Enantioenriched Piperidinyl Allylic Boronates: From Mechanism to Drug Discovery

by

Mohamad Estaitie

A thesis submitted in partial fulfillment of the requirements for the degree of

Doctor of Philosophy

Department of Chemistry
University of Alberta

Abstract

Functionalized piperidine rings are frequently found in a variety of alkaloids and pharmaceuticals attesting to the importance of this class of heterocycles in drug discovery. According to recent data, the piperidine ring is the most abundant heterocycle found in FDA approved drugs. Thus, gaining access towards enantioenriched piperidines through convenient and cost-effective methods is highly desirable. One approach to access such heterocycles is the use of enantioenriched alkyl boronic esters. Alkyl boronic esters have gained attention as versatile building blocks in organic transformations and drug discovery due to their low toxicity and configurational stability. This thesis focuses on the development and optimization of synthetic methodologies towards the synthesis of functionalized enantioenriched piperidines using chiral boronic ester intermediates. In addition, this thesis also focuses on the application of such intermediates in drug discovery.

Chapter 2 describes a collaborative effort of a mechanistic study on the borylative migration reaction, which is a robust methodology previously reported by our group to access enantioenriched tetrahydropyran and piperidine derivatives. The study uses a combination of experimental and computational approaches to decipher the mechanistic pathway of this reaction. The aim of this project is gain insights about the reaction, which would be useful in expanding the scope of the borylative migration towards other heterocyclic systems.

Since its discovery of the borylative migration, the synthetic applications of obtained products were limited to allylboration on aldehydes and $C_{sp}{}^3$–$C_{sp}{}^2$ Suzuki–Miyaura cross-coupling reactions. Chapter 3 of this thesis describes our recent efforts to expand the application of the piperidinyl allylic boronic intermediates towards a stereospecific $C_{sp}{}^3$–$C_{sp}{}^3$ cross-coupling

reactions. This gives access to novel enantioenriched 2-substitued piperidines bearing a cinnamyl moiety.

Chapter 4 focuses on a collaborative project for the application of the borylative migration reaction in drug discovery. The synthesis of vacquinol-1 analogs, potential drugs in the treatment of glioblastoma multiforme (GBM) is described. In addition, *in vitro* biological testing of these analogs against GBM cell lines is also presented.

Preface

Chapter 2 of this thesis was published as H. A. Clement, M. Estaitie, Y. Kim, D. G. Hall, C. Y. Legault "Mechanism of the Palladium-Catalyzed Asymmetric Borylative Migration of Enol Perfluorosulfonates: Insights into an Enantiofacial-Selective Transmetalation" *ACS Catal.* **2021**, *11*, 8902–8914. This project was collaborative effort with Dr. Claude Y. Legault from Université de Sherbrooke. H. A. Clement was responsible for the experimental investigations described in Section 2.2, where I was responsible for experimental investigation of the inhibitory effect of the side product of the borylative migration reaction. C. Y. Legault was responsible for all DFT calculations regarding the studied reaction. I assisted in writing the supporting information in collaboration with H. A. Clement. D. G. Hall and C. Y. Legault were the supervisory authors of this project.

Chapter 3 of this thesis was published as M. Estaitie, D. G. Hall "Regiocontrolled Synthesis of Enantioenriched 2-Substituted Dehydropiperidines by Stereospecific Allyl Allyl Cross-Coupling of a Chiral Allylic Boronate" *ChemComm* **2022**, *58*, 1370–1373. I was responsible for the reaction optimization, study of the substrate scope, data collection, analysis and writing of the supporting information. I was also responsible for writing the manuscript with assistance from D. G. Hall. D. G. Hall was the supervisory author of this work.

Chapter 4 is an ongoing collaborative effort with Dr. Roseline Godbout from the Department of Oncology at the University of Alberta. This project is a continuation of Samantha Kwok's and Rory McDonald's master's theses. Samantha Kwok's and Rory McDonald's efforts in this project are summarized in Section 4.2. I was responsible for synthesis and characterization

of the new vacquinol-1 analogs. The in vitro testing of vacquinol-1 analogs was done by Dr. Saket Jain and Dr. Mansi Garg from the Godbout Group.

Acknowledgements

I would like to give thanks to my supervisor Prof. Dennis Hall for giving me the opportunity to join his research team. He has been an incredible mentor throughout my PhD program. His support, patience and hands-on approach made me a better organic chemist today than I was 5 years ago. Attending his group meetings expanded my scope in organic chemistry beyond the projects I was working on.

I am so grateful to the amazing Hall Group members starting from Jason Rygus and Dr. Helen Clement for their support and help during my research. I would like to extend my gratitude all my colleagues, specifically to Zain Kazmi, Dawson Konowalchuk, Jake Blackner, Olivia Schneider, Ashley Ponich, Geneviève O'Keefe, Martin Lessard, Jingkai Sun and Jingning Zhou. In addition, I would like to also thank all past group members specially Rory McDonald, Carl Estrada, Dr. Marco Paladino, Kevin Nguyen, and Dr. Hwee Ting Ang.

I would like to give my appreciation to the organic chemistry teaching staff specifically to the awesome Dr. Hayley Wan and Connor Part for being very supportive and helpful during my teaching assistantship duties.

A gracious thank you to all research and administrative services staff at the University of Alberta including the NMR staff, mass spectrometry, analytical labs and storeroom. Special thanks to Ed Fu, the analytical technician of Hall Group for his contribution in HPLC and chiral separation used in my project. I would like to also thank the NMR expert Mark Miskolzie for his help in my kinetic studies.

Lastly, I would like to give my gratitude to my friends specifically Ahmed Alloush, Mohammad Charaf and Jacqueline Eleanor Evans for their help and support throughout my PhD

years. I am also very grateful to my parents, Huda Hassiba and Khalid Estaitie and my siblings Hiba, Waleed and Hussam for supporting the youngest member of the family.

Table of Contents

List of Tables

List of Figures

List of Schemes

List of Abbreviations

Å	Angstrom
Ac	Acetyl
Ad	Adamantyl
aq.	Aqueous
Ar	Aryl
atm	Atmosphere
Bn	Benzyl
Boc	*tert*-Butyloxycarbonyl
cal	Calorie
cat.	Catalytic
Cbz	Benzyl chloroformate
cm^{-1}	Wavenumber
COD	1,5-Cyclooctadiene
CPME	Cyclopentyl methyl ether
Cy	Cyclohexyl
d	Doublet
dba	Dibenzylideneacetone
DCM	Dichloromethane
de	Diastereomeric excess

DIBAL	Diisobutylaluminium hydride
DIPEA	*N,N*-Diisopropylethylamine
DMA	Dimethylaniline
DMF	Dimethylformamide
DMP	Dess–Martin periodinane
DPEphos	Bis[(2-diphenylphosphino)phenyl] ether
dppf	1,1′-Ferrocenediyl-bis(diphenylphosphine)
dppp	1,3-Bis(diphenylphosphino)propane
dr	Diastereomeric ratio
E	Electrophile
EDCI	1-Ethyl-3-(3-dimethylaminopropyl)carbodiimide
EDG	Electron donating group
ee	Enantiomeric excess
er	Enantiomeric ratio
es	Enantiospecificity
Et	Ethyl
EWG	Electron withdrawing group
FG	Functional Group
h	Hour
HOBt	Hydroxybenzotriazole

Hz	Hertz
IBX	2-Iodoxybenzoic acid
*i*Pr	*iso*-Propyl
k	Kilo
L	Liter
LG	Leaving group
LiHMDS	Lithium bis(trimethylsilyl)amide
M	Molar
m	Multiplet
M.S.	Molecular sieves
*m*CPBA	*meta*-Chloroperoxybenzoic acid
Me	Methyl
Mes	Mesityl
mg	Milligram
min	Minute
mL	Millilitre
mol	Mole
MTBE	Methyl tert-butyl ether
n.d.	Not detected
nbd	Norbornadiene

n-Bu	Normal butyl
Nf	Nonaflate
NHC	*N*-Heterocyclic carbene
NMR	Nuclear magnetic resonance
Nu	Nucleophile
PG	Protecting Group
pin	Pinacol
PMA	Phosphomolybdic acid
PMB	*para*-Methoxybenzyl
q	Quartet
R	Alkyl
rac	Racemic
rt	Room temperature
t	Triplet
TBAF	Tetrabutylammonium fluoride
TBDPS	*tert*-Butyldiphenylsilyl
t-Bu	*tert*-Butyl
Tf	Triflate
TFA	Trifluoroacetic acid
THF	Tetrahydrofuran

TLC	Thin layer chromatography
TMS	Trimethylsilyl
Ts	Tosyl
UV	Ultraviolet
VQ-1	Vacquinol-1
μ	Micro
μW	Microwave

Chapter 1: Piperidine Rings as Invaluable Building Blocks in Drug Discovery

1.1 Introduction

Alkaloids are nitrogen-bearing compounds that are part of the most complex chemicals found in nature. Most of these compounds have significant biological properties and play substantial roles in the human body.[1] The piperidine moiety can be found in a plethora of examples of this class of chemicals. This six-membered ring containing a nitrogen atom and five methylene units was named after the *Piper* genus, pepper vines, from which numerous piperidine alkaloids were isolated.[2] Due to their biological properties, many piperidine alkaloids have been utilized as scaffolds for the development of pharmaceuticals.[3,4]

1.1.1 Piperidines in natural products

Historically, the alkaloid piperine **1-1** was isolated from black pepper in 1820.[5] Upon treating this natural product with aqueous alkali solution, a basic product was isolated and given the name piperidine. However, the cyclic structure of piperidine was not determined until 1883.[5] Presently, piperine is known to have several biological activities. In addition to being responsible for the spiciness of black pepper, it was shown that this piperidine derivative has a beneficial influence on the bioavailability of a number of other chemicals such as curcumin, propranolol and theophylline.[6,7] According to *in vitro* and *in vivo* studies, piperine exhibited inhibition activities on a range of drug-metabolizing enzymes including ethylmorphine-*N*-demethylase, whereas it can enhance the activity of other enzymes such lipases, trypsin and disaccharidases.[8-10] An additional example of a pharmaceutically relevant piperidine natural product is lobeline **1-2**, which was isolated from *lobelia inflata*.[11] It has been used in the treatment of several respiratory conditions including bronchitis, asthma, and pneumonia.[12] One of the most established piperidine alkaloid is quinine **1-3**, which was used to treat malaria as early as the 1600's.[13] Initially, it was administered as a component of grounded barks of cinchona trees until it was successfully isolated in 1820.[13]

Despite that more effective synthetic anti-malarial drugs becoming available in the 1920's, it is still recommended as a second-line treatment for malaria by 2022 World Health Organization (WHO) guidelines.[14]

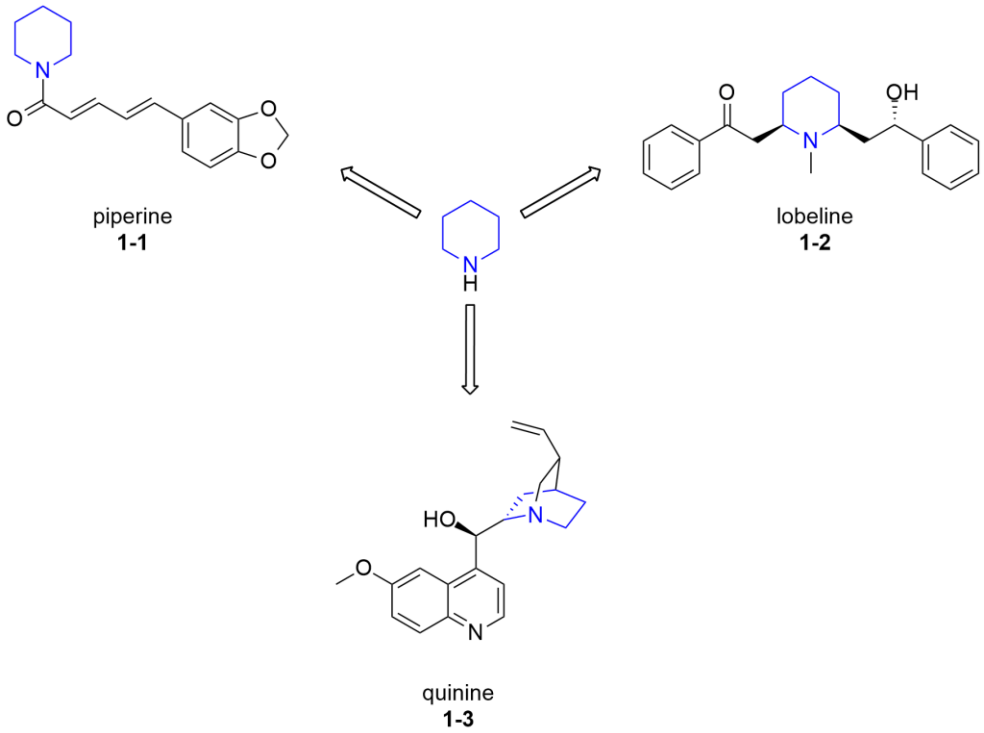

Figure 1-1. Selective examples of natural products containing a piperidine unit.

1.1.2 Piperidines in pharmaceuticals

Due to the fact that several natural products containing piperidine units have biological activity, it is not surprising that this structural motif can also be found in pharmaceutical drugs. In fact, the piperidine moiety is the most abundant heterocycle found in synthetic medications earning its classification as a "privileged scaffold" (Figure 1-2).[15-17] An example of piperidine-containing pharmaceuticals is the antidiarrheal loperamide **1-4**. This strong μ-opioid receptor agonist is listed on the *WHO Model Lists of Essential Medicines*.[18,19] An additional illustration of a widely used piperidine-containing medication is the antidepressant paroxetine **1-5**, which is a selective serotonin reuptake inhibitor (SSRI).[20] The antimalarial mefloquine **1-6** is another instance of a drug containing the piperidine unit that is listed on *WHO Model List of Essential Medicines*.[18]

Studies suggest that mefloquine targets the eukaryotic ribosome of the parasitic *Plasmodium falciparum*, which inhibits its protein biosynthesis process.[21] Ibrutinib **1-7** is one more case of a drug containing the piperidine motif. This pharmaceutical is used in the treatment of chronic lymphocytic leukemia.[22] The drug's mode of action occurs by irreversible binding to Bruton's tyrosine kinase protein, which inhibits the proliferation of B-cells.[22]

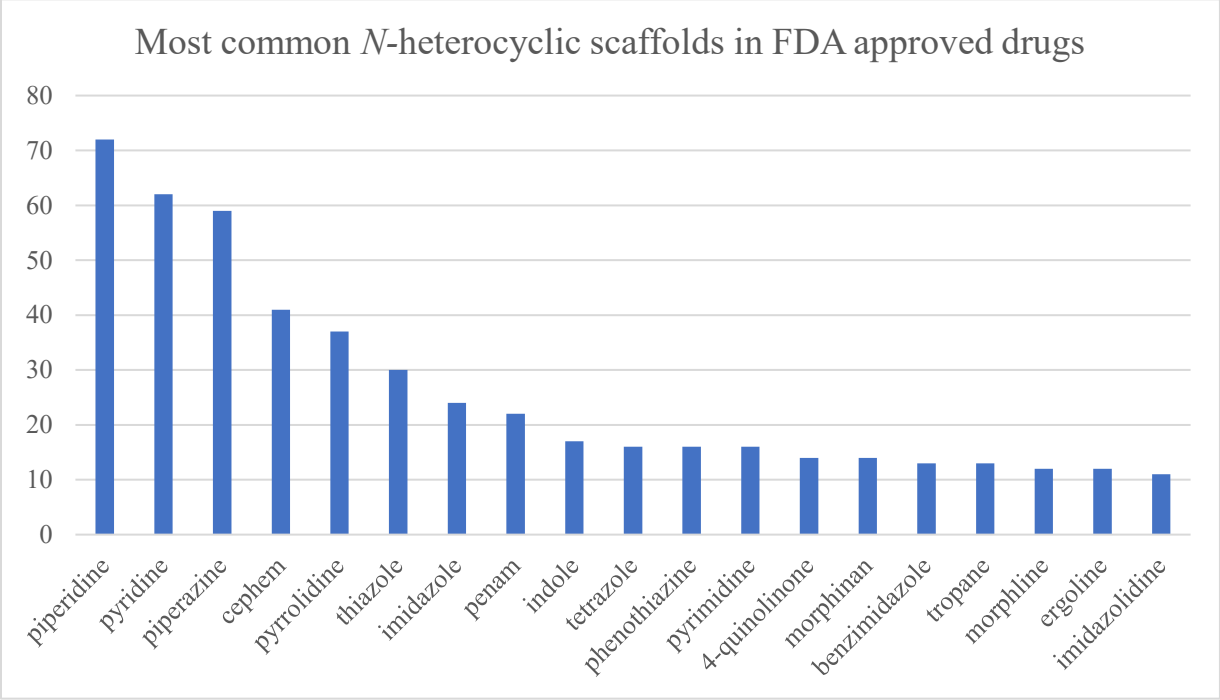

Figure 1-2. Most frequent *N*-heterocycles found in Food and Drug Administration (FDA) approved drugs.

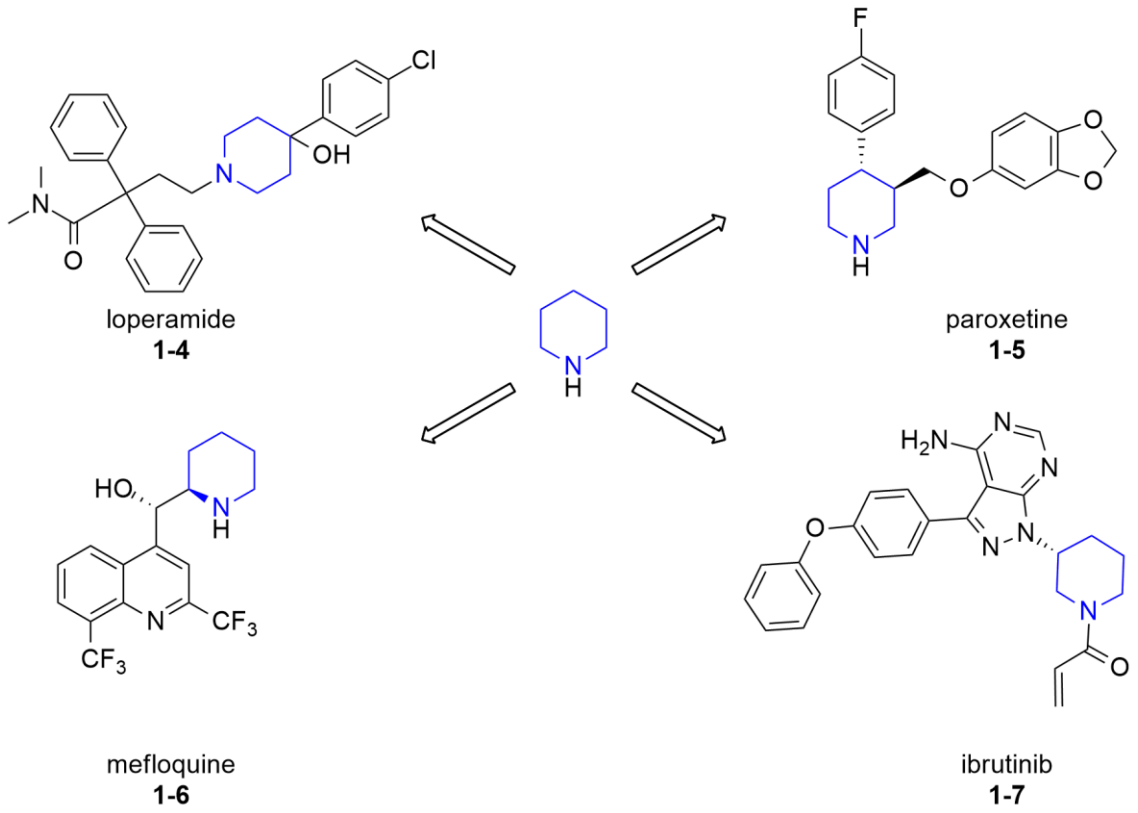

Figure 1-3. Selective examples of synthetic pharmaceuticals containing a piperidine unit.

1.2 Common Methods for the Synthesis of Piperidines

From the aforementioned relevance of the piperidine ring in natural products and the pharmaceutical industry, it is desirable to develop convenient stereoselective methods towards the synthesis of this pharmaceutically relevant moiety. For this reason, organic chemists have made numerous efforts to synthesize enantioenriched piperidines utilizing efficient and cost-friendly methods. The following sections will discuss in detail some selected recent examples towards the enantioselective synthesis of piperidines.

1.2.1 Reduction of pyridines

Obtaining piperidines by the reduction of pyridines is a robust strategy due to the widespread availability of pyridine derivatives. This transformation can occur through the reduction of the entirety of the pyridine ring, or through sequential formation of the corresponding dihydro- and tetrahydropyridines, which allows for further modification of these intermediates. The reduction

can occur stereoselectively, forming multiple stereocenters in the process. This could occur either in an enantioselective manner by using a chiral catalytic system or diastereoselectively by utilizing the presence of a pyridine substituent with a stereogenic center to discriminate between the two faces of the ring during the reduction.

1.2.1.1 Organocatalyzed hydrogenation

One strategy for the catalytic asymmetric reduction of substituted pyridines is the use of chiral phosphoric acids in the presence of a transfer hydrogenation reagent. Reuping and Antonchick reported the first example of this chemistry using a catalytic amount of 9-anthryl-substituted BINOL phosphoric acid and two equivalents of Hantzch ester (Scheme 1-1a).[23] Diverse 2,3,6-trisubstituted pyridines **1-8** were successfully reduced to the corresponding enantioenriched tetrahydropyridines **1-9** in high yields and excellent enantioselectivities. The presence of an electron-withdrawing substituent at the 3-position of the pyridine ring played a major role in the success of this transformation, accelerating the reduction of the heteroarene and stabilizing the tetrahydropyridine products *via* a push-pull substitution pattern.[23] A more recent example of this strategy was reported by You and co-workers.[24] In their work, they employed a chiral spirocyclic phosphoric acid catalyst in a cascade hydrogenative coupling of pyridines **1-10** and pyrrole nucleophiles **1-11** (Scheme 1-1b). The mechanism of this asymmetric transformation involves protonation of the pyridine by the phosphoric acid catalyst to form the pyridinium salt **Int-1-1**. Next, reduction of the salt by a 1,4-hydride transfer from the Hantzch ester generates **Int-1-2**, which isomerizes to the corresponding iminium **Int-1-3** in the presence of the acid catalyst. The subsequent asymmetric nucleophilic attack of the pyrrole on the iminium intermediate releases the product **1-12** and regenerates the catalyst.[24] The stereoinduction of the attack is governed by the chirality of the conjugate base of the chiral phosphoric acid. A major drawback of this strategy is the need for an electron withdrawing group at the 3-position, which limits the substrates that can be employed.

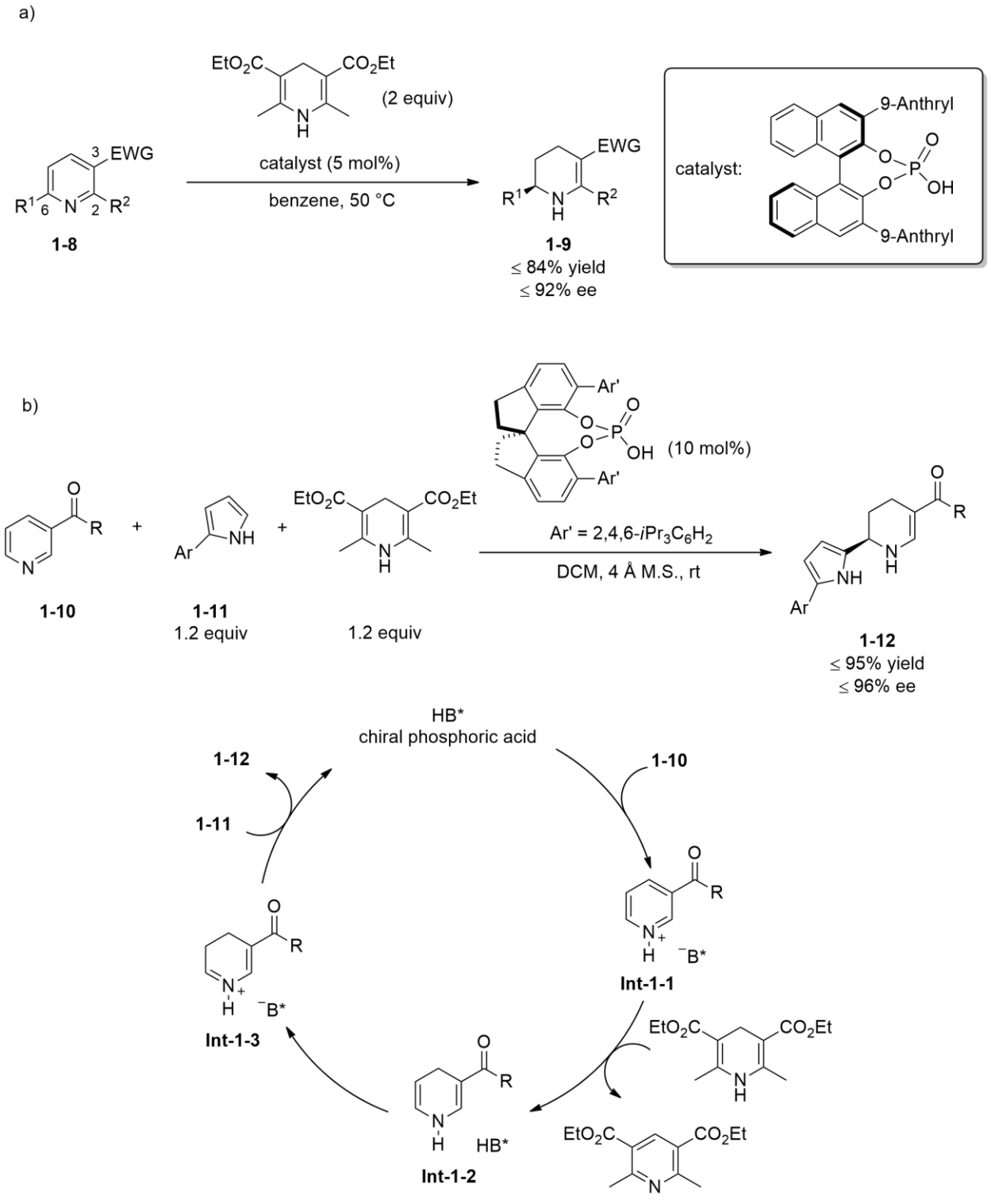

Scheme 1-1. a) Asymmetric catalytic hydrogenation of pyridines using chiral phosphoric acid. b) Cascade transformation catalyzed by chiral phosphoric acid.

1.2.1.2 Transition metal-catalyzed hydrogenation

Another strategy employed in the synthesis of enantioenriched piperidines *via* the reduction of pyridines is through the use of transition metal catalysis. This method is challenged by the inhibitory effect caused by the coordination ability of pyridine nitrogen atom towards transition metal catalysts. Studer et al. reported the first example of this strategy in the full hydrogenation of monosubstituted pyridines.[25] Their method used a homogenous rhodium catalyst with chiral diphosphine ligands; however, the products were obtained in low enantioselectivity (Scheme 1-2a). To circumvent the inhibition effect of the nitrogen, efforts were made towards strategies that included substrate activation. For example, Legault and Charette reported an asymmetric hydrogenation of *N*-iminopyridinium ylides using chiral iridium catalysis.[26] Following this work, different pyridinium salts were investigated in the synthesis of enantioenriched piperidines from a parent pyridine moiety including *N*-benzylpyridinium and pyridinium hydrohalide salts (Scheme 1-2b).[27-32] A recent example from the Zhou Group reported the synthesis of highly enantioenriched piperidines through asymmetric hydrogenation directly from pyridines to bypass the need for substrate pre-activation.[33] Their method employed an *in situ* substrate activation using chiral iridium catalysis in the presence of trichloroisocyanuric acid as a traceless activator. Using this strategy, the Zhou Group was able to obtain enantioenriched substituted piperidines in high yields and enantiomeric excess (Scheme 1-2c). Major drawbacks of this type of reduction methods include the requirement for a prior substrate activation step and the presence of substituents in a close vicinity to the heteroatom.

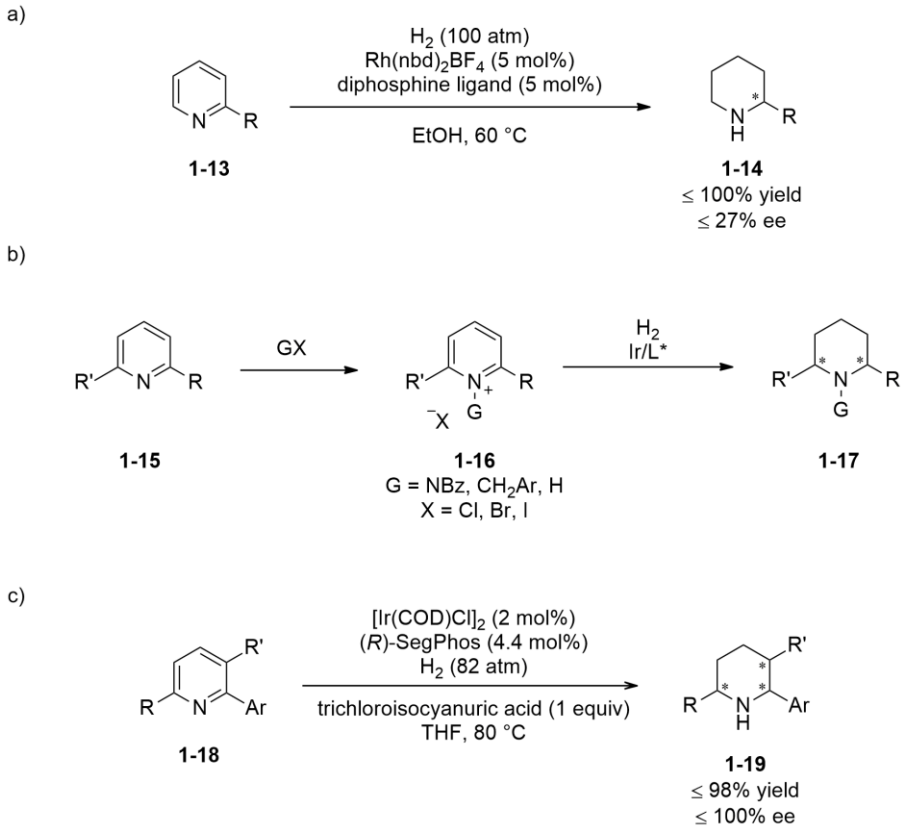

Scheme 1-2. a) Early example of asymmetric pyridine hydrogenation using rhodium catalysis. b) General strategy of iridium-catalyzed asymmetric hydrogenation of pyridines. c) Zhou Group's asymmetric hydrogenation of pyridines.

1.2.2 Piperidines from aza-Diels–Alder cycloaddition

The aza-Diels–Alder reaction is a powerful synthetic method for the assembly of pharmaceutically relevant piperidines.[34] Using this method, piperidines can be synthesized in a highly regio- and diastereoselective fashion. If asymmetric catalysts are employed, this type of [4 + 2] cycloaddition allows access to enantioenriched functionalized piperidines.[35,36] Similar to other types of Diels–Alder reactions, aza-Diels–Alder cycloadditions can be classified into normal and inverse electron demand types (Figure 1-4). A normal electron demand aza-Diels–Alder reaction (NED aza-DAR) describes the reaction between electron-rich 1,3-dienes with electron-deficient dienophiles, including imines and electron-deficient alkenes.[37] On the other hand, inverse electron demand aza-Diels–Alder reaction (IED aza-DAR) refers to the involvement of electron-deficient 1,3-dienes, such as 1- or 2-aza-1,3-dienes, and electron-rich dienophiles.[38,39]

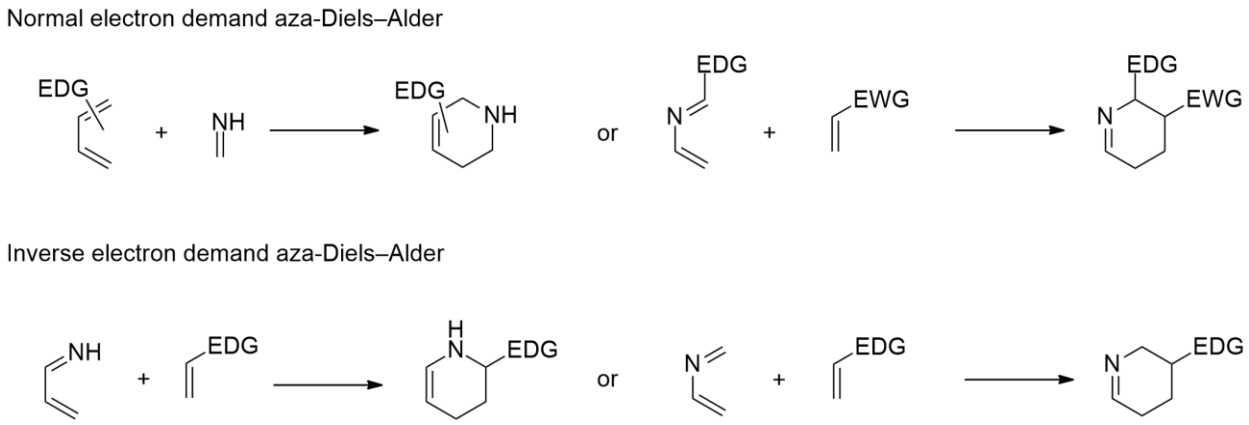

Figure 1-4. Normal and inverse electron demand aza-Diels–Alder reactions.

From the beginning of the 21st century, a number of catalytic enantioselective variations of the aza-DAR have been established. These were enabled by the use of chiral Lewis acidic metals or chiral organic compounds such as Brønsted acids and amines.[40-42] The first example of a catalytic asymmetric aza-DAR to obtain piperidine derivatives was reported by Kobayashi and co-workers using chiral Lewis acid catalysis.[43] In their method, they used imine **1-20** with Danishefsky diene **1-21** in the presence of a chiral zirconium-binol complex, which afforded the cycloadduct **1-22** in high yields and enantioselectivity (Scheme 1-3). The stereoinduction observed in this chemistry was attributed to the dual complexation of dienophile **1-20** with the zirconium catalyst through the imine nitrogen and the hydroxy group.[34,43]

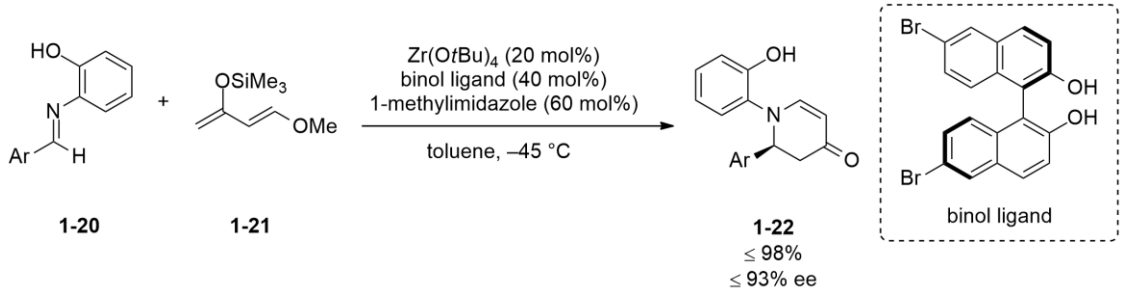

Scheme 1-3. First catalytic enantioselective aza-DAR for piperidine synthesis *via* zirconium catalysis by Kobayashi and co-workers.

Following this discovery, several efforts have been made to expand the application of chiral metal catalysis using a variety of ligands in aza-DAR.[44-46] Recently, Rovis and co-workers reported

an enantio- and diastereoselective formal [4 + 2] cycloaddition of silicon-free 1-azadienes **1-23** as weakly nucleophilic dienes with α-nitroalkenes **1-24** as highly electrophilic dienophiles.[47] This methodology was achieved by the use of zinc catalysis with enantioenriched bis(oxazoline) ligands. The observed stereochemistry was rationalized by the mechanism shown in Scheme 1-4. First, Michael addition of the aza-diene **1-23** to the zinc-coordinated nitroalkene **1-24** occurs to from **Int-1-4**. Next, an intramolecular cyclization of **Int-1-4** delivers the desired product **1-25** after the subsequent chemoselective reduction.[47]

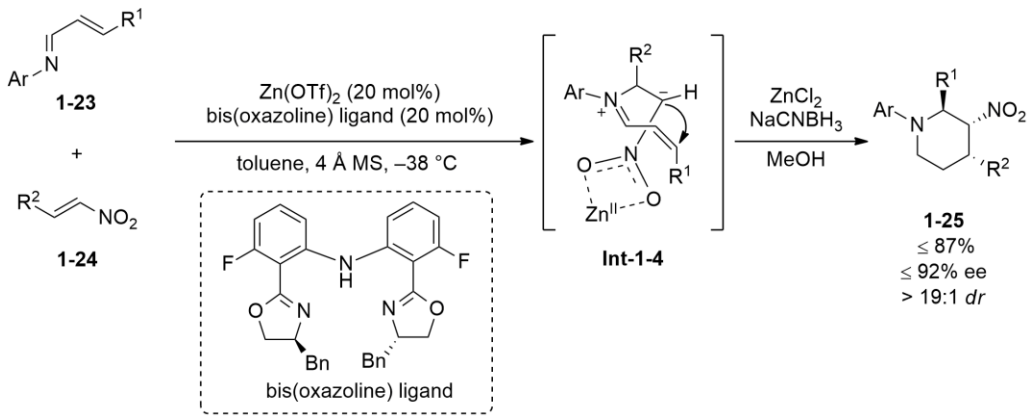

Scheme 1-4. Zinc catalyzed asymmetric formal aza-Diels–Alder reaction.

In addition to NED aza-DAR, the IED aza-DAR method could also be applied to prepare enantioenriched piperidines. One of the general strategies applied in this method is the use of chiral Lewis base organocatalysts to promote stereoinduction during the cycloaddition as reported by several research groups such as the Chen Group and the Ye Group (Scheme 1-5a).[48-50] The Zhao Group reported a recent example of this strategy in the synthesis of enantioenriched benzofuran fused piperidines (Scheme 1-5b).[51] Their method employed a chiral proline derivative with a low catalytic loading in the [4 + 2] cycloaddition reaction between benzofuran derivative **1-26** and aldehyde **1-27**. This cycloaddition generated a hemiaminal intermediate that was directly used in the subsequent reduction to afford the desired benzofuran fused piperidines **1-28** in high yields and enantioselectivity.[51] One of the drawbacks of the aza-Diels Alder reaction is that the regio-

and diastereoselectivity is governed by the substituents of the reactants, which limits the diversity of substrates that can be used in this reaction.

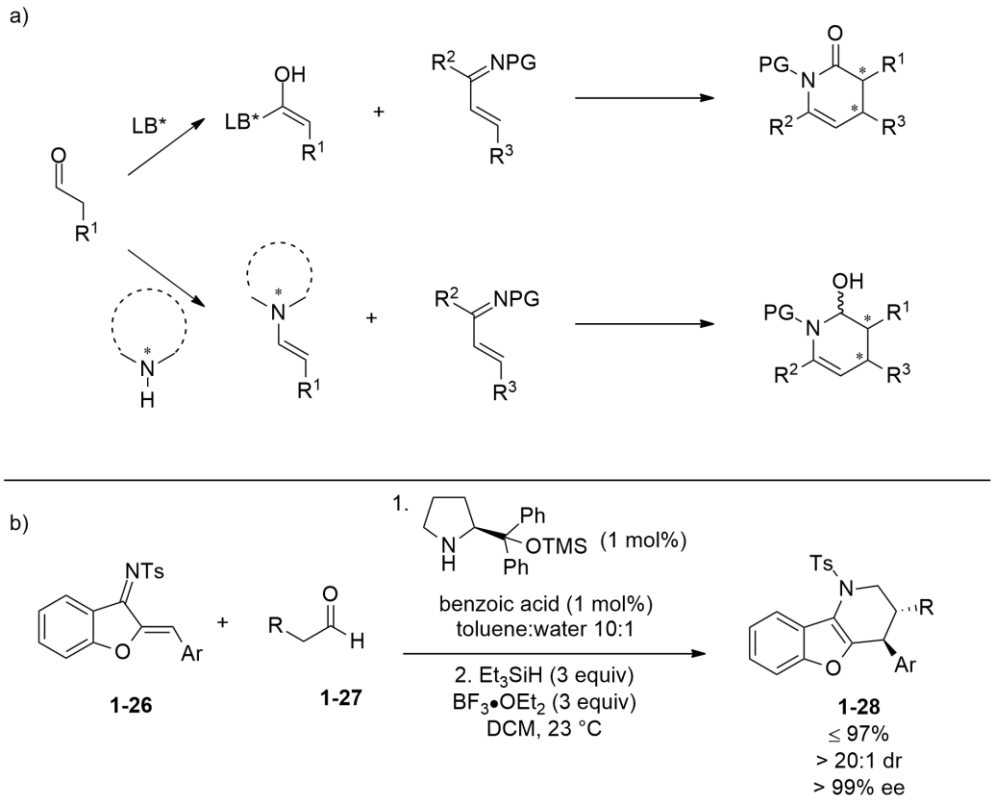

Scheme 1-5. a) General strategy employed in IED aza-DAR. b) Recent method for the synthesis of enantioenriched benzofuran fused piperidines.

1.2.3 Ring-closing metathesis

Ring-closing metathesis (RCM) is an effective strategy for the formation of carbon–carbon bonds *via* a transition metal-catalyzed intramolecular olefin metathesis reaction. This success could be attributed to the development of stable, reactive, and highly functional group tolerant metal alkylidenes.[52] The driving force of this transformation is the formation of a volatile by-product and alkene stability of the product as illustrated in the mechanism (Scheme 1-6a). The first example of RCM used in the synthesis of piperidine derivatives was reported by Grubbs and Fu in 1992 using molybdenum alkylidene catalysis, where an unsaturated piperidine derivative **1-30** was produced in high yield (Scheme 1-6b).[53] This strategy has subsequently been applied in the synthesis of many natural products containing the piperidinyl moiety. Early examples include the

synthesis of (−)-coniine **1-32** and (+)-sedamine **1-35** as reported by the Vankar Group and the Cossy Group respectively (Scheme 1-6c).[54,55]

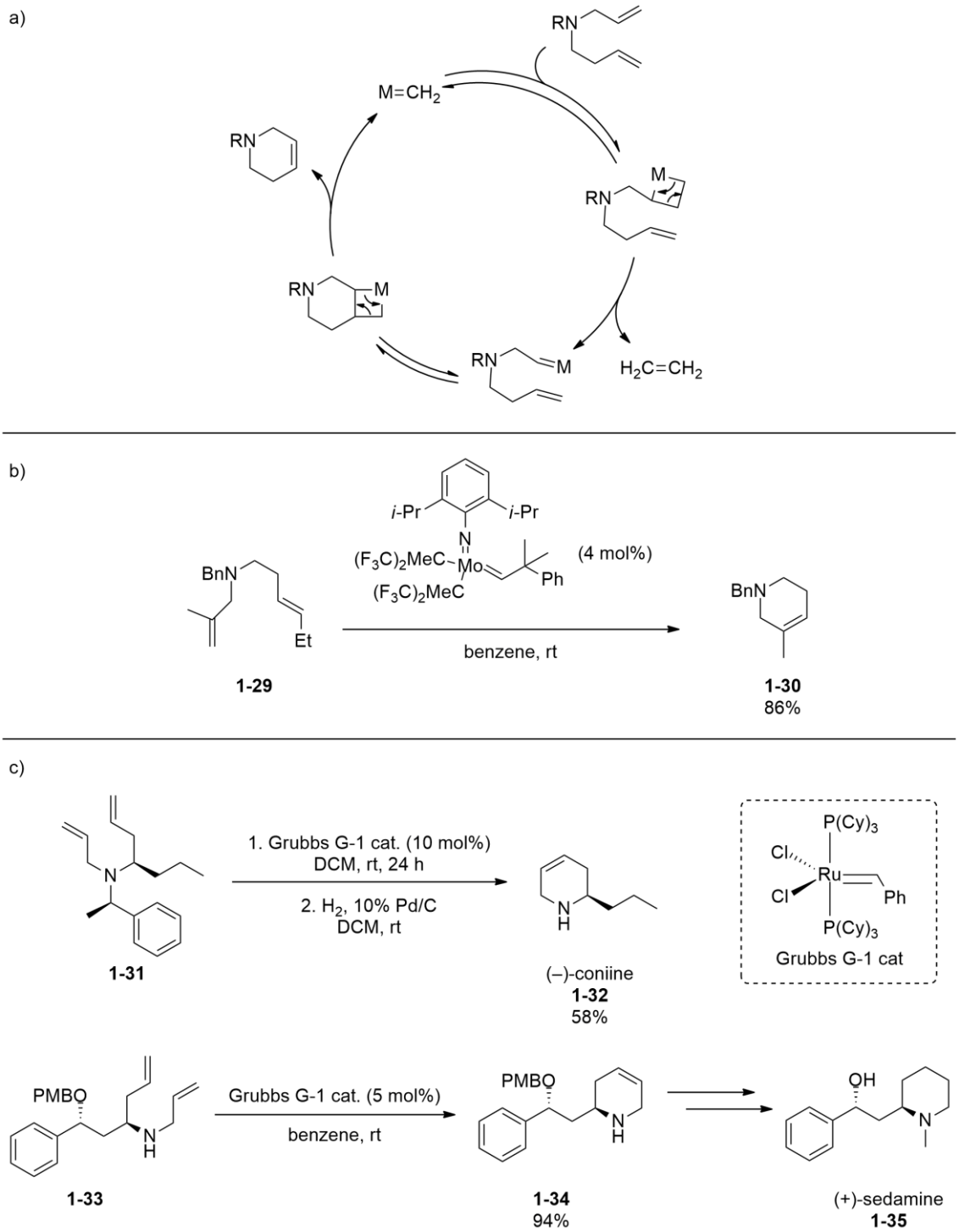

Scheme 1-6. a) General mechanism of RCM. b) First example of piperidine derivative synthesis using RCM as reported by Grubbs and Fu. c) Early examples of total synthesis using RCM as a key step.

As shown by the aforementioned examples, the prevalent drawback of using RCM in the synthesis of enantioenriched substrates is the necessity of installing the stereogenic centers prior to the cyclization reaction. Efforts have been made to mitigate this drawback by employing different strategies, such as kinetic resolution of dienes or desymmetrization of trienes.[56] A few research groups successfully utilized chiral molybdenum alkylidenes to access heterocycles in an enantioselective manner.[57-60] One example of these efforts is the work of Hoveyda and co-workers in the desymmetrization of nitrogen-containing trienes to synthesize enantioenriched piperidines and azepanes in high yields and enantiomeric excess (Scheme 1-7).[60]

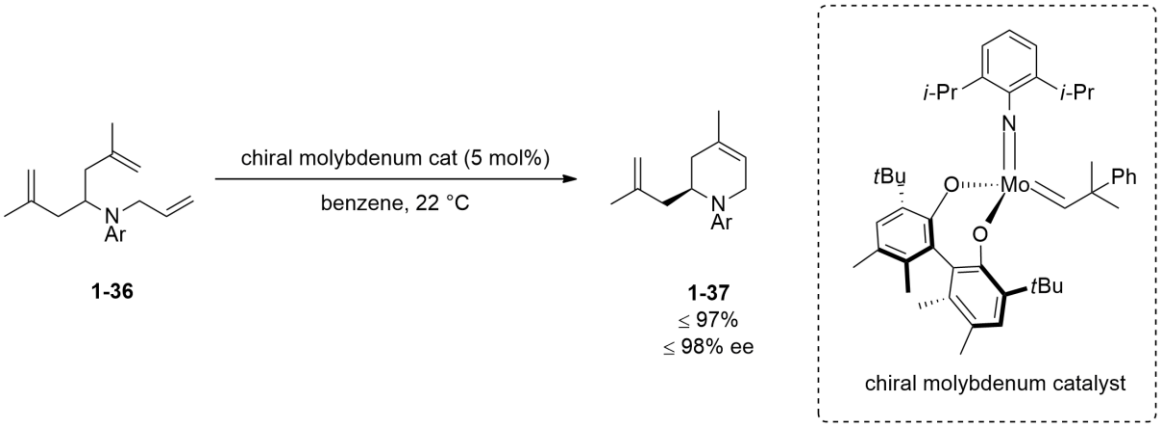

Scheme 1-7. Hoveyda and Shrock's asymmetric RCM using chiral molybdenum catalysis.

1.2.4 Piperidines *via* ring expansion

Ring expansion reactions enable chemists to access medium to large ring moieties and it is an alternative strategy to the conventional cyclization reactions. In the case of piperidine heterocycles, 3- and 4-substituted piperidines can be prepared by ring expansion of strained aziridinium and azetidinium salts respectively. An early example of this strategy was reported by Cossy and co-workers in 1999, where 2-substituted pyrroline derivatives **1-38** were used in the synthesis of enantioenriched 3-substituted piperidines **1-40** *via* the aziridinium salt **1-39**, which is generated *in situ*.[61] The authors used this strategy in the synthesis of (–)-velbanamine natural product **1-43** (Scheme 1-8).[62]

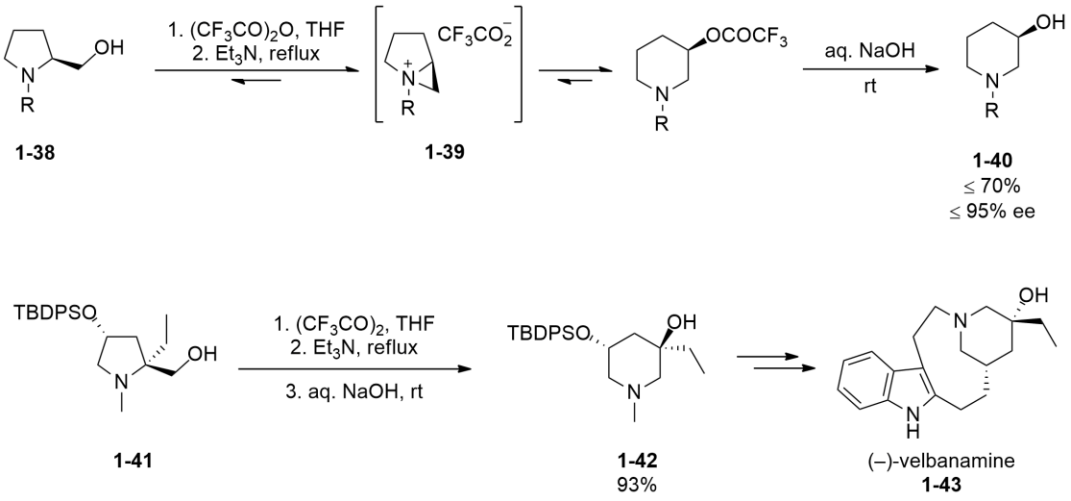

Scheme 1-8. Early example of using aziridinium salts in the preparation of enantioenriched piperidine derivatives and their application in the total synthesis of (–)-velbanamine.

In 2011, the Charette Group improved on this strategy by making the transformation irreversible and regioselective at the more hindered electrophilic center. This achievement was enabled by employing α,β-unsaturated aziridinium intermediates. This unsaturation further activates the allylic position towards nucleophilic attack, and promotes regioselective ring-opening at the most hindered site to form the desired piperidine (Scheme 1-9).[63]

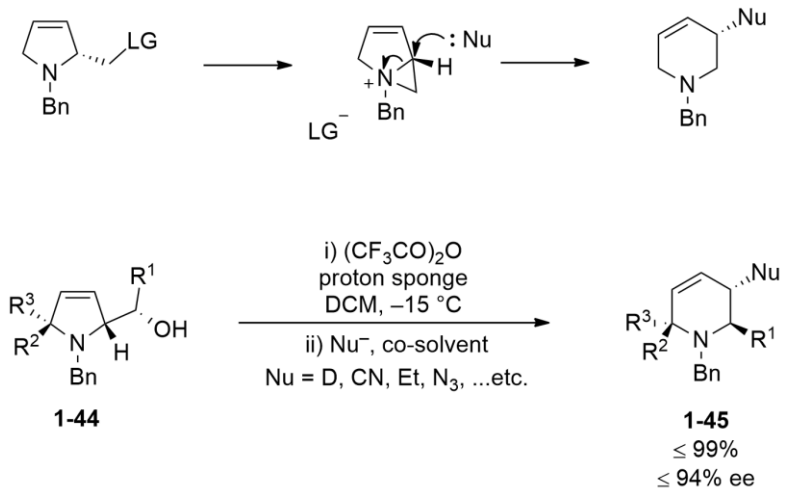

Scheme 1-9. Charette's improvement on Cossy's work of ring expansion of aziridinium salts to piperidines.

Alternatively, 4-substitued piperidines are accessible by ring expansion using azetidinium salts. This strategy was explored by De Kimpe and co-workers in 2006, who reported that 4-bromo

piperidines **1-48** could be obtained in high yields and stereoselectivity upon refluxing bromo azetidines **1-46** in acetonitrile. The reaction proceeds through an intramolecular S_N2 attack to form the azabicyclic intermediate **1-47**, which is subjected to a subsequent ring opening nucleophilic attack.[64] Later, the same laboratory expanded on this chemistry by using azetidines bearing a mesylate leaving group and subjecting them to various nucleophiles, which diversified the products that can be obtained using this method. The main drawback of these ring expansion methods is the requirement for the stereochemistry to be present in the substrates prior to the transformation (Scheme 1-10).[65]

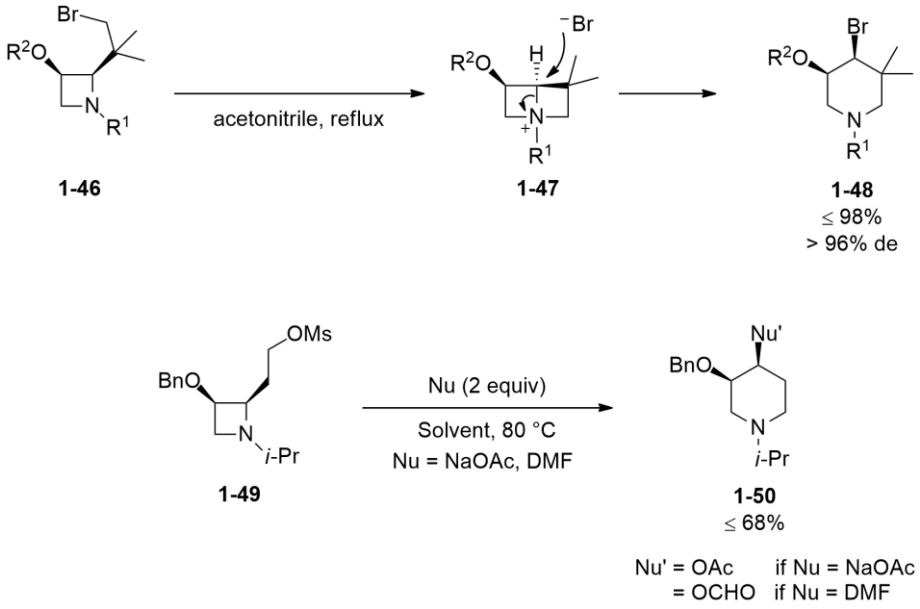

Scheme 1-10. De Kimpe's ring expansion of azetidines to form 4-substituted piperidines.

1.2.5 Alkylative cyclization

Intramolecular nucleophilic attack of nitrogen atoms on an electrophilic carbon center is a well-established strategy for the synthesis of piperidine rings. This strategy includes nucleophilic substitution, reductive amination, and Michael addition. This direct cyclization approach is commonly employed in the synthesis of pharmaceutically relevant *N*-containing molecules, which, according to chemoinformatics studies, show that almost half of the C–N bond forming

transformations used in the pharmaceutical industry are performed *via N*-substitution and reductive amination.[66]

Chiral piperidine substrates can be obtained from intramolecular substitution reactions by employing auxiliary-based strategies. Such auxiliaries include *tert*-butyl- or tolylsulfinamides, which were initially explored by the Ellman Group and the Davis Group respectively.[67,68] A recent examples of this method was reported by Mangelinckx and co-workers in the synthesis of 2,3-disubstituted enantioenriched piperidines.[69] In their work, chiral *N*-sulfinyl imidate **1-51** was employed in an anti-selective enolate addition to an aldimine derivative **1-52** to obtain anti-adducts **1-53**. The consequent intramolecular cyclization reaction of the resulting sulfonamides **1-53** furnished the desired piperidine derivatives **1-54** (Scheme 1-11).[69]

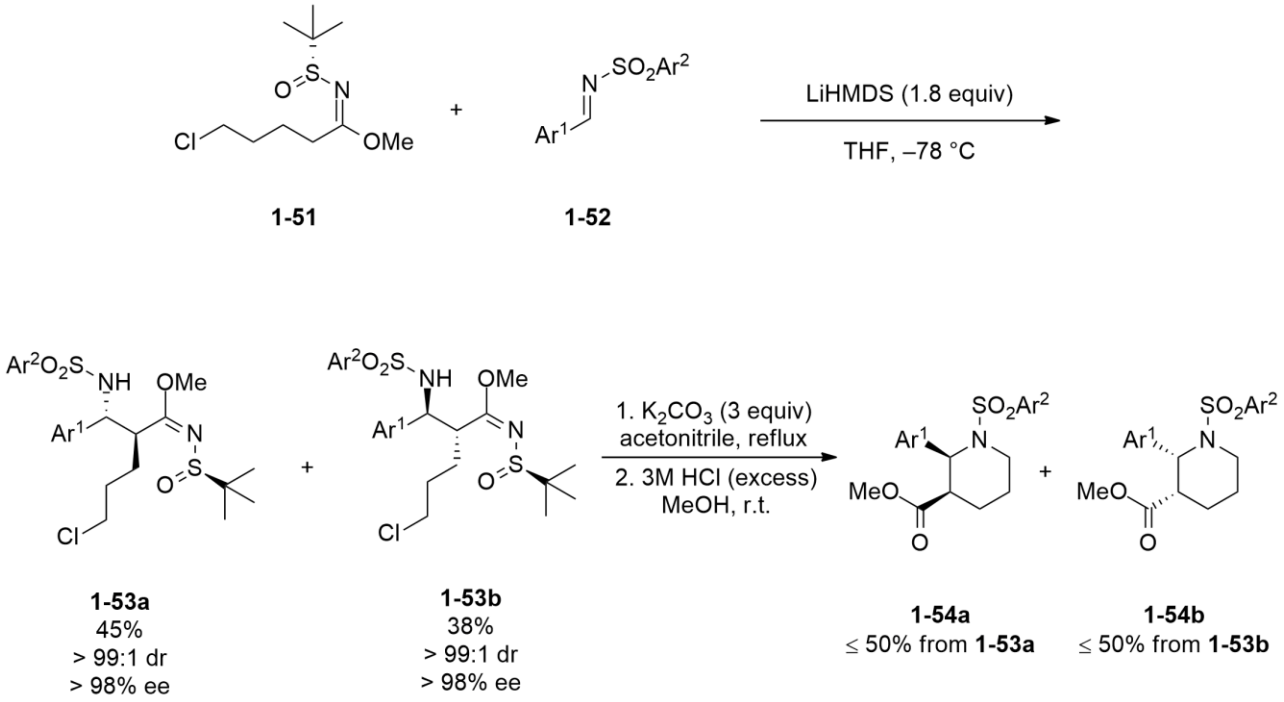

Scheme 1-11. Example of intramolecular cyclative nucleophilic substitution reaction reported by Mangelinckx.

In addition to the cyclative nucleophilic substitution strategy, reductive amination is an effective method to synthesize disubstituted piperidines with high diastereoselectivity. This was demonstrated by Szolcsányi and co-workers in the synthesis of (+)-dihydropinidine and (–)-epidhydropinidine. In their work, the diastereoselectivity of the lithium aluminum hydride (LAH) reduction of imine **1-55** was controlled by the addition of trimethylaluminium as a chelating agent. The stereoselectivity of the reaction can be explained by the steric effects between the reducing agent and the $AlMe_3$-chelated imine to favor the pseudo-equatorial attack to form anti-product **1-56**. On the other hand, the absence of a chelating agent favors the formation of the syn-product **1-57** by a pseudo-axial attack (Scheme 1-12).[70]

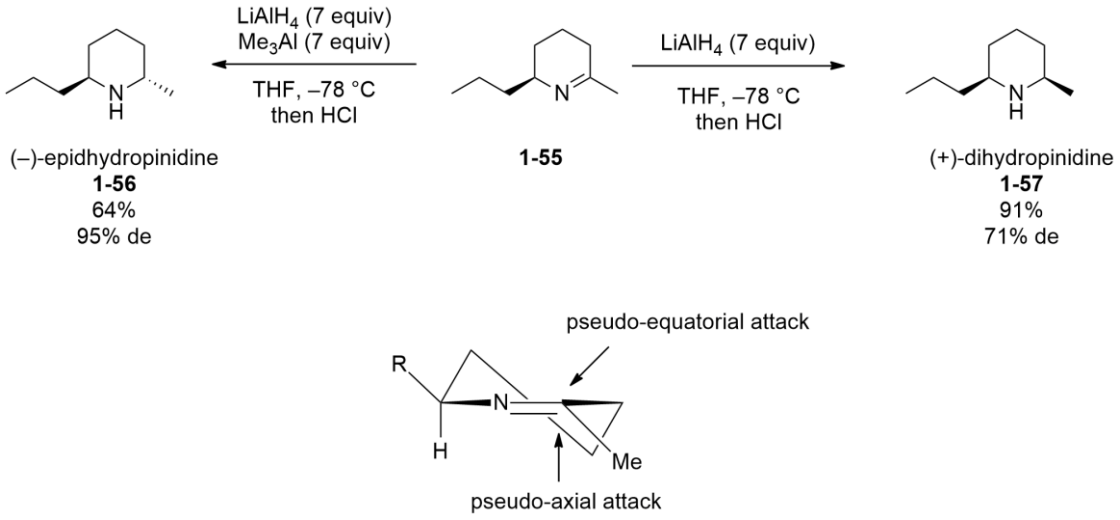

Scheme 1-12. Synthesis of (+)-dihydropinidine and (–)-epidhydropinidine reported by Szolcsányi.

α,β-Unsaturated carbonyls bearing an amino moiety can also be employed in the preparation of piperidines through an intramolecular aza-Michael-addition. Numerous efforts have been reported towards stereoselective Michael addition by utilizing chiral organocatalysis.[71-73] This method was recently used by the del Pozo Group in their enantioselective synthesis of 2-substituted piperidines.[74] The stereochemical induction in this strategy was enabled by using a hydroquinine catalyst, which forms a chiral *α,β*-unsaturated iminium salt intermediate that undergoes an intramolecular Michael-type nucleophilic attack from the amino moiety.[75] In this

way, enantioenriched piperidine derivatives **1-59** were successfully obtained from *α,β*-unsaturated ketone **1-58** bearing vinyl sulfonamide moiety (Scheme 1-13).[74]

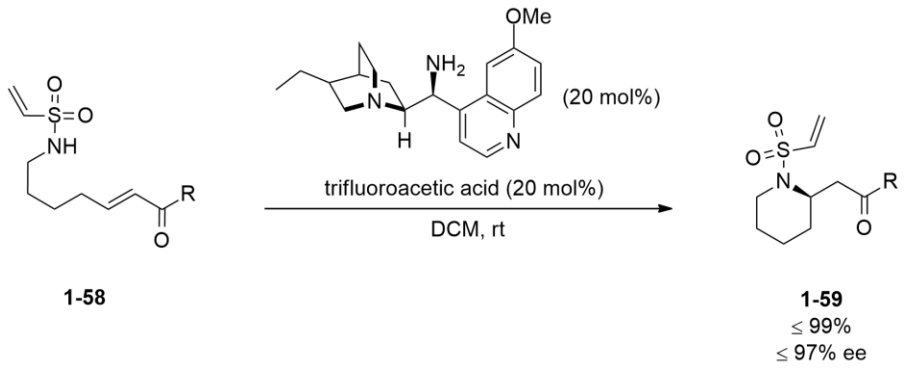

Scheme 1-13. Enantioselective intramolecular aza-Michael addition example reported by del Pozo.

As discussed in this section, there are a variety of synthetic methods towards the preparation of piperidines. However, each method has its own drawbacks and limitations, which include the necessity of highly functionalized starting substrates for a late-stage ring formation. These limitations narrow the possible set of piperidines that can be produced *via* these methods. In addition, for some of these aforementioned examples, the regio- and stereoselectivity remain a challenge. Therefore, exploring alternative strategies towards the synthesis of piperidine derivatives from unfunctionalized or slightly functionalized piperidine rings in a stereoselective fashion is desirable. One example of such a strategy is the use of chiral allylic boronates as a building block, which display several advantages in synthetic organic chemistry that will be discussed in the following section.

1.3 Applications of Chiral Allylic Boronic Esters

Allylic boronic esters (and by extension alkyl boronic esters) are a versatile class of building blocks for numerous transformations in organic chemistry. The versatility of these reagents arise from the Lewis acidic nature of the boron atom in the tricoordinate state and the electron rich nature in the tetracoordinate state.[76] Furthermore, upon borate formation, the C–B bond is sufficiently nucleophilic that it can react with various electrophiles. Another feature that is specific to allylic boronic esters compared to other organoboron compounds is the presence of two sites of reactivity

as shown in Figure 1-5a. Due to these aforementioned features, there have been a myriad of methodologies that employ chiral boronic esters in various stereospecific transformations. This section provides a brief overview of the general methods towards boronic esters functionalization, which have been comprehensively reviewed elsewhere.[77]

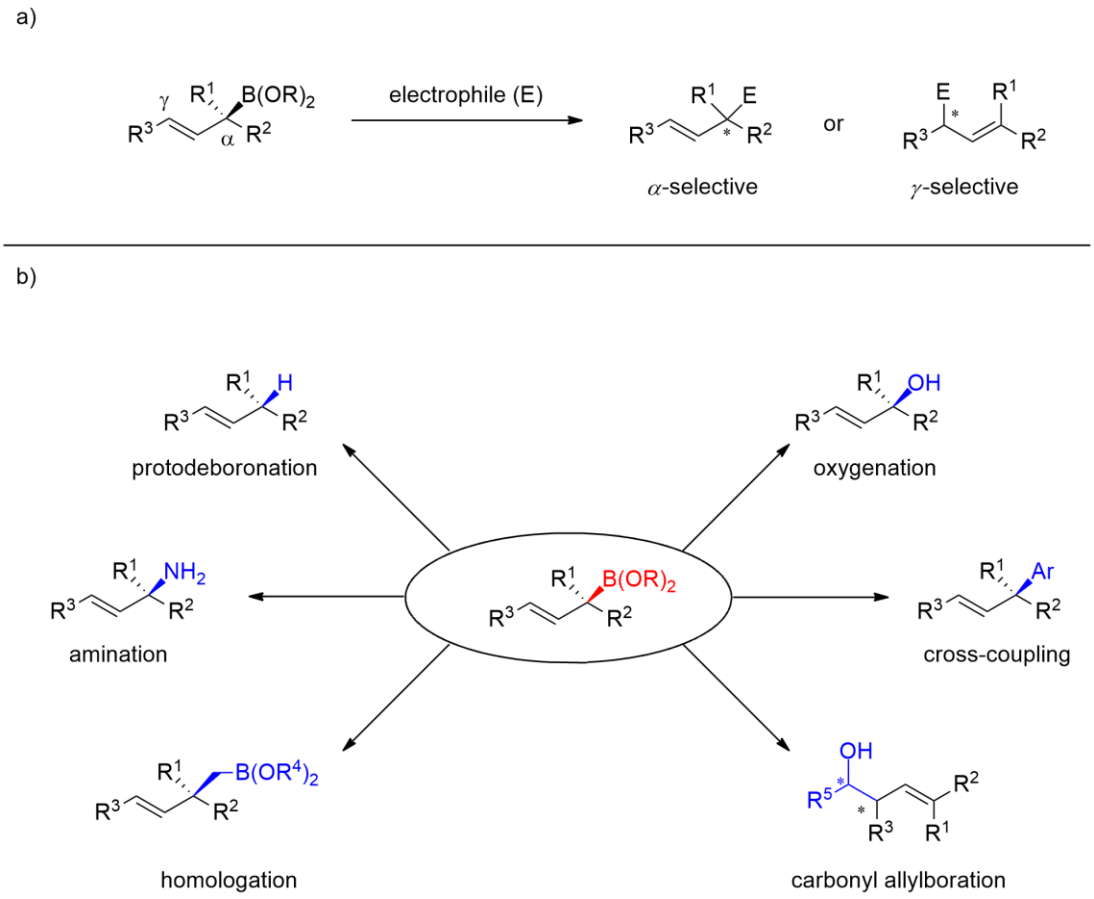

Figure 1-5. a) Allyl boronic esters mode of reactivity. b) Synthetic applications of allylic boronic esters.

1.3.1 Oxidation methods

Oxidation of alkylboronic esters to their analogous alcohols is the most common transformation of boronic esters. Oxygenation of C–B bonds in organoboron compounds is a well-established and robust reaction. The typical conditions for the oxidation of organoboron compounds include treatment of the substrate with an alkaline hydrogen peroxide solution in an organic solvent. Improvement on this method allowed the use of sodium perborate as a milder oxidant.[78] The mechanism of the C–B oxidation involves coordination of the peroxide anion to generate the

tetracoordinated borate species. Then, the borate undergoes a 1,2-metallate shift to furnish the desired alcohol in a stereospecific manner after hydrolysis (Scheme 1-14). Furthermore, amines can also be obtained stereospecifically directly from alkylboronic esters by using the highly nucleophilic alkoxy amines as devised by Morken and co-workers.[79,80]

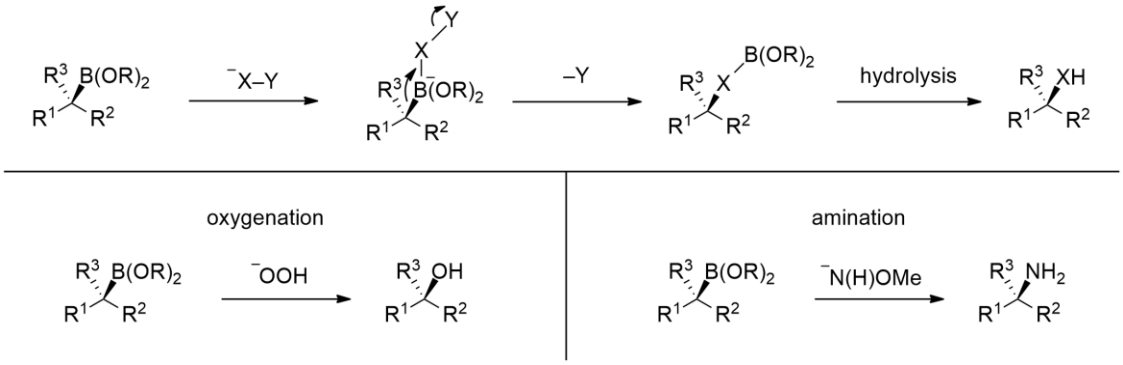

Scheme 1-14. Brief overview of stereospecific C-B bond oxidation to alcohols and amines.

1.3.2 Protodeboronation

Protodeboronation involves protonolysis of organoboron compounds, where C–B bonds are converted to C–H bonds. Typically, protodeboronation is a common undesired side transformation during organoboron functionalization reactions. However, stereospecific protodeboronation of tertiary alkylboronic esters enables access to enantioenriched methine moieties. A general stereoretentive protodeboronation protocol of diaryl and benzylic boronic esters **1-60** was reported by the Aggarwal Group.[81] The stereoretentive nature of the transformation was believed to arise from a hydrogen bonded boronate complex **1-61** that undergoes the protodeboronation to afford the desired product **1-62** (Scheme 1-15).[81]

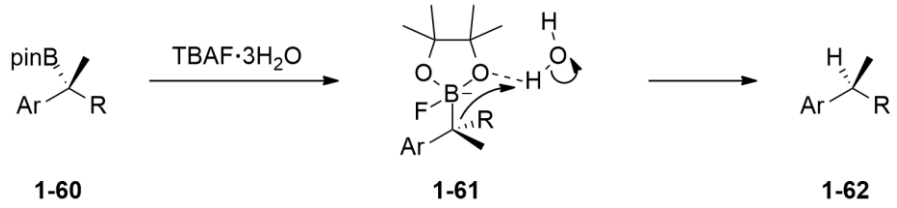

Scheme 1-15. Stereoretentive protodeboronation reported by the Aggarwal Group.

1.3.3 Carbon-carbon bond formation

1.3.3.1 Homologation reactions

Homologation reactions are described as the extension of a hydrocarbon chain by one carbon, typically, a methylene unit. The homologation of organoboron compounds are explored extensively by organic chemists for carbon-carbon bond formation. This strategy involves incorporation of aliphatic nucleophiles bearing a leaving group at the α-position. This transformation is applicable to secondary and tertiary alkylboronic esters, which makes it a feasible strategy for stereospecific C–C bond formation due to the stereoretentive nature of this chemistry. An example of this strategy is the well-established Matteson homologation reaction, where coordination of a lithiated dichloro- or dibromomethane to a chiral alkylboronic ester forms a tetracoordinate intermediate, which undergoes a stereoretentive 1,2-metallate shift to afford the product **1-64** (Scheme 1-16).[77]

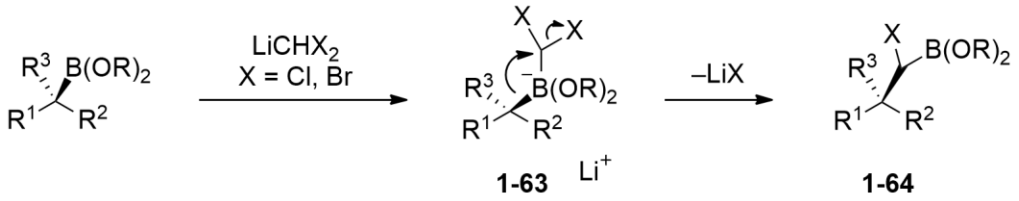

Scheme 1-16. Traditional Matteson homologation reaction.

1.3.3.2 Allylboration reactions

The nucleophilic addition of allyl boronic esters to carbonyl electrophiles to afford homoallylic alcohols, generally referred to as allylboration, is one of the most valuable transformations in organic chemistry to form new C–C bonds in a stereocontrolled fashion. The control of the stereoselectivity of the allylboration reaction arises from the closed Zimmerman–Traxler chair-like transition state **1-65**, where the carbonyl is activated by coordination to the boron atom (Scheme 1-17). This method enables diastereoselective synthesis of homoallylic alcohols by using enantioenriched allylic boronic esters. In addition, the Hall Group showcased the application of Lewis and Brønsted acid catalysis in allylborations to accelerate the reaction or enhance the

stereocontrol during the transformation.[82,83] Compared to aldehydes, the allylboration of ketones is more challenging. Thus, efforts have been made to promote catalytic ketone activation to afford tertiary homoallylic alcohols as reported by Schaus.[84] Furthermore, Aggarwal reported uncatalyzed ketone activation methods to access similar products.[85] For more insights about this transformation the reader is directed to more thorough reviews.[86,87]

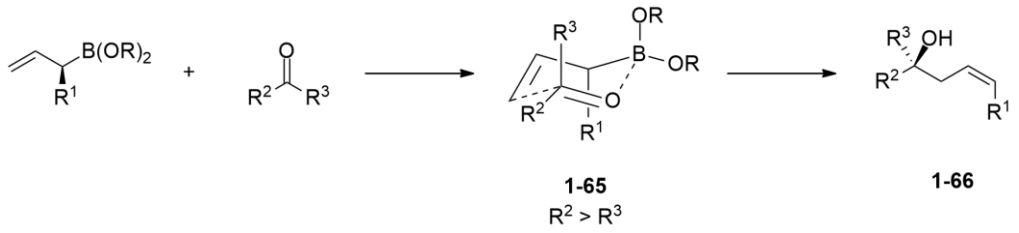

Scheme 1-17. General allylboration reactions of enantioenriched allylic boronic esters on carbonyl compounds.

1.3.3.3 Suzuki–Miyaura cross-coupling

The Suzuki–Miyaura cross-coupling reaction is one of the most effective methods for C–C bond formation. Due to the advantageous cost-effective and scalable nature of this reaction, it has been applied in the synthesis of various pharmaceuticals. In fact, it is listed as the second most employed reaction in medicinal chemistry after amide bond formation.[88] The Suzuki–Miyaura reaction is well-established for the C_{sp}^2–C_{sp}^2 bond formation between alkenyl or aryl organoboron compounds and alkenyl- or aryl halides and pseudohalides. On the other hand, C_{sp}^3–C_{sp}^2 and C_{sp}^3–C_{sp}^3 bond connections are challenging and relatively limited due to undesired *β*-hydride elimination that can occur during the process. Thus, efforts have been made to overcome this problem and enable stereoselective cross-coupling reactions of alkyl boronates. During the cross-coupling reaction of enantioenriched alkyl boronic esters, transmetalation can occur *via* either retention or inversion, which can be controlled by utilizing the proper catalytic system for the transformation (Scheme 1-18).[77,89,90]

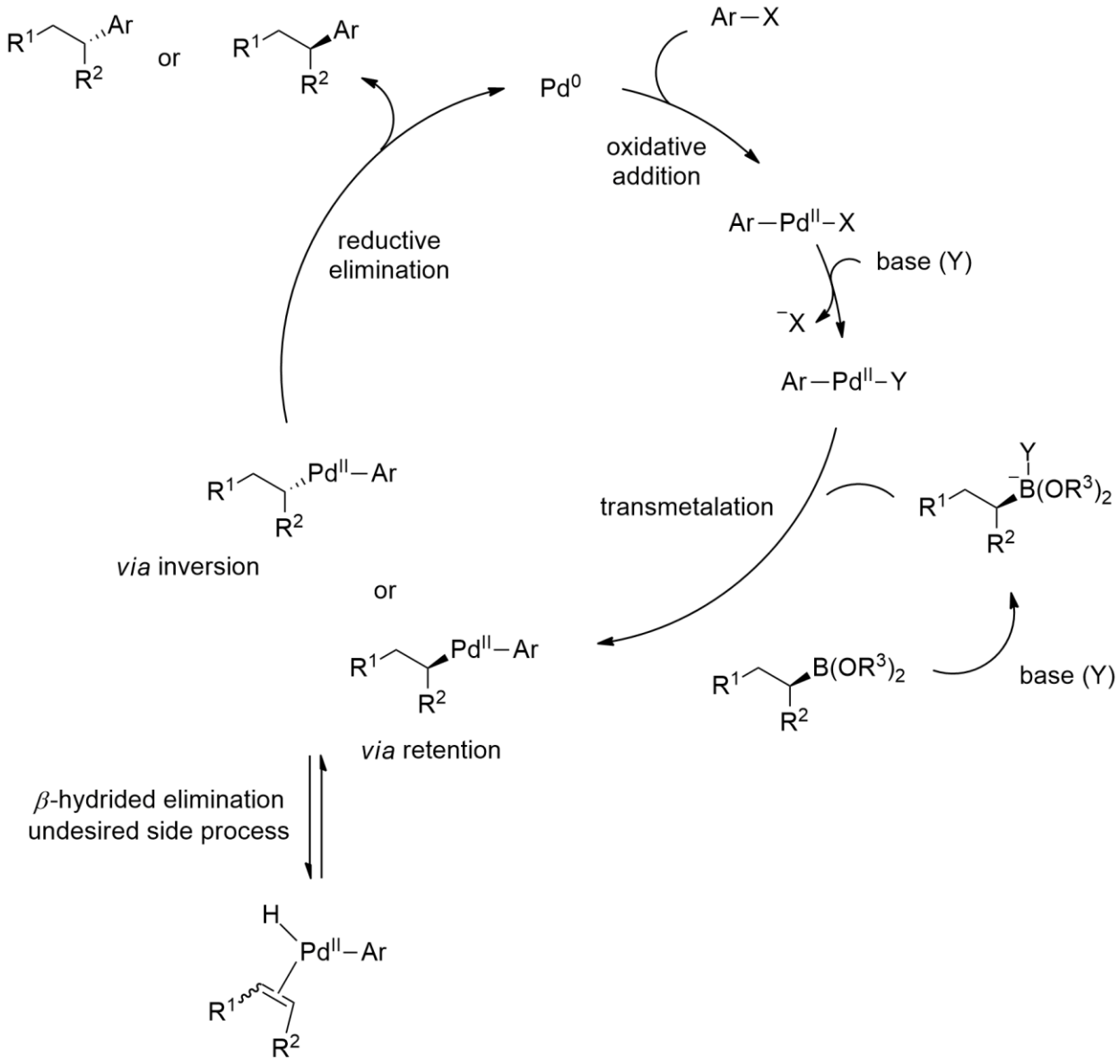

Scheme 1-18. General mechanism of Suzuki–Miyaura reaction of enantioenriched alkyl boronates and the possible *β*-hydride elimination undesired side process.

1.4 Synthetic Methods Towards Enantioenriched Cyclic Allylic Boronic Esters

Due to the rise of interest in chiral allylic boronic esters as a synthetic building block (*vide supra,* Section 1.3), it is beneficial to expand the realm of synthetic methodologies that enable straightforward access to such building blocks in a convenient and cost-friendly fashion. Allylic boronic esters can be synthesized through conventional methods, such as conjugate borylation and hydro/diboration.[91,92] However, these general methods will not be discussed in this section due to the lack of examples of cyclic products. Instead, the reader is directed towards a recent review of these general transformations and only several methodologies to obtain cyclic allylic boronates will be discussed.[93]

1.4.1 Allylic borylation

The copper-catalyzed borylation of allylic substrates is one of the main methodologies that can be used to access chiral allylic boronic esters. The first example of this strategy was reported by the Ito Group, where they employed *Z*-allylic carbonates **1-67** to access enantioenriched allylic boronic esters **1-68** in high enantiomeric ratio and good yields (Scheme 1-19a). The proposed mechanism of this transformation involves σ-bond metathesis between the copper alkoxide **1-69** and B_2pin_2 to form the copper–boryl intermediate **Int-1-5**. Next, alkene insertion on allylic carbonate **1-67** affords the γ-borylated alkyl copper complex **Int-1-6**. Finally, the catalytic species **1-69** is then regenerated through β-alkoxy elimination to form the desired chiral allylic boronic ester **1-68** (Scheme 1-19b).[94] Several related examples of this chemistry have been reported by Hoveyda and McQuade using Cu-NHC catalysis.[95,96] In addition, this generic allylic borylation chemistry has been expanded to incorporate other elimination approaches such as β-Br, β-F, β-C and β-N eliminations.[97-100]

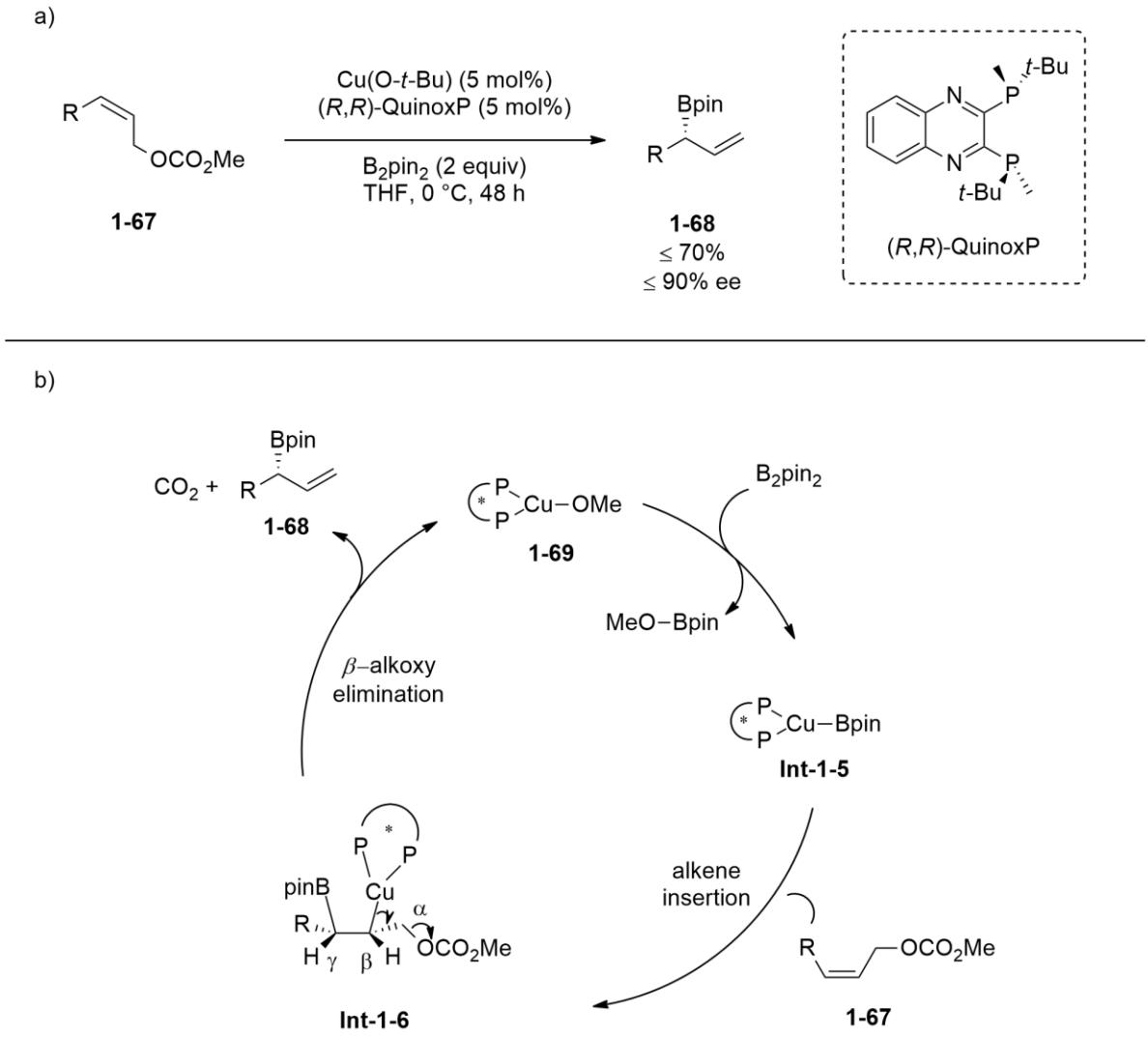

Scheme 1-19. a) First example of stereoselective Cu-catalyzed allylic borylation. b) Proposed general mechanism of allylic borylation chemistry.

An early application of this strategy for the synthesis of enantioenriched cyclic allylic boronic esters was reported by Ito and co-workers, where racemic allylic ethers **1-70** were used in an enantioconvergent allylic borylation to produce allylic boronic esters **1-71**.[101] These allylic boronic esters were used in stereospecific allylboration reactions on aldehydes to afford homoallylic alcohols **1-72** (Scheme 1-20a). The enantioconvergence of this transformation arises from opposite facial selectivity in the nucleophilic attack of the Cu-Bpin complex on each enantiomer of the racemic allylic ether mixture (Scheme 1-20b).[101]

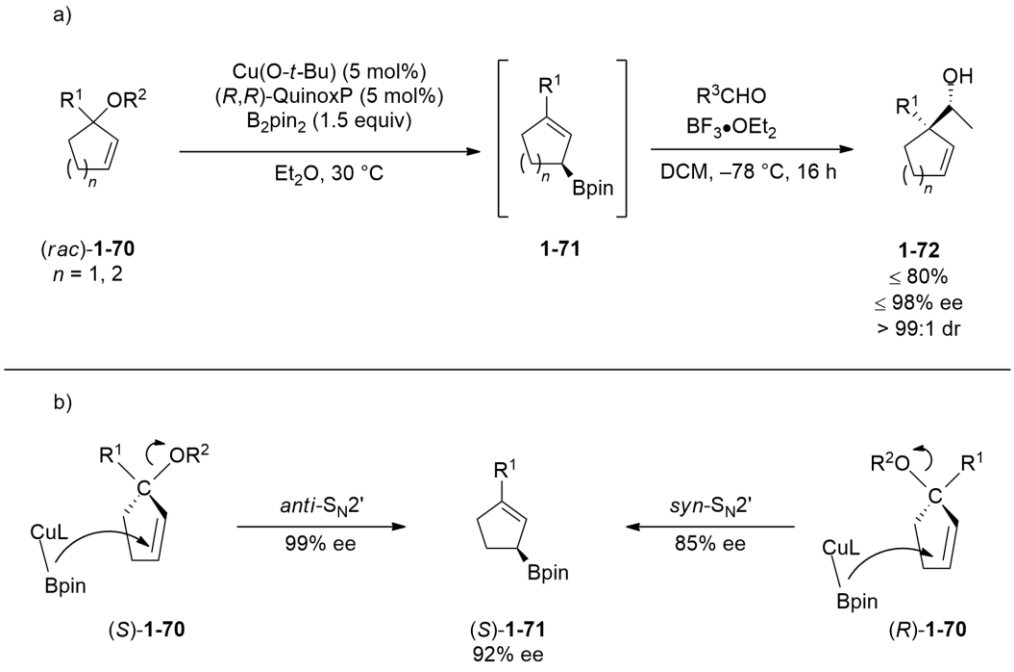

Scheme 1-20. a) Copper-catalyzed enantioconvergent allylic borylation reaction. b) Rationale for the enantioconvergence.

A more recent example of the synthesis of enantioenriched cyclic allylic boronic esters through an allylic borylation strategy is the work of the Tan Group (Scheme 1-21).[102] In their work, secondary and tertiary cyclic allylic boronic esters **1-75** and **1-76** were obtained in high enantioselectivity using an enantioconvergent copper-catalyzed transformation similar to Ito's work. To date, it is one of the few known examples of stereoselective protocols enabling access to tertiary cyclic allylic boronic esters.[102]

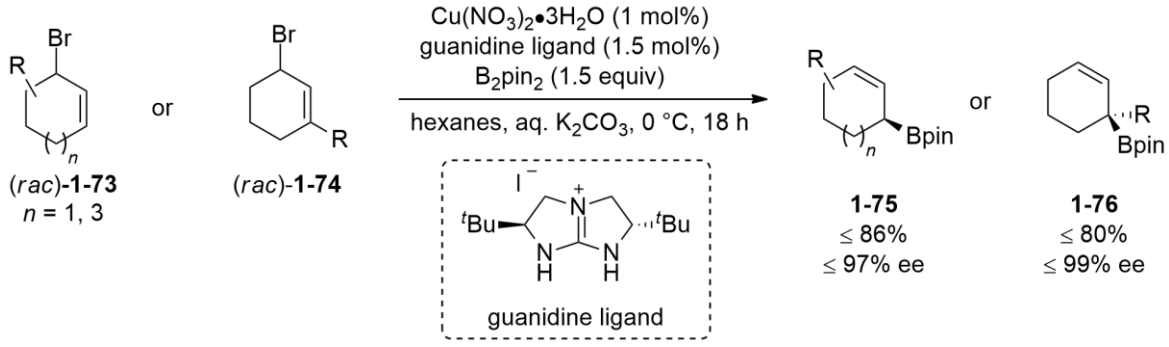

Scheme 1-21. Enantioselective Cu-catalyzed allylic borylation towards the synthesis of secondary and tertiary allylic boronic esters.

1.4.2 Hetero-Diels–Alder cycloaddition

Seeking efficient means towards the synthesis of pharmaceutically relevant heterocycles, the Hall Group reported a catalytic enantioselective approach to obtain heterocyclic allylic boronic esters **1-77** using chiral chromium catalysis in a [4 + 2] hetero-Diels–Alder cycloaddition. The authors devised a three-component one pot reaction protocol to gain access to piperidine and dihydropyran derivatives **1-78** with high enantio- and diastereoselectivity (Scheme 1-22a).[103] This protocol was used in the synthesis of marine natural products thiomarinol **1-79** and palmerolide A.[104-106] In addition, the same group reported a different hetero-Diels–Alder cycloaddition approach towards the synthesis of bicyclic piperidine derivatives **1-83** in high regio- and enantioselectivity (Scheme 1-22c).[107] This approached utilized an inexpensive Waldner's chiral dienophile **1-81** in the multicomponent reaction with borono-hydrazono-diene **1-80** and an aldehyde. In this reaction, the *endo*-adducts were exclusively formed away from the sulfoxide oxygen. This methodology was used in the total synthesis of (–)-methyl palustramate **1-84** and (–)-methyl dihydropalustramate **1-85**.[107,108]

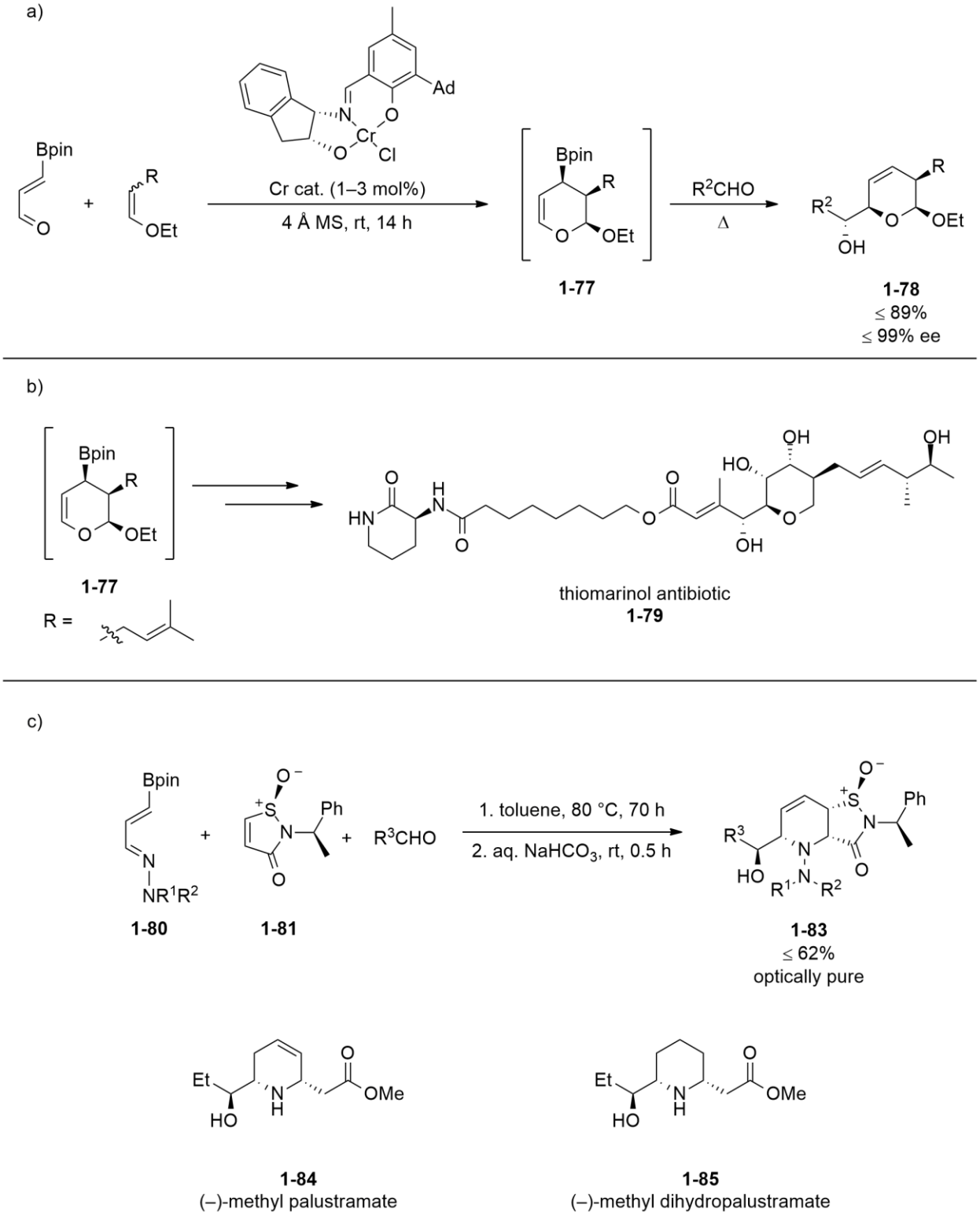

Scheme 1-22. a) Hall Group's enantioselective Cr-catalyzed hetero-Diels–Alder towards the synthesis of cyclic allylic boronic esters. b) Application of Hall Group's hetero-Diels–Alder in the synthesis of thiomarinol natural product. c) Enantioselective multicomponent reaction towards the synthesis of bicyclic piperidines by the Hall Group.

1.4.3 Borylative Migration

The palladium-catalyzed borylative migration reaction is a different approach towards the synthesis of chiral heterocyclic allylic boronic esters that was introduced by the Hall Group in 2009.[109] This method enables access to useful heterocyclic building blocks by desymmetrization of low-cost piperidones and tetrahydropyranones starting materials. The Hall Group was inspired by an observation from the work of Masuda and co-workers, where a heterocyclic allylic boronic ester was formed instead of the expected alkenyl derivative in their optimized borylation reaction for alkenyl triflate as substrates (Scheme 1-23a).[110] In this method, heterocyclic alkenyl triflates or nonaflates are subjected to a palladium-catalyzed transformation to afford the desired allylic boronic esters **1-87** in high enantioselectivity (Scheme 1-23b). The impact of this method was demonstrated by utilizing the allylic boronate products in subsequent stereoselective allylboration and ligand-controlled α- or γ-selective cross-coupling reactions.[111,112] In addition, the Hall Group was successful in using this method in several total and formal syntheses of pharmaceuticals and natural products such as mefloquine, anabasine and paroxetine (Scheme 1-23c). More details of the borylative migration reaction are presented in Chapters 2 and 3.

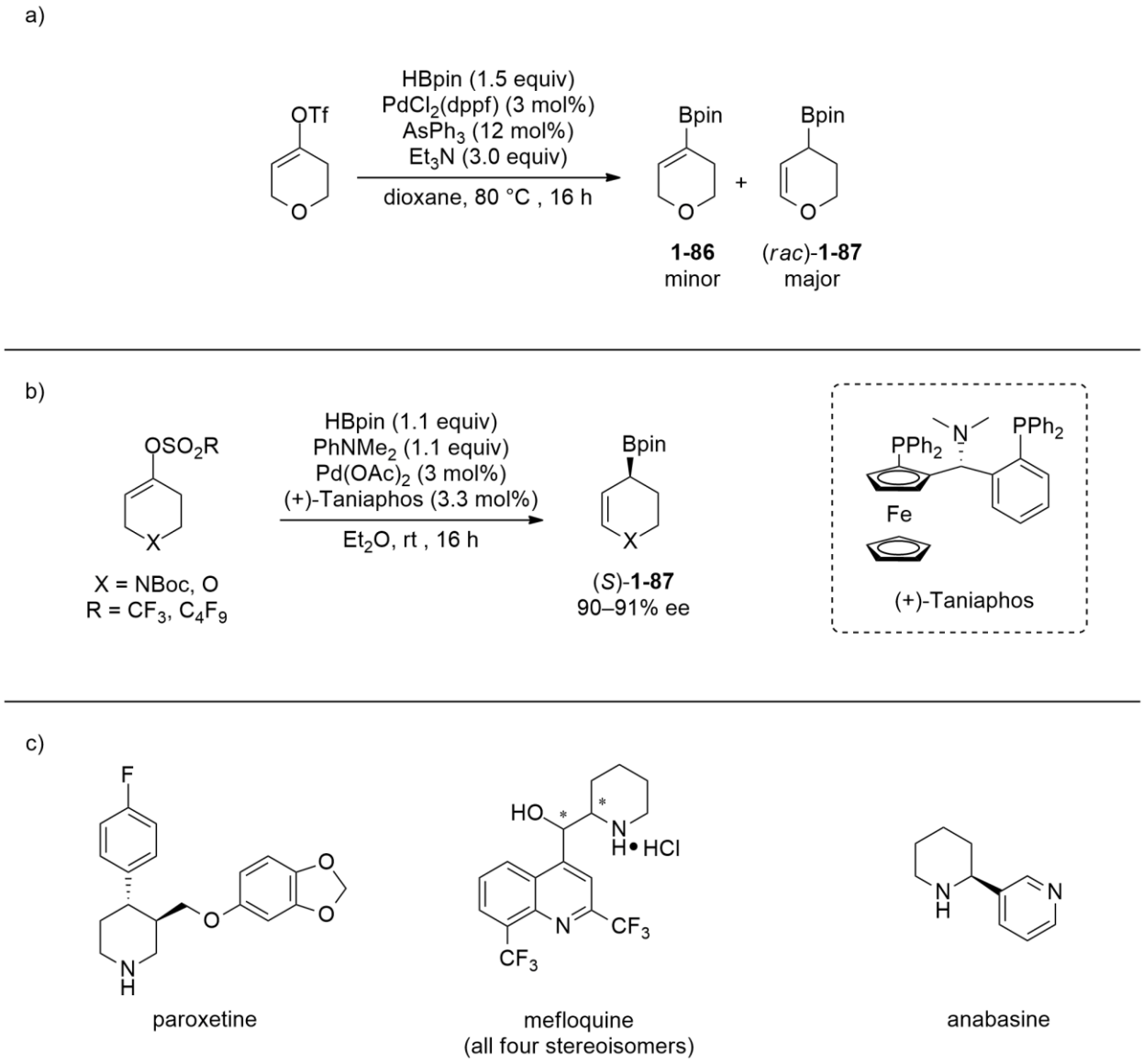

Scheme 1-23. a) Inspiration for the borylative migration method. b) Optimized conditions for the borylative migration. c) Application of borylative migration in the synthesis of pharmaceuticals and natural products.

1.5 Thesis Objective

Chiral allylic boronic esters are robust building blocks for various chemical transformations in organic chemistry. Hence, it is advantageous for organic chemists to have a satisfactory understanding of the current methods towards the synthesis of such building blocks and extend their utility in useful transformations. For this reason, the goal of the work discussed in this thesis is to gain more understanding of the borylative migration reaction and expand its utility in organic

synthesis and medicinal chemistry. The objectives of this thesis are summarized in the following list:

- Gaining definitive mechanistic insights of the borylative migration reaction.
- Expanding the utility of the borylative migration products in C_{sp}^3–C_{sp}^3 cross-coupling reaction enabling the synthesis of enantioenriched piperidines.
- Further applying the borylative migration methodology in medicinal chemistry by synthesizing piperidine derivatives for the treatment of glioblastoma multiforme.

Our laboratory showcased the impact of the borylative migration reaction in various transformations. However, it is crucial to have a clearer picture of the mechanistic pathways involved in this reaction to expand its application to different piperidine derivatives and heterocycles of different sizes. Chapter 2 of this thesis will discuss my recent collaborative efforts with Prof. Claude Legault towards the mechanistic investigation of this reaction. The investigation relies on both experimental and computational studies. The work accomplished in this chapter focuses on rationalizing the effect of a side product on the kinetics of the reaction.

In addition to the successful application of the borylative migration product in stereoselective allylboration and C_{sp}^3–C_{sp}^2 cross-coupling reactions, our group is also interested in expanding the application of this chemistry to other useful transformations. Thus, Chapter 3 describes the application of piperidinyl allylic boronic ester formed from the borylative migration reaction in an enantiospecific allyl-allyl C_{sp}^3–C_{sp}^3 palladium-catalyzed cross-coupling reaction. The described method allows access to enantioenriched piperidine derivatives bearing a cinnamyl motif at the 2-position.

In Chapter 4, my recent efforts in expanding the library of vacquinol-1 analogs towards the treatment of glioblastoma multiforme will be discussed. The analogs were accessible *via* the borylative migration reaction, which further highlights this method's effectiveness in the synthesis of pharmaceutically relevant enantioenriched piperidines.

1.6 References

[1] Gao, B.; Yang, B.; Feng, X.; Li, C. *Nat. Prod. Rep.* **2022**, *39*, 139.

[2] Parmar, V. S.; Jain, S. C.; Bisht, K. S.; Jain, R.; Taneja, P.; Jha, A.; Tyagi, O. D.; Prasad, A. K.; Wengel, J.; Olsen, C. E.; Boll, P. M. *Phytochemistry* **1997**, *46*, 597.

[3] Butler, M. S. *Nat. Prod. Rep.* **2008**, *25*, 475.

[4] Cordell, G. A.; Quinn-Beattie, M. L.; Farnsworth, N. R. *Phytother. Res.* **2001**, *15*, 183.

[5] Warnhoff, E. W. *Bull. Hist. Chem.* **1998**, *22*, 29.

[6] Shoba, G.; Joy, D.; Joseph, T.; Majeed, M.; Rajendran, R.; Srinivas, P. *Planta Med.* **1998**, *64*, 353.

[7] Bano, G.; Raina, R.; Zutshi, U.; Bedi, K.; Johri, R.; Sharma, S. *Eur. J. Clin. Pharmacol.* **1991**, *41*, 615.

[8] Atal, C.; Dubey, R. K.; Singh, J. *J. Pharmacol. Exp. Ther.* **1985**, *232*, 258.

[9] Platel, K.; Srinivasan, K. *Nahrung* **2000**, *44*, 42.

[10] Platel, K.; Srinivasan, K. *Int. J. Food Sci. Nutr.* **1996**, *47*, 55.

[11] Felpin, F. X.; Lebreton, J. *ChemInform* **2005**, *36*.

[12] Stansbury, J.; Saunders, P. R.; Zampieron, E. *J. Restor. Med.* **2013**, *2*, 94.

[13] Achan, J.; Talisuna, A. O.; Erhart, A.; Yeka, A.; Tibenderana, J. K.; Baliraine, F. N.; Rosenthal, P. J.; D'Alessandro, U. *Malar. J.* **2011**, *10*, 144.

[14] WHO: Guidelines for Malaria. 2022. https://app.magicapp.org/#/guideline/6236, accessed April 5th, 2022

[15] Baumann, M.; Baxendale, I. R. *Beilstein J. Org. Chem.* **2013**, *9*, 2265.

[16] Welsch, M. E.; Snyder, S. A.; Stockwell, B. R. *Curr. Opin. Chem. Biol.* **2010**, *14*, 347.

[17] Vitaku, E.; Smith, D. T.; Njardarson, J. T. *J. Med. Chem.* **2014**, *57*, 10257.

[18] WHO Model Lists of Essential Medicines. 2021.

https://apps.who.int/iris/rest/bitstreams/1374779/retrieve, accessed April 6th, 2022

[19] Gründer, G.; Hippius, H.; Carlsson, A. *Nat. Rev. Drug Discov.* **2009**, *8*, 197.

[20] Wagstaff, A. J.; Cheer, S. M.; Matheson, A. J.; Ormrod, D.; Goa, K. L. *Drugs* **2002**, *62*, 655.

[21] Wong, W.; Bai, X.-C.; Sleebs, B. E.; Triglia, T.; Brown, A.; Thompson, J. K.; Jackson, K. E.; Hanssen, E.; Marapana, D. S.; Fernandez, I. S.; Ralph, S. A.; Cowman, A. F.; Scheres, S. H. W.; Baum, J. *Nat. Microbiol.* **2017**, *2*, 17031.

[22] Peter, H.; Joris, D.; Nollaig, H.; Wafae, I.; Johan, A.; Mark, W. *Haematologica* **2018**, *103*, e204.

[23] Rueping, M.; Antonchick, A. P. *Angew. Chem. Int. Ed.* **2007**, *46*, 4562.

[24] Wang, S.-G.; You, S.-L. *Angew. Chem. Int. Ed.* **2014**, *53*, 2194.

[25] Studer, M.; Wedemeyer-Exl, C.; Spindler, F.; Blaser, H.-U. *Monatsh. Chem.* **2000**, *131*, 1335.

[26] Legault, C. Y.; Charette, A. B. *J. Am. Chem. Soc.* **2005**, *127*, 8966.

[27] Ye, Z.-S.; Chen, M.-W.; Chen, Q.-A.; Shi, L.; Duan, Y.; Zhou, Y.-G. *Angew. Chem. Int. Ed.* **2012**, *51*, 10181.

[28] Renom-Carrasco, M.; Gajewski, P.; Pignataro, L.; de Vries, J. G.; Piarulli, U.; Gennari, C.; Lefort, L. *Chem. Eur. J.* **2016**, *22*, 9528.

[29] Huang, W.-X.; Yu, C.-B.; Ji, Y.; Liu, L.-J.; Zhou, Y.-G. *ACS Catal.* **2016**, *6*, 2368.

[30] Kita, Y.; Iimuro, A.; Hida, S.; Mashima, K. *Chem. Lett.* **2014**, *43*, 284.

[31] Chen, M.-W.; Ye, Z.-S.; Chen, Z.-P.; Wu, B.; Zhou, Y.-G. *Org. Chem. Front.* **2015**, *2*, 586.

[32] Li, W.; Zhang, S.; Yu, X.; Feng, X.; Yamamoto, Y.; Bao, M. *J. Org. Chem.* **2021**, *86*, 10773.

[33] Chen, M.-W.; Ji, Y.; Wang, J.; Chen, Q.-A.; Shi, L.; Zhou, Y.-G. *Org. Lett.* **2017**, *19*, 4988.

[34] Vinogradov, M. G.; Turova, O. V.; Zlotin, S. G. *Adv. Synth. Catal.* **2021**, *363*, 1466.

[35] Moyano, A.; Rios, R. *Chem. Rev.* **2011**, *111*, 4703.

[36] Cao, M.-H.; Green, N. J.; Xu, S.-Z. *Org. Biomol. Chem.* **2017**, *15*, 3105.

[37] Rowland, B. G.; Rowland, B. E.; Zhang, Q.; Antilla, C. J. *Curr. Org. Chem.* **2006**, *10*, 981.

[38] Fochi, M.; Caruana, L.; Bernardi, L. *Synthesis* **2014**, *46*, 135.

[39] Xie, M.; Lin, L.; Feng, X. *Chem. Rec.* **2017**, *17*, 1184.

[40] Liu, X.; Zheng, H.; Xia, Y.; Lin, L.; Feng, X. *Acc. Chem. Res.* **2017**, *50*, 2621.

[41] Rahman, A.; Lin, X. *Org. Biomol. Chem.* **2018**, *16*, 4753.

[42] Klier, L.; Tur, F.; Poulsen, P. H.; Jørgensen, K. A. *Chem. Soc. Rev.* **2017**, *46*, 1080.

[43] Kobayashi, S.; Komiyama, S.; Ishitani, H. *Angew. Chem. Int. Ed.* **1998**, *37*, 979.

[44] Yao, S.; Saaby, S.; Hazell, R. G.; Jørgensen, K. A. *Chem. Eur. J.* **2000**, *6*, 2435.

[45] Mancheño, O. G.; Gómez Arrayás, R.; Adrio, J.; Carretero, J. C. *J. Org. Chem.* **2007**, *72*, 10294.

[46] Mandai, H.; Mandai, K.; Snapper, M. L.; Hoveyda, A. H. *J. Am. Chem. Soc.* **2008**, *130*, 17961.

[47] Chu, J. C. K.; Dalton, D. M.; Rovis, T. *J. Am. Chem. Soc.* **2015**, *137*, 4445.

[48] Han, B.; Li, J.-L.; Ma, C.; Zhang, S.-J.; Chen, Y.-C. *Angew. Chem. Int. Ed.* **2008**, *47*, 9971.

[49] Li, Q.-Z.; Ma, L.; Dong, L.; Chen, Y.-C. *ChemCatChem* **2012**, *4*, 1139.

[50] Jian, T.-Y.; Sun, L.-H.; Ye, S. *Chem. Commun.* **2012**, *48*, 10907.

[51] Rong, Z.-Q.; Wang, M.; Chow, C. H. E.; Zhao, Y. *Chem. Eur. J.* **2016**, *22*, 9483.

[52] Felpin, F.-X.; Lebreton, J. *Eur. J. Org. Chem.* **2003**, 3693.

[53] Fu, G. C.; Grubbs, R. H. *J. Am. Chem. Soc.* **1992**, *114*, 7324.

[54] Pachamuthu, K.; Vankar, Y. D. *J. Organomet. Chem.* **2001**, *624*, 359.

[55] Cossy, J.; Willis, C.; Bellosta, V.; Bouzbouz, S. *Synlett* **2000**, *2000*, 1461.

[56] Alexander, J. B.; La, D. S.; Cefalo, D. R.; Hoveyda, A. H.; Schrock, R. R. *J. Am. Chem. Soc.* **1998**, *120*, 4041.

[57] La, D. S.; Alexander, J. B.; Cefalo, D. R.; Graf, D. D.; Hoveyda, A. H.; Schrock, R. R. *J. Am. Chem. Soc.* **1998**, *120*, 9720.

[58] Cefalo, D. R.; Kiely, A. F.; Wuchrer, M.; Jamieson, J. Y.; Schrock, R. R.; Hoveyda, A. H. *J. Am. Chem. Soc.* **2001**, *123*, 3139.

[59] Sattely, E. S.; Cortez, G. A.; Moebius, D. C.; Schrock, R. R.; Hoveyda, A. H. *J. Am. Chem. Soc.* **2005**, *127*, 8526.

[60] Dolman, S. J.; Sattely, E. S.; Hoveyda, A. H.; Schrock, R. R. *J. Am. Chem. Soc.* **2002**, *124*, 6991.

[61] Cossy, J.; Dumas, C.; Pardo, D. G. *Eur. J. Org. Chem.* **1999**, 1693.

[62] Cossy, J.; Mirguet, O.; Pardo, D. G. *Synlett* **2001**, *2001*, 1575.

[63] Jarvis, S. B. D.; Charette, A. B. *Org. Lett.* **2011**, *13*, 3830.

[64] Van Brabandt, W.; Van Landeghem, R.; De Kimpe, N. *Org. Lett.* **2006**, *8*, 1105.

[65] Mollet, K.; Catak, S.; Waroquier, M.; Van Speybroeck, V.; D'hooghe, M.; De Kimpe, N. *J. Org. Chem.* **2011**, *76*, 8364.

[66] Roughley, S. D.; Jordan, A. M. *J. Med. Chem.* **2011**, *54*, 3451.

[67] Davis, F. A.; Reddy, R. E.; Szewczyk, J. M.; Reddy, G. V.; Portonovo, P. S.; Zhang, H.; Fanelli, D.; Zhou, P.; Carroll, P. J. *J. Org. Chem.* **1997**, *62*, 2555.

[68] Liu, G.; Cogan, D. A.; Ellman, J. A. *J. Am. Chem. Soc.* **1997**, *119*, 9913.

[69] Semina, E.; Colpaert, F.; Van Hecke, K.; De Kimpe, N.; Mangelinckx, S. *Eur. J. Org. Chem.* **2015**, 4847.

[70] Kavala, M.; Mathia, F.; Kožíšek, J.; Szolcsányi, P. *J. Nat. Prod.* **2011**, *74*, 803.

[71] Fustero, S.; Jiménez, D.; Moscardó, J.; Catalán, S.; del Pozo, C. *Org. Lett.* **2007**, *9*, 5283.

[72] Liu, J.-D.; Chen, Y.-C.; Zhang, G.-B.; Li, Z.-Q.; Chen, P.; Du, J.-Y.; Tu, Y.-Q.; Fan, C.-A. *Adv. Synth. Catal.* **2011**, *353*, 2721.

[73] Sun, Z.; Winschel, G. A.; Zimmerman, P. M.; Nagorny, P. *Angew. Chem. Int. Ed.* **2014**, *53*, 11194.

[74] Mulet, C.; Escolano, M.; Llopis, S.; Sanz, S.; Ramírez de Arellano, C.; Sánchez-Roselló, M.; Fustero, S.; del Pozo, C. *Adv. Synth. Catal.* **2018**, *360*, 2885.

[75] Fustero , S.; del Pozo, C.; Mulet, C.; Lazaro, R.; Sánchez-Roselló, M. *Chem. Eur. J.* **2011**, *17*, 14267.

[76] Hall, D. G. *Boronic Acids*; 2nd Edition, Wiley: Weinheim, 2011.

[77] Sandford, C.; Aggarwal, V. K. *Chem. Commun.* **2017**, *53*, 5481.

[78] McKillop, A.; Sanderson, W. R. *Tetrahedron* **1995**, *51*, 6145.

[79] Mlynarski, S. N.; Karns, A. S.; Morken, J. P. *J. Am. Chem. Soc.* **2012**, *134*, 16449.

[80] Edelstein, E. K.; Grote, A. C.; Palkowitz, M. D.; Morken, J. P. *Synlett* **2018**, *29*, 1749.

[81] Nave, S.; Sonawane, R. P.; Elford, T. G.; Aggarwal, V. K. *J. Am. Chem. Soc.* **2010**, *132*, 17096.

[82] Kennedy, J. W. J.; Hall, D. G. *J. Am. Chem. Soc.* **2002**, *124*, 11586.

[83] Rauniyar, V.; Zhai, H.; Hall, D. G. *J. Am. Chem. Soc.* **2008**, *130*, 8481.

[84] Lou, S.; Moquist, P. N.; Schaus, S. E. *J. Am. Chem. Soc.* **2006**, *128*, 12660.

[85] Chen, J. L.-Y.; Aggarwal, V. K. *Angew. Chem. Int. Ed.* **2014**, *53*, 10992.

[86] Lachance, H.; Hall, D. G. *Allylboration of Carbonyl Compounds*. In *Organic Reactions*; Denmark, S. E., Ed. 2009, p 1–574.

[87] Clement, H. A.; Hall, D. G. *Recent Advances in the Stereoselective Additions of Allylic Boronates to Carbonyl Compounds*. In *PATAI'S Chemistry of Functional Groups*; Rappoport, Z., Ed. 2020, p 1–86.

[88] Buskes, M. J.; Blanco, M.-J. *Molecules* **2020**, *25*, 3493.

[89] Zhao, S.; Gensch, T.; Murray, B.; Niemeyer, Z. L.; Sigman, M. S.; Biscoe, M. R. *Science* **2018**, *362*, 670.

[90] Lehmann, J. W.; Crouch, I. T.; Blair, D. J.; Trobe, M.; Wang, P.; Li, J.; Burke, M. D. *Nat. Commun.* **2019**, *10*, 1263.

[91] Luo, Y.; Wales, S. M.; Korkis, S. E.; Roy, I. D.; Lewis, W.; Lam, H. W. *Chem. Eur. J.* **2018**, *24*, 8315.

[92] Lee, H.; Yun, J. *Org. Lett.* **2018**, *20*, 7961.

[93] Hu, J.; Ferger, M.; Shi, Z.; Marder, T. B. *Chem. Soc. Rev.* **2021**, *50*, 13129.

[94] Ito, H.; Ito, S.; Sasaki, Y.; Matsuura, K.; Sawamura, M. *J. Am. Chem. Soc.* **2007**, *129*, 14856.

[95] Guzman-Martinez, A.; Hoveyda, A. H. *J. Am. Chem. Soc.* **2010**, *132*, 10634.

[96] Park, J. K.; Lackey, H. H.; Ondrusek, B. A.; McQuade, D. T. *J. Am. Chem. Soc.* **2011**, *133*, 2410.

[97] Rivera-Chao, E.; Mitxelena, M.; Varela, J. A.; Fañanás-Mastral, M. *Angew. Chem. Int. Ed.* **2019**, *58*, 18230.

[98] Kojima, R.; Akiyama, S.; Ito, H. *Angew. Chem. Int. Ed.* **2018**, *57*, 7196.

[99] Chen, C.; Shen, X.; Chen, J.; Hong, X.; Lu, Z. *Org. Lett.* **2017**, *19*, 5422.

[100] Lee, H.; Han, J. T.; Yun, J. *ACS Catal.* **2016**, *6*, 6487.

[101] Ito, H.; Kunii, S.; Sawamura, M. *Nat. Chem.* **2010**, *2*, 972.

[102] Ge, Y.; Cui, X.-Y.; Tan, S. M.; Jiang, H.; Ren, J.; Lee, N.; Lee, R.; Tan, C.-H. *Angew. Chem. Int. Ed.* **2019**, *58*, 2382.

[103] Gao, X.; Hall, D. G. *J. Am. Chem. Soc.* **2003**, *125*, 9308.

[104] Hall, D. G.; Rybak, T.; Verdelet, T. *Acc. Chem. Res.* **2016**, *49*, 2489.

[105] Gao, X.; Hall, D. G. *J. Am. Chem. Soc.* **2005**, *127*, 1628.

[106] Penner, M.; Rauniyar, V.; Kaspar, L. T.; Hall, D. G. *J. Am. Chem. Soc.* **2009**, *131*, 14216.

[107] Touré, B. B.; Hall, D. G. *J. Org. Chem.* **2004**, *69*, 8429.

[108] Touré, B. B.; Hall, D. G. *Angew. Chem. Int. Ed.* **2004**, *43*, 2001.

[109] Lessard, S.; Peng, F.; Hall, D. G. *J. Am. Chem. Soc.* **2009**, *131*, 9612.

[110] Murata, M.; Oyama, T.; Watanabe, S.; Masuda, Y. *Synthesis* **2000**, *2000*, 778.

[111] Kim, Y.-R.; Hall, D. G. *Org. Biomol. Chem.* **2016**, *14*, 4739.

[112] Ding, J.; Rybak, T.; Hall, D. G. *Nat. Commun.* **2014**, *5*, 5474.

Chapter 2: Mechanistic Analysis of a Palladium-Catalyzed Borylative Migration

2.1 Introduction

As described in Chapter 1, desymmetrization of prochiral piperidine derivatives is an attractive approach to access enantioenriched heterocycles. With this objective in sight, the Hall Group developed a borylative migration protocol to obtain enantioenriched allylic boronate heterocycles (Scheme 2.1a).[1,2] This methodology has provided a pathway towards the enantioselective synthesis of a plethora of pharmaceutically relevant molecules, which will be discussed in detail in Chapter 3.[1,2] However, expanding the borylative migration reaction to different ring sizes has proven difficult.[3] Therefore, it was deemed a priority to gain a proper understanding of the reaction mechanism. Although a mechanistic proposal was elaborated in the original report of this chemistry in 2009,[4] there was little experimental evidence to support this hypothesis.

The borylative migration reaction equation is shown in Scheme 2-1a,[5] and the hypothesized mechanism in the initial report is shown in Scheme 2-1b.[4] The proposed catalytic cycle revolves around the allylic borylation of an allyl triflate intermediate that was delivered by the hydropalladation of enol triflate **3-1**. Theoretically, oxidative addition of pinacolborane could generate the catalytic palladium hydride complex **Int-2-1** *in situ*. The formed electron-poor palladium(II) intermediate **Int-2-1** would be prone to alkene coordination with alkenyl triflate **3-1** to deliver the π-complex **Int-2-2** followed by an alkene insertion to furnish the hydropalladation complex **Int-2-3**. β-Hydride elimination of **Int-2-3** yields the palladium-coordinated allylic triflate species **Int-2-4,** which undergoes ligand dissociation to deliver the free allylic triflate intermediate **2-1′**. The allylic triflate intermediate could then undergo an oxidative addition to another equivalent of the palladium(0) catalyst to form allylpalladium(II) intermediate **Int-2-5**. Transmetalation between intermediate **Int-2-5** and pinacolborane delivers the borylated palladium(II) species **Int-2-6**; where the desired product **2-5** could be generated by a regioselective reductive elimination step. Furthermore, it was proposed that the alkenyl boronate side product **2-**

7 was obtained through a chain-walking mechanism from allyl to alkenyl boronate from product **2-5** and palladium hydride complex **Int-2-1**. This proposed mechanism was based on an experiment with DBpin, in which 85% D-incorporation was observed at the allylic position of the product **2-5** (Scheme, 2-1c). However, little precedence could be found in the literature supporting the initial oxidative addition step of palladium(0) with pinacolborane as shown in Scheme 2-1b.

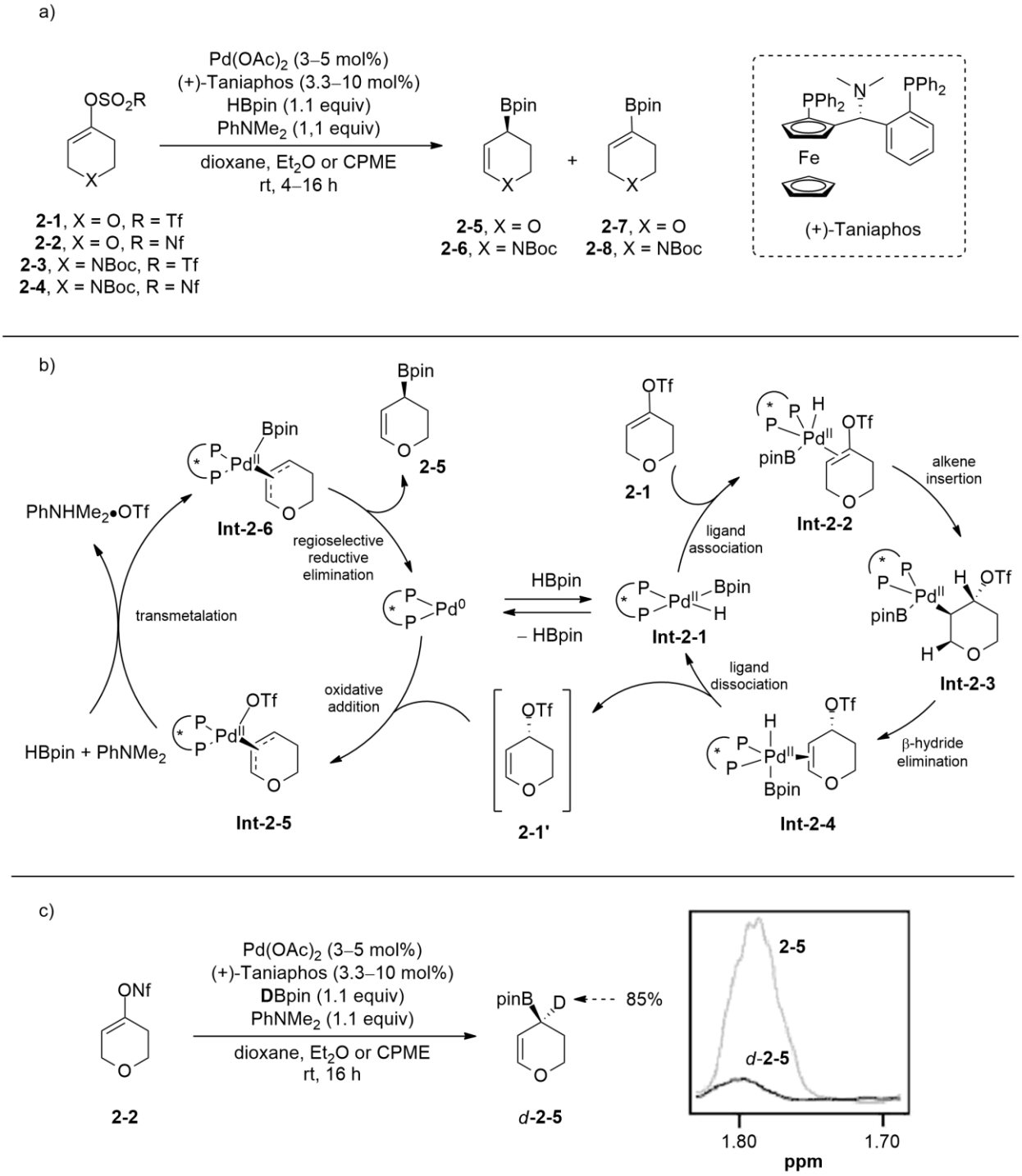

Scheme 2-1. a) Summary of the borylative migration reaction. b) Mechanistic proposal from the initial report. c) Results of the D-labelling experiments with DBpin analyzed by ^{1}H NMR spectroscopy.

To acquire a deeper understanding of the plausible mechanistic pathways, a summary of the relevant literature of the borylative migration is necessary. The borylative migration methodology was developed in 2009 by the Hall Group after they were inspired by an undesired side product observed by Masuda and co-workers.[6] In contrast to the traditional Miyaura borylation conditions that use bis(pinacolato)diboron and potassium acetate, the Masuda Group developed a borylation protocol for aryl and alkenyl electrophiles using pinacolborane and an amine base.[7,8] In their report, it was found that when using alkenyl triflate **2-1** as an electrophile, their borylation procedure affords the racemic allylic boronate **2-5** instead of the desired alkenyl boronate **2-7** (Scheme 2-2a). It was proposed the undesired allylic boronate **2-5** forms through an alkene isomerization. In addition, the Masuda Group proposed a mechanistic cycle for their developed borylation (Scheme 2-2b).[9,10] The authors rationalized the reaction would proceed through an oxidative addition of the aryl electrophile with palladium, followed by a transmetalation step involving ligand exchange with a boryl anion formed from an interaction between triethylamine and pinacolborane. Reductive elimination of the boron-aryl palladium(II) complex would furnish the borylation product and regenerate the active palladium(0) catalyst.

The proposed mechanistic cycle shown in Scheme 2-2b by Masuda and co-workers involves the generation of a boryl anion from an acid-base reaction prior to the transmetalation step.[11] The pinacolborane deprotonation step by an amine is questionable since it has little precedence in the literature.[12] This step is considered to be implausible and counter-intuitive due to the hydridic nature of the hydrogen of pinacolborane. For this reason, this type of transmetalation will not be considered for the mechanistic investigation of the borylative migration reaction.

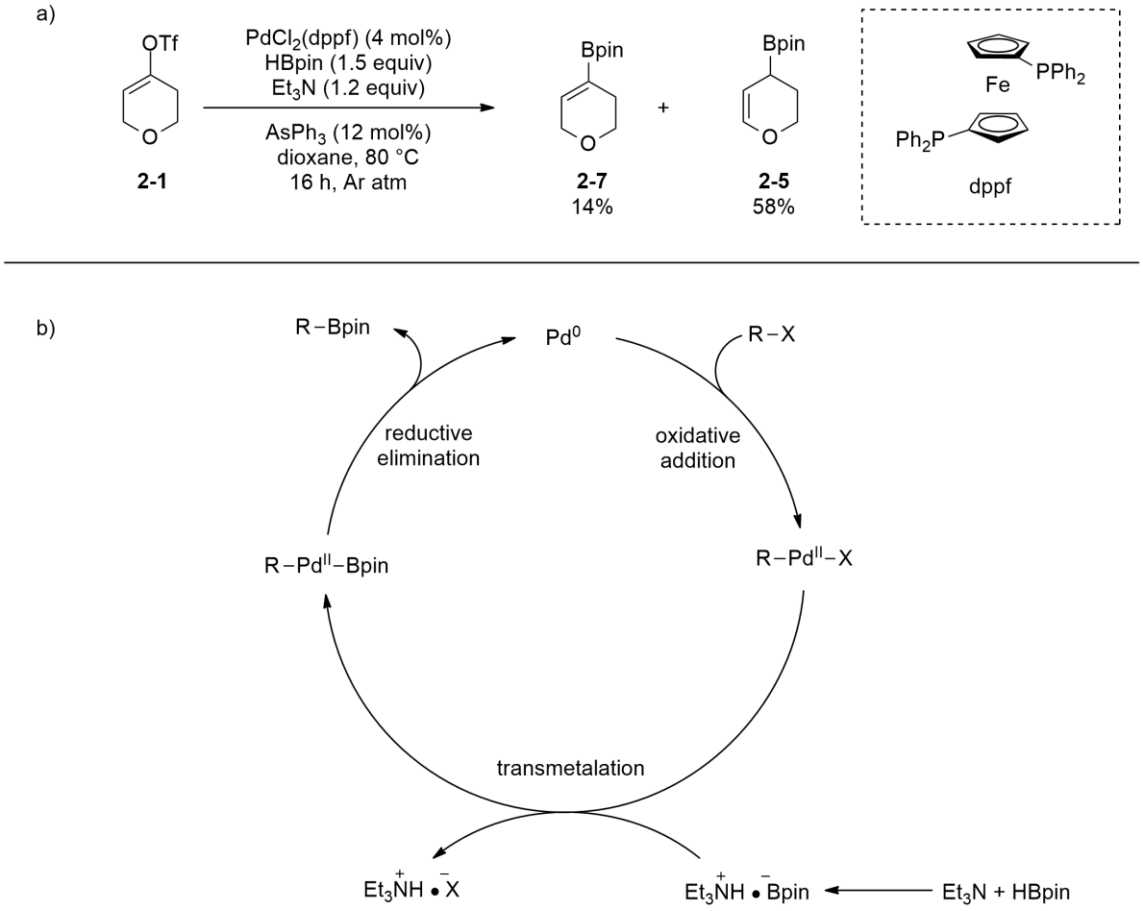

Scheme 2-2. a) Anomalous Miyaura borylation of **2-1** with pinacolborane reported by Masuda and co-workers. b) Proposed mechanistic cycle by Masuda and co-workers.

With respect to the aforementioned concerns regarding Masuda's mechanistic proposal, Lin and co-workers reported a computational mechanistic investigation of the Miyaura borylation with pinacolborane using a simplified model reaction (Scheme 2-3).[11] The authors argued that the most preferable pathway involves an essential σ-bond metathesis step between a cationic aryl palladium(II) intermediate and pinacolborane. The proposed catalytic cycle starts by an oxidative addition of aryl iodide to form an aryl palladium(II) complex. Next, an amine assisted ionization occurs to deliver a cationic palladium complex, which can undergo a σ-bond metathesis with pinacolborane to obtain the Miyaura borylation product and a cationic palladium hydride complex. An amine induced reduction of the palladium hydride complex occurs to regenerate the catalyst. These mechanistic findings could be relevant in the borylative migration mechanism. However, in

the preliminary report by the Hall Group,[4] it was found that the undesired side product alkenyl boronate **2-7** is not an intermediate in the reaction and instead may be formed *via* an off-cycle side reaction. This finding contradicts the expectation for a borylative migration reaction mechanism similar to Lin's mechanistic proposal.

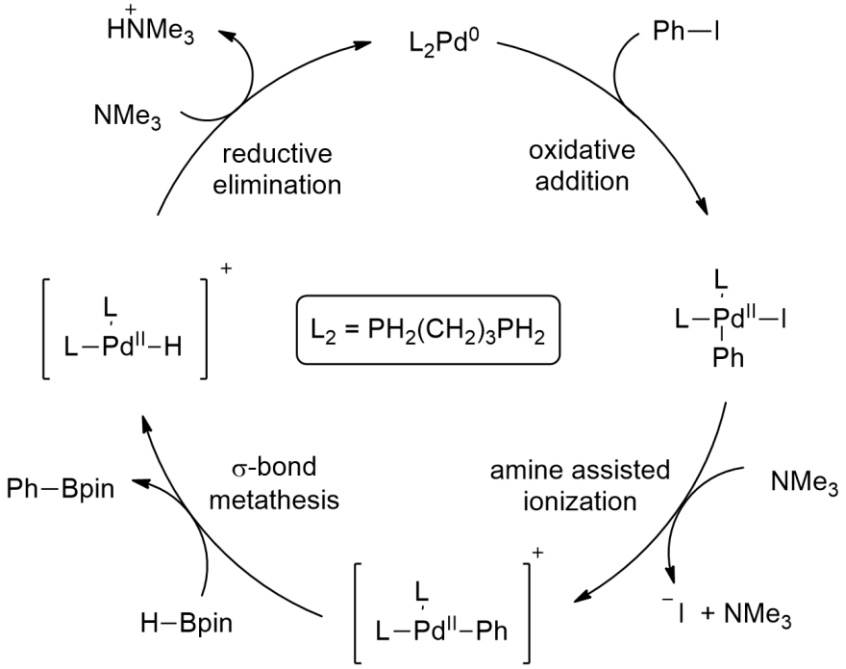

Scheme 2-3. Lin's and co-workers' mechanistic proposal of the Miyaura borylation reaction.

A mechanistic investigation is essential to facilitate the use of this chemistry to a broader variety of substrates. Until recently, many aspects concerning the mechanism of the borylative migration reaction remained unresolved, such as the nature of the rate-determining step, the factors that control the alkene isomerization step, and the origin of the enantiomeric induction. Described below are the Hall Group's recent investigative efforts on the mechanism of the borylative migration reaction to address the aforementioned aspects by combining experimental investigation guided by density functional theory (DFT) computational calculations.[13,14]

2.2 Recent Mechanistic Investigations of the Borylative Migration Reaction

This project was initiated as a collaboration between Dr. Helen Clement from the Hall Group and Dr. Claude Legault (University of Sherbrooke). DFT calculations were completed by Dr. Legault

using the pyranyl alkenyl triflate substrate **2-1**. Values of free energies were reported in kcal/mol relative to the dissociated alkenyl triflate **2-1** and palladium ligand-bound catalyst, arbitrarily set to 0 kcal/mol, using a M06-D3/6-31+G(d,p)/SDD(Pd)(SMD, Dioxane)//M06-D3/6-31G(d)/LANL2DZ(Pd) basis set. The following subsections summarize Dr. Clement and Dr. Legault's recent experimental and computational studies towards the mechanistic investigation of the borylation migration.

2.2.1 Feasibility of the Miyaura borylation pathway

In comparison to the reaction pathway described in the original report,[4] the oxidative addition of nonaflates and triflates with a palladium(0) catalyst is a well-established process in transition metal catalyzed cross-coupling reactions.[15] In fact, the calculations showed that the oxidative addition is initiated by an energetically preferred coordination of **2-1** to form complex **Int-2-7** (Scheme 2-4). A direct oxidative addition of **Int-2-7** through transition state **TS-2-1** leads to a square-planar palladium complex **Int-2-8**, with an overall energetic barrier of 12.5 kcal/mol.

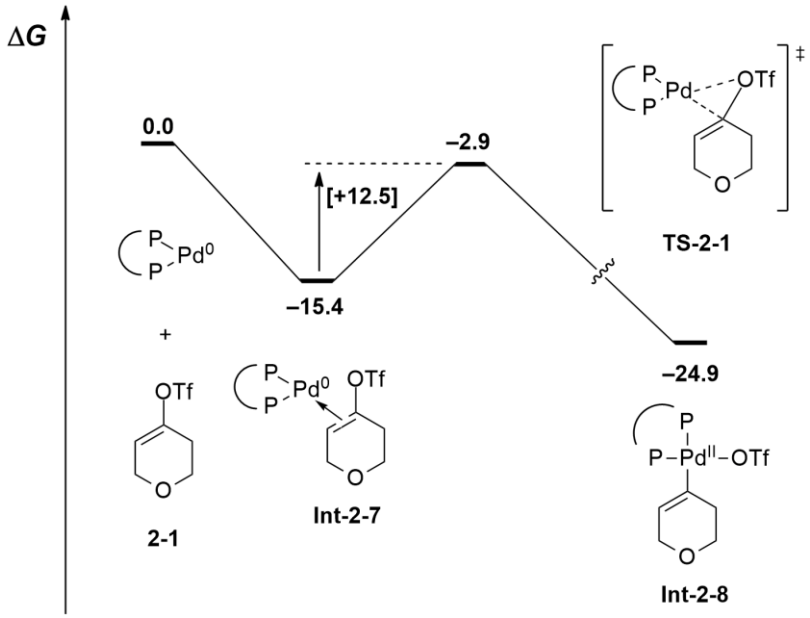

Scheme 2-4. Energy diagram (in kcal/mol) of the oxidative addition process.

2.2.2 Borylation of the alkenyl triflate and nonaflate

At this stage of the reaction, the borylation step was suspected to occur with a highly electrophilic cationic palladium complex similar to that proposed by Lin and co-workers.[11] To confirm this hypothesis, an experimental investigation was performed by Dr. Clement running the borylative migration reaction in the presence of a nucleophilic iodide source. It was observed that the addition of only 6 mol% tetrabutylammonium iodide suppressed product formation (Table 2-1, entries 1–2), whereas a stoichiometric amount delivered alkenyl iodide **2-9** (Table 2-1, entry 3). Based on these results, it was suggested that perfluorosulfonates act as weakly nucleophilic anions to allow the reaction to proceed beyond the oxidative addition step. Moreover, these observations support the presence of a cationic palladium species in the borylation step.

Table 2-1. Effect of n-Bu_4NI additive in the reaction.

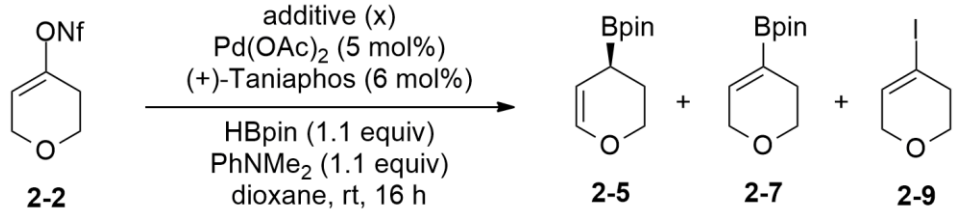

entry	additive	x	yield of 2-5[a]	yield of 2-7[a]	yield of 2-9[a]
1	*n*-Bu_4NOTF	1 equiv	70%	10%	—
2	*n*-Bu_4NI	6 mol%	3%	5%	—
3	*n*-Bu_4NI	1 equiv	4%	2%	15%

[a] Determined by crude ^1H NMR. "—" indicates not observed.

The experimental confirmation of the cationic palladium pathway was accompanied by a DFT calculation study on the borylation step. The energy diagram for the palladium ionization and transmetalation is shown in Scheme 2-5. The amine assisted ionization of the Pd(II)-OTf complex was simplified by considering **Int-2-8** and **Int-2-8**$^+$ to be equienergetic as these processes tend to be difficult to model accurately. Next, the introduction of the boryl unit was examined. For the complexation of pinacolborane to palladium(II) species to occur, a ligand exchange between dimethylaniline and pinacolborane is required. Dissociation of the aniline was proposed to occur

due to the steric hindrance around the palladium center. It was found that the dissociation step has an energy barrier of 5.2 kcal/mol leading to the cationic intermediate **Int-2-9**. Complexation of pinacolborane to **Int-2-9** to form **Int-2-10** is exergonic by 3.0 kcal/mol. Finally, a regioselective σ-bond metathesis furnishes the borylated product **Int-2-11**. This process occurs through a well-established spiro-like 4-membered transition state.[11]

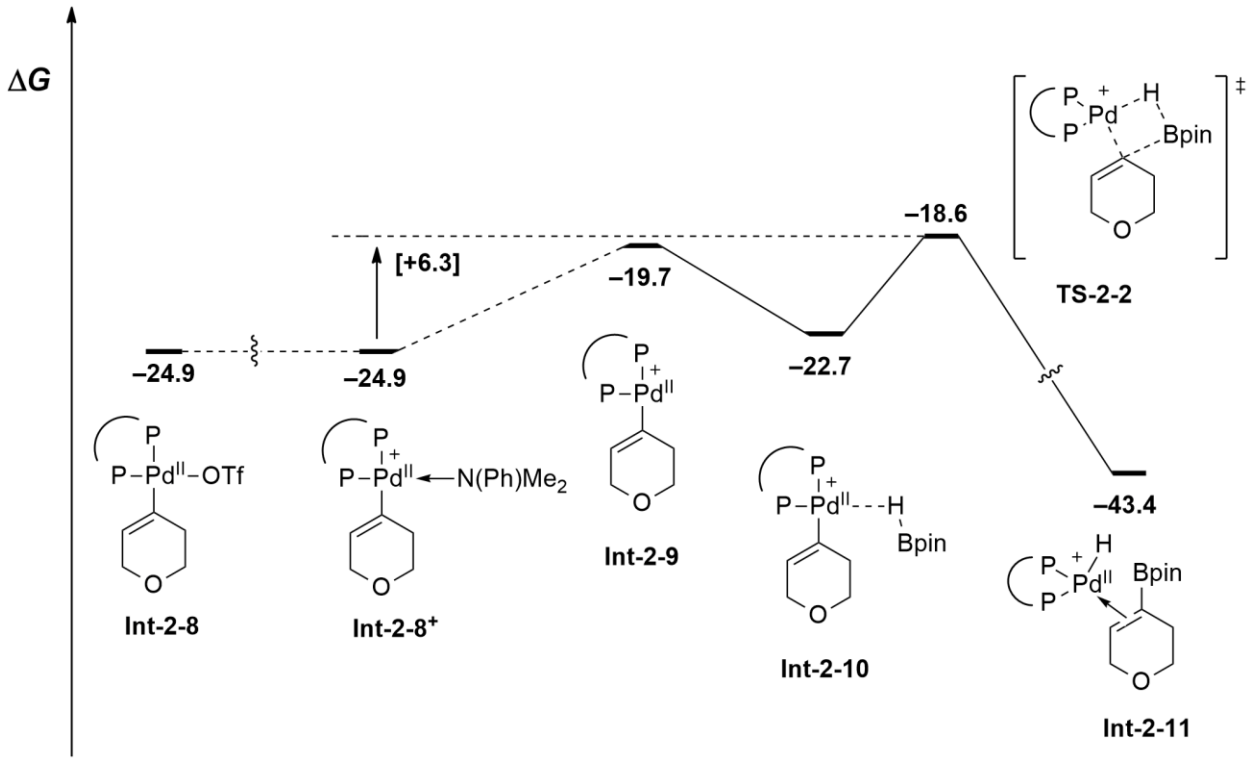

Scheme 2-5. Energy diagram (in kcal/mol) for the palladium ionization and transmetalation from **Int-2-8**.

2.2.3 Isomerization of the alkenyl boronate

After the borylation leading to **Int-2-11**, it was hypothesized that the alkene isomerization step could occur by either alkene insertion into the Pd-H bond followed by a *β*-hydride elimination, or a deprotonation pathway as illustrated in Scheme 2-6 (black and red pathways, respectively).[16] As the DFT calculations show, the energy barrier for the allylic deprotonation of **Int-2-11** via **TS-2-3** was found to be too high to be considered as a competing pathway in the isomerization step. In contrast, the regioselective hydropalladation was found to be fundamentally barrierless to furnish **Int-2-12** *via* **TS-2-5**, which is consistent with the results from the isotopic labelling experiments (Scheme 2-1c). **Int-2-13** is accessible through a subsequent *β*-hydride elimination, which leads to complex **Int-2-14** upon reductive deprotonation. Alternatively, the alkenyl side product **2-7** is obtained through the deprotonation of **Int-2-11** (Scheme 2-6, in blue). However, it was found that this route is more energetically demanding than the isomerization pathway.

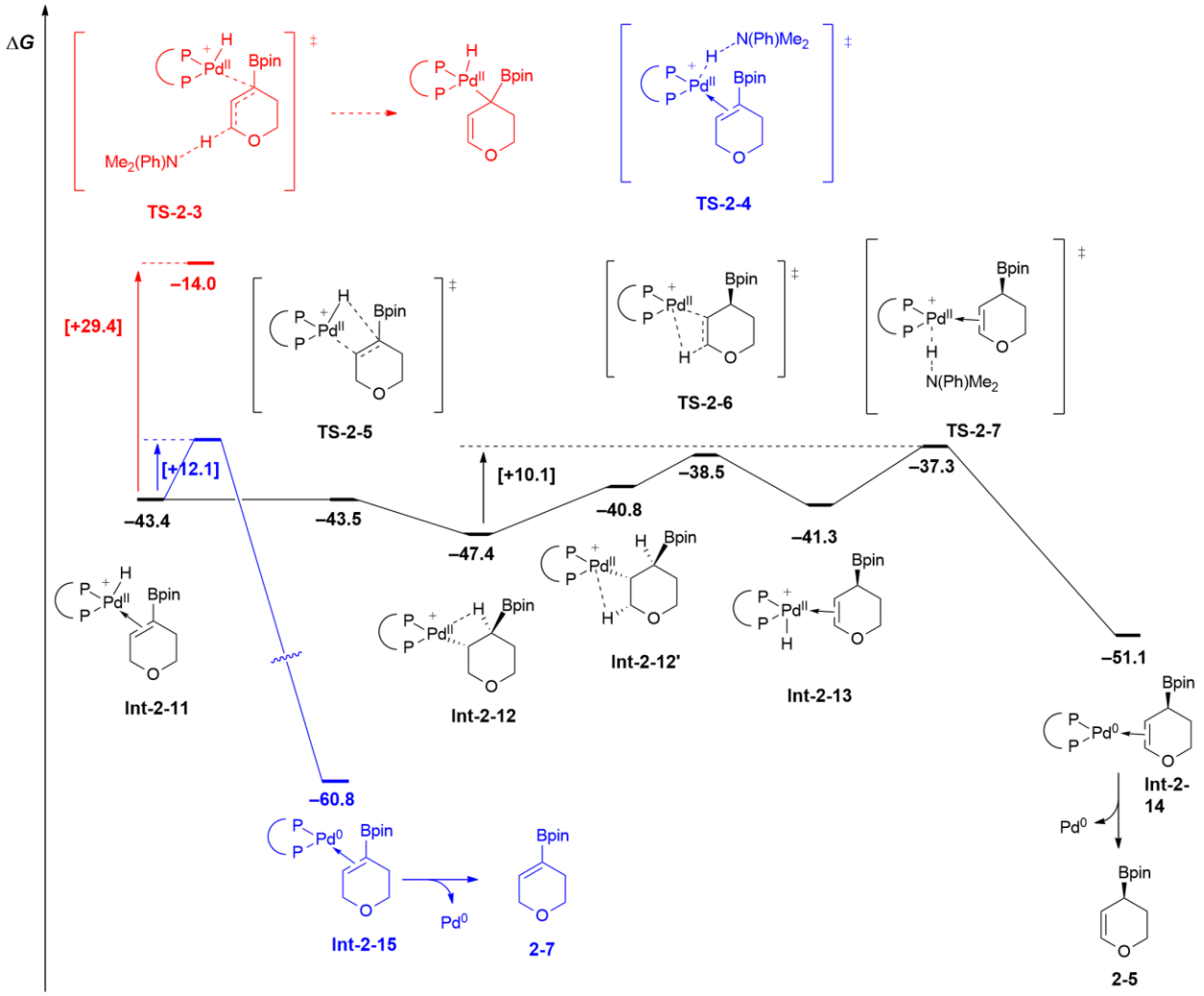

Scheme 2-6. Comparison of hydridic and protic alkene isomerization pathways from **Int-6** (free energies in kcal/mol)

2.2.4 Influence of the heteroatom on product formation and enantioselectivity

As shown above, the effectiveness of the borylative migration relies on the favorable alkene isomerization step to furnish allyl boronate **2-5** over the alternative reductive deprotonation of **Int-2-11**. Due to the conjugation involving the oxygen atom in **Int-2-13**, it was suggested that the nature of the heteroatom at the homoallylic position might influence the ratio of the allylic boronate to the alkenyl boronate produced in the reaction. Thus, a brief experimental study was conducted by Dr. Clement to compare four different alkenyl nonaflates in the borylative migration reaction. It was found that the ratio of allyl to alkenyl boronate products was dependent on the identity of

the heteroatom. As illustrated in Table 2-2, the allyl to alkenyl boronate ratio decreases from X = O > NBoc > $NC(O)CF_3$ > CH_2.

Table 2-2. Effect of the heteroatom on the product distribution

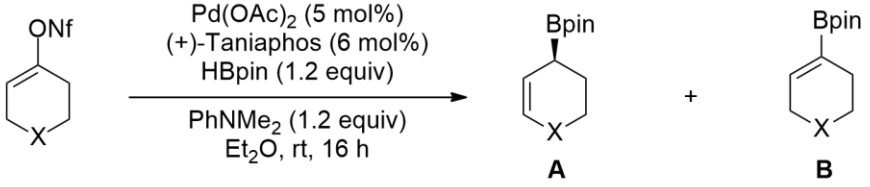

2-2, X = O
2-4, X = NBoc
2-10, X = $NCOCF_3$
2-13, X = CH_2

2-5, X = O
2-6, X = NBoc
2-11, X = $NCOCF_3$
2-14, X = CH_2

2-7, X = O
2-8, X = NBoc
2-12, X = $NCOCF_3$
2-15, X = CH_2

entry	substrate	yield of A[a]	ratio A/B[a]	ee
1	**2-2**	72%	8:1	90%
2	**2-4**	80%	4:1	89%
3	**2-10**	57%	2.5:1	89%
4	**2-13**	34%	1:2	<2%

[a] Yield and product ratios are estimated by crude ^{1}H NMR.

In addition to the outcome of the allyl to the alkenyl boronate ratio in the borylative migration reaction, the presence of a heteroatom also influences the enantioselectivity of the reaction. As shown in Table 2-2, the absence of a heteroatom at the homoallylic position results in the loss of enantioselectivity (Table 2-2, entry 4). From the collective experimental and computational results described above, it was suggested that transmetalation of **Int-2-10** leading to **Int-2-11** is an irreversible process and is the stereochemistry-determining step of the reaction. However, for this hypothesis to be valid, free Pd–H cannot be present in solution, which could be generated by the dissociation from complex **Int-2-4**. Consequently, an experimental investigation for the presence of free Pd–H in solution was undertaken by subjecting nonaflate **2-2** to the borylative migration reaction conditions in the presence of alkenyl boronate **2-7** (Table 2-3). It was observed that alkenyl boronate **2-7** did not participate in the reaction and it was mostly recovered (Table 2-3, entry 2). This observation suggests that alkenyl boronate **2-7** is not an intermediate in the reaction and that free Pd–H is not present in the solution.

Table 2-3. Probing for a dissociative alkene isomerization pathway.

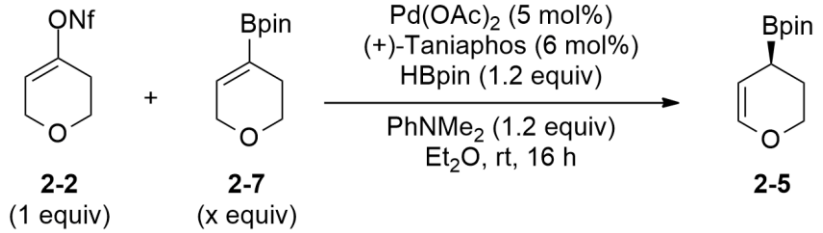

entry	x	yield of 2-5[a]	ee of 2-5	recovered 2-7
1	0	72%	90	9%
2	1.0	81%	90	92%

[a] Yield and product ratios are estimated by crude ^{1}H NMR.

2.2.5 Kinetic studies

The DFT calculations indicate that the rate-determining step of the reaction is the oxidative addition of the alkenyl nonaflates or triflates. However, it was thought that probing the rate-determining step experimentally through kinetic analysis would add value to the overall mechanistic study.[17,18] Owing to recent advances in visual kinetics analysis developed by Blackmond and Burés, and coworkers, general rate dependence information can be obtained in only a few experiments.[19-21] This approach allows access to information regarding rate-dependence from direct comparison of concentration against time data. Thus, experimental studies were performed to confirm the nature of oxidative addition being the rate-determining step. The rate-dependence of the dehydropiperidinyl nonaflate **2-4**, pinacolborane, $PhNMe_2$ and the catalyst on the reaction was investigated using slightly modified reaction conditions with *in situ* ^{1}H NMR monitoring. The results of the kinetic study suggest that the reaction is zero order in pinacolborane, $PhNMe_2$, and first order in catalyst respectively. Furthermore, it was observed that the reaction is 0.6 order in the nonaflate **2-4**. A partial first-order suggests that the alkenyl nonaflate **2-4** is involved in the reaction during the rate-determining step, however it may also indicate an inhibition effect from the product or side product of the reaction. Thus, a computational analysis studying the energetics of catalyst turnover and product release was conducted. It was observed that the release of the desired product **2-5** to form **Int-2-7** is favorable by 5.8 kcal/mol, whereas

the release of the side product **2-7** has an energy barrier of 3.3 kcal/mol (Scheme 2-7). The endergonic release of the side product lowers the effectiveness of the catalyst, which is in agreement to the observed partial first-order of the nonaflate starting material.

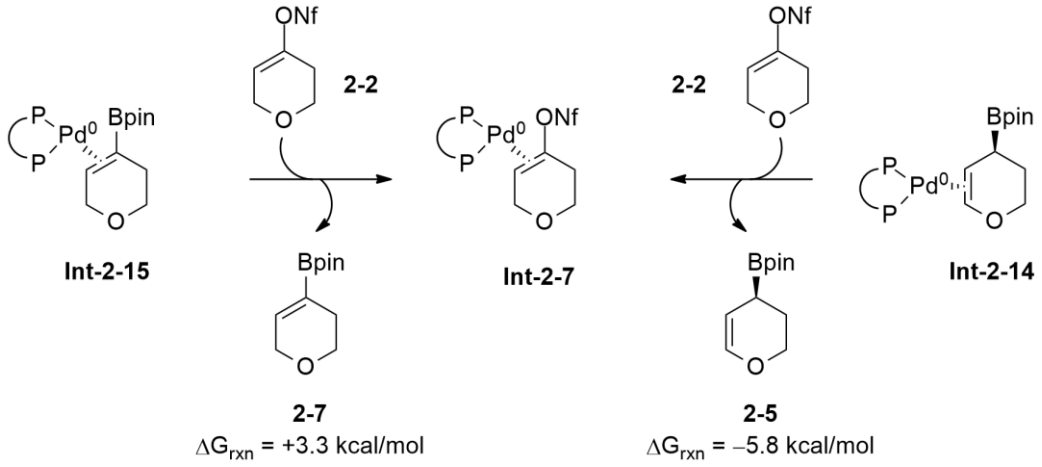

Scheme 2-7. Energetics for catalyst turnover comparing products/substrate exchange.

2.3 Objective

As shown above, the extensive mechanistic investigation by Dr. Helen Clement and Dr. Claude Legault on the borylative migration provided a significant understanding of the reaction mechanism. However, some aspects of the mechanism concerning the inhibitory effect of the alkenyl boronate side products were left under speculation. Thus, it is essential to experimentally investigate and confirm the inhibition effect of the alkenyl boronate **2-7** to gain further insight about the mechanism and complete the full picture of the mechanistic cycle. This section describes my contribution to address this gap.

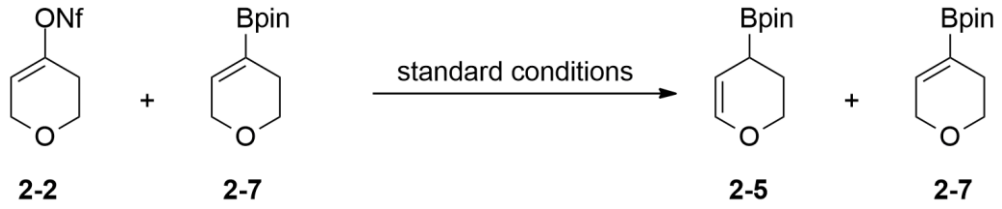

Scheme 2-8. Proposal for investigating the inhibition effect of alkenyl boronate **2-7**.

2.4 Inhibition Effect of Alkenyl Boronate Side Product

To study the effect of the alkenyl boronate on the borylative migration reaction, I performed a product inhibition study by adding different amounts of the alkenyl boronate side product **2-7** at the start of borylative migration reaction. The inhibition effect is then assessed by comparing the consumption of alkenyl nonaflate **2-2** from ^{1}H NMR spectra of the crude mixture.[5] The alkenyl boronate **2-7** can be synthesized using the standard Miyaura borylation conditions from alkenyl nonflate **2-2** (Scheme 2-9).[8] The results of the inhibition studies are summarized in Table 2-4. As shown below, when the alkenyl boronate **2-7** is not present in solution at the beginning of the reaction, the starting material nonaflate **2-2** is mostly consumed within 1 h (Table 2-4, entry 1). However, it was observed that the consumption of **2-2** decreases as the initial concentration of the alkenyl boronate **2-7** increases (Table 2-4, entries 2–4). These observed results could be attributed to the strong binding affinity of alkenyl boronate **2-7** to the palladium catalyst.

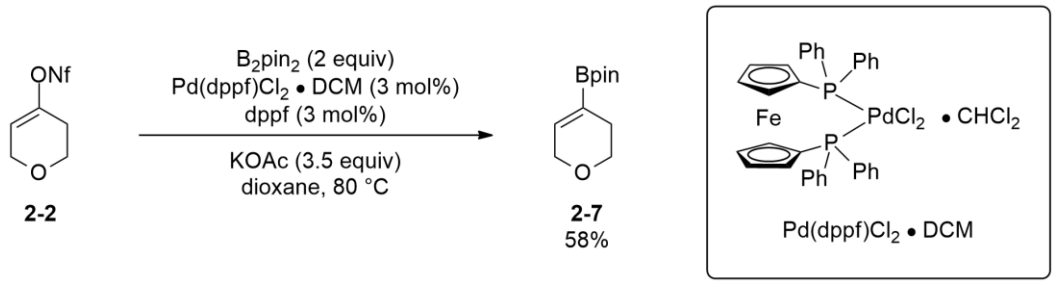

Scheme 2-9. Preparation of the alkenyl boronate **2-7**.

Table 2-4. Effect of alkenyl boronate **2-7** on the borylative migration reaction.

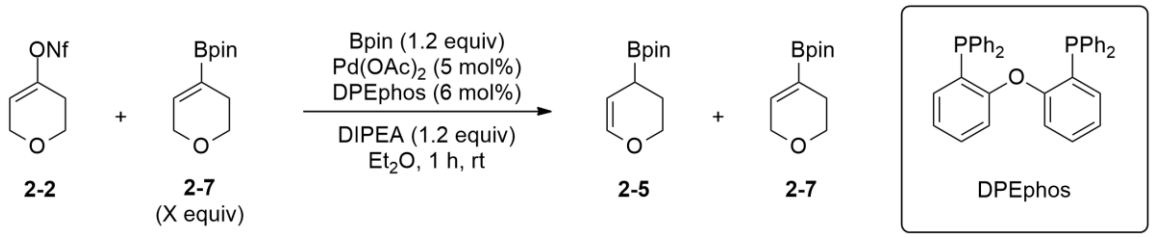

entry	X	remainder of 2-2 (%)[a]
1	0	4
2	0.1	17
3	0.2	24
4	0.5	57

[a] Determined by crude ^{1}H NMR with 1,3,5-trimethoxybenzene as a standard.

In addition to the parallel experiments, I performed kinetic *in situ* ^{1}H NMR studies were conducted to observe the inhibition effect of alkenyl boronate **2-7** on the borylative migration in real time. Preliminary studies showed that the reaction is extremely fast using the standard conditions, which makes monitoring the reaction profile challenging. Therefore, these experiments were run with slightly modified reaction conditions using $Pd_2(dba)_3$ as a catalyst and 1,3,5-trimethoxybenzene as an internal NMR standard. A control experiment, performed in the absence of the alkenyl boronate at the start of the reaction, shows that most of the nonaflate starting material **2-2** was consumed within 1 h of the reaction time (Figure 2-1, in blue). Next, addition of 1 mol% of alkenyl boronate **2-7** at the start of the reaction was enough to drastically slow the reaction with ~ 2% overall consumption of alkenyl nonaflate **2-2** within 1 h (Figure 2-1, in red). Finally, 1 mol%

of **2-7** was added 5 min after the initiation of the reaction (Figure 2-1, in green). In this experiment, the reaction had a similar kinetic profile to the control experiment at the beginning of the reaction (Figure 2-1, in blue), however, a drastic decrease of the reaction rate is observed, comparable to the addition of 1 mol% of **2-7** at the start of the reaction profile (Figure 2-1, in red). Overall, these observations are in agreement with the observed partial first-order of the nonaflate **2-2** and the computed endergonic nature of side product **2-7** release from the catalyst to continue the catalytic cycle.

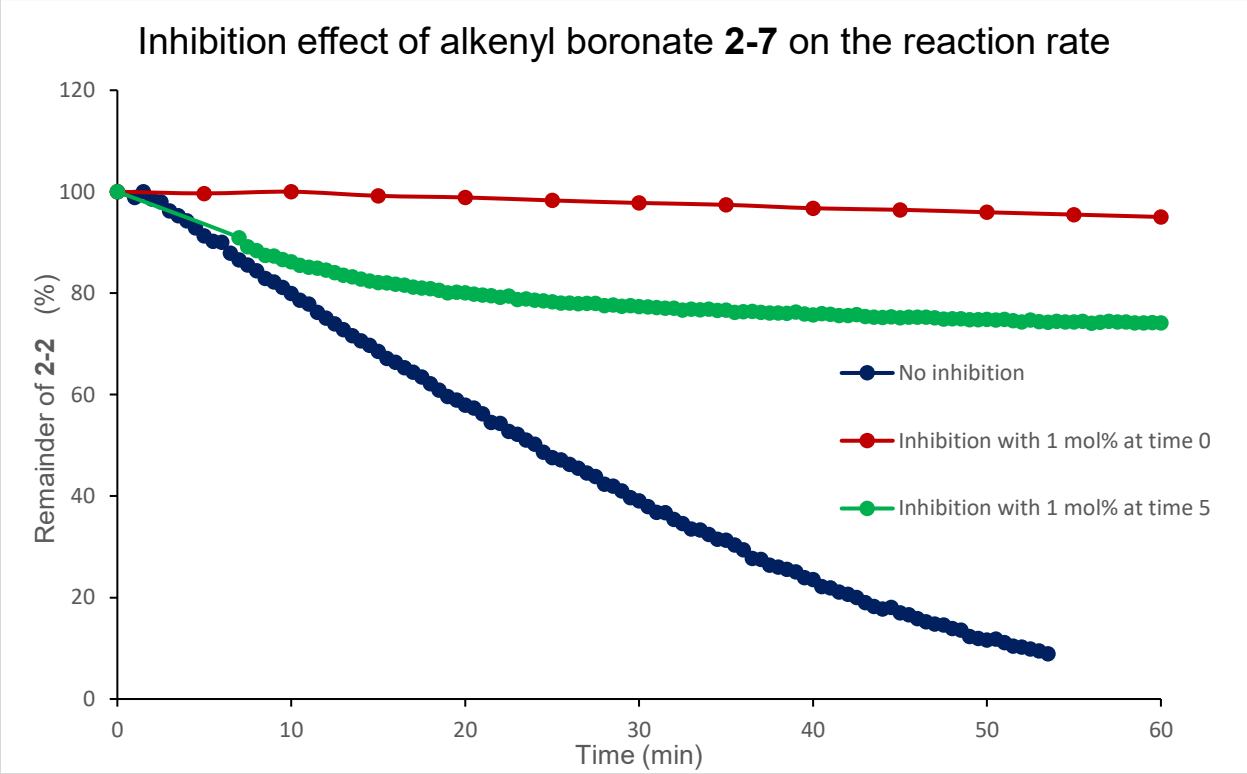

Figure 2-1. Kinetic profiles of inhibition studies of **2-7** on the borylative migration reaction.

2.5 Catalytic Cycle

Based on the extensive mechanistic studies described above, including this confirmation of the inhibitory effect of the alkenyl boronate side product, a full catalytic cycle can be proposed as shown in Scheme 2-10. As indicated by the experiments and computational studies, the cycle is initiated by a Miyaura-type borylation, followed by an alkene isomerization with an electrophilic cationic palladium species . Initially, an oxidative addition occurs to afford the complex **Int-2-8**, which is the rate-determining step of the reaction. Next, an ionization of the palladium complex furnishes the amine-coordinated cationic palladium complex **Int-2-8***, followed by the complexation of pinacolborane to the cationic palladium complex to form **Int-2-10**. The borylated intermediate **Int-2-11** is afforded by an unprecedented enantio-determining σ-bond metathesis *via* **TS-2-2**, a step considered to be irreversible. Deprotonation of **Int-2-11** results in reductive elimination, leading to **Int-2-15** and to the sequential release of alkenyl boronate side product **2-7**. On the other hand, **Int-2-11** undergoes the preferred pathway of palladium chain walking involving an alkene insertion step followed by a β-hydride elimination affording **Int-2-13**. Finally, the subsequent deprotonation of **Int-2-13** furnishes the allylic boronate product **2-5** and the regenerated palladium(0) catalyst upon release from **Int-2-14**.

In addition, the off-cycle complex **Int-2-15** causes catalyst inhibition that explains the partial first-order in electrophile **2-2** according to the kinetic analysis and calculations. This outcome could be explained by the endergonic release of side product **2-7,** which lowers the effective concentration of the active catalyst available to reinitiate the catalytic cycle. The ratio of allyl boronate **2-5** to alkenyl boronate **2-7** formed is dependent on the π-stabilization of palladium hydride complex **Int-2-13**, which is controlled by the electron-donating ability of the heteroatom at the homoallylic position. Furthermore, the heteroatom plays an important role in the enantioselectivity of the reaction by acting as a roadblock to prevent the chain walking of palladium across the ring, which leads to racemization as observed in the case of cyclohexenyl perfluorosulfonate substrates.

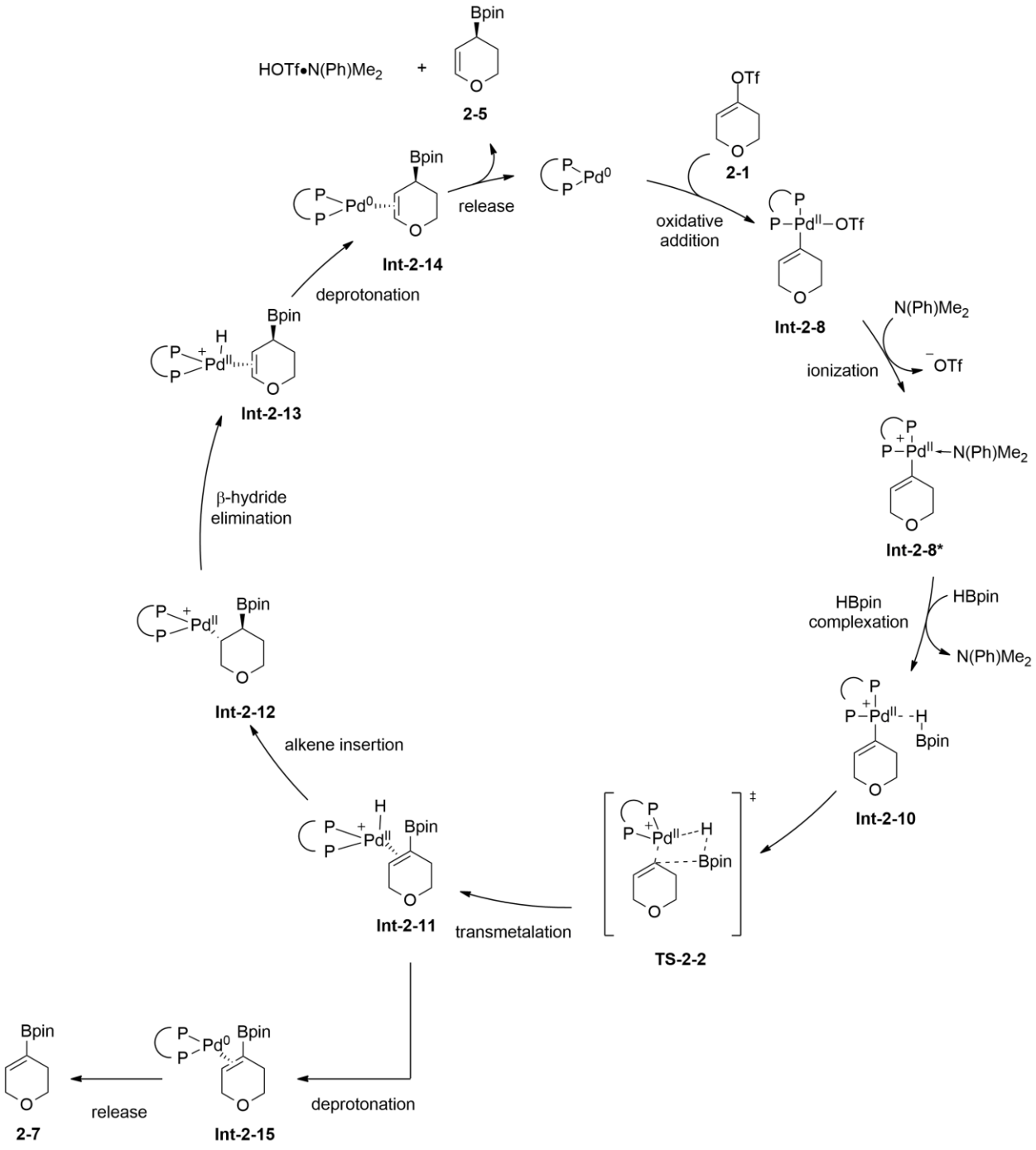

Scheme 2-10. Catalytic cycle of the Pd-catalyzed enantioselective borylative migration.

2.6 Summary

In conclusion, a mechanistic depiction of the borylative migration reaction has been established using experimental and computational data with insight regarding the regio- and enantioselectivity of this reaction. The studies revealed that the reaction proceeds by a Miyaura-type borylation followed by an alkene isomerization pathway with an electrophilic cationic palladium intermediate to deliver the desired allylic boronate product. In addition, the studies suggest that the oxidative addition is the rate-determining step and the stereoselectivity is controlled by an irreversible σ-bond metathesis. Furthermore, it was found and confirmed in this chapter's investigation that the alkenyl boronate side product exerts an inhibitory effect on the reaction due to its strong binding to the palladium catalyst. By gaining mechanistic insight about the borylative migration reaction, access to other heterocyclic allylic boronate could be enabled by rational design approach using new electrophiles. Finally, the efforts and conclusions reported herein have the potential to provide further mechanistic insight in other metal-catalyzed borylation and palladium-catalyzed asymmetric methodologies.

2.7 Experimental

2.7.1 General information

All reactions were performed under nitrogen atmosphere in flame dried glassware, unless otherwise stated. Diethyl ether (Et_2O) was distilled over CaH_2. Dioxane was distilled over sodium/benzophenone ketyl. *N,N*-Diisopropylethylamine (DIPEA) was purchased from Sigma-Aldrich and distilled over CaH_2 under nitrogen prior to use. 1,8-Diazabicyclo[5.4.0.]undec-7-ene (DBU) was purchased from Combi-Blocks Inc., and distilled over CaH_2 under vacuum prior to use. Pinacolborane was purchased from Oakwood Chemicals and used without further purification. 1-*tert*-Butoxycarbonyl-4-piperidone, 1-carbobenzoxy-4-piperidone, perfluorobutanesulfonyl fluoride (NfF) and tris(dibenzylideneacetone)dipalladium(0) were purchased from Combi-Blocks Inc. and used as purchased without further purification. Palladium(II) acetate and DPEphos were purchased from STREM Chemicals and used without further purification. Thin layer chromatography (TLC)

was performed on Merck Silica Gel 60 F254 plates and visualized using UV light, phosphomolybdic acid (PMA) stain, and $KMnO_4$ stain. Flash chromatography was performed on ultra-pure silica gel 230-400 mesh. Nuclear magnetic resonance (NMR) spectra were recorded on Agilent/Varian INOVA-400 or INOVA 500 MHz instruments. The residual solvent proton (^1H) and carbon (^{13}C) signals were used as internal references. ^1H NMR data are represented as follows: Chemical Shift in ppm (δ) downfield from trimethylsilane (multiplicity, coupling constant, integration). The following abbreviations are used in reporting NMR data: s, singlet; br s, broad singlet; t, triplet; app t, apparent triplet; dd, doublet of doublets; dt, doublet of triplets; m, multiplet. The error of coupling constants from ^1H NMR spectra is estimated to be ± 0.3 Hz. High-resolution mass spectra were recorded by the University of Alberta Mass Spectrometry Services Laboratory using electrospray ionization (ESI) method. Infrared spectra were obtained from a Nicolet Magna-IR machine with frequencies expressed in cm^{-1}.

2.7.2 Compound synthesis and characterization

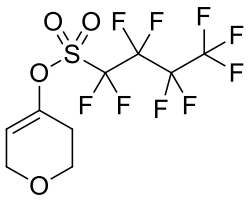

3,6-Dihydro-2*H*-pyran-4-yl 1,1,2,2,3,3,4,4,4-nonafluorobutane-1-sulfonate (2-2). In a flame dried round bottom flask equipped with a stir bar, Tetrahydro-4*H*-pyran-4-one (4.00 g, 40.0 mmol, 1.00 equiv) was dissolved in THF (80.0 mL, 0.500 M) under a nitrogen atmosphere. The solution was cooled down to 0 °C using an ice-bath and stirred for 5 min. DBU (7.00 mL, 44.0 mmol, 1.10 equiv) and perfluorobutanesulfonyl fluoride (12.6 g, 42.0 mmol, 1.05 equiv) were added respectively. The ice-bath was removed, and the solution was allowed to stir at room temperature overnight. The reaction mixture was quenched by slow addition of water and extracted with Et_2O (100 mL × 3). The organic layers were combined and washed with brine, dried over Na_2SO_4, filtered, and concentrated *in vacuo*. The brown crude oil was then purified by chromatography (15% Et_2O/pentane) to afford a clear, colourless oil (10.6 g, 69% yield): ^1H NMR (700 MHz,

$CDCl_3$)**:** δ 5.85–5.81 (m, 1H), 4.26 (dt, *J* = 2.9, 2.9 Hz, 2H), 3.89 (t, *J* = 5.5 Hz, 2H), 2.46 (ttd, *J* = 5.5, 2.8, 1.4 Hz, 2H); ^{13}C NMR (101 MHz, $CDCl_3$, ^{19}F decoupled)**:** δ 146.0, 117.1, 117.0, 114.3, 109.9, 108.5, 77.4, 77.1, 76.7, 64.2, 64.0, 28.5; ^{19}F NMR (377 MHz, $CDCl_3$)**:** δ –80.8, –109.9, –121.1, –126.0; **HRMS**: (EI) for $C_9H_7F_9O_4S$ calcd. 381.9921; found 381.9914.

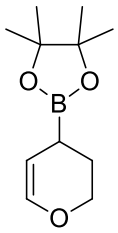

(±)-2-(3,4-Dihydro-*2H*-pyran-4-yl)-4,4,5,5-tetramethyl-1,3,2-dioxaborolane [(±)-2-5]. In a flame dried flask equipped with a stir bar under nitrogen atmosphere, $Pd(OAc)_2$ (13 mg, 0.075 mmol, 5.0 mol%) and DPEPhos (43 mg, 0.080 mmol, 5.3 mol%) were dissolved in Et_2O (6.0 mL, 0.33 M) and stirred for 20 minutes. DIPEA (0.38 mL, 2.2 mmol, 1.1 equiv), HBpin (0.32 mL, 2.2 mmol, 1.1 equiv) and alkenyl nonaflate **2-2** (766 mg, 2.00 mmol, 1.00 equiv) were sequentially added and the reaction was left to stir at room temperature for 16 hours. The crude reaction mixture was filtered through a short silica plug with Et_2O (100 mL) and the volatiles were removed *in vacuo*. The crude reaction mixture was purified by column chromatography (15% Et_2O in pentane) to afford a clear, colourless oil (302 mg, 72% yield). **^{1}H NMR** (400 MHz, $CDCl_3$): δ 6.35 (dd, *J* = 6.2, 2.4 Hz, 1H), 4.68 (dd, *J* = 6.3, 3.7 Hz, 1H), 3.99 (ddd, *J* = 10.2, 6.5, 3.5 Hz, 1H), 3.92 (ddd, *J* = 10.3, 6.7, 3.5 Hz, 1H), 2.01–1.83 (m, 2H), 1.83–1.73 (m, 1H), 1.23 (s, 12H); **^{13}C NMR** (176 MHz, $CDCl_3$): δ 143.0, 101.1, 83.4, 77.2, 77.1, 76.9, 65.7, 24.8, 24.7, 24.2, 16.3 (br); **^{11}B NMR** (128 MHz, $CDCl_3$): δ 32.9; **IR** (microscope, cm^{-1}): 3060, 2931, 2869, 1642, 1372, 1327, 1244, 1218, 1145, 863; **HRMS:** (EI) for $C_{11}H_{19}{}^{11}BO_3$ calcd. 210.1427; found 210.1425.

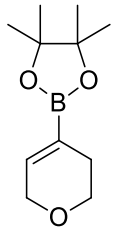

2-(3,6-Dihydro-*2H*-pyran-4-yl)-4,4,5,5-tetramethyl-1,3,2-dioxaborolane (2-7). In a flame dried flask equipped with a stir bar under nitrogen atmosphere, $Pd(dppf)Cl_2 \bullet CH_2Cl_2$ (109 mg, 0.144 mmol, 3.00 mol%), dppf (82.5 mg, 0.144 mmol, 3.00 mol%), bis(pinacolato)diboron (2.44 g, 9.60 mmol, 2.00 equiv), and potassium acetate (1.68 g, 16.8 mmol, 3.50 equiv) were dissolved in dioxane (10.7 mL, 0.449 M) and alkenyl nonaflate **2-2** (1.91 g, 4.8 mmol, 1.0 equiv) was added. The reaction was left to stir at 80 °C for 16 hours. The reaction was cooled to room temperature, diluted in water (25 mL) and extracted with Et_2O (3 × 25 mL). The organic layers were combined and washed with brine, dried over Na_2SO_4, filtered, and concentrated *in vacuo*. The crude mixture was purified by a short silica plug (1:4 EtOAc:Hex) and concentrated *in vacuo* to obtain the desired product as a mixture with bis(pinolato)diboron. The mixture was dissolved in EtOAc (68 mL, 0.070 M) and a few drops of water were added followed by IBX (3.90 g, 13.9 mmol, 2.90 equiv). The reaction was heated to 80 °C with vigorous stirring for 3 hours. Upon cooling to room temperature, the reaction mixture was filtered through a short silica plug (100% EtOAc) and the volatiles were removed *in vacuo*. The crude reaction mixture was purified by column chromatography (5% ethyl acetate in hexanes) to afford a white solid (590 mg, 58% yield). **^{1}H NMR** (400 MHz, $CDCl_3$) δ 6.52 (tt, *J* = 2.3, 2.3 Hz, 1H), 4.19 (dt, *J* = 2.8, 2.8 Hz, 2H), 3.75 (t, *J* = 5.4 Hz, 2H), 2.22 (ttd, *J* = 5.3, 2.8, 2.3 Hz, 2H), 1.27 (s, 12H); **^{13}C NMR** (126 MHz, $CDCl_3$) δ 141.0, 83.4, 66.2, 64.3, 26.2, 24.9 (the boron-bound carbon was not detected due to quadrupolar relaxation of boron);**^{11}B NMR** (128 MHz, $CDCl_3$) δ 29.5; **IR** (microscope, cm^{-1}) 3029, 2983, 2955, 2894, 2813, 1640, 1379, 1326, 1294, 1129; **HRMS** (EI) for $C_{11}H_{19}{}^{11}BO_3$ calcd. 210.1427; found 210.1430.

2.7.3 Effect of alkenyl boronate additive on the reaction progress

2.7.3.1 Experimental procedure with no alkenyl boronate additive

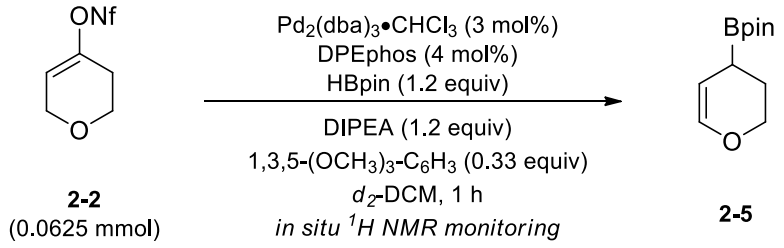

$Pd_2(dba)_3$•$CHCl_3$ (1.8 mg, 1.9 µmol, 3.0 mol%), DPEphos (1.3 mg, 2.5 µmol, 4.0 mol%) and 1,3,5-trimethoxybenzene (3.6 mg, 21 µmol, 0.33 equiv) were added to an oven-dried J-Young NMR tube containing a small stir bar and capped with a septum, which was evacuated and re-filled with argon four times. Dry d_2-DCM (0.75 mL) was added, and the reaction mixture was stirred for 15 minutes. The small stir bar was quickly removed, and the headspace of the NMR tube was flushed with argon for 5 minutes. DIPEA (14 µL, 79 µmol, 1.3 equiv) and HBpin (11 µL, 76 µmol, 1.2 equiv) were measured in separate gas-tight syringes and capped with a septum under nitrogen. Alkenyl nonaflate **2-2** (23.9 mg, 62.5 µmol, 1.00 equiv) was weighed into a tared gas-tight syringe and capped with a septum. Once the array parameters were set using a standard sample containing d_2-DCM, DIPEA, HBpin, and the alkenyl nonaflate **2-2** were sequentially added. The septum was quickly replaced with the J-Young NMR tube cap. The reaction mixture was shaken vigorously for ten seconds, and the sample was inserted into the magnet. All measurements were acquired via continuous measurement arrays using a pre-acquisition delay (PAD) using Agilent instruments with the following parameters: steps = 120; starting value = 10; array increment = 0; nt = 4; ss = 0; pad[1] = 0. All spectra were phased, baseline-corrected, and the data obtained using VnmrJ software. The data was transferred to an excel spreadsheet and manipulated as required according to Burés and co-workers to obtained concentration over time by relative integration to the 1,3,5-trimethoxybenzene internal standard (IS).[19,22]

2.7.3.2 Experimental procedure with 1 mol% of alkenyl boronate additive

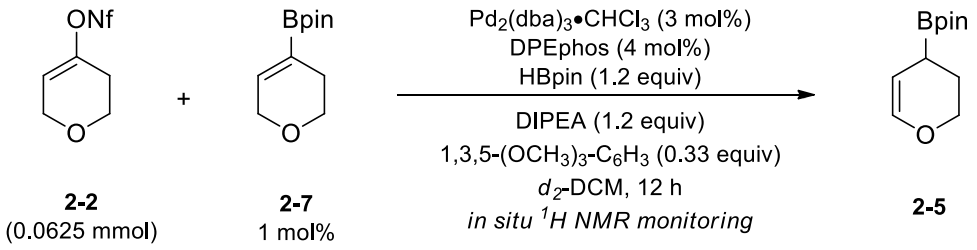

The inhibition experiment was performed according to General Procedure A, with 0.01 equivalent of alkenyl boronate **2-7** in d_2-DCM (48 mM, 13 µL, 0.63 µmol, 0.01 equiv) being added to the reaction mixture after the addition of HBpin and prior to the addition of alkenyl nonaflate **1b**. The PAD parameters were as the following: steps = 120; starting value = 300; array increment = 0; nt = 8; ss = 0; pad[1] = 0. All spectra were phased, baseline-corrected, and the data obtained using VnmrJ software. The data was transferred to an excel spreadsheet and manipulated as required according to Burés and co-workers to obtained concentration over time by relative integration to the 1,3,5-trimethoxybenzene internal standard (IS).[19,22]

2.7.3.3 Experimental procedure with 1 mol% of alkenyl boronate added after 5 min.

The inhibition experiment was performed according to General Procedure A, with 0.01 equivalent of alkenyl boronate **5** in d_2-DCM (48 mM, 13 µL, 0.63 µmol, 0.01 equiv) being added to the reaction mixture five minutes after the addition of the alkenyl nonaflate **1b**. The PAD parameters were as the following: steps = 120; starting value = 10; array increment = 0; nt = 4; ss = 0; pad[1] = 0. All spectra were phased, baseline-corrected, and the data obtained using VnmrJ software. The data was transferred to an excel spreadsheet and manipulated as required according to Burés and co-workers to obtained concentration over time by relative integration to the 1,3,5-trimethoxybenzene internal standard (IS).[19,22]

2.8 References

[1] Ding, J.; Hall, D. G. *Angew. Chem. Int. Ed.* **2013**, *125*, 8227.

[2] Ding, J.; Rybak, T.; Hall, D. G. *Nat. Commun.* **2014**, *5*, 5474.

[3] Clement, H. A.; Hall, D. G. *Tetrahedron Lett.* **2018**, *59*, 4334.

[4] Lessard, S.; Peng, F.; Hall, D. G. *J. Am. Chem. Soc.* **2009**, *131*, 9612.

[5] Kim, Y.-R.; Hall, D. G. *Org. Biomol. Chem.* **2016**, *14*, 4739.

[6] Murata, M.; Oyama, T.; Watanabe, S.; Masuda, Y. *Synthesis* **2000**, *2000*, 778.

[7] Chow, W. K.; Yuen, O. Y.; Choy, P. Y.; So, C. M.; Lau, C. P.; Wong, W. T.; Kwong, F. Y. *RSC Adv.* **2013**, *3*, 12518.

[8] Ishiyama, T.; Murata, M.; Miyaura, N. *J. Org. Chem.* **1995**, *60*, 7508.

[9] Murata, M.; Watanabe, S.; Masuda, Y. *J. Org. Chem.* **1997**, *62*, 6458.

[10] Murata, M.; Oyama, T.; Watanabe, S.; Masuda, Y. *J. Org. Chem.* **2000**, *65*, 164.

[11] Lam, K. C.; Marder, T. B.; Lin, Z. *Organometallics* **2010**, *29*, 1849.

[12] Yamashita, M.; Nozaki, K. *Topics in Organometallic Chemistry, Springer, Cham* **2015**, 2.

[13] Yamamoto, Y.; Nogi, K.; Yorimitsu, H.; Osuka, A. *ChemistrySelect* **2017**, *2*, 1723.

[14] Murata, M.; Oda, T.; Sogabe, Y.; Tone, H.; Namikoshi, T.; Watanabe, S. *Chem. Lett.* **2011**, *40*, 962.

[15] Beletskaya, I. P.; Cheprakov, A. V. *Chem. Rev.* **2000**, *100*, 3009.

[16] Sommer, H.; Juliá-Hernández, F.; Martin, R.; Marek, I. *ACS Cent. Sci.* **2018**, *4*, 153.

[17] Mathew, J. S.; Klussmann, M.; Iwamura, H.; Valera, F.; Futran, A.; Emanuelsson, E. A. C.; Blackmond, D. G. *J. Org. Chem.* **2006**, *71*, 4711.

[18] Blackmond, D. G. *J. Am. Chem. Soc.* **2015**, *137*, 10852.

[19] Burés, J. *Angew. Chem. Int. Ed.* **2016**, *55*, 16084.

[20] Thomas, B. N.; Moon, P. J.; Yin, S.; Brown, A.; Lundgren, R. J. *Chem. Sci.* **2018**, *9*, 238.

[21] Nielsen, C. D. T.; Burés, J. *Chem. Sci.* **2019**, *10*, 348.

[22] Burés, J. *Angew. Chem. Int. Ed.* **2016**, *55*, 2028.

Chapter 3: Regiocontrolled and Enantiospecific Allyl-Allyl Cross-Coupling of Enantioenriched Piperidinyl Allylic Boronates

3.1 Introduction

As discussed in Chapter 1, due to their importance in pharmaceutical industry, numerous synthetic methods have been reported to gain access to enantioenriched piperidine heterocycles in an efficient and cost-effective manner. However, many of these methods require employment of pre-functionalized acyclic substrates which syntheses require laborious stereocontrolled multistep sequences. *N*-cyclization reactions[1] and ring-closing metathesis (RCM)[2] are examples of such approaches (Scheme 3-1a). To circumvent the need for such acyclic substrates, one approach to be considered is the desymmetrization of readily available simple prochiral piperidine derivatives. Using this approach would provide access to desirable enantioenriched piperidines in few steps. For this reason, the Hall Group developed a novel enantioselective borylative migration reaction using prochiral heterocyclic enol perfluorosulfonates **3-1** and **3-2** to afford enantioenriched allylic boronic esters **3-3** and **3-4** (Scheme 3-1b).[3,4] This methodology transforms readily available prochiral heterocycles to enantioenriched heterocyclic allylic boronic esters in two steps. Allylic boronic esters are useful in various carbon-carbon bond formation methods, including the allylboration of carbonyls[5] and the Suzuki–Miyaura cross-coupling.[6] The Hall Group made efforts to employ the optically enriched allyl boronic ester heterocycles obtained by the borylative migration protocol in several chemical transformations. One example of such efforts is the stereospecific allylboration of aldehydes to afford products with high diastereo- and enantioselectivities.[7] Another example is the development of regiocontrolled allylic Suzuki–Miyaura cross-coupling reactions, where the type of ligands used in these reactions dictates the regioselectivity outcome of the product (Scheme 3-1 b).[8] These methods were applied in the total synthesis of pharmaceutical drugs (Scheme 3-1c).[7,8]

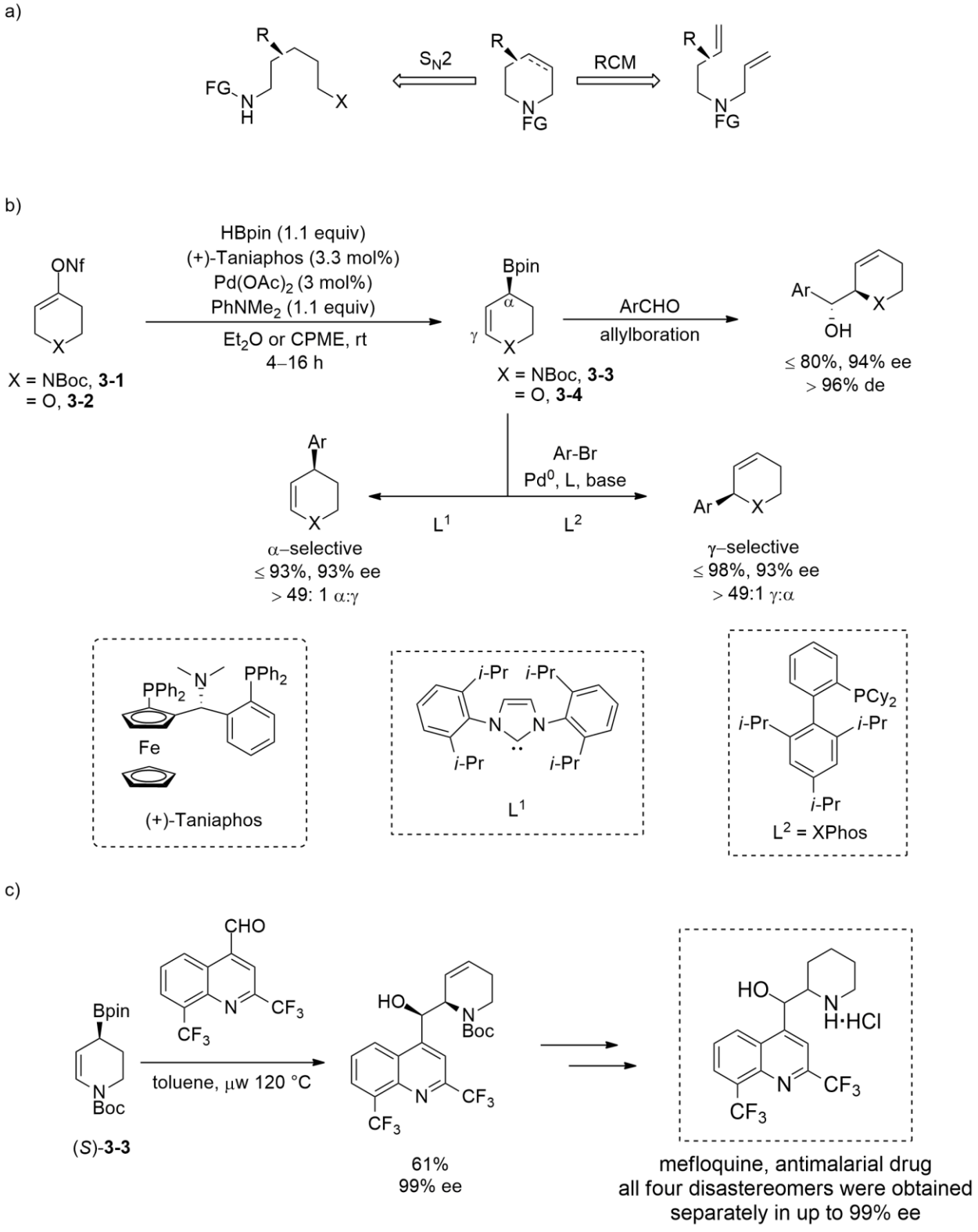

Scheme 3-1. a) Examples of chiral piperidine synthesis from acyclic substrates. b) Hall Group's enantioselective borylative migration methodology. c) Total synthesis application of mefloquine, an antimalarial drug, from chiral piperidinyl allylic boronate **3-3**.

In spite of the fact that the optically enriched allylic boronic ester **3-3** was successfully implemented in Suzuki–Miyaura cross-coupling with various aryl and alkenyl bromides,[8] there have been no examples of its application in C_{sp}^3–C_{sp}^3 coupling reactions. The formation of C_{sp}^3–C_{sp}^3 bonds through palladium-catalyzed cross-coupling means is inherently difficult due to the tendency of alkylpalladium intermediates to undergo *β*-hydride elimination, which leads to undesired byproducts (Scheme 3-2a).[9] *β*-Hydride elimination occurs exclusively to alkylmetal species containing a syn coplanar H atom on the to the *β*-carbon. To circumvent this issue, Morken and co-worker developed a palladium-catalyzed allyl-allyl cross-coupling reaction of cinnamyl and benzylic allylic electrophiles.[10] Employing such electrophiles renders the *β*-hydride elimination not possible due to the absence of an aliphatic *β*-C–H bond (Scheme 3-2b). This study revealed that the regioselectivity to afford either branched or linear products can be controlled based on the type of phosphine ligand used.[10] Linear products were obtained using monodentate ligands, whereas bidentate ligands afford the branched products selectively.[10] In addition, this cross-coupling reaction can be modified to afford enantioenriched branched products using the chiral bidentate phosphine ligand (*R*)-MeO-furyl-BIPHEB (Scheme 3-2b).[10] However, a limitation of this study is the scope of nucleophilic coupling partners; most of the allylic boronic esters used in the reaction are simple linear allyl or crotyl boronates without any substituents.

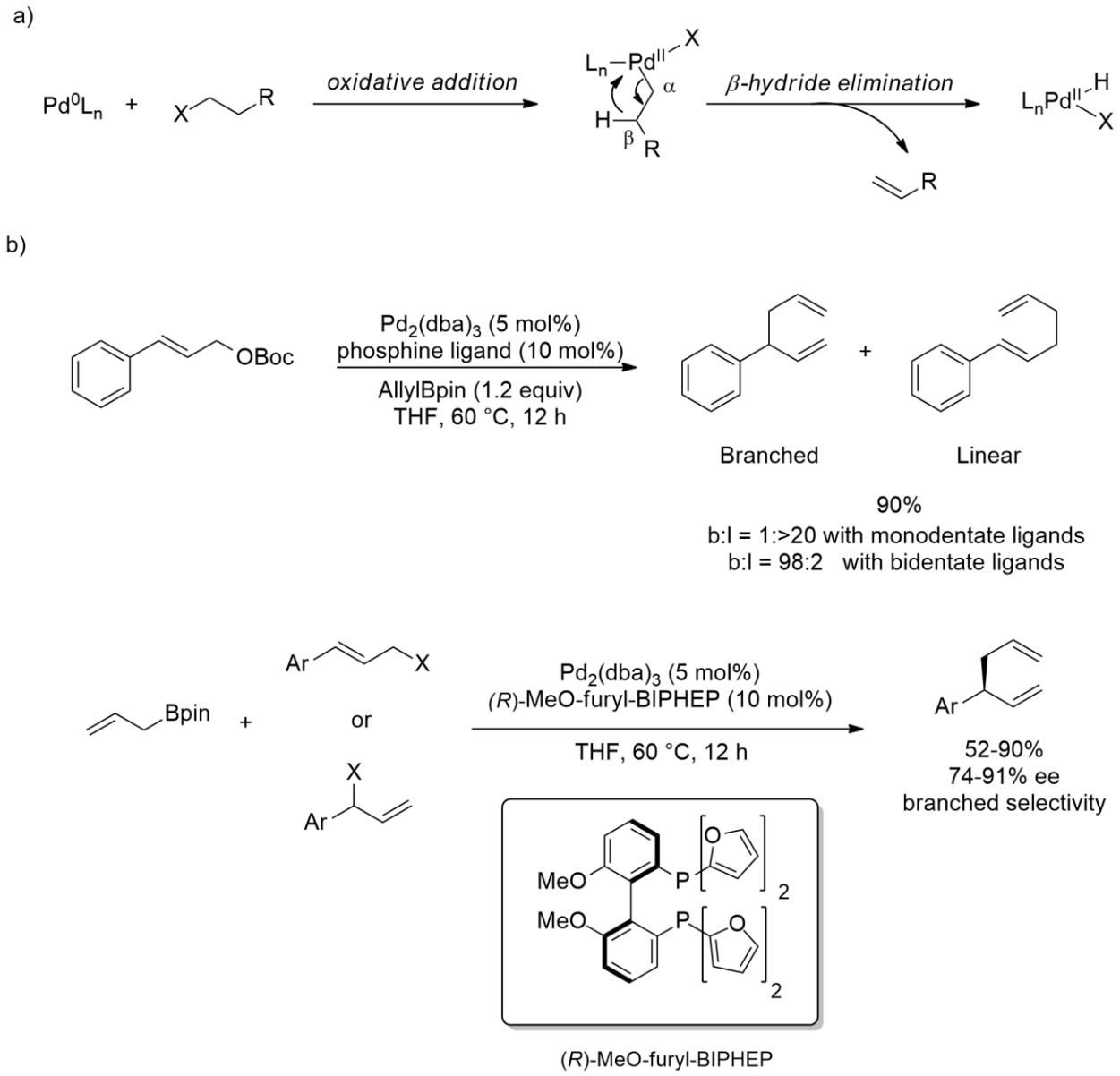

Scheme 3-2. a) β-Hydride elimination side reaction in palladium catalyzed cross-coupling using alkyl halides. b) Morken's allyl-allyl cross-coupling methodology and its enantioselective modification.

3.2 Objective

In Section 2.1, the efficacy of the borylative migration methodology in accessing piperidinyl allylic boronates was demonstrated. Therefore, the Hall Group is interested in expanding the synthetic utility of these piperidinyl allylic boronates beyond their initial applications, considering the pharmaceutical importance of such heterocycles.[11] To date, these heterocycles were only employed in aldehyde allylboration and Csp^3–Csp^2 cross-coupling reactions.[4,8] Inspired by Morken's efforts,

I was interested in using this opportunity, and surmised that enantioenriched piperidinyl allylic boronate **3-3** could be employed in Morken's allyl-allyl cross-coupling protocol to deliver enantioenriched allylated piperidine derivatives. However, the likelihood of forming four regioisomers when using two unsymmetrical allylic substrates poses a challenge for this approach (Scheme 3-3). Hence, the objective of this project is to develop a new allyl-allyl cross-coupling reaction between allylic boronate **3-3** and cinnamyl and allylic carbonate derivatives and optimize the reaction conditions to obtain high regioselectivity and high enantiospecificity. Furthermore, efforts to derivatize the resulting cross-coupling products will be made to emphasize on the potential application of the newly developed method in medicinal chemistry.

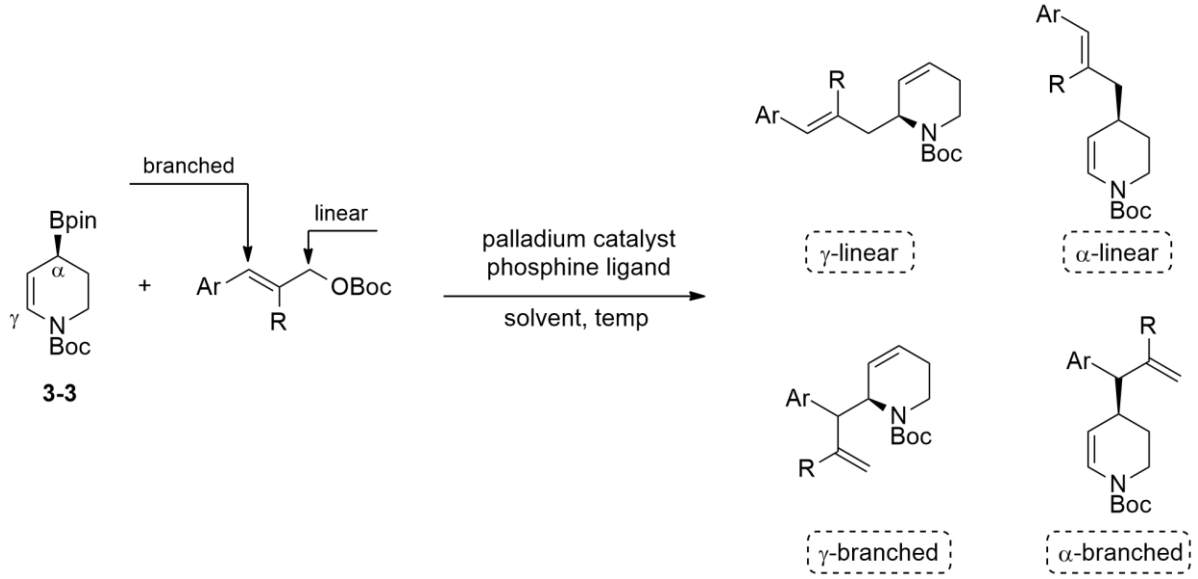

Scheme 3-3. Proposed allyl-allyl cross-coupling reaction between allylic boronate **3-2a** and allylic electrophiles with the four possible regioisomers.

3.3 Initial Screening and Optimization of the Allyl-Allyl Cross-Coupling Reaction Using Racemic Allylic Boronates

3.3.1 Preparation of starting materials for the initial screening

To avoid wasting enantioenriched materials, Initial testing of the allyl-allyl cross-coupling reaction was conducted using racemic allylic boron ester (*rac*)-**3-3**. Allylic boronic ester (*rac*)-**3-3** was synthesized in two steps from commercially available 1-Boc-4-piperidone using DPEphos, an inexpensive ligand, in the borylative migration step, instead of the valuable enantioenriched Taniaphos (Scheme 3-4a).[4] In addition, cinnamyl *tert*-butyl carbonate **3-5** was chosen as the electrophilic coupling partner in the screening as a cost-friendly alternative to cinnamyl halides.[12] The allylic carbonate can be synthesized using a O-Boc protection from commercially available cinnamyl alcohol and di-tert-butyl dicarbonate (Scheme 3-4b).

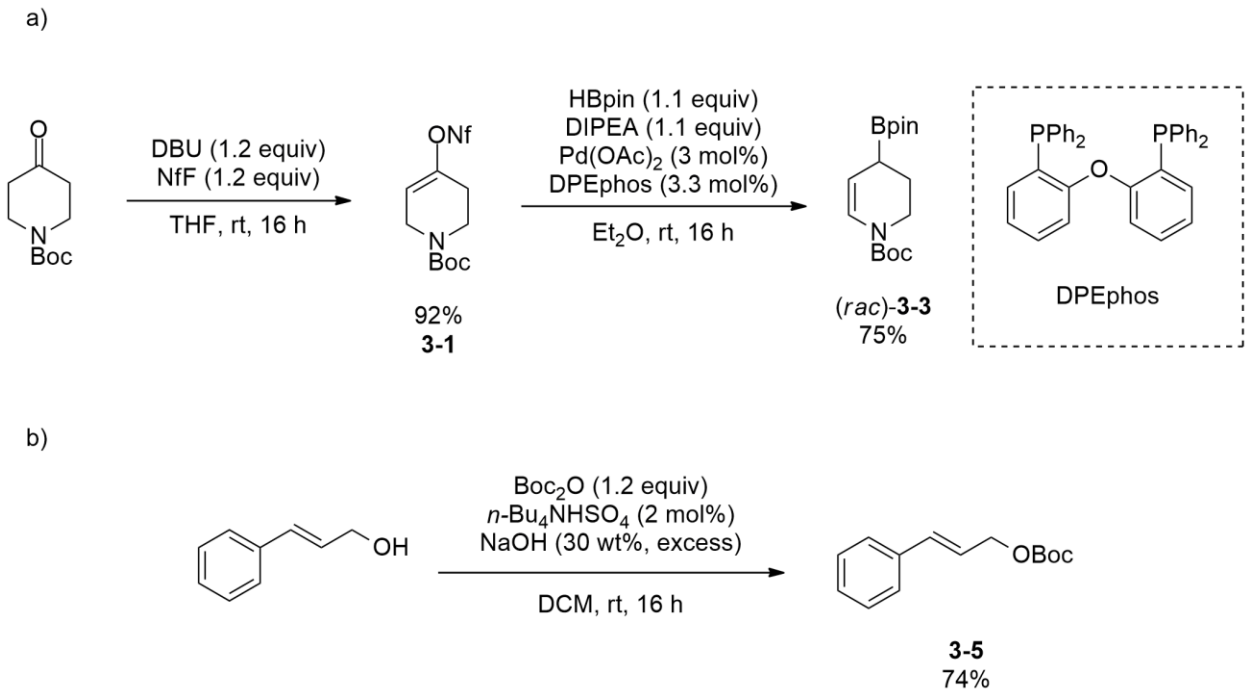

Scheme 3-4. Preparation of the starting materials for the initial screening: a) Synthesis of racemic allyl boronic ester **3-2a**. b) Synthesis of cinnamyl carbonate **3-3**.

3.3.2 Initial screening using racemic boronic esters

Initial screening of the cross-coupling reaction was conducted using nucleophile (*rac*)-**3-3** and electrophile **3-5** as standard substrates. Initially, the conditions reported by Morken and co-worker were employed,[13] using triphenylphosphine as a ligand, affording the γ-linear product (*rac*)-**3-6** in a low yield (Table 3-1, entry 1). Crude mixture ^{1}H NMR analysis of the reaction mixture confirmed that the γ-linear product was the sole isomer. A variety of other ligands were tested for their availability to enhance the reaction yield, however, there was no improvement of the reaction yield observed with bidentate ligands, including MeO-furyl-BIPHEB (Table 3-1, entries 2–4). Furthermore, dialkylbiarylphosphine ligands such as XPhos, CyJohnPhos and *t*-BuXPhos did not improve the yield of the γ-linear product (Table 3-1, entries 5–7). In previous work with aryl halides as the electrophile, the employment of palladium–NHC catalytic systems led to α-selective cross-coupling,[8] however, there was no product observed when Pd-PEPPSI-IPr was used in this reaction (Table 3-1, entries 8–9). Furthermore, switching the electrophilic coupling partner to allyl bromide provided no reactivity (Table 3-1, entry 10).

In the Pd-catalyzed cross-coupling of organoboron compounds, a base is typically required to enable transmetalation of the carbon fragment from boron to palladium. This process is believed to occur through the formation of Pd-O-B linkages, although the exact nature of pre-transmetalation intermediates remains a subject of intense interest.[14] Initially, no basic additives were added to the reaction mixture as it was thought that the *tert*-butoxide formed from the oxidative addition step is basic enough to promote the transmetalation step.[10] Nevertheless, due to the low yields from the initial screening, basic additives were considered to enhance the reaction yield. Hence, a variety of basic additives such as silver carbonate and cesium fluoride were tested, and it was observed that fluoride anion significantly improved the reaction yield (Table 3-1, entries 11–12). This observation can be rationalized by the affinity of fluoride ions to the boronic ester to form fluoroborate ions, which are active towards the transmetalation with palladium.[15] The addition of basic additives also enabled the use of allyl halides as electrophilic coupling partners

(Table 3-1, entries 13–15). A variety of solvents were tested to monitor their effect on the reaction yield; however, the initial solvent, tetrahydrofuran, was shown to be the most suitable solvent for this reaction (Table 3-1, entries 16–19). Lastly, a significant decrease of reactivity was noticed when the ligand loading was lowered (Table 3-1, entry 20). In general, the use of triphenylphosphine as a ligand and cesium fluoride as a basic additive (Table 3-1, entry 12) were determined to be the optimal reaction conditions**,** furnishing a good yield of the γ-linear product as the only isomer observed.

Table 3-1. Reaction screening of the allyl-allyl cross-coupling with (rac)-**3-3**.

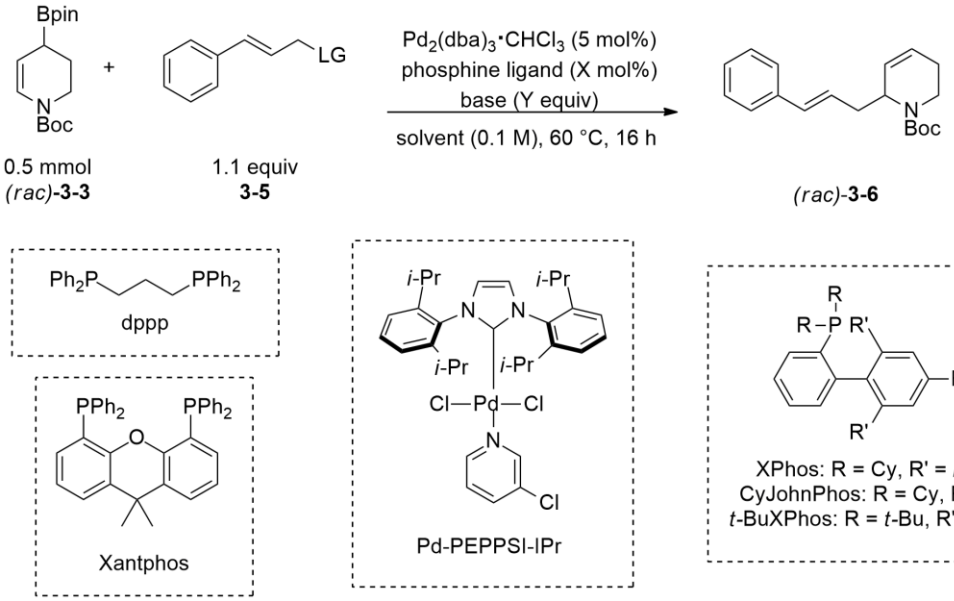

entry	LG	solvent	ligand	X	base	Y	yield[a]
1	OBoc	THF	PPh_3	10	—	—	31%
2	OBoc	THF	dppp	5	—	—	20%
3	OBoc	THF	Xantphos	5	—	—	20%
4	OBoc	THF	MeO-furyl-BIPHEP	5	—	—	n.d.[b]
5	OBoc	THF	XPhos	10	—	—	< 5%
6	OBoc	THF	CyJohnPhos	10	—	—	< 5%
7	OBoc	THF	*t*-BuXPhos	10	—	—	< 5%
8[c]	OBoc	THF	—	—	—	—	n.d.[b]
9[c]	OBoc	THF	—	—	Cs_2CO_3	2.5	n.d.[b]
10	Br	THF	PPh_3	10	—	—	n.d.[b]
11	OBoc	THF	PPh_3	10	Ag_2CO_3	2.5	64%
12	OBoc	THF	PPh_3	10	CsF	5	75%
13	Br	THF	PPh_3	10	Ag_2CO_3	2.5	59%
14	Cl	THF	PPh_3	10	Ag_2CO_3	2.5	37%
15	Cl	THF	PPh_3	10	CsF	5	62%
16	OBoc	DCE	PPh_3	10	CsF	5	48%
17	OBoc	MeCN	PPh_3	10	CsF	5	50%
18	OBoc	EtOH	PPh_3	10	CsF	5	n.d.[b]
19	OBoc	toluene	PPh_3	10	CsF	5	52%
20	OBoc	THF	PPh_3	5	CsF	5	< 5%

[a] Isolated yield. [b] n.d.: not detected. [c] Catalyst used: Pd-PEPPSI-IPr

3.4 Optimization of the Reaction Conditions for the Chiral Allylic Boronic Esters

Optically enriched piperidine allylic boronic ester **3-3** (87% ee), which is readily accessible by the borylative migration protocol,[4] was subjected to a cross-coupling reaction with cinnamyl carbonate **3-5** using the optimal reactions conditions identified in Section 3.3 (Table 3-1, entry 12). At the outset, the substituted piperidine product (*S*)-**3-6** showed significant erosion of the optical purity with mediocre enantiospecificity (57% es) (Scheme 3-5a). The observed erosion from the reaction was tentatively thought to be caused by the intermediacy of chiral palladium(II) complex **3-7** which may undergo a reversible Pd–Pd displacement from free palladium(0) in the solution. This process would cause partial racemization of the pre-reductive-elimination complex **3-7** and erode the enantiofacial selectivity of the transmetalation step (Scheme 3-5b).[16] This assumption was based on the work of the Bäckvall Group in studying the isomerization of π-allyl palladium complexes.[16] In their work, they demonstrated that π-allyl palladium complexes undergo isomerization *via* Pd–Pd displacement. If this tentative assumption is correct, the rate of the racemization of the palladium(II) complex **3-7** can be controlled by altering factors such as the reaction temperature, concentration and the electronic characteristics of the triarylphosphine ligand.

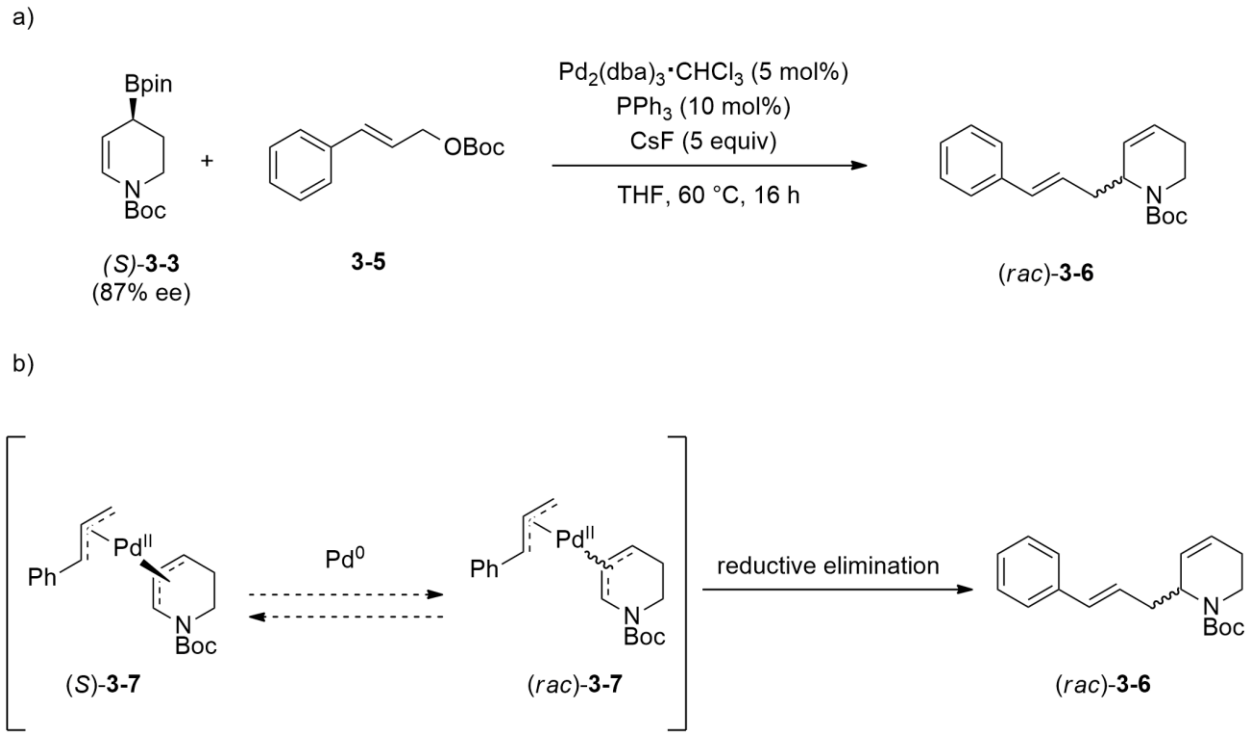

Scheme 3-5. a) Cross-coupling reaction chiral allylic boronate **3-3** using the optimal conditions of Table 3-1. b) Rationale for the stereochemical erosion during the cross-coupling reaction.

Therefore, in an effort to improve the optical purity of the cross-coupling product, other reaction parameters such as the temperature, electronic nature of the triarylphosphine ligand and the reaction concentration were explored (Table 3-2). Performing the reaction at room temperature showed a slight improvement of the enantiospecificity of the reaction (Table 3-2, entry 2). On the other hand, when the electron-poor triarylphosphine ligand, $(p\text{-}CF_3C_6H_4)_3P$, was employed in the reaction, significantly enhanced enantiospecificity was observed, albeit with low yield. In contrast, use of an electron-rich triarylphosphine, $(p\text{-}MeOC_6H_4)_3P$, resulted in further erosion of the optical purity of the reaction product (Table 3-2, entries 3–4). The improved enantiospecificity observed with an electron-deficient ligand can be rationalized by one of two following reasons: 1) reduction of the nucleophilicity of the palladium catalyst, mitigating stereorandomizing addition to the π-allyl palladium(II) complex **3-7**; or, 2) the destabilization of the palladium(II) complex intermediate **3-7** with a consequent increase of the reductive elimination rate,[17,18] which in turn can help suppress the undesired competitive epimerization process. To examine the extent of the

electron-poor triarylphosphine ligands to enhance the stereospecificity of the reaction, tris(pentafluorophenyl)phosphine was employed, however, there was no reactivity observed (Table 3-2, entry 5). To address the low yield of the reaction when (p-$CF_3C_6H_4)_3P$ is used, different reaction parameters were tested. Firstly, due to the difficulty of separating dibenzylideneacetone from the desired product, the palladium source was switched to $Pd(OAc)_2$. Furthermore, employing the allylic boronic ester in excess caused significant increase in the yield of the reaction.

Table 3-2. Optimization of the allyl-allyl cross-coupling reaction with optically enriched boronate **3-3**.

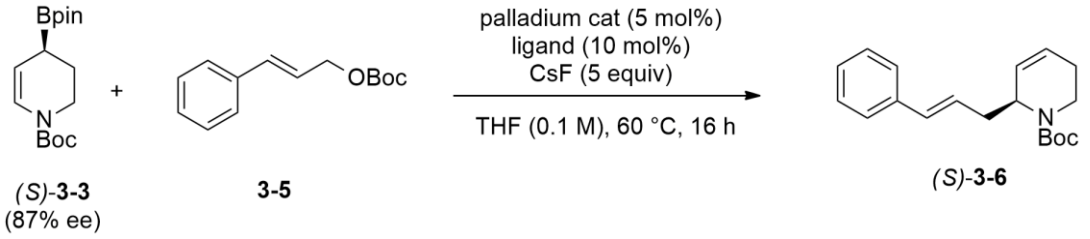

(S)-**3-3** (87% ee) | **3-5** | *(S)*-**3-6**

entry	palladium source	ligand	yield (%)[a]	es (%)[b]
1	$Pd_2(dba)_3 \bullet CHCl_3$	PPh_3	72	57
2[c]	$Pd_2(dba)_3 \bullet CHCl_3$	PPh_3	40	63
3	$Pd_2(dba)_3 \bullet CHCl_3$	(p-$CF_3C_6H_4)_3P$	25	94
4	$Pd_2(dba)_3 \bullet CHCl_3$	(p-$MeOC_6H_4)_3P$	60	40
5	$Pd_2(dba)_3 \bullet CHCl_3$	$(C_6F_5)_3P$	n.r.[d]	n/a
6[e]	$Pd(OAc)_2$	(p-$CF_3C_6H_4)_3P$	68	97
7[f]	$Pd(OAc)_2$	(p-$CF_3C_6H_4)_3P$	67	97

[a] Isolated yield. [b] Enantiospecifity (% es): (% ee of product/% ee of SM) × 100. [c] Reaction performed at room temperature. [d] n.r. = no reaction. [e] Reaction was performed with 0.20 mmol of **3-5**, 0.24 mmol of (*S*)-**3-3** (1.2 equiv), and 1.0 mmol of CsF (5 equiv). [f] Concentration = 0.025 M.

Satisfyingly, it was found that combining $Pd(OAc)_2$ as the precatalyst with (p-$CF_3C_6H_4)_3P$ as the ligand and switching the limiting reagent to the allyl carbonate electrophile **3-5** afforded the cross-coupling product (*S*)-**3-6** with excellent enantiospecificity and good yield (Table 3-2, entry

6). Lastly, it was found that running the reaction at a low concentration did not affect the enantiospecificity of the reaction (Table 3-2, entry 7).

Table 3-3. Optimization of the ligand and basic additive loading in the reaction using racemic boronate **3-3**.

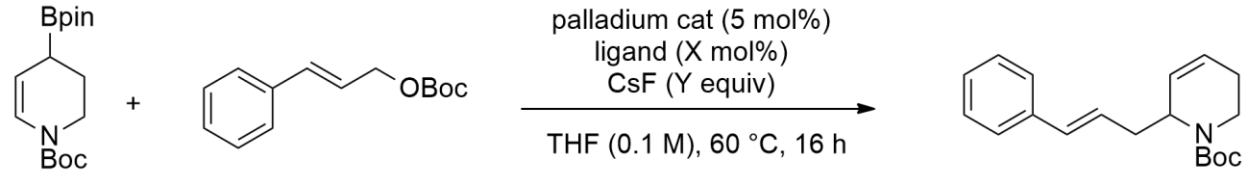

(*rac*)-**3-3** **3-5** (*rac*)-**3-6**

entry	X (mol%)	Y (equiv)	isolated yield (%)
1	10	5	76
2	10	3	78
3	10	2	75
4	10	1.5	30
5	5	2.5	n.d.
6	7.5	2.5	n.d.

After identifying the optimal ligand affording the highest enantiospecificity in the reaction, further optimization of the ligand loading and basic additive were examined using racemic allylic boronic ester **3-3** (Table 3-3). It was found that there was no significant change in the reaction yield by decreasing the loading of cesium fluoride to two equivalents compared to the allylic carbonate electrophile, whilst a significant drop in the yield was observed by employing a stoichiometry lower than two equivalents (Table 3-3, entries 1-4). Furthermore, it was found that the optimal precatalyst to ligand ratio is 1:2. It is likely that the precatalyst $Pd(OAc)_2$ requires oxidation of an equivalent of the ligand to be reduced to the active palladium(0) complex at the start of the reaction (Table 3-3, entries 5–6).[19]

Overall, a regioselective and enantiospecific allyl-allyl cross-coupling reaction between chiral piperidinyl allylic boronate **3-3** and cinnamyl carbonate derivatives was optimized. It was found that the use of $(p\text{-}CF_3C_6H_4)_3P$ as a ligand is optimal to achieve high enantiospecificity. In addition, good yields were obtained by using $Pd(OAc)_2$ as a precatalyst and two equivalents of cesium fluoride, with respect to the cinnamyl carbonate electrophile, as a basic additive.

3.5 Substrate Scope of the Allyl-Allyl Cross-Coupling Reaction

3.5.1 Preparation of the allylic carbonate starting materials

To test the scope of this reaction with respect to substituted allylic carbonates, various electrophilic coupling partners were prepared from different starting materials depending on their commercial availability. One route to access primary allylic carbonates is through reduction of the cinnamyl aldehydes to the corresponding alcohols followed by O-Boc protection to afford the desired starting materials **3-5** for the reaction scope (Scheme 3-6, route A).[10] Alternatively, these primary allyl carbonates can be accessed from the corresponding benzaldehyde derivatives through the Doebner modification of the Knoevenagel condensation[20] reactions with malonic acid, followed by acid catalyzed esterification, diisobutylaluminium hydride (DIBAL) reduction then O-Boc protection to furnish the desired derivatives **3-5** (Scheme 3-6, route B). Because the mechanism of the allyl-allyl cross-coupling is thought to be proceed by the formation of a π-allyl palladium(II) complex, secondary allylic benzylic carbonate electrophiles **3-5′** were expected to participate in the cross-coupling reaction to afford the γ-linear. These substrates were prepared by Grignard reaction using the corresponding benzaldehydes and vinylmagnesium bromide followed by O-Boc protection (Scheme 3-6, route C).[10] These branched allylic carbonates may provide an alternative route to the synthesis of the γ-linear products and would provide mechanistic insights about the reaction.

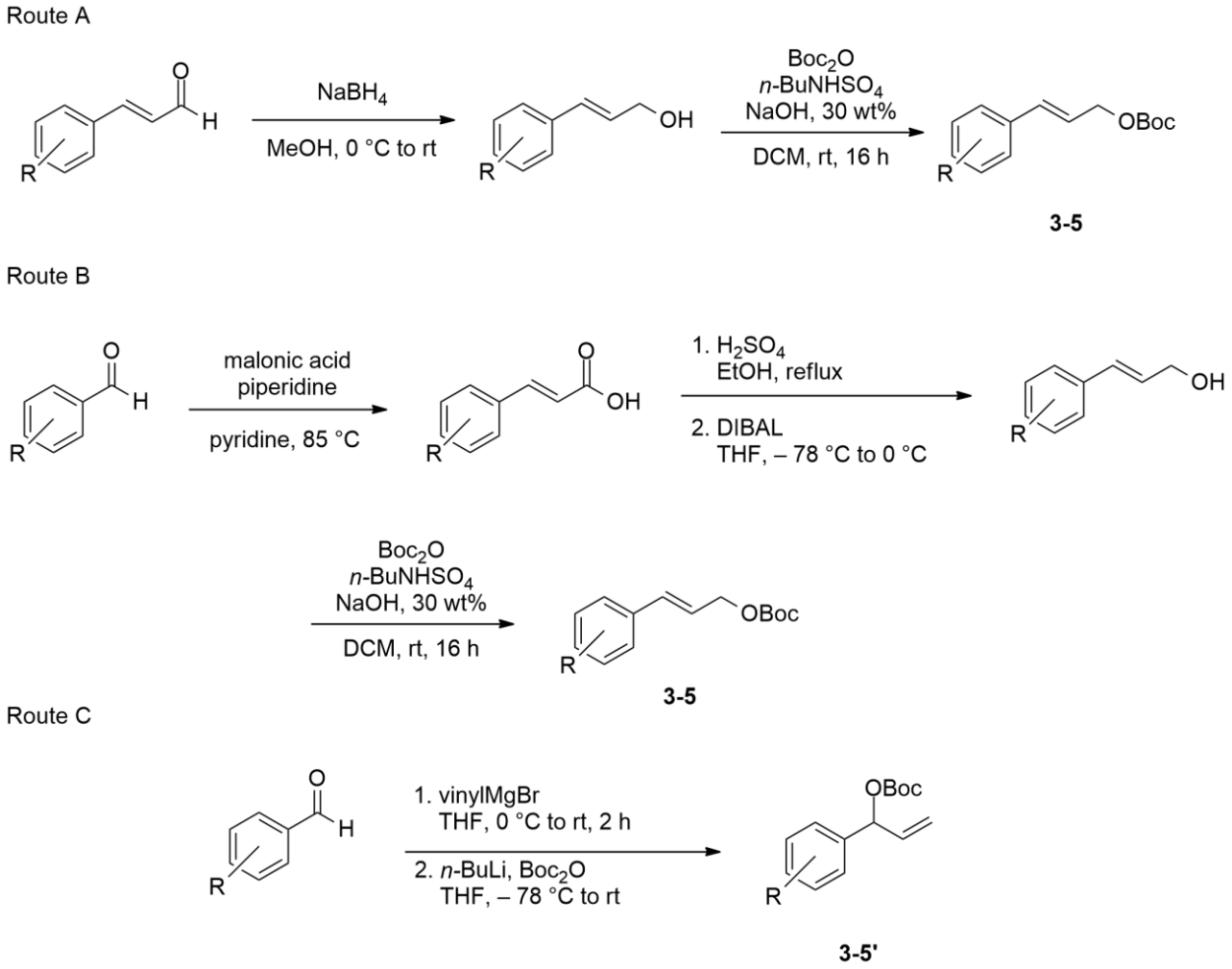

Scheme 3-6. Different synthetic routes for the formation of the electrophilic coupling partners.

3.5.2 Substrate scope of the reaction

With the optimal reaction conditions in hand, the scope of cinnamyl carbonates as the electrophilic coupling partners was examined with optically enriched (*S*)/(*R*)-**3-3** (Scheme 3-7). The reaction with *ortho*-, *meta*-, and *para*-methylcinnamic carbonates **3-5b**–**d** furnished the corresponding 2-cinnamyl dehydropiperidine products (**3-6b**–**d**) in good yields (65–76%) and outstanding enantiospecifities (>98%). *o*-Methoxy substituted cinnamyl carbonate was cross-coupled to give product **3-6e** in low yield (25%), however with high enantiospecifity (97%). Products with oxygen containing rings and substituents were obtained in good yields as shown with the examples of 1,3-benzodioxole **3-6f** (63%, >99% es) and the chromene derivative **3-6g** (75%, 96% es).

Different electron withdrawing groups such as chlorine and trifluoromethyl groups, as well as a thioether were tolerated to afford the respective products **3-6h–j** in moderate yield with high enantiospecificity. The regioisomeric secondary allylic carbonates **3-5′** can also be employed to give the same product without loss in yield and enantiospecificity. Thus, when **3-5d′** was combined with (*S*)**-3-3**, product **3-6d** was isolated in a yield and es similar to that observed when **3-5d** was employed. In the same manner, products **3-6k** and **3-6l** were isolated in good yield and high es from the corresponding secondary allylic carbonates **3-5k′** and **3-5l′**. Overall, in all of the successful examples, the γ-linear isomer **3-6** was the only isolated product.

Several substrates were unsuccessful in affording the desired γ-linear product (Figure 3-1). The naphthyl carbonate derivative and propargyl carbonate did not show any reactivity in the cross-coupling reaction and most of the starting materials were recovered. However, when *p*-methyl ester cinnamyl carbonate was employed, the crude reaction product showed substantial decomposition in the reaction as no predicted product or starting materials were identified by the ^{1}H NMR spectra. When aliphatic allylic carbonates were employed, most of the starting materials were recovered without formation of desired product.

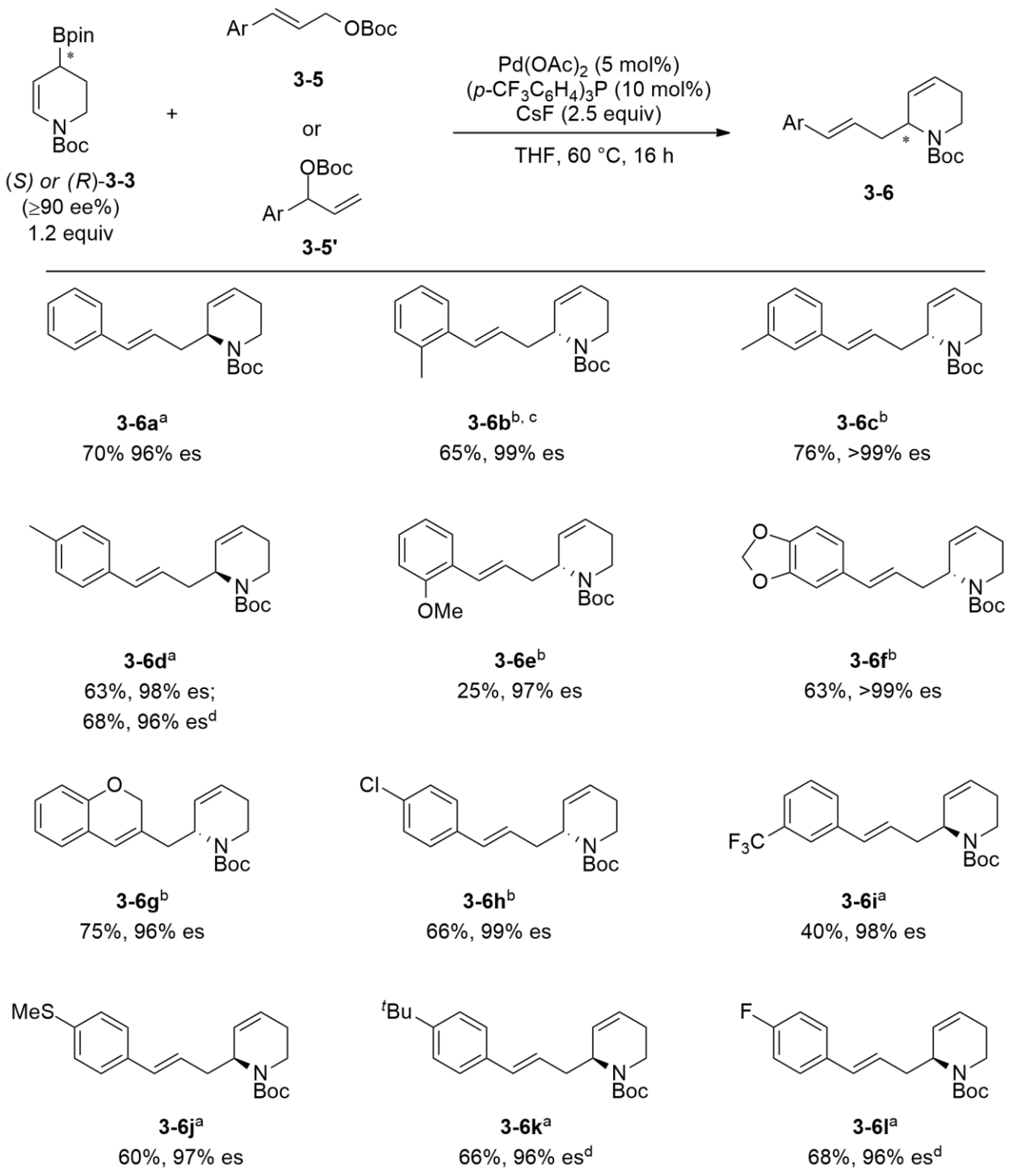

Scheme 3-7. Substrate scope of the allyl-allyl cross-coupling reaction. All reactions were performed using 0.20 mmol of **3-5** and 0.24 mmol of **3-3** (1.2 equiv). [a] Using (S)-**3-2**. [b] Using (R)-**3-2**. [c] Reaction performed at 35 °C. [d] Using **3-5′**.

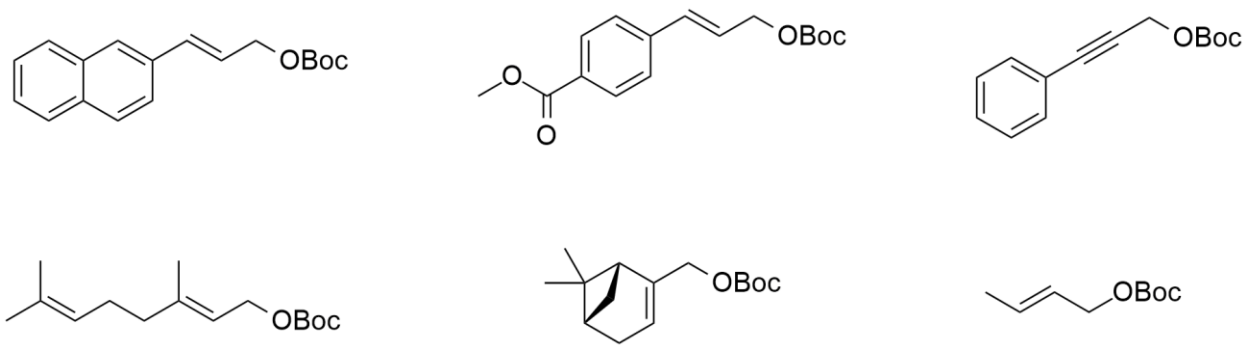

Figure 3-1. Examples of allylic carbonate substrates that were unsuccessful in the cross-coupling reaction.

3.6 Mechanism of the Allyl-Allyl Cross-Coupling Reaction

3.6.1 Proposed catalytic cycle

Based on the collective observations of the cross-coupling reaction involving electrophiles **3-5** and **3-5′**, a catalytic cycle can be proposed (Scheme 3-8).[21] First, the active palladium(0) catalyst undergoes oxidative addition with allylic carbonate **3-5** or **3-5′** to provide palladium(II) π-allyl complex **3-8**. The fluoride anion coordinates to the allyl boronate (*S*)-**3-4** to form a fluoroborate anion before the subsequent transmetalation step.[15] According to mechanistic studies by Braun, cross-coupling reactions proceed through cationic palladium species in the presence of cesium fluoride as a base.[22] According to the previous work of Miyaura and Szabo, when triarylphophines are used as ligands, the transmetalation between the fluoroborate anion and the cationic allylpalladium(II) complexes is thought to occur *via* a S_E2' process.[6,23-26] During this step, the fluoride anion acts as a bridging ligand between the two species as shown in the transition structure **3-9**, delivering the palladium atom at the γ-position in a stereoretentive manner forming intermediate **3-10**. In previous work with boronate **3-3** from the Hall Group, the use of triarylphosphine ligands in cross-coupling reactions favored the formation of α-palladium complexes of such allylic heterocyclic systems.[8] This can take place through σ-π-σ equilibrium resulting in intermediate **3-11** *via* complex **3-7**. Subsequent reductive elimination from these allyl-allyl palladium(II) complexes can occur through 1,1′ or 3,3′ carbon-carbon connectivity. According to the experimental and computational studies by Ardolino and Morken, it was found

that in systems using monophosphine ligands, the 3,3′ reductive elimination of the isomer intermediate with the least hindered 3,3′ termini is energetically favored.[21] Therefore, between the two isomeric α-palladium complexes **3-12** and **3-13**, the γ-linear product can be delivered preferably *via* a 3,3′ reductive elimination from complex **3-12**.

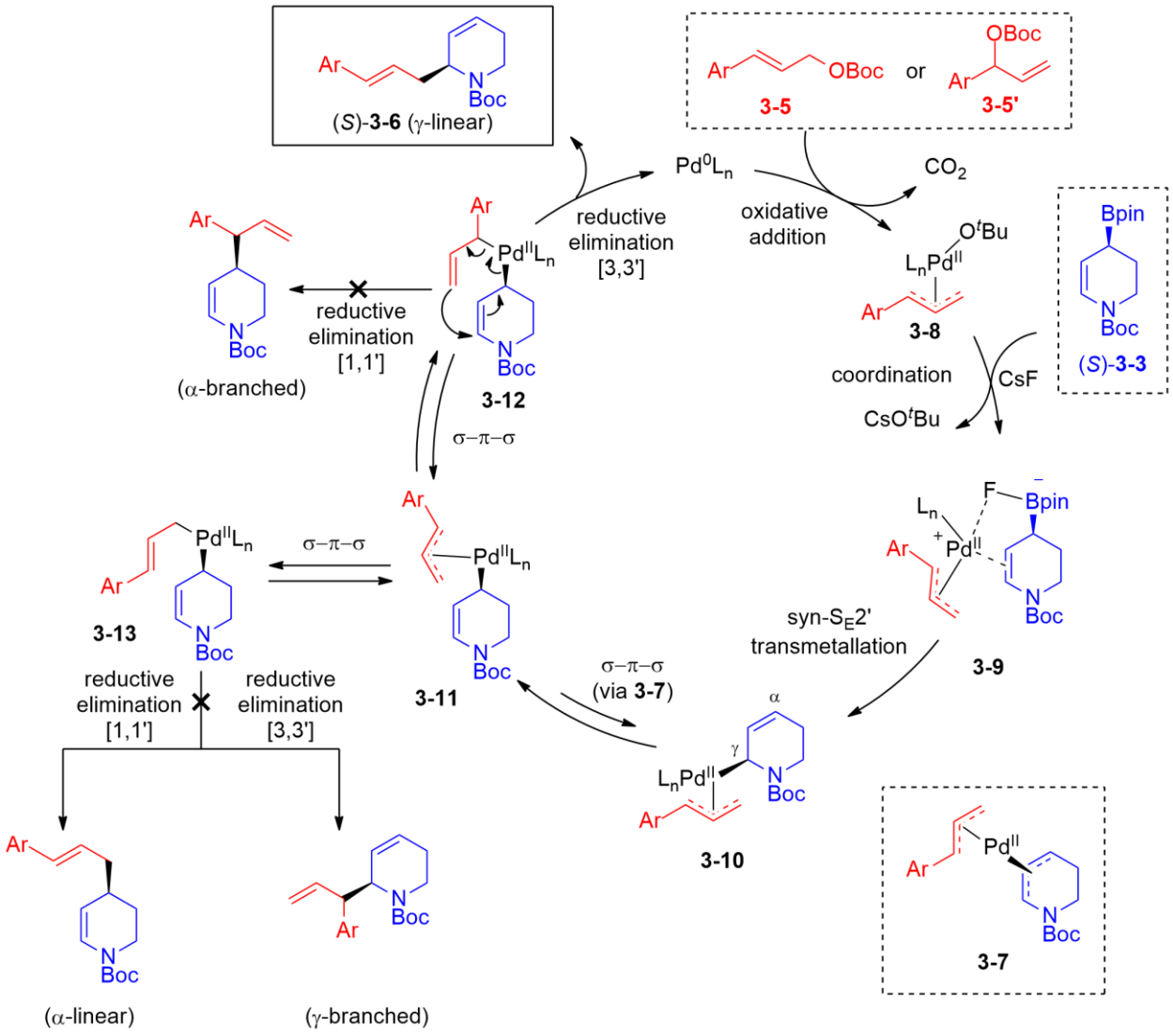

Scheme 3-8. Proposed catalytic cycle of the allyl-allyl cross-coupling reaction.

3.6.2 Determination of the absolute stereochemistry of the allyl-allyl products

Based on the proposed mechanism, the allyl fragment is expected to be delivered from the same face as the boronate moiety. This prediction can be rationalized by a 6-membered cyclic transition state in the transmetalation step that would deliver the palladium atom of α-palladium complex **3-10** from the same face of the allyl boronate (Scheme 3-10a). However, confirmation of the absolute stereochemistry of the coupled products would be essential to this study. Due to the physical nature of the products, i.e., liquid at room temperature, obtaining an X-ray crystallographic structure to confirm the absolute stereochemistry is not feasible. One way to circumvent this issue is by derivatizing compound (*S*)-**3-6a** into the previously reported compound (*S*)-**3-14** and compare the measured optical rotation against the reported value. If the compounds have similar optical activity, i.e., rotate a polarized light in the same direction, the compounds are assumed to share the same absolute configuration. Thus, compound **3-4a** was derivatized to **3-14** by hydrogenation followed by removal of the Boc group and its optical rotation was compared to the reported value (Scheme 3-10b).[27] It was found that the synthesized compound (*S*)-**3-14** had the same optical rotation sign as the reported (*S*)-2-(3-phenylpropyl)piperidine, which confirms its absolute stereochemistry. The absolute stereochemistry of all products in this study was assessed by analogy with (*S*)-**3-6a** and the stereofacial-retentive mechanism of the cross-coupling

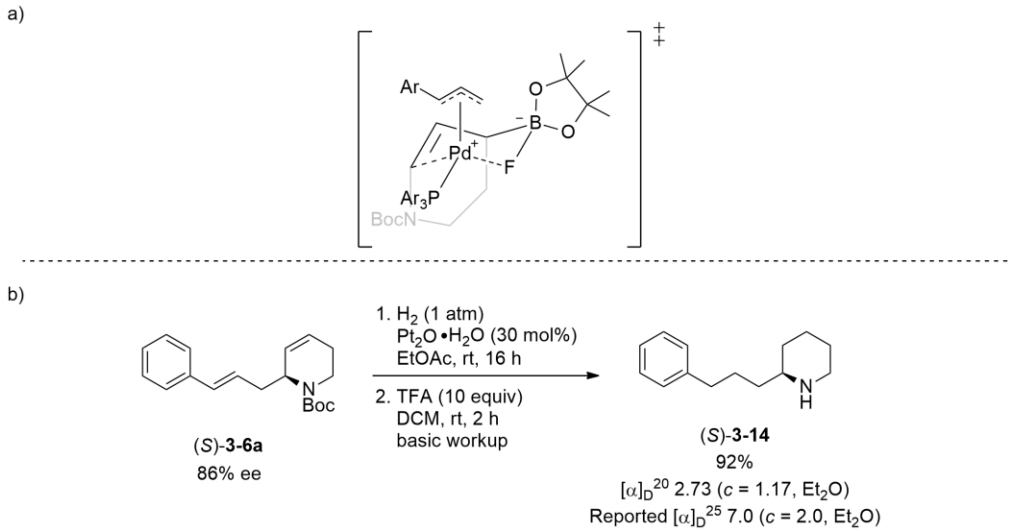

Scheme 3-9. a) Rationale for the observed stereochemistry of the products. b) Confirmation of the stereochemistry of **3-6a**.

3.7 Synthetic Applications of the Allyl-Allyl Cross-Coupled Products

To evaluate the robustness and versatility of the newly optimized cross-coupling protocol, further chemical transformations of the cross-coupling product **3-6d** were examined. Firstly, the allyl-allyl cross-coupling reaction could be readily scaled up from 0.2 mmol to 2.0 mmol scale without erosion of the yields (Scheme 3-10a). In addition, the reaction was tested using benzyloxycarbonyl (Cbz), a different amine protecting group, and it provided similar yields and regioselectivity (Scheme 3-10a). One of the features of the cross-coupled compounds is the presence of a protected amine functional group, which can be employed in various chemical transformations. One example of these transformations is the reductive amination of carbonyl compounds. Hence substrate (*rac*)-**3-6d** was subjected to deprotection under acidic conditions to obtain the free amine **3-15**, followed by a reductive amination with *p*-anisaldehyde to deliver tertiary amine **3-16** (Scheme 3-10b).[28] Lastly, complete hydrogenation of the substrate was achieved by using heterogenous catalysis to yield the fully hydrogenated product **3-17** (Scheme 3-10b).

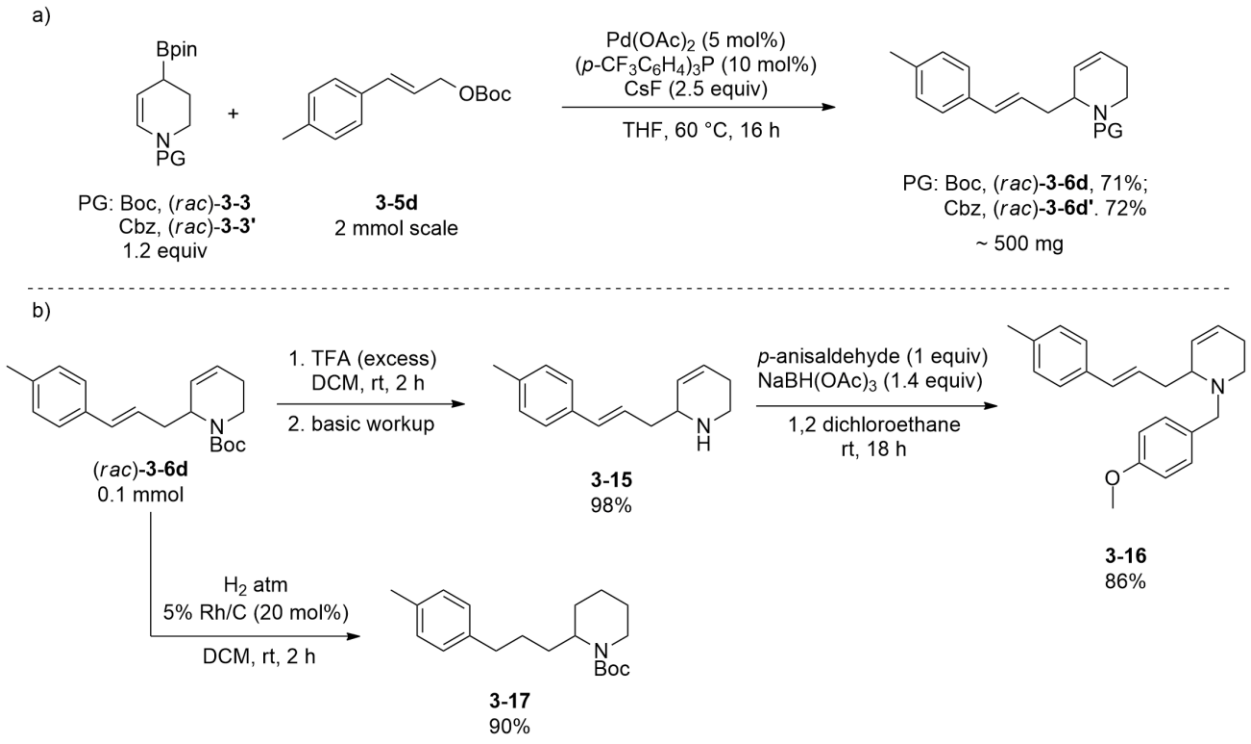

Scheme 3-10. a) Scalability of the cross-coupling reaction using different protecting groups. b) Successful chemical transformations of (rac)-**3-6d**.

3.8 Summary

In summary, a regiocontrolled and enantiospecific palladium-catalyzed allyl-allyl cross-coupling reaction between cinnamyl carbonates and a chiral piperidinyl allylic boronic ester has been developed. The choice of ligand was essential to achieve high regioselectivity and enantiospecificity. Employing the electron-deficient monodentate ligand (p-$CF_3C_6H_4)_3P$ in the reaction enables high regioselectivity towards the γ-linear cross-coupled products and up to 99% enantiospecificity. The robustness of this new methodology was tested using various cinnamyl carbonate derivatives delivering the corresponding products in moderate to good yields while maintaining high enantiospecificity. A mechanism of the reaction was proposed to provide an explanation for the observed regioselectivity and high enantiospecifity. The key features of this catalytic cycle are the stereoretentive transmetalation, and the 3,3′ reductive elimination of the allyl-allyl-palladium complex with the least sterically hindered 3,3′ ends to deliver high regioselectivity for the γ-linear products. Lastly, the cross-coupled products were subjected to

further chemical modification to emphasize the importance of these compounds in drug discovery application and natural product synthesis.

3.9 Experimental

3.9.1 General information

All reactions were performed under nitrogen atmosphere in flame dried glassware, unless otherwise stated. Tetrahydrofuran (THF), dichloromethane (DCM) and toluene were purified using a cartridge solvent purification system. Diethyl ether (Et_2O) was distilled over CaH_2. Cyclopentyl methyl ether (CPME) was purchased from Sigma-Aldrich and used as received. *N,N*-Diisopropylethylamine (DIPEA) was purchased from Sigma-Aldrich and distilled over CaH_2 under nitrogen prior to use. *N,N*-dimethylaniline (DMA) and 1,8-diazabicyclo[5.4.0.]undec-7-ene (DBU) were purchased from Sigma Aldrich and Combi-Blocks Inc., respectively, and distilled over CaH_2 under vacuum prior to use. Pinacolborane was purchased from Oakwood Chemicals and used without further purification. 1-*tert*-Butoxycarbonyl-4-piperidone, 1-carbobenzoxy-4-piperidone, perfluorobutanesulfonyl fluoride (NfF) and tris(dibenzylideneacetone)dipalladium(0) were purchased from Combi-Blocks Inc. and used as purchased without further purification. Palladium(II) acetate, Taniaphos, and DPEphos were purchased from STREM Chemicals. Thin layer chromatography (TLC) was performed on Merck Silica Gel 60 F254 plates and visualized using UV light, phosphomolybdic acid (PMA) stain, and $KMnO_4$ stain. Flash chromatography was performed on ultra-pure silica gel 230-400 mesh. Nuclear magnetic resonance (NMR) spectra were recorded on Agilent/Varian INOVA-400, INOVA 500, INOVA-600 or INOVA-700 MHz instruments. The residual solvent proton (^1H) and carbon (^{13}C) signals were used as internal references. ^1H NMR data are represented as follows: Chemical Shift in ppm (δ) downfield from trimehtylsilane (multiplicity, coupling constant, integration). The following abbreviations are used in reporting NMR data: s, singlet; br s, broad singlet; t, triplet; app t, apparent triplet; dd, doublet of doublets; dt, doublet of triplets; m, multiplet. The error of coupling constants from ^1H NMR spectra is estimated to be ± 0.3 Hz. High-resolution mass spectra were recorded by the University

of Alberta Mass Spectrometry Services Laboratory using electrospray ionization (ESI) method. Infrared spectra were obtained from a Nicolet Magna-IR machine with frequencies expressed in cm^{-1}. The enantiomeric excess ratios for optically enriched compounds were determined using a HPLC Agilent instrument with a Chiralcel-OD or Chiralpak IA or IB or IC column as specified in the following individual procedures.

3.9.2 Preparation of Cinnamyl Alcohol Derivatives

Representative Procedure A

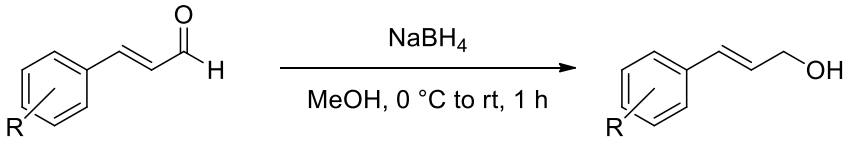

In a round bottom flask equipped with a stir bar, 4-methoxycinnamaldehyde (405 mg, 2.50 mmol) was mixed with methanol (10 mL) and cooled down to 0 °C and kept stirring for 5 min. $NaBH_4$ (94.6 mg, 2.50 mmol) was then added to the solution in three portions. The ice bath was removed, and the reaction mixture was allowed to stir at room temperature for 1 h. The reaction was quenched with H_2O and extracted with Et_2O (40 mL × 3). The organic layers were washed with brine, dried over Na_2SO_4, filtered, and then concentrated *in vacuo* to afford 4-methoxycinnamal alcohol as a yellow oil which was used in the next step without further purification.

Representative Procedure B

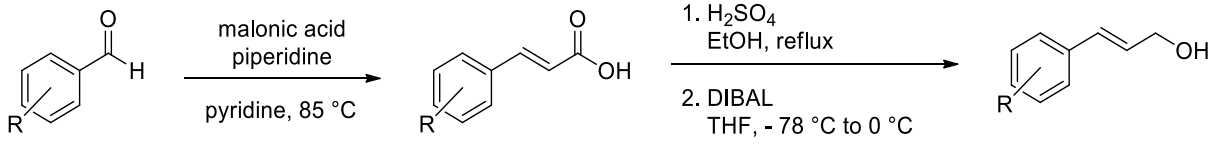

To a stirred solution of malonic acid (1.62 g, 15.6 mmol) in pyridine (10.0 mL) and piperidine (102 µL, 1.20 mmol) in a round bottom flask, 3, 5-dimethylbenzaldehyde was added slowly under 85 °C. The resulting reaction mixture was allowed to stir for 6 h then cooled down to 0 °C before it was neutralized with 10% hydrochloric acid aqueous mixture where a white solid was precipitated. The solid was filtered and washed with cooled water and dried under vacuum at 60 °C

overnight to afford the corresponding (2*E*)-3-(3,5-dimethylphenyl)-2-propenoic acid (666 mg, 78%).

The acid (666 mg, 3.78 mmol) was mixed with ethanol (50 mL) in a round bottom flask and a few drops of H_2SO_4 were added. The reaction mixture was allowed to stir at reflux overnight. The mixture was diluted with H_2O and extracted with EtOAc (50 mL × 3). The organic layer was washed with saturated aqueous $NaHCO_3$, water, brine, then dried over Na_2SO_4, filtered and the solvent was removed. The crude mixture was then transferred into a flame dried round bottom flask equipped with a stir bar and mixed with THF (30.0 mL) under N_2 atmosphere. The reaction flask was cooled down to –78 °C then DIBAL (9.50 mL, 9.50 mmol, 1.00 M in THF) was added slowly to the reaction mixture. Upon complete addition of DIBAL, the solution was warmed up to 0 °C and kept stirring for 1 h. The reaction mixture was quenched with 15% aqueous NaOH, after which $MgSO_4$ (4.0 g) was added and the mixture was stirred for 5 minutes. The solids were filtered out and the organic layer was concentrated *in vacuo*. The corresponding crude alcohol was used in the next step without further purification.

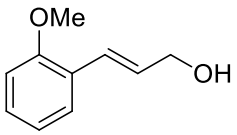

(*E*)-3-(2-Methoxyphenyl)prop-2-en-1-ol (3-18). Prepared according to representative procedure A from commercial 4-methoxycinnamaldehyde (1.00 g, 6.20 mmol), $NaBH_4$ (234 mg, 6.20 mmol): yellow oil (955 mg, 97% crude yield). Spectral data are in accordance with the literature:[29] **^{1}H NMR** (400 MHz, $CDCl_3$): δ 7.41 (dd, *J* = 7.6, 1.8 Hz, 1H), 7.29–7.21 (m, 1H), 6.95–6.85 (m, 3H), 6.40–6.32 (m, 1H), 4.30 (d, *J* = 5.8 Hz, 2H), 3.82 (s, 3H); **^{13}C NMR** (101 MHz, $CDCl_3$): δ 156.6, 129.3, 128.7, 127.0, 126.2, 125.6, 120.9, 110.7, 64.2, 55.4.

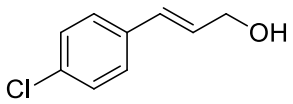

(*E*)-3-(4-Chlorophenyl)prop-2-en-1-ol (3-19). Prepared according to representative procedure A from commercial 4-chlorocinnamaldehyde (415 mg, 2.50 mmol), $NaBH_4$ (94.5 mg, 2.50 mmol): yellow oil (371 mg, 88% crude yield). Spectral data are in accordance with the literature:[29]

^{1}H NMR (400 MHz, $CDCl_3$): δ 7.31–7.26 (m, 4H), 6.56 (dt, *J* = 15.9, 1.4 Hz, 6.31 (dt, *J* = 16.0, 5.6 Hz, 1H), 4.31 (dd, *J* = 5.6, 1.3 Hz, 2H); **^{13}C NMR** (101 MHz, $CDCl_3$): δ 135.3, 133.1, 129.8, 129.1, 128.7, 127.8, 63.5.

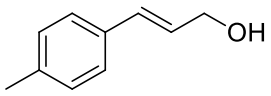

(*E*)-3-(*p*-Tolyl)prop-2-en-1-ol (3-20). Prepared according to representative procedure A from commercial (*E*)-3-(*p*-tolyl)acrylaldehyde (500 mg, 3.40 mmol), $NaBH_4$ (129 mg, 3.40 mmol): yellow oil (468 mg, 93% crude yield). Spectral data are in accordance with the literature:[29] **^{1}H NMR** (400 MHz, $CDCl_3$): δ 7.29 (d, *J* = 8.1 Hz, 2H), 7.13 (d, *J* = 7.9 Hz, 2H), 6.57 (d, *J* = 15.9, 1H), 6.33 (dt, *J* = 15.8, 5.7 Hz, 1H), 4.32 (d, *J* = 5.7 Hz, 2H); **^{13}C NMR** (101 MHz, $CDCl_3$): δ 137.7, 134.0, 131.2, 129.5, 127.4, 126.4, 63.8, 21.3.

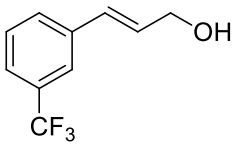

(*E*)-3-(3-(Trifluoromethyl)phenyl)prop-2-en-1-ol (3-21). Prepared according to representative procedure B from commercial 3-(trifluoromethyl)benzaldehyde. Spectral data are in accordance with the literature:[30] **^{1}H NMR** (498 MHz, $CDCl_3$): δ 7.62 (s, 1H), 7.54 (d, *J* = 7.7 Hz, 1H), 7.49 (d, *J* = 7.8 Hz, 1H), 7.43 (t, *J* = 7.7 Hz, 1H), 6.66 (dt, *J* = 15.9, 1.7 Hz, 1H), 6.44 (dt, *J* = 15.9, 5.4 Hz, 1H), 4.36 (dd, *J* = 5.4, 1.6 Hz, 2H).

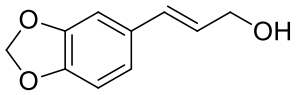

(*E*)-3-(Benzo[*d*][1,3]dioxol-5-yl)prop-2-en-1-ol (3-22). Prepared according to representative procedure B from commercial piperonal. Spectral data are in accordance with the literature:[30] **^{1}H NMR** (498 MHz, $CDCl_3$): δ 6.93 (d, *J* = 1.7 Hz, 1H), 6.82 (dd, *J* = 8.0, 1.7 Hz, 1H), 6.76 (d, *J* = 8.0 Hz, 1H), 6.53 (dt, *J* = 15.8, 1.5 Hz, 1H), 6.20 (dt, *J* = 15.8, 5.9 Hz, 1H), 5.96 (s, 2H), 4.29 (td,

J = 5.9, 1.5 Hz, 2H); **^{13}C NMR** (125 MHz, $CDCl_3$): δ = 148.2, 147.5, 131.2, 131.2, 126.8, 121.3, 108.4, 105.9, 101.2, 63.9.

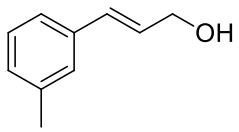

(*E*)-3-(*m*-Tolyl)prop-2-en-1-ol (3-23). Prepared according to representative procedure B from commercial *m*-tolualdehyde. Spectral data are in accordance with the literature:[29] **^{1}H NMR** (400 MHz, $CDCl_3$): δ 7.33–7.11 (m, 3H), 7.08–6.93 (m, 1H), 6.55 (dd, *J* = 15.8, 1.6 Hz, 1H), 6.32 (dt, *J* = 15.9, 6.5 Hz, 1H), 4.28 (d, *J* = 5.7 Hz, 2H), 2.34 (s, 3H); **^{13}C NMR** (101 MHz, $CDCl_3$): δ 138.1, 136.8, 131.1, 128.4, 128.5, 128.6, 127.2, 123.5, 63.6, 21.4.

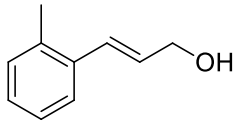

(*E*)-3-(*o*-Tolyl)prop-2-en-1-ol (3-24). Prepared according to representative procedure B from commercial *o*-tolualdehyde. Spectral data are in accordance with the literature:[31] **^{1}H NMR** (498 MHz, $CDCl_3$): δ 7.47–7.42 (m, 1H), 7.19–7.12 (m, 3H), 6.83 (dt, *J* = 15.8, 1.6 Hz, 1H), 6.25 (dt, *J* = 15.7, 5.7 Hz, 1H), 4.34 (td, *J* = 5.8, 1.6 Hz, 2H), 2.35 (s, 3H).

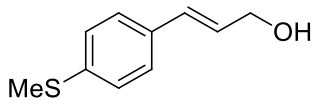

(*E*)-3-(4-(Methylthio)phenyl)prop-2-en-1-ol (3-25). Prepared according to representative procedure B from commercial 4-(Methylthio)benzaldehyde. Spectral data are in accordance with the literature:[32] **^{1}H NMR** (498 MHz, $CDCl_3$): δ 7.32–7.27 (m, 2H), 7.22–7.17 (m, 2H), 6.56 (dt, *J* = 15.9, 1.6 Hz, 1H), 6.32 (dt, *J* = 15.9, 5.8 Hz, 1H), 4.30 (td, *J* = 5.7, 1.6 Hz, 2H), 2.48 (s, 3H).

3.9.3 General Procedure for the Synthesis of Cinnamyl Carbonate Derivatives

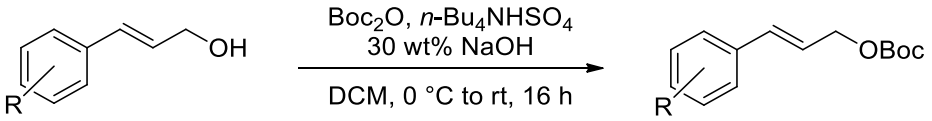

In a round bottom flask equipped with a stir bar, cinnamyl alcohol (500 mg, 3.73 mmol) and DCM (5.00 ml) were added. To the resulting solution, *n*-Bu_4NHSO_4 (25.0 mg, 0.0730 mmol) and Boc_2O (888 mg, 4.07 mmol) at room temperature. The solution was cooled to 0 °C and aqueous solution of NaOH (2.50 mL, 30 wt% solution) was added slowly. The ice-water bath was removed after 10 min and the reaction flask was allowed to stir at room temperature overnight. The reaction mixture was diluted with Et_2O and 1M HCl aqueous solution and was extracted with Et_2O (50 mL × 3). the combined organic layers were washed with water followed by brine and then dried over Na_2SO_4, filtered and then concentrated *in vacuo*. The crude mixture was purified on silica gel (5% Et_2O/ pentane) to afford 646 mg (74%) of a clear oil.

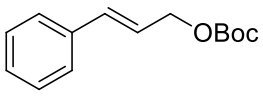

***tert*-Butyl cinnamyl carbonate (3-5a).** The reaction was performed according to the general procedure using commercial cinnamyl alcohol (500 mg, 3.73 mmol), Bu_4NHSO_4 (25.0 mg, 0.0730 mmol), Boc_2O (888 mg, 4.07 mmol) and NaOH (2.50 mL, 30 wt% solution). The crude reaction mixture was purified on silica gel (5% Et_2O/pentane) to afford the product as colorless oil (646 mg, 74% yield). Spectral data are in accordance with the literature:[33] **^{1}H NMR** (498 MHz, $CDCl_3$): δ 7.41–7.37 (m, 2H), 7.35–7.30 (m, 2H), 7.29–7.23 (m, 1H), 6.67 (dt, *J* = 15.9, 1.4 Hz, 1H), 6.30 (dt, *J* = 16.0, 6.4 Hz, 1H), 4.72 (dd, *J* = 6.4, 1.4 Hz, 2H), 1.51 (s, 9H).

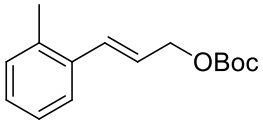

(*E*)-*tert*-Butyl (3-(*o*-tolyl)allyl) carbonate (3-5b). The reaction was performed according to the general procedure using (*E*)-3-(*o*-tolyl)prop-2-en-1-ol (1.48 g, 10.0 mmol), Bu_4NHSO_4 (67.8 mg,

0.200 mmol), Boc_2O (2.62 g, 12.0 mmol) and NaOH (5.00 mL, 30 wt% solution). The crude reaction mixture was purified on a silica plug (5% Et_2O/pentane) to afford the product as a colorless oil (1.69 g, 68% yield). Spectral data are in accordance with the literature:[34] **^{1}H NMR** (500 MHz, $CDCl_3$): δ 7.47–7.40 (m, 1H), 7.22–7.11 (m, 3H), 6.89 (dd, *J* = 15.8, 1.4 Hz, 1H), 6.18 (dt, *J* = 15.6, 6.4 Hz, 1H), 4.74 (dd, *J* = 6.4, 1.4 Hz, 2H), 2.35 (s, 3H), 1.51 (s, 9H); **^{13}C NMR** (125 MHz, $CDCl_3$): δ 153.4, 135.7, 135.4, 132.5, 130.3, 128.0, 126.2, 125.9, 124.3, 82.2, 77.3, 77.3, 77.1, 76.8, 67.72, 27.8, 19.7.

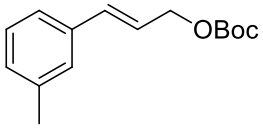

(*E*)-*tert*-Butyl (3-(*m*-tolyl)allyl) carbonate (3-5c). The reaction was performed according to the general procedure using (*E*)-3-(*m*-tolyl)prop-2-en-1-ol (1.63 g, 11.0 mmol), Bu_4NHSO_4 (74.7 mg, 0.220 mmol), Boc_2O (2.64 g, 12.1 mmol) and NaOH (5.00 mL, 30 wt% solution). The crude reaction mixture was purified on a silica plug (5% Et_2O/pentane) to afford the product as a colorless oil (1.94 g, 71% yield). Spectral data are in accordance with the literature:[34] **^{1}H NMR** (500 MHz, $CDCl_3$): δ 7.24–7.16 (m, 3H), 7.11–7.03 (m, 1H), 6.64 (dd, *J* = 15.8, 1.6 Hz, 1H), 6.28 (dt, *J* = 15.9, 6.5 Hz, 1H), 4.71 (dd, *J* = 6.5, 1.3 Hz, 2H), 2.34 (s, 3H), 1.50 (s, 9H); **^{13}C NMR** (125 MHz, $CDCl_3$): δ 153.4, 138.2, 136.2, 134.6, 128.9, 128.5, 127.5, 123.9, 122.8, 82.2, 67.6, 27.8, 21.4.

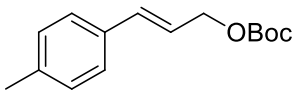

(*E*)-*tert*-Butyl (3-(*p*-tolyl)allyl) carbonate (3-5d). The reaction was performed according to the general procedure using (*E*)-3-(*p*-tolyl)prop-2-en-1-ol (468 mg, 3.16 mmol), Bu_4NHSO_4 (21 mg, 0.063 mmol), Boc_2O (758 mg, 3.48 mmol) and NaOH (2.50 mL, 30 wt% solution). The crude reaction mixture was purified on a silica gel (10% Et_2O/pentane) to afford the product as a white solid (514 mg, 66% yield). Spectral data are in accordance with the literature:[35] **^{1}H NMR** (500 MHz, $CDCl_3$): δ 7.30–7.27 (m, 2H), 7.13 (d, *J* = 7.8 Hz, 2H), 6.64 (dt, *J* = 15.9, 1.4 Hz, 1H), 6.24

(dt, J = 15.8, 6.5 Hz, 1H), 4.71 (dd, J = 6.5, 1.3 Hz, 2H), 2.34 (s, 3H), 1.50 (s, 9H); **^{13}C NMR** (125 MHz, $CDCl_3$): δ 153.4, 138.0, 134.5, 133.4, 129.3, 126.6, 121.8, 82.1, 67.6, 27.8, 21.2.

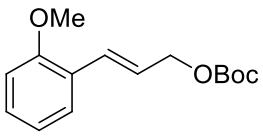

***(E)*-*tert*-Butyl (3-(2-methoxyphenyl)allyl) carbonate (3-5e).** The reaction was performed according to the general procedure using (*E*)-3-(2-methoxyphenyl)prop-2-en-1-ol (985 mg, 6.01 mmol), Bu_4NHSO_4 (42 mg, 0.124 mmol), Boc_2O (1.46 g, 6.70 mmol) and NaOH (4.00 mL, 30 wt% solution). The crude reaction mixture was purified on a silica plug (4% Et_2O/pentane) to afford the product as yellow oil (1.51 g, 95% yield). Spectral data are in accordance with the literature:[36] **^{1}H NMR** (700 MHz, $CDCl_3$): δ 7.42 (dd, J = 7.7, 1.7 Hz, 1H), 7.24 (ddd, J = 8.2, 7.4, 1.7 Hz, 1H), 6.99 (dt, J = 16.0, 1.4 Hz, 1H), 6.92 (td, J = 7.5, 1.0 Hz, 1H), 6.86 (dd, J = 8.2, 1.0 Hz, 1H), 4.73 (dd, J = 6.6, 1.4 Hz, 2H), 3.84 (s, 3H), 1.50 (s, 9H); **^{13}C NMR** (176 MHz, $CDCl_3$): δ 157.0, 153.4, 129.6, 129.2, 127.2, 125.3, 123.5, 120.7, 110.9, 82.1, 68.1, 55.5, 27.8.

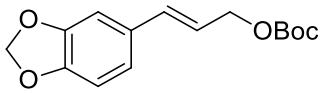

(*E*)-3-(Benzo[*d*][1,3]dioxol-5-yl)allyl *tert*-butyl carbonate (3-5f). The reaction was performed according to the general procedure using (*E*)-3-(benzo[*d*][1,3]dioxol-5-yl)prop-2-en-1-ol (567 mg, 3.18 mmol), Bu_4NHSO_4 (22 mg, 0.063 mmol), Boc_2O (763 mg, 3.50 mmol) and NaOH (2.50 mL, 30 wt% solution). The crude reaction mixture was purified on a silica plug (10% Et_2O/pentane) to afford the product as a colorless oil (533 mg, 64% yield). Spectral data are in accordance with the literature:[10] **^{1}H NMR** (500 MHz, $CDCl_3$): δ 6.91 (d, J = 1.7 Hz, 1H), 6.81 (dd, J = 8.0, 1.7 Hz, 1H), 6.74 (d, J = 8.0 Hz, 1H), 6.56 (dt, J = 15.7, 1.4 Hz, 1H), 6.11 (dt, J = 15.8, 6.6 Hz, 1H), 5.94 (s, 2H), 4.67 (dd, J = 6.6, 1.3 Hz, 2H), 1.49 (s, 9H): **^{13}C NMR** (125 MHz, $CDCl_3$): δ 153.3, 148.0, 147.6, 134.3, 130.6, 121.5, 121.1, 108.3, 105.8, 101.1, 82.1, 67.5, 27.8.

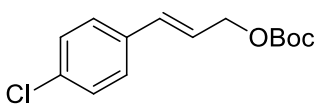

(*E*)-*tert*-Butyl (3-(4-chlorophenyl)allyl) carbonate (3-5h). The reaction was performed according to the general procedure using (*E*)-3-(4-chlorophenyl)prop-2-en-1-ol (371 mg, 2.20 mmol), Bu_4NHSO_4 (14 mg, 0.041 mmol), Boc_2O (528 mg, 2.42 mmol) and NaOH (2.50 mL, 30 wt% solution). The crude reaction mixture was purified on a silica plug (5% Et_2O/pentane) to afford the product as yellow solid (357 mg, 60% yield). Spectral data are in accordance with the literature:[10] **^{1}H NMR** (400 MHz, $CDCl_3$): δ 7.37–7.23 (m, 4H), 6.62 (dt, *J* = 15.9, 1.4 Hz, 1H), 6.26 (dt, *J* = 15.9, 6.4 Hz, 1H), 4.71 (dd, *J* = 6.4, 1.3 Hz, 2H), 1.50 (s, 9H); **^{13}C NMR** (101 MHz, $CDCl_3$): δ 153.3, 134.8, 133.8, 133.1, 128.8, 127.9, 123.7, 82.4, 67.2, 27.8.

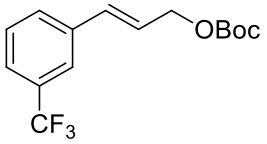

(*E*)-*tert*-Butyl (3-(3-(trifluoromethyl)phenyl)allyl) carbonate (3-5i). The reaction was performed according to the general procedure using (*E*)-3-(3-(trifluoromethyl)phenyl)prop-2-en-1-ol. (485 mg, 2.40 mmol), Bu_4NHSO_4 (16.0 mg, 0.0480 mmol), Boc_2O (575 mg, 2.64 mmol) and NaOH (2.00 mL, 30 wt% solution). The crude reaction mixture was purified on a silica plug (5% Et_2O/pentane) to afford the product as a yellow oil (482 mg, 67% yield). Spectral data are in accordance with the literature:[35] **^{1}H NMR** (700 MHz, $CDCl_3$): δ 7.62 (d, *J* = 1.7 Hz, 1H), 7.55 (d, *J* = 7.6 Hz, 1H), 7.52–7.49 (m, 1H), 7.44 (t, *J* = 7.8 Hz, 1H), 6.70 (dt, *J* = 15.8, 1.5 Hz, 1H), 6.36 (dt, *J* = 15.9, 6.2 Hz, 1H), 4.74 (dd, *J* = 6.2, 1.5 Hz, 2H), 1.51 (s, 9H); **^{13}C NMR** (176 MHz, $CDCl_3$): δ 153.3, 137.1, 132.6, 131.4, 131.2, 131.0, 130.9, 129.8, 129.1, 125.1, 124.8, 124.6, 123.4, 82.5, 67.0, 27.8.

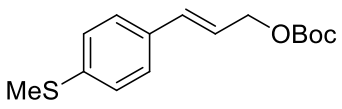

(*E*)-*tert*-Butyl (3-(4-(methylthio)phenyl)allyl) carbonate (3-5j). The reaction was performed according to the general procedure using (*E*)-3-(4-(methylthio)phenyl)prop-2-en-1-ol (900 mg,

5.00 mmol), Bu_4NHSO_4 (33.9 mg, 0.100 mmol), Boc_2O (1.20 g, 5.50 mmol) and NaOH (4.00 mL, 30 wt% solution). The crude reaction mixture was purified on a silica gel (10% Et_2O/pentane) to afford the product as a white solid (1.17 g, 82% yield): **m.p.** = 56.5-58.3 °C; **^{1}H NMR** (399.794 MHz, $CDCl_3$): δ 7.31 (d, *J* = 8.4 Hz, 2H), 7.20 (d, *J* = 8.4 Hz, 2H), 6.62 (d, *J* = 15.9 Hz, 1H), 6.25 (dt, *J* = 15.9, 6.5 Hz, 1H), 4.71 (dd, *J* = 6.5, 1.3 Hz, 2H), 2.48 (s, 3H), 1.50 (s, 9H); **^{13}C NMR** (100.539 MHz, $CDCl_3$): δ 152.9, 138.1, 133.5, 132.7, 126.6, 126.1, 121.9, 81.8, 67.1, 27.4, 15.3; **IR** (microscope, cm^{-1}) 3074, 2980, 2923, 1739, 1477, 1274, 1254, 1161; **HRMS** (ESI-TOF): For $C_{15}H_{20}NaO_3S$ $(M + Na)^+$: calcd. 303.1025; found 303.1025.

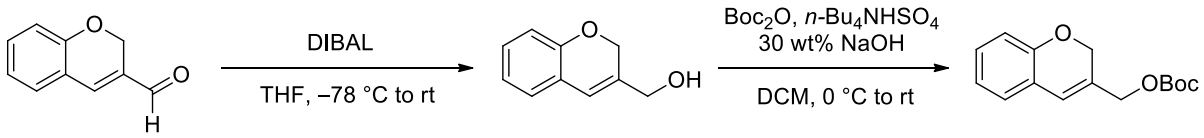

(2*H*-Chromen-3-yl)methyl *tert*-butyl carbonate (3-5g). To a stirred solution of 2*H*-chromene-3-carbaldehyde (400 mg, 2.50 mmol) in THF (8 mL), DIBAL (7.00 mL, 1.10 M solution in hexane, 7.70 mmol, 3.10 equiv) was added dropwise at –78 °C and kept stirring for 1 h. The reaction was quenched with MeOH and kept stirring for another hour and filtered through a pad of celite. The filtrate was concentrated *in vacuo* to give the allylic alcohol which was used with no further purification in the next step. In a round bottom flask equipped with a stir bar, the alcohol intermediate (2.50 mmol) and DCM (5.00 ml) were added. To the resulting solution, *n*-Bu_4NHSO_4 (17.0 mg, 0.0500 mmol) and Boc_2O (655 mg, 3.00 mmol) at room temperature. The solution was cooled to 0 °C and aqueous solution of NaOH (1.40 mL, 30 wt% solution) was added slowly. The ice-water bath was removed after 10 min and the reaction flask was allowed to stir at room temperature overnight. The reaction mixture was diluted with Et_2O and 1M HCl aqueous solution and was extracted with Et_2O (50 mL × 3). the combined organic layers were washed with water followed by a brine wash and then dried over Na_2SO_4, filtered and then concentrated *in vacuo*. The crude mixture was purified on silica gel (5% Et_2O/pentane) to afford 472 mg (72%) of a yellow oil: **^{1}H NMR** (500 MHz, $CDCl_3$): δ 7.12 (td, *J* = 7.9, 1.6 Hz, 1H), 6.99 (dd, *J* = 7.5, 1.6 Hz, 1H), 6.87 (td, *J* = 7.4, 1.1 Hz, 1H), 6.79 (d, *J* = 8.1 Hz, 1H), 6.46 (s, 1H), 4.80 (s, 22H), 4.63 (s, 2H),

1.50 (s, 9H); **^{13}C NMR** (126 MHz, $CDCl_3$): δ 153.5, 153.4, 129.6, 128.2, 127.0, 123.5, 121.8, 121.5, 115.7, 82.7, 67.1, 66.3, 27.8; **IR** (microscope, cm^{-1}) 2980, 2935, 1742, 1487, 1369, 1282 1254 1161; **HRMS** (ESI-TOF): For $C_{15}H_{18}NaO_4$ $(M + Na)^+$: calcd. 285.1097; found 285.1094.

3.9.4 General Procedure for the Synthesis of Benzylic Allylic Secondary Carbonates

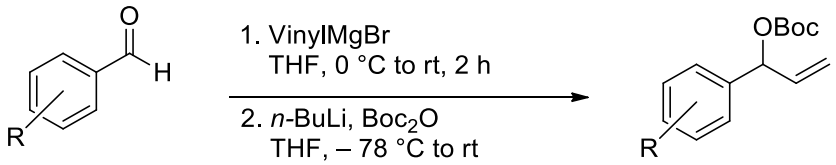

Representative Procedure A: In a flamed dried round bottom flask equipped with a stir bar under nitrogen atmosphere, *p*-tolyl aldehyde (600 mg, 5.0 mmol) was dissolved in 20 mL of THF, and the solution was kept stirring at 0 °C for 10 minutes. Vinylmagnesium bromide solution in THF (6.5 mL, 1.0 M, 1.3 equiv) was added to the solution dropwise over 10 min. The reaction was then warmed to room temperature and stirred for 2 h. The reaction mixture was quenched with NH_4Cl (20 mL) and extracted with EtOAc (50 × 3 mL). The organic layers were washed with brine, dried with Na_2SO_4, filtered, and concentrated *in vacuo*. The concentrated crude mixture was then transferred into a round bottom flask charged with a stir bar and mixed with THF (20 mL). The solution was cooled down to –78 °C and *n*-BuLi in THF (2.2 mL, 2.5 M, 1.1 equiv) was added dropwise. The solution stirred for 30 minutes, then Boc_2O (1.6 g, 7.5 mmol, 1.5 equiv) was added. The reaction mixture was warmed to room temperature and kept stirred for 16 h. The reaction was quenched with water (20 mL) and extracted with Et_2O (50 mL × 3). The combined organic layers were washed with brine, dried with Na_2SO_4, filtered, and concentrated *in vacuo*. The crude mixture was purified on silica gel (5% Et_2O/ pentane) to afford 820 mg (66%) of a clear oil.

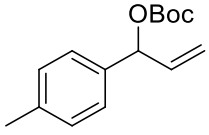

***tert*-Butyl (1-(*p*-tolyl)allyl) carbonate (3-5d′).** The reaction was performed according to the representative procedure A using *p*-tolyl aldehyde (601 mg, 5.00 mmol), Vinylmagnesium bromide solution in THF (6.5 mL, 1 M, 1.3 equiv), nBuLi in THF (2.2 mL, 2.5 M, 1.1 equiv), and Boc_2O (1.6 g, 7.5 mmol, 1.5 equiv) The crude product was purified on silica gel (5% Et_2O/pentane) to afford 820 mg (66%) of a clear oil. Spectral data are in accordance with the literature:[37] **^{1}H NMR** (500 MHz, $CDCl_3$): δ ppm 7.31–7.25 (m, 2H), 7.16 (d, *J* = 7.8 Hz, 2H), 6.10–5.94 (m, 2H), 5.36–5.30 (m, 1H), 5.26–5.19 (m, 1H), 2.35 (s, 3H), 1.48 (s, 9H).

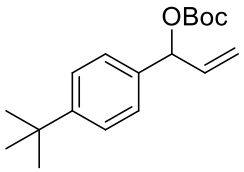

***tert*-Butyl (1-(4-(*tert*-butyl)phenyl)allyl) carbonate (3-5k′).** The reaction was performed according to the representative procedure A using 4-(*tert*-butyl)benzaldehyde (810 mg, 5.00 mmol), Vinylmagnesium bromide solution in THF (6.5 mL, 1.0 M, 1.3 equiv), nBuLi in THF (2.2 mL, 2.5 M, 1.1 equiv), and Boc_2O (1.6 g, 7.5 mmol, 1.5 equiv) The crude product was purified on silica gel (5% Et_2O/pentane) to afford 790 mg (54%) of a white solid. Spectral data are in accordance with the literature:[38] **1H NMR** (500 MHz, $CDCl_3$): δ 7.41 (d, *J* = 8.4 Hz, 2H), 7.34 (d, *J* = 8.4 Hz, 2H), 6.11–6.03 (m, 2H), 5.36 (d, *J* = 16.4 Hz, 1H), 5.27 (d, *J* = 10.5 Hz, 1H), 1.51 (s, 9H), 1.35 (s, 9H); **13C NMR** (126 MHz, $CDCl_3$): δ 152.6, 151.2, 136.4, 135.8, 126.7, 125.5, 116.8, 82.2, 79.0, 34.7, 31.3, 27.9.

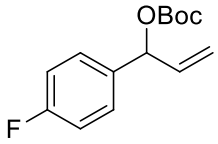

***tert*-Butyl (1-(4-fluorophenyl)allyl) carbonate (3-5l′).** The reaction was performed according to the representative procedure A using 4-fluorobenzaldehyde (620 mg, 5.00 mmol), Vinylmagnesium bromide solution in THF (6.5 mL, 1.0 M, 1.3 equiv), nBuLi in THF (2.2 mL, 2.5 M, 1.1 equiv), and Boc_2O (1.6 g, 7.5 mmol, 1.5 equiv) The crude mixture was purified on silica

gel (5% Et_2O/pentane) to afford 770 mg (61%) of a clear oil. Spectral data are in accordance with the literature:[39] **^{1}H NMR** (400 MHz, $CDCl_3$): δ 7.39–7.31 (m, 2H), 7.08–6.99 (m, 2H), 6.07–5.94 (m, 2H), 5.35–5.21 (m, 2H), 1.47 (s, 9H).

3.9.5 Synthesis of Allyl Piperidinyl Boronate

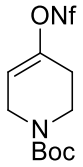

***tert*-Butyl 4-(((perfluorobutyl)sulfonyl)oxy)-5,6-dihydropyridine-1(2*H*)-carboxylate (3-1).** In a flame dried round bottom flask equipped with a stir bar, 1-Boc-4-piperidone (5.0 g, 25 mmol) was dissolved in THF (125 mL) under a nitrogen atmosphere. The solution was cooled down to 0 °C using an ice-bath and stirred for 5 min. DBU (4.5 mL, 30 mmol) and perfluorobutanesulfonyl fluoride (5.4 mL, 30 mmol) were added respectively. The ice-bath was removed, and the solution was allowed to stir at room temperature overnight. The reaction mixture was quenched by slow addition of water and extracted with Et_2O (100 mL × 3). the organic layers were washed with brine, dried over Na_2SO_4, filtered and concentrated *in vacuo*. The brown crude oil was then purified by silica gel (15% Et_2O/pentane). Spectral data are in accordance with the literature:[4] **^{1}H NMR** (400 MHz, $CDCl_3$): δ 5.77 (s, 1H), 4.11–3.99 (m, 2H), 3.63 (t, J = 5.7 Hz, 2H), 2.48–2.39 (m, 2H), 1.47 (s, 9H).

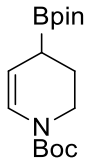

***tert*-Butyl 4-(4,4,5,5-tetramethyl-1,3,2-dioxaborolan-2-yl)-3,4-dihydropyridine-1(2*H*)-carboxylate ((*rac*)-3-3)**. In a flame dried round bottom flask equipped with a stir bar, palladium acetate (54 mg, 0.24 mmol) and DPEphos (140 mg, 0.26 mmol) were mixed with freshly distilled Et_2O (24 mL) and stirred at room temperature for 10 min. DIPEA (1.5 mL, 8.8 mmol),

pinacolborane (1.3 mL, 8.8 mmol) and *tert*-butyl-4-(nonafluorobutylsulfonyloxy)-5,6-dihydropyridine-1(*2H*)-carboxylate **3-1** (3.9 g, 8.0 mmol) were added respectively, and the mixture was stirred at room temperature for 16 h. The mixture was filtered through a short silica plug (100% Et_2O) and concentrated *in vacuo*, the crude mixture was purified by silica gel (15% Et_2O/pentane) which provided the allylic boronate as a colorless oil (1.66 g, 67% yield). Spectral data are in accordance with the literature:[4] **^{1}H NMR** (700 MHz, $CDCl_3$, rotamers are present): δ 6.84–6.71 (m, 1H), 5.02–4.76 (m, 1H), 3.62–3.44 (m, 2H), 1.92–1.77 (m, 3H), 1.45 (s, 9H), 1.21 (s, 12H); **^{13}C NMR** (176 MHz, $CDCl_3$, rotamers are present): δ 152.7, 152.3, 124.5, 124.2, 106.3, 105.8, 83.4, 83.4, 80.3, 80.2, 42.4, 41.3, 28.4, 24.8, 24.7, 23.3, 18.3.

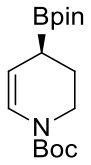

(*4S*)-*tert*-Butyl 4-(4,4,5,5-tetramethyl-1,3,2-dioxaborolan-2-yl)-3,4-dihydropyridine-1(*2H*)-carboxylate (*(S)*-3-3). In a flame dried round bottom flask equipped with a stir bar, palladium acetate (25 mg, 0.11 mmol) and (+)-Taniaphos (110 mg, 0.17 mmol) were mixed with CPME (12 mL) and stirred at room temperature for 10 min. *N*,*N*-dimethylaniline (510 µL, 4.1 mmol), pinacolborane (590 µL, 4.1 mmol) and *tert*-butyl-4-(nonafluorobutylsulfonyloxy)-5,6-dihydropyridine-1(*2H*)-carboxylate **3-1** (1.8 g, 3.7 mmol) were added respectively, and the mixture was stirred at room temperature for 16 h. The mixture was filtered through a short silica plug (100% Et_2O) and concentrated *in vacuo*, the crude mixture was purified by silica gel (15% Et_2O/pentane) which provided the allylic boronate as a colorless oil (910 mg, 79% yield). Spectral data are in accordance with the literature:[4] **^{1}H NMR** (700 MHz, $CDCl_3$, rotamers are present): δ 6.84–6.71 (m, 1H), 5.02–4.76 (m, 1H), 3.62–3.44 (m, 2H), 1.92–1.77 (m, 3H), 1.45 (s, 9H), 1.21 (s, 12H); **^{13}C NMR** (176 MHz, $CDCl_3$, rotamers are present): δ 152.7, 152.3, 124.5, 124.2, 106.3, 105.8, 83.4, 83.4, 80.3, 80.2, 42.4, 41.3, 28.4, 24.8, 24.7, 23.3, 18.3.

3.9.6 Substrate Scope of the Allyl-Ally Cross-Coupling Reaction

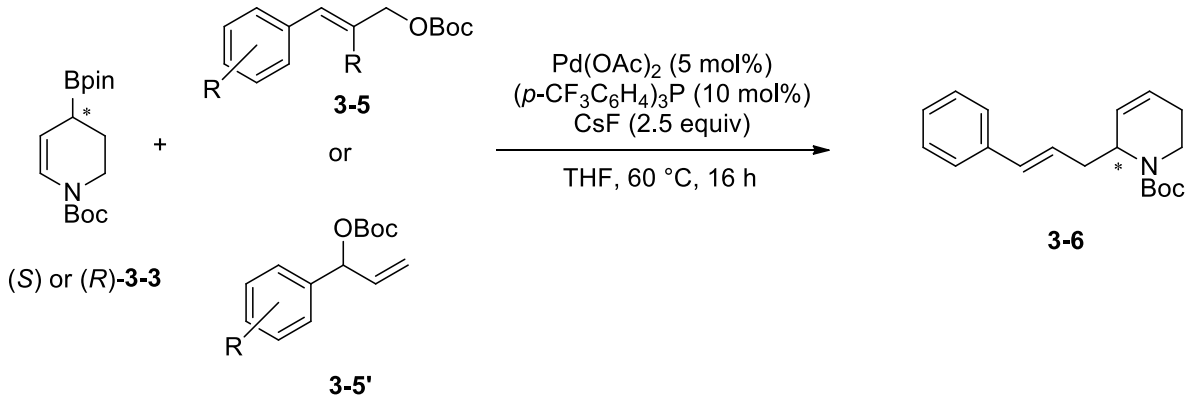

Example procedure A. In a flame dried sealed tube equipped with a stir bar, palladium acetate (2.2 mg, 0.010 mmol), tris(4-trifluoromethylphenyl)phosphine (9.3 mg, 0.020 mmol) and cesium fluoride (76 mg, 0.50 mmol) were mixed with THF under an argon atmosphere and stirred for 5 min. Then, (*E*)-*tert*-butyl (3-(2-methoxyphenyl)allyl) carbonate **3-5**e (53 mg, 0.20 mmol) and (*S*) or (*R*) allylic boronate **3-3** (74 mg, 0.24 mmol) were added respectively. The reaction tube was sealed and heated to 60 °C and kept stirring for 16 h. The reaction mixture was filtered through a silica plug (100% Et_2O) and concentrated *in vacuo*. The crude product was purified by silica gel (0-5% Et_2O/pentane) to afford the product as a colorless oil (16 mg, 25%).

Example procedure B. In a glovebox, palladium acetate (2.2 mg, 0.010 mmol), tris(4-trifluoromethylphenyl)phosphine (9.3 mg, 0.020 mmol) and cesium fluoride (76 mg, 0.50 mmol) were mixed with THF under an argon atmosphere in an oven dried sealed reaction tube and stirred for 5 min. Then, (*E*)-*tert*-butyl (3-(4-(methylthio)phenyl)allyl) carbonate **3-5j** (56 mg, 0.20 mmol) and (*S*) or (*R*) allylic boronate **3-3** (74 mg, 0.24 mmol) were added respectively. The reaction tube was sealed, taken out of the glovebox and heated to 60 °C and kept stirring for 16 h. The reaction mixture was filtered through a silica plug (100% Et_2O) and concentrated *in vacuo*. The crude mixture was purified by silica gel (0-5% Et_2O/pentane) to afford the product as a colorless oil (41 mg, 59%).

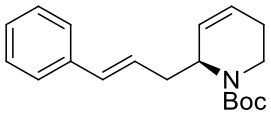

***(S)-tert*-Butyl 2-cinnamyl-5,6-dihydropyridine-1(2*H*)-carboxylate (3-6a).** Prepared by example procedure A using *tert*-butyl cinnamyl carbonate **3-5a** (47 mg, 0.50 mmol) and of (*S*)-**3-3** (74 mg, 0.60 mmol). Flash chromatography afforded the product as a clear oil (100 mg, 68%): **^{1}H NMR** (500 MHz, $CDCl_3$), rotamers are present: δ 7.34 (d, *J* = 7.5 Hz, 2H), 7.29 (t, *J* = 8.0 Hz, 2H), 7.20 (t, *J* = 8.0 Hz, 1H), 6.41 (d, *J* = 16.0 Hz, 1H), 6.24 (br s, 1H), 5.86 (br s, 1H), 5.71 (br s, 1H), 4.70–4.34 (m, 1H), 4.30–3.92 (m, 1H), 2.88 (br s, 1H), 2.48 (t, *J* = 6.0 Hz, 2H), 2.20 (br s, 1H), 1.96 (d, *J* = 16.2 Hz, 1H), 1.43 (s, 9H); **^{13}C NMR** (126 MHz, $CDCl_3$), rotamers are present: δ 154.6, 137.5, 132.2, 128.5, 128.0, 127.1, 126.6, 126.1, 125.8, 79.5, 52.7, 38.0, 36.4, 28.7, 24.9; **IR** (microscope, cm^{-1}) 3027, 3006, 2974, 2928, 1693, 1416, 1364, 1171, 1109; **HRMS** (ESI-TOF): for $C_{19}H_{25}NNaO_2$ $(M + Na)^+$: calcd. 322.1778; found 322.1777; **[α]$_D^{20}$**: 123 (*c* = 1.04, CH_2Cl_2); **HPLC** (Chiralpak IC) 2:98 iso-propanol:hexanes, 0.5 mL/min, 20 °C, λ = 280 nm, T_{minor} = 9.7 min, T_{major} = 11.4 min, er = 93.0:7.0.

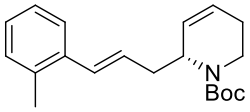

***(R,E)-tert*-Butyl 2-(3-(*o*-tolyl)allyl)-5,6-dihydropyridine-1(2*H*)-carboxylate (3-6b).** Prepared by example procedure A using (*E*)-*tert*-butyl (3-(*o*-tolyl)allyl) carbonate **3-5b** (50 mg, 0.20 mmol) and (*R*)-**3-3** (74 mg, 0.24 mmol). Flash chromatography afforded the product as a yellow oil (40 mg, 65%): **^{1}H NMR** (500 MHz, $CDCl_3$), rotamers are present: δ 7.40 (dd, *J* = 6.0, 1.5 Hz, 1H), 7.20–7.09 (m, 3H), 6.61 (d, *J* = 16.0 Hz, 1H), 6.16–6.00 (m, 1H), 6.87 (br s, 1H), 5.73 (br s, 1H), 4.66–4.35 (m, 1H), 4.30–3.95 (m, 1H), 2.87 (br s, 1H), 2.50 (t, *J* = 5.0 Hz, 2H), 2.30 (s, 3H), 2.20 (br s, 1H), 1.96 (d, *J* = 17.3 Hz, 1H), 1.44 (s, 9H); **^{13}C NMR** (126 MHz, $CDCl_3$), rotamers are present: δ 154.6, 136.6, 135.0, 130.1, 127.9, 127.1, 126.0, 125.7, 79.5, 52.8, 51.5, 38.5, 36.4, 28.6, 25.0, 19.8.; **IR** (microscope, cm^{-1}) 3064, 3017, 2974, 2926, 2869, 2838, 1694, 1416, 1364, 1172,

1110, 761; **HRMS** (ESI-TOF): For $C_{20}H_{27}NNaO_2$ $(M + Na)^+$: calcd. 336.1934; found 336.1935; **[α]D^{20}**: –95.7 (*c* = 1.53, CH_2Cl_2); **HPLC** (Chiralpak IA) 2:98 iso-propanol:hexanes, 0.5 mL/min, 20 °C, λ = 254 nm, T_{major} = 11.0 min, T_{minor} = 11.8 min, er = 94.3:5.7.

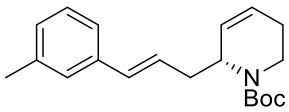

***(R,E)-tert*-Butyl 2-(3-(*m*-tolyl)allyl)-5,6-dihydropyridine-1(2*H*)-carboxylate (3-6c).** Prepared by example procedure A using (*E*)-*tert*-butyl (3-(*m*-tolyl)allyl) carbonate **3-5c** (50 mg, 0.20 mmol) and (*R*)-**3-3** (74 mg, 0.24 mmol). Flash chromatography afforded the product as a yellow oil (48 mg, 76%): **^{1}H NMR** (500 MHz, $CDCl_3$), rotamers are present: δ 7.21–7.11 (m, 3H), 7.02 (d, *J* = 7.0 Hz, 1H), 6.38 (d, *J* = 15.0 Hz, 1H), 6.28–6.11 (m, 1H), 5.86 (br s, 1H), 5.70 (br s, 1H), 4.65–4.35 (m, 1H), 4.28–3.90 (m, 1H), 2.88 (br s, 1H), 2.46 (t, *J* = 6.5, 2H), 2.33 (s, 3H), 2.20 (br s, 1H), 1.96 (d, *J* = 15.9 Hz, 1H), 1.45 (s, 9H); **^{13}C NMR** (126 MHz, $CDCl_3$), rotamers are present: δ 154.6, 138.0, 137.5, 132.3, 128.4, 128.1, 127.9, 126.8, 126.4, 125.8, 123.3, 79.6, 52.6, 38.1, 36.2, 28.5, 24.9, 21.4; **IR** (microscope, cm^{-1}) 3030, 2974, 2926, 2870, 1693, 1416, 1364, 1171, 1110, 771; **HRMS** (ESI-TOF): For $C_{20}H_{27}NNaO_2$ $(M + Na)^+$: calcd. 336.1934; found 336.1934; **[α]D^{20}**: –9.3 (*c* = 1.8, CH_2Cl_2); **HPLC** (Chiralpak IC) 2:98 iso-propanol:hexanes, 0.5 mL/min, 20 °C, λ = 280 nm, T_{major} = 11.8 min, T_{minor} = 11.7 min, er = 94.8:5.2.

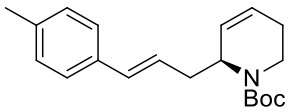

(*S,E*)-*tert*-Butyl 2-(3-(*p*-tolyl)allyl)-5,6-dihydropyridine-1(2*H*)-carboxylate (3-6d). Prepared by example procedure A using (*E*)-*tert*-butyl (3-(*p*-tolyl)allyl) carbonate **3-5d** (50 mg, 0.20 mmol) and (*S*)-**3-3** (74 mg, 0.24 mmol). Flash chromatography afforded the product as a yellow oil (40 mg, 63%): **^{1}H NMR** (500 MHz, $CDCl_3$), rotamers are present: δ 7.23 (d, *J* = 7.5 Hz, 2H), 7.10 (d, *J* = 7.5 Hz, 2H), 6.38 (d, *J* = 15.5 Hz, 1H), 6.16 (br s, 1H), 5.86 (br s, 1H), 5.70 (br s, 1H), 4.68–4.34 (m, 1H), 4.29–3.94 (m, 1H), 2.87 (br s, 1H), 2.47 (t, *J* = 7.3, 2H), 2.32 (s, 3H), 2.20 (br

s, 1H), 1.96 (d, *J* = 17.4 Hz, 1H), 1.44 (s, 9H); **^{13}C NMR** (126 MHz, $CDCl_3$), rotamers are present: δ 154.5, 138.8, 134.7, 132.0, 129.1, 128.1, 125.9, 125.7, 125.5, 79.5, 52.7, 38.0, 36.3, 28.7, 25.1, 21.2; **IR** (microscope, cm^{-1}) 3022, 3006, 2974, 2924, 1693, 1417, 1171, 967; **HRMS** (ESI-TOF): For $C_{20}H_{27}NNaO_2$ $(M + Na)^+$: calcd. 336.1934; found 336.1932; **[α]$_D^{20}$**: 129 (*c* = 0.540, CH_2Cl_2); **HPLC** (Chiralpak IC) 2:98 iso-propanol:hexanes, 0.5 mL/min, 20 °C, λ = 280 nm, T_{minor} = 10.3 min, T_{major} = 12.4 min, er = 93.0:7.0.

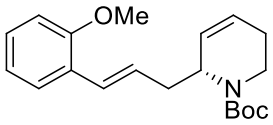

***(R,E)-tert*-Butyl 2-(3-(2-methoxyphenyl)allyl)-5,6-dihydropyridine-1(2*H*)-carboxylate (3-6e).** Prepared by example procedure A using (*E*)-*tert*-butyl (3-(2-methoxyphenyl)allyl) carbonate **3-5e** (53 mg, 0.20 mmol) and (*R*)-**3-3** (74 mg, 0.24 mmol). Flash chromatography afforded the product as a clear oil (17 mg, 25%): **^{1}H NMR** (500 MHz, $CDCl_3$), rotamers are present: δ 7.41 (dd, *J* = 8.0, 1.5 Hz, 1H), 7.18 (td, *J* = 7.8, 1.5 Hz, 1H), 6.90 (t, *J* = 7.5 Hz, 1H), 6.85 (d, *J* = 8.0 Hz, 1H), 6.73 (d, *J* = 15.0 Hz, 1H), 6.22 (dt, *J* = 16.0, 7.0 Hz), 6.85 (br s, 1H), 5.72 (br s, 1H), 4.65–4.33 (m, 1H), 4.30–3.94 (m, 1H), 3.83 (s, 3H), 2.90 (br s, 1H), 2.50 (t, *J* = 6.5 Hz, 2H), 2.20 (br s, 1H), 1.96 (d, *J* = 15.6 Hz, 1H), 1.45 (s, 9H); **^{13}C NMR** (126 MHz, $CDCl_3$), rotamers are present: δ 156.4, 154.6, 128.1, 127.2, 126.8, 126.6, 125.6, 120.6, 110.9, 79.4, 55.5, 52.7, 38.4, 36.4, 28.6, 25.1; **IR** (microscope, cm^{-1}) 3012, 2975, 2930, 1692, 1491, 1367, 756; **HRMS** (ESI-TOF): For $C_{20}H_{27}NNaO_3$ $(M + Na)^+$: calcd. 352.1883; found 352.1880; **[α]$_D^{20}$**: 11.3 (*c* = 0.710, CH_2Cl_2); **HPLC** (Chiralpak IC) 2:98 iso-propanol:hexanes, 0.5 mL/min, 20 °C, λ = 254 nm, T_{major} = 16.9 min, T_{minor} = 20.7 min, er = 92.7:7.3.

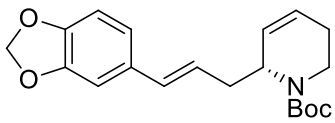

(*R,E*)-*tert*-Butyl 2-(3-(benzo[*d*][1,3]dioxol-5-yl)allyl)-5,6-dihydropyridine-1(2*H*)-carboxylate (3-6f). Prepared by example procedure A using (*E*)-3-(benzo[*d*][1,3]dioxol-5-yl)allyl *tert*-butyl

carbonate **3-5f** (56 mg, 0.20 mmol) and (*R*)-**3-3** (74 mg, 0.24 mmol). Flash chromatography afforded the product as a pale-yellow oil (43 mg, 43.3%): **^{1}H NMR** (500 MHz, $CDCl_3$), rotamers are present: δ 6.88 (d, *J* = 1.4 Hz, 1H), 6.78–6.69 (m, 2H), 6.31 (d, *J* = 15.7 Hz, 1H), 6.04 (br s, 1H), 5.93 (s, 2H), 5.85 (br s, 1H), 5.69 (br s, 1H), 4.62–4.31 (m, 1H), 4.27–3.90 (m, 1H), 2.85 (br s, 1H), 2.44 (t, *J* = 6.7 Hz, 2H), 2.19 (br s, 1H), 1.95 (d, *J* = 16.5 Hz, 1H), 1.44 (s, 9H); **^{13}C NMR** (126 MHz, $CDCl_3$), rotamers are present: δ 154.6, 147.9, 146.8, 132.2, 131.7, 128.6, 128.2, 125.7, 124.9, 120.5, 108.2, 105.6, 100.9, 79.5, 52.6, 51.5, 37.9, 36.4, 28.6, 28.5, 25.0; **IR** (microscope, cm^{-1}) 3031, 2975, 2926, 2838, 1689, 1490 1416, 1248, 1170, 1039, 813, 768; **HRMS** (ESI-TOF): For $C_{20}H_{25}NNaO_4$ $(M + Na)^+$: calcd. 366.1676; found 366.1676; **$[\alpha]_D^{20}$**: –4.0 (*c* = 1.2, CH_2Cl_2); **HPLC** (Chiralpak IC) 2:98 iso-propanol:hexanes, 0.5 mL/min, 20 °C, λ = 254 nm, T_{major} = 17.2 min, T_{minor} = 18.3 min, er = 95.4:4.6.

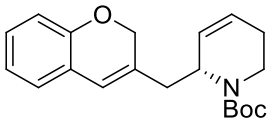

***(R)-tert*-Butyl 2-((2*H*-chromen-3-yl)methyl)-5,6-dihydropyridine-1(2*H*)-carboxylate (3-6g).** Prepared by general example A using (2*H*-chromen-3-yl)methyl *tert*-butyl carbonate (52 mg, 0.20 mmol) **3-5g** and (*R*)-**3-3** (74 mg, 0.24 mmol). Flash chromatography afforded the product as a clear oil (49.1 mg, 75%): **^{1}H NMR** (500 MHz, $CDCl_3$), rotamers are present: δ 7.05 (t, *J* = 8.0 Hz, 1H), 6.91 (dd, *J* = 7.0, 1.0 Hz, 1H), 6.83 (t, *J* = 7.0 Hz, 1H), 6.76 (d, *J* = 8.0 Hz, 1H), 6.19 (s, 1H), 5.87 (br s, 1H), 5.70 (br s, 1H), 4.76 (s, 2H), 4.65–4.35 (m, 1H), 4.30–3.90 (m, 1H), 2.87 (br s, 1H), 2.46–2.12 (m, 3H), 1.97 (d, *J* = 15.7 Hz, 1H), 1.43 (s, 9H); **^{13}C NMR** (126 MHz, $CDCl_3$), rotamers are present: δ 154.4, 152.9, 131.1, 128.5, 127.6, 126.1, 122.7, 121.8, 121.3, 115.3, 79.9, 68.3, 50.9, 38.3, 35.9, 28.4, 25.0; **IR** (microscope, cm^{-1}) 3031, 2974, 2928, 2870, 1691, 1417, 1365, 1240, 1170, 902; **HRMS** (ESI-TOF): For $C_{20}H_{25}NNaO_3$ $(M + Na)^+$: calcd. 350.1727; found 350.1721; **$[\alpha]_D^{20}$**: –8.5 (*c* = 0.47, CH_2Cl_2); **HPLC** (Chiralpak IC) 5:95 iso-propanol:hexanes, 0.5 mL/min, 20 °C, λ = 280 nm, T_{major} = 13.9 min, T_{minor} = 14.9 min, er = 92.5:7.5.

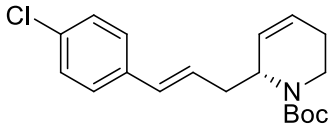

(*R*,*E*)-*tert*-Butyl 2-(3-(4-chlorophenyl)allyl)-5,6-dihydropyridine-1(2*H*)-carboxylate (3-6h). Prepared by general example A using (*E*)-*tert*-butyl (3-(4-chlorophenyl)allyl) carbonate **3-5h** (54 mg, 0.20 mmol) and (*R*)-**3-3** (74 mg, 0.24 mmol). Flash chromatography afforded the product as a pale-yellow oil (44.1 mg, 66%): **^{1}H NMR** (500 MHz, $CDCl_3$), rotamers are present: δ 7.24 (s, 4H), 6.34 (d, *J* = 15.5 Hz, 1H), 6.20 (br s, 1H), 5.85 (br s, 1H), 5.68 (br s, 1H), 4.66–4.32 (m, 1H), 4.29–3.90 (m, 1H), 2.85 (br s, 1H), 2.45 (t, *J* = 6.5 Hz, 2H), 2.19 (br s, 1H), 1.95 (d, *J* = 16.0 Hz, 1H), 1.42 (s, 9H); **^{13}C NMR** (126 MHz, $CDCl_3$), rotamers are present: δ 154.6, 135.9, 132.6, 130.9, 128.6, 127.9, 127.5, 127.3, 126.0, 79.6, 52.7, 38.1, 36.3, 28.5, 24.9; **IR** (microscope, cm^{-1}) 3004, 2974, 2927, 1694, 1417, 1365, 1171, 816; **HRMS** (ESI-TOF): For $C_{19}H_{24}ClNNaO_2$ $(M + Na)^+$: calcd. 356.1388; found 356.1390; **$[\alpha]_D^{20}$**: –4.5 (*c* = 0.63, CH_2Cl_2); **HPLC** (Chiralpak IC) 2:98 iso-propanol:hexanes, 0.5 mL/min, 20 °C, λ = 254 nm, T_{major} = 9.7 min, T_{minor} = 10.4 min, er = 94.9:5.1.

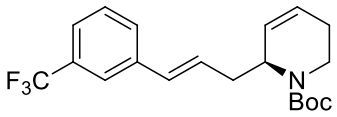

(*S*,*E*)-*tert*-Butyl 2-(3-(3-(trifluoromethyl)phenyl)allyl)-5,6-dihydropyridine-1(2*H*)-carboxylate (3-6i). Prepared by example procedure B using (*E*)-*tert*-butyl (3-(3-(trifluoromethyl)phenyl)allyl) carbonate **3-5i** (61 mg, 0.20 mmol) and (*S*)-**3-3** (74 mg, 0.24 mmol). Flash chromatography afforded the product as a pale-yellow oil (29 mg, 40%): **^{1}H NMR** (500 MHz, $CDCl_3$), rotamers are present: δ 7.58 (s, 1H), 7.49 (d, *J* = 7.5 Hz, 1H), 7.44 (d, *J* = 7.3 Hz, 1H), 7.39 (t, *J* = 7.6 Hz, 1H), 6.42 (d, *J* = 15.8 Hz, 1H), 6.37–6.25 (m, 1H), 5.87 (br s, 1H), 5.69 (br s, 1H), 4.68–4.37 (m, 1H), 4.32–3.94 (m, 1H), 2.87 (br s, 1H), 2.49 (t, *J* = 6.8 Hz, 2H), 2.21 (br s, 1H), 1.96 (d, *J* = 16.6 Hz, 1H), 1.42 (s, 9H); **^{13}C NMR** (126 MHz, $CDCl_3$), rotamers are present: δ 154.6, 138.4, 130.7, 129.3, 128.9, 128.5, 127.9, 126.2, 125.8, 125.3, 123.6, 123.1, 122.7, 79.6, 52.4, 51.3,

38.1, 36.3, 28.5, 25.2; **^{19}F NMR** (469 MHz, $CDCl_3$): δ –62.7; **IR** (microscope, cm^{-1}) 3012, 2974, 2922, 1693, 1477, 1454, 1365, 1170, 814; **HRMS** (ESI-TOF): For $C_{20}H_{24}F_3NNaO_2$ $(M + Na)^+$: calcd. 390.1651; found 390.1652; **$[\alpha]_D^{20}$**: –4.0 (*c* = 0.42, CH_2Cl_2); **HPLC** (Chiralpak IC) 2:98 iso-propanol:hexanes, 0.5 mL/min, 20 °C, λ = 280 nm, T_{minor} = 7.3 min, T_{major} = 7.6 min, er = 94.4:5.6.

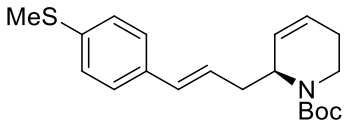

(*S,E*)-*tert*-Butyl 2-(3-(4-(methylthio)phenyl)allyl)-5,6-dihydropyridine-1(2*H*)-carboxylate (3-6j). Prepared by example procedure B using (*E*)-*tert*-butyl (3-(4-(methylthio)phenyl)allyl) carbonate (56 mg, 0.20 mmol) **3-5j** and (*S*)-**3-3** (74 mg, 0.24 mmol). Flash chromatography afforded the product as a pale-yellow oil (42 mg, 60%): **^{1}H NMR** (500 MHz, $CDCl_3$), rotamers are present: δ 7.29 (d, *J* = 8.3 Hz, 2H), 7.21 (d, *J* = 8.4 Hz, 2H), 6.38 (d, *J* = 15.8 Hz, 1H), 6.22 (br s, 1H), 5.88 (br s, 1H), 5.72 (br s, 1H), 4.68–4.34 (m, 1H), 4.32–3.96 (m, 1H), 2.89 (br s, 1H), 2.55–2.44 (m, 5H), 2.22 (br s, 1H), 1.98 (d, *J* = 16.3 Hz, 1H), 1.46 (s, 9H); **^{13}C NMR** (126 MHz, $CDCl_3$), rotamers are present: δ 154.6, 136.9, 134.5, 131.5, 128.6, 127.9, 126.8, 126.5, 126.2, 79.5, 52.7, 51.4, 37.9, 36.5, 28.5, 25.0, 16.1; **IR** (microscope, cm^{-1}) 3029, 2975, 2922, 2837, 1690, 1454, 1416, 1171, 815; **HRMS** (ESI-TOF): For $C_{20}H_{27}NNaO_2S$ $(M + Na)^+$: calcd. 368.1655; found 368.1653; **$[\alpha]_D^{20}$**: 0.68 (*c* = 0.46, CH_2Cl_2); **HPLC** (Chiralpak IC) 2:98 iso-propanol:hexanes, 0.5 mL/min, 20 °C, λ = 280 nm, T_{minor} = 7.3 min, T_{major} = 7.6 min, er = 94.4:5.6.

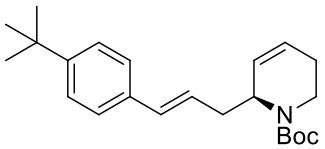

(*S,E*)-*tert*-Butyl 2-(3-(4-(tert-butyl)phenyl)allyl)-5,6-dihydropyridine-1(2*H*)-carboxylate (3-6k). Prepared by example procedure B using *tert*-butyl (1-(4-(*tert*-butyl)phenyl)allyl) carbonate **3-5k** (58 mg, 0.20 mmol) and (*S*)-**3-3** (74 mg, 0.24 mmol). Flash chromatography afforded the

product as a clear oil (47 mg, 66%): **^{1}H NMR** (500 MHz, $CDCl_3$), rotamers are present: δ 7.32 (d, *J* = 8.5 Hz, 2H), 7.28 (d, *J* = 8.4 Hz, 2H), 6.39 (d, *J* = 15.8 Hz, 1H), 6.18 (br s, 1H), 5.85 (br s, 1H), 5.70 (br s, 1H), 4.62–4.32 (m, 1H), 4.82–3.93 (m, 1H), 2.88 (br s, 1H), 2.47 (t, *J* = 6.4 Hz, 2H), 2.19 (br s, 1H), 1.95 (d, *J* = 16.3 Hz, 1H), 1.45 (s, 9H), 1.31 (s, 9H); **^{13}C NMR** (126 MHz, $CDCl_3$), rotamers are present: δ 154.6, 150.2, 134.4, 132.0, 128.5, 128.1, 125.8, 125.4, 79.5, 52.5, 51.4, 37.8, 36.4, 34.6, 31.4, 28.6, 24.9; **IR** (microscope, cm^{-1}) 3030, 2964, 2929, 2869, 1694, 1415, 1364, 1171, 1109, 825; **HRMS** (ESI-TOF): For $C_{23}H_{33}NNaO_2$ $(M + Na)^+$: calcd. 378.2404; found 378.2409; **[α]$_D^{20}$**: 11.3 (*c* = 0.710, CH_2Cl_2); **HPLC** (Chiralpak IC) 2:98 iso-propanol:hexanes, 0.5 mL/min, 20 °C, λ = 254 nm, T_{minor} = 8.1 min, T_{major} = 8.9 min, er = 92.7:7.3.

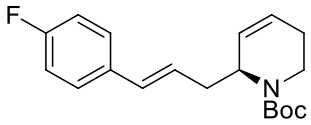

(*S*,*E*)-*tert*-Butyl 2-(3-(4-fluorophenyl)allyl)-5,6-dihydropyridine-1(2*H*)-carboxylate (3-6l). Prepared by example procedure B using *tert*-butyl (1-(4-fluorophenyl)allyl) carbonate (51 mg, 0.20 mmol) **3-5l** and (*S*)-**3-3** (74 mg, 0.24 mmol). Flash chromatography afforded the product as a pale-yellow oil (35.5 mg, 56%): **^{1}H NMR** (500 MHz, $CDCl_3$), rotamers are present: δ 7.32–7.27 (m, 2H), 6.97 (t, *J* = 8.6 Hz, 2H), 6.35 (d, *J* = 15.5 Hz, 1H), 6.14 (br s, 1H), 5.85 (br s, 1H), 5.69 (br s, 1H), 4.63–4.34 (m, 1H), 4.30–3.91 (m, 1H), 2.86 (br s, 1H), 2.45 (t, *J* = 7.2 Hz, 2H), 2.20 (br s, 1H), 1.95 (d, *J* = 17.2 Hz, 1H), 1.42 (s, 9H); **^{13}C NMR** (126 MHz, $CDCl_3$), rotamers are present: δ 163.0, 161.1, 154.6, 133.7, 130.9, 128.6, 128.2, 127.5, 126.6, 125.8, 125.5, 115.4, 115.2, 79.5, 52.7, 51.3, 37.7, 36.3, 28.5, 24.9; **^{19}F NMR** (469 MHz, $CDCl_3$): δ –115.4; **IR** (microscope, cm^{-1}) 3034, 2973, 2928, 2832, 1726, 1692, 1508, 1417, 1364, 1228, 1172, 821; **HRMS** (ESI-TOF): For $C_{19}H_{24}FNNaO_2$ $(M + Na)^+$: calcd. 340.1683; found 340.1688; **[α]$_D^{20}$**: 119 (*c* = 0.550, CH_2Cl_2); **HPLC** (Chiralpak IC) 2:98 iso-propanol:hexanes, 0.5 mL/min, 20 °C, λ = 254 nm, T_{minor} = 7.1 min, T_{major} = 7.6 min, er = 93.5:6.5.

3.9.7 Applications of Allyl-Allyl Products

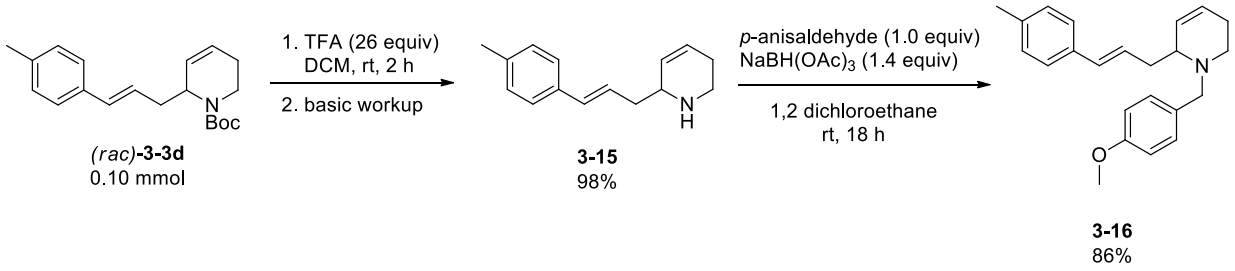

(rac)-**3-3d**
0.10 mmol

3-15
98%

3-16
86%

(±)-(*E*)-1-(4-Methoxybenzyl)-6-(3-(*p*-tolyl)allyl)-1,2,3,6-tetrahydropyridine (3-16). In a 1-dram vial equipped with a stir bar, compound (*rac*)-**3-6d** (31.3 mg, 0.10 mmol) was dissolved in DCM (2 mL), then trifluoracetic acid (0.20 mL, 2.6 mmol, 26 equiv) was added dropwise. The reaction mixture was allowed to stir for 2 hours. The reaction mixture was then concentrated *in vacuo* to remove the excess acid. The crude mixture was then redissolved in dichloromethane (10 mL) and washed with NaOH (10 mL) and extracted with dichloromethane (10 mL × 3). The combined organic layers were dried over Na_2SO_4, filtered, and concentrated *in vacuo* to afford free amine **3-15** as a yellow oil (20.9 mg, 98%): **^{1}H NMR** (500 MHz, $CDCl_3$): δ 7.18 (d, *J* = 7.8 Hz, 2H), 7.03 (d, *J* = 7.9 Hz, 2H), 6.39 (d, *J* = 15.8 Hz, 1H), 6.08 (dt, *J* = 15.8, 7.0, 1H), 5.74 (ddt, *J* = 9.7, 4.7, 2.3 Hz, 1H), 5.59 (dq, *J* = 10.2, 2.0 Hz, 1H), 3.36 (dq, *J* = 5.3, 2.7 Hz, 1H), 3.02 (ddd, *J* = 12.0, 5.7, 2.8 Hz, 1H), 2.79 (ddd, *J* = 12.1, 9.6, 4.6 Hz, 1H), 2.35–2.19 (m, 5H), 2.09 (dddq, *J* = 18.0, 9.0, 5.9, 2.8 Hz, 1H), 1.94–1.83 (m, 1H), 1.67 (br s, 1H); **^{13}C NMR** (126 MHz, $CDCl_3$): δ 136.9, 134.6, 132.6, 130.6, 129.2, 126.2, 126.0, 125.9, 53.7, 42.3, 39.9, 25.9, 21.2; **IR** (microscope, cm^{-1}) 3330, 3022, 2943, 2915, 2832, 1512, 1429, 1114; **HRMS** (ESI-TOF): For $C_{15}H_{20}N$ $(M + H)^+$: calcd. 214.1590; found 214.1586.

Free amine **3-15** was then subjected to a reductive amination reaction according to the following procedure: in a flame dried round bottom flask equipped with a stir bar, free amine **3-15** (21 mg, 0.098 mmol) and *p*-anisaldehyde (12 µL, 0.098 mmol, 1.0 equiv) were mixed in 1,2-Dichloroethane (1 mL) under N_2 atmosphere. The mixture was stirred at room temperature for 30 min. Sodium triacetoxyborohydride (29 mg, 0.14 mmol, 1.4 equiv) was added to the reaction

mixture which then was allowed to stir at room temperature for 16 h. The reaction mixture was quenched with saturated solution of $NaHCO_3$ and extracted with ethyl acetate (10 mL × 3). The combined organic layers were dried over anhydrous Na_2SO_4, filtered, and concentrated *in vacuo*. The crude product was purified on an HPLC Agilent instrument using a XDB-C18 column, (9.4 × 250mm, 5μm) with the following instrument conditions and eluent: 3.0 mL/min, 40 °C M.P.A: 0.1% formic acid in H_2O M.P.B: 0.1% formic acid in acetonitrile to afford the formic acid salt of compound **12** which was treated with NaOH (1.0 M, 10 mL) and extracted with dichloromethane (10 mL × 3). The organic layers were then dried over Na_2SO_4, filtered and concentrated *in vacuo* to afford compound **3-16** as a dark brown oil (28 mg, 86%): **^{1}H NMR** (500 MHz, $CDCl_3$): δ 7.28 (d, *J* = 8.6 Hz, 2H), 7.25 (d, *J* = 8.1 Hz, 2H), 7.11 (d, *J* = 7.9 Hz, 2H), 6.85 (d, *J* = 8.6 Hz, 2H), 6.39 (d, *J* = 15.9 Hz, 1H), 6.20 (dtd, *J* = 15.5, 7.0, 1.0 Hz, 1H), 5.82 (ddd, *J* = 9.6, 3.7, 2.0 Hz, 1H), 5.67 (dq, *J* = 10.1, 1.9 Hz, 1H), 3.93 (d, *J* = 13.4 Hz, 1H), 3.80 (s, 3H), 3.42 (d, *J* = 13.4 Hz, 1H), 3.08 (ddt, *J* = 7.1, 4.6, 2.3 Hz, 1H), 2.90 (dt, *J* = 11.4, 5.4 Hz, 1H), 2.58 (dt, *J* = 12.5, 6.2 Hz, 1H), 2.43 (dq, *J* = 11.9, 6.5, 5.5 Hz, 2H), 2.34 (s, 3H), 2.07–2.00 (m, 2H): **^{13}C NMR** (126 MHz, $CDCl_3$): δ 158.6, 136.6, 135.1, 131.6, 131.2, 130.0, 129.7, 129.1, 126.9, 125.9, 125.5, 113.5, 58.9, 57.6, 55.2, 46.1, 37.0, 24.3, 21.1; **IR** (microscope, cm^{-1}) 3024, 2912, 2834, 2794, 1611, 1511, 1245, 834; **HRMS** (ESI-TOF): For $C_{23}H_{28}NO$ $(M + H)^+$: calcd. 334.2165; found 334.2162.

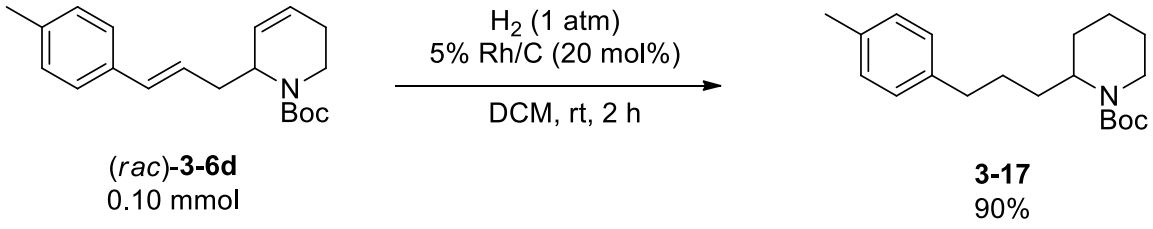

(*rac*)-**3-6d**
0.10 mmol

3-17
90%

***tert*-Butyl 2-(3-(*p*-tolyl)propyl)piperidine-1-carboxylate (3-17).** In a flame-dried 10 mL pear flask charged with a stir bar was added 5% rhodium on carbon (41 mg, 0.020 mmol, 0.20 equiv), and compound (*rac*)-**3-6d** (31.3 mg, 0.10 mmol). The flask was evacuated and backfilled with nitrogen for three cycles. Dichloromethane (3.0 mL) was added to the flask *via* syringe and mixture was stirred for 5 min. The solution was purged with a hydrogen balloon for 10 min. The balloon

was then moved into the flask's headspace, and the reaction then stirred for two hours. The mixture was then filtered through a silica plug with (100% dichloromethane), then concentrated *in vacuo*. The crude product was purified on HPLC Agilent instrument using a XDB-C18 column, (9.4 × 250mm, 5µm) with the following instrument conditions and eluent: 3.0 mL/min, 40 °C M.P.A: 0.1% formic acid in H_2O M.P.B: 0.1% formic acid in acetonitrile to afford compound **3-17** as a clear oil (28.5 mg, 90%): **^{1}H NMR** (500 MHz, $CDCl_3$), rotamers are present: δ 7.10–7.04 (m, 4H), 4.23 (br s, 1H), 3.95 (d, *J* = 10.7 Hz, 1H), 2.71 (td, *J* = 14.0, 5.0 Hz, 1H), 2.66–2.54 (m, 2H), 2.31 (s, 3H), 1.75–1.65 (m, 1H), 1.54 (m, 7H), 1.46–1.30 (m, 11H). **^{13}C NMR** (126 MHz, $CDCl_3$), rotamers are present: δ 155.2, 139.4, 135.1, 128.9, 128.3, 79.1, 50.3, 38.8, 35.2, 30.4, 29.2, 28.6, 28.1, 25.7, 21.0, 19.1; **IR** (microscope, cm^{-1}) 3002, 2973, 2932, 2861, 1689, 1415, 1364, 1157; **HRMS** (ESI-TOF): For $C_{20}H_{31}NNaO_2$ $(M + Na)^+$: calcd. 340.2247; found 340.2244.

3.9.8 Proof of absolute stereochemistry

To confirm the absolute configuration of the cross-coupled products, compound (*S*)-**3-6a** was derivatized to the previously reported compound (*S*)-**3-14**, (*S*)-2-(3-phenylpropyl)piperidine,[27] and their optical rotation values were compared.

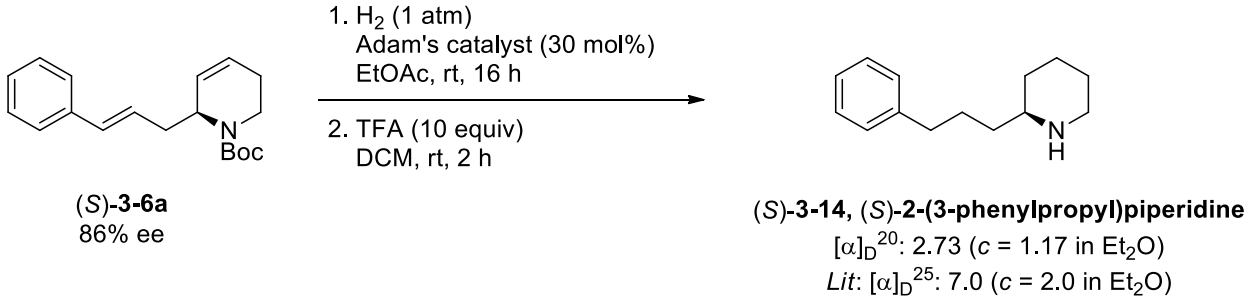

(*S*)-**3-6a**
86% ee

(*S*)-**3-14,** (*S*)-**2-(3-phenylpropyl)piperidine**
$[\alpha]_D^{20}$: 2.73 (*c* = 1.17 in Et_2O)
Lit: $[\alpha]_D^{25}$: 7.0 (*c* = 2.0 in Et_2O)

(*S*)-2-(3-Phenylpropyl)piperidine ((*S*)-3-14). In a flame dried 10 mL pear-shaped flask charged with a stir bar was added Adams' catalyst (4.9 mg, 20 µmol, 0.30 equiv), and compound (*S*)-**3-6a** (20 mg, 67 µmol) and evacuated and backfilled with nitrogen for three cycles. Ethyl acetate (5.0 mL) was added to the flask via syringe and mixture was stirred for 5 min. The solution was purged with a hydrogen balloon for 10 min. The balloon was then moved into the flask's headspace, and the reaction then stirred for 16 h. The mixture was then filtered through a silica plug with (100% EtOAc), then concentrated *in vacuo* and used in the next deprotection step without further purification. The deprotection step was carried out using the same procedure as mentioned for the preparation of compound **3-18**, delivering compound (*S*)-**3-14** (11.7 mg, 86% overall yield). Spectral data matches those previously reported: **^{1}H NMR** (400 MHz, $CDCl_3$): δ 7.23–7.18 (5 H, m), 3.07–3.02 (m, 1H), 2.60 (t, *J* = 7.6 Hz, 2H), 2.52–2.46 (m, 2H), 1.00–1.80 (m, 11H).

$[\alpha]_D^{20}$: 2.73 (*c* = 1.17 in Et_2O), (*Lit*[27]: 7.0, *c* = 2.0 in Et_2O, 91% ee).

3.9.9 Example of cross-coupling reaction with Cbz protected piperidine

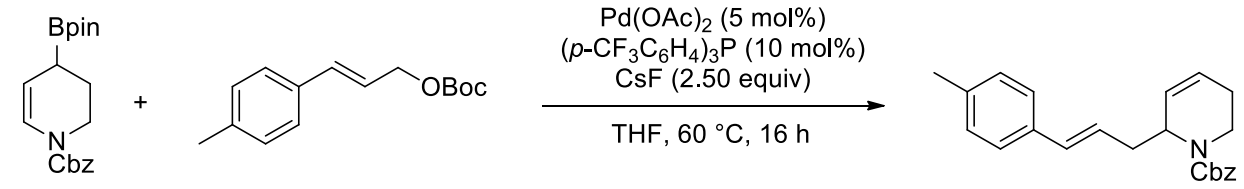

(*rac*)-**3-3'**
1.20 equiv

3-5
1.00 mmol

(*rac*)-**3-6d'**
72%

(*E*)-benzyl 2-(3-(*p*-tolyl)allyl)-5,6-dihydropyridine-1(2*H*)-carboxylate ((*rac*)-3-6d′). Prepared by example procedure A under Section 3.9.6 using (*E*)-*tert*-butyl (3-(*p*-tolyl)allyl) carbonate **3-5d** (246 mg, 1.00 mmol) and (*rac*)-**3-3′** (412 mg, 1.20 mmol). Flash chromatography afforded the product as a yellow oil (250 mg, 72%): **^{1}H NMR** (500 MHz, $CDCl_3$): δ 7.40–7.28 (m Hz, 5H), 7.27–7.16 (m, 2H), 7.10 (d, *J* = 7.7 Hz, 2H), 6.47–6.28 (m, 1H), 6.26–6.4.05 (s, 1H), 5.87 (br s, 1H), 5.80–5.64 (m, 1H), 5.14 (s, 2H), 4.69–4.46 (m, 1H), 4.33–4.05 (m, 1H), 2.97 (br s, 1H), 2.59–2.41 (m, 2H), 2.34 (s, 3H), 2.30–2.13 (m, 1H), 2.08–1.89 (m, 1H); **^{13}C NMR** (126 MHz, $CDCl_3$): δ 155.4, 137.0, 134.8, 132.3, 129.2, 128.5, 128.2, 127.9, 126.0, 125.8, 125.4, 125.1, 125.1, 67.2, 52.5, 38.1, 37.8, 37.2, 25.1, 24.8, 21.2; **IR** (microscope, cm^{-1}): 3031, 2921, 2837, 1699, 1424, 1391, 1248, 1105, 697; **HRMS** (ESI-TOF): For $C_{23}H_{25}NNaO_2$ $(M + Na)^+$: calcd. 370.1778; found 370.1772.

3.10 References

[1] Larsen, M. A.; Hennessy, E. T.; Deem, M. C.; Lam, Y.-h.; Saurí, J.; Sather, A. C. *J. Am. Chem. Soc.* **2020**, *142*, 726.

[2] Deardorff, D. R.; Niman, S. W.; Paulsen, M. I.; Sookezian, A.; Whalen, M. E.; Finlayson, C. J.; Frivold, C.; Brown, H. C.; Cannon, J. S. *ACS Omega* **2020**, *5*, 2005.

[3] Lessard, S.; Peng, F.; Hall, D. G. *J. Am. Chem. Soc.* **2009**, *131*, 9612.

[4] Kim, Y.-R.; Hall, D. G. *Org. Biomol. Chem.* **2016**, *14*, 4739.

[5] Clement, H. A.; Hall, D. G. *Recent Advances in the Stereoselective Additions of Allylic Boronates to Carbonyl Compounds*. In *PATAI'S Chemistry of Functional Groups*; Rappoport, Z., Ed. 2020, p 1-86.

[6] Glasspoole, B. W.; Ghozati, K.; Moir, J. W.; Crudden, C. M. *Chem. Commun.* **2012**, *48*, 1230.

[7] Ding, J.; Hall, D. G. *Angew. Chem. Int. Ed.* **2013**, *52*, 8069.

[8] Ding, J.; Rybak, T.; Hall, D. G. *Nat. Commun.* **2014**, *5*, 5474.

[9] Jana, R.; Pathak, T. P.; Sigman, M. S. *Chem. Rev.* **2011**, *111*, 1417.

[10] Zhang, P.; Brozek, L. A.; Morken, J. P. *J. Am. Chem. Soc.* **2010**, *132*, 10686.

[11] Vitaku, E.; Smith, D. T.; Njardarson, J. T. *J. Med. Chem.* **2014**, *57*, 10257.

[12] Quasdorf, K. W.; Riener, M.; Petrova, K. V.; Garg, N. K. *J. Am. Chem. Soc.* **2009**, *131*, 17748.

[13] Brozek, L. A.; Ardolino, M. J.; Morken, J. P. *J. Am. Chem. Soc.* **2011**, *133*, 16778.

[14] Thomas, A. A.; Zahrt, A. F.; Delaney, C. P.; Denmark, S. E. *J. Am. Chem. Soc.* **2018**, *140*, 4401.

[15] Wright, S. W.; Hageman, D. L.; McClure, L. D. *J. Org. Chem.* **1994**, *59*, 6095.

[16] Granberg, K. L.; Bäckvall, J. E. *J. Am. Chem. Soc.* **1992**, *114*, 6858.

[17] Hartwig, J. F. *Inorg. Chem.* **2007**, *46*, 1936.

[18] Zhang, S.-L.; Huang, L.; Sun, L.-J. *Dalton Trans.* **2015**, *44*, 4613.

[19] Amatore, C.; Jutand, A.; M'Barki, M. A. *Organometallics* **1992**, *11*, 3009.

[20] Doebner, O. *Ber. Dtsch. Chem. Ges.* **1902**, *35*, 1136.

[21] Ardolino, M. J.; Morken, J. P. *Tetrahedron* **2015**, *71*, 6409.

[22] Kohlmann, J.; Braun, T.; Laubenstein, R.; Herrmann, R. *Chem. Eur. J.* **2017**, *23*, 12218.

[23] Yamamoto, Y.; Takada, S.; Miyaura, N.; Iyama, T.; Tachikawa, H. *Organometallics* **2009**, *28*, 152.

[24] Yamamoto, Y.; Takada, S.; Miyaura, N. *Chem. Lett.* **2006**, *35*, 1368.

[25] Yamamoto, Y.; Takada, S.; Miyaura, N. *Chem. Lett.* **2006**, *35*, 704.

[26] Sebelius, S.; Olsson, V. J.; Wallner, O. A.; Szabó, K. J. *J. Am. Chem. Soc.* **2006**, *128*, 8150.

[27] Meyers, A. I.; Dickman, D. A.; Bailey, T. R. *J. Am. Chem. Soc.* **1985**, *107*, 7974.

[28] Podyacheva, E.; Afanasyev, O. I.; Tsygankov, A. A.; Makarova, M.; Chusov, D. *Synthesis* **2019**, *51*, 2667.

[29] Liu, X.; Liu, S.; Wang, Q.; Zhou, G.; Yao, L.; Ouyang, Q.; Jiang, R.; Lan, Y.; Chen, W. *Org. Lett.* **2020**, *22*, 3149.

[30] Yang, B.; Wang, Z.-X. *Org. Lett.* **2019**, *21*, 7965.

[31] Guo, Y.; Shen, Z. *Org. Bio. Chem.* **2019**, *17*, 3103.

[32] Li, F.; Wang, Z.-H.; Zhao, L.; Xiong, F.-J.; He, Q.-Q.; Chen, F.-E. *Tetrahedron: Asymmetry* **2011**, *22*, 1337.

[33] Weix, D. J.; Markovic, D.; Ueda, M.; Hartwig, J. F. *Org. Lett.* **2009**, *11*, 2944.

[34] Yuan, Q.; Yao, K.; Liu, D.; Zhang, W. *Chem. Commun.* **2015**, *51*, 11834.

[35] Lin, L.-Z.; Che, Y.-Y.; Bai, P.-B.; Feng, C. *Org. Lett.* **2019**, *21*, 7424.

[36] Bai, X.-D.; Zhang, Q.-F.; He, Y. *Chem. Commun.* **2019**, *55*, 5547.

[37] Davis, C. R.; Luvaga, I. K.; Ready, J. M. *J. Am. Chem. Soc.* **2021**, *143*, 4921.

[38] Daley, R. A.; Topczewski, J. J. *Org. Biomol. Chem.* **2019**, *17*, 1709.

[39] Stambasky, J.; Malkov, A. V.; Kocovsky, P. *J. Org. Chem.* **2008**, *73*, 9148.

Chapter 4: Towards a New Treatment of Glioblastoma Multiforme: Pharmaceutical Application of Enantioenriched Allylic Piperidinyl Boronates towards the Synthesis of Novel Vacquinol-1 Analogs

4.1 Introduction

4.1.1 Glioblastoma multiforme

Glioblastoma multiforme (GBM) is an aggressive malignant brain tumor with an average incidence rate of 3.19 per 100,000 population.[1,2] As reported by population-based studies, this cancer has a low survival rate of 3.3% two years following the patients' diagnosis.[3] There are two categories of GBM: primary and secondary.[4,5] Primary GBM is *de novo* tumor, i.e., it develops without any clinical or histologic evidence preceding the diagnosis, that accounts for 90% of all GBM cases and usually targets elderly patients. [4-7] Primary GBM is classified as a grade IV tumor, which are well-known for their ability to grow fast, spread to various areas of the brain with ease, and their abnormal blood vessel growth.[7,8] On the other hand, secondary GBM cover the remaining 10% of cases and usually manifests itself in younger patients.[5,9] In addition, secondary GBM ranges from slowly growing grade II astrocytoma, to a low malignancy grade III anaplastic astrocytoma.[5,9] According to data, 15% of primary intracranial tumors are diagnosed as GBM, which illustrates the impact of this type of cancer on the population.[10]

Based on its histopathological features, GBM can be categorized into three different subtypes: small cell glioblastoma, glioblastoma with oligodendroglioma component, and glioneuronal tumor with neuropil-like islands.[11] Individual subtypes of GBM are determined from a combination of distinct glial cells, a variety of histopathological features, and a unique pattern of gene expression.[11-14] Furthermore, GBM can be categorized into four additional subtypes based on its gene expression: proneural, neural, classical and mesenchymal.[15] In addition the morphology of GBM consists of nuclear atypia, cellular pleomorphism, mitotic activity, vascular thrombosis,

microvascular proliferation, and necrosis.[5] These attributes provide diverseness to GBM and the rationale behind the multiforme categorization.[16]

The treatment of GBM is exceptionally difficult due to its location, physical permutations, and genetic factors. The conventional treatment is surgical removal of the tumor, followed by a combination of radiotherapy and oral temozolomide (TMZ) chemotherapy.[17] TMZ is a prodrug that is converted to the active metabolite imidazole-4-carboximide (MTIC) *in vivo* (Scheme 4-1). MTIC promotes apoptosis of cancer cells preceded by alkylation of their DNA.[7] TMZ has a reported half maximal inhibitory concentration (IC_{50}) of ~20 μM against U251 GBM cell lines.[18] However, the effectiveness of this treatment method is impeded by the localization of the tumor within the brain, as surgery can only be employed if the tumor is reasonably accessible. In addition, GBM cells are located in hypoxic (oxygen-lacking) environments, which render them highly resistant to radiotherapy.[7] Furthermore, TMZ is hardly effective due to the various biological mechanism of resistance of GBM. This is illustrated by high IC_{50} values that can reach up to 1585 μM when TMZ is tested against patient derived GBM cell lines.[18] An example of such mechanism is the DNA repair pathway through O^6-methylguanine-DNA methyltransferase (MGMT), which reverses the DNA alkylation induced by MTIC.[19] Additionally, GBM is known for containing cancer stem cells (CSCs), which remain dormant during treatment of GBM and become active after treatment to repopulate the brain with more resistant GBM cancer cells.[20] The drawbacks of the current treatment methods, combined with the resilience of GBM are responsible for the low survivability of the disease. Typically, patients with GBM have a median survival period of 14.6 months, and <10% survival rate after five years.[20,21] For this reason, it is essential to gain access to better treatment methods that can mitigate the resistance mechanism of this incurable deadly ailment.

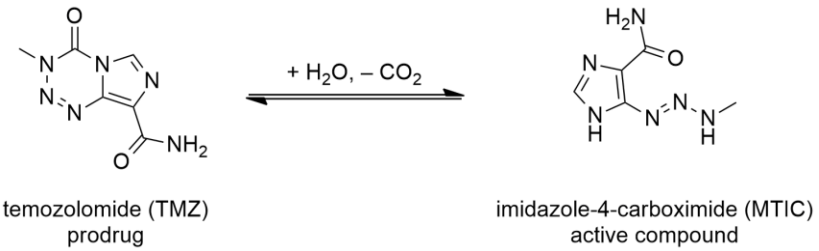

Scheme 4-1. Chemical transformation of prodrug TMZ to the active MTIC form.

4.1.2 The discovery of vacquinol-1 for the treatment of GBM

In order to develop better treatments against GBM and bypass its resistance mechanisms, Patrik Ernfors and co-workers conducted a high-throughput screening (HTS) experiment using 1364 compounds from the National Institute of Health (NIH).[22] HTS has accelerated the drug discovery process in pharmaceutical industry as it can screen large numbers of compounds in short periods of time.[23]

In their study, Ernfors and co-workers used an unbiased phenotypic screening for active compounds that could alter the shape or size of GBM cells, rather than using a target-based approach.[22,24] One design feature is the use of primary GBM cultures derived from two different patients instead of long-established GBM cell lines.[22,24] The phenotype and genotype of established GBM cell lines are suspected to be diverged from the original GBM cells, which would potentially invalidate the screening results for active compounds.[22,24,25] This strategy employed by Ernfors and co-workers generated 234 hits. Focusing on the potential toxicity of the hits rather than the potency, the authors followed up by screening these hits against GBM cultures derived from seven more patients to confirm anti-GBM activity.[22,24] In addition, these hits were counter-screened against healthy mouse embryonic stem cells, human fibroblasts, and an *in vivo* assay using a zebrafish GBM model to exclude nonspecifically toxic compounds. This rigorous analysis led to the discovery of vacquinol-1 (VQ-1) as a drug candidate for the treatment of GBM.[22,24] It is worth noting that the original study by Ernfors and co-workers was retracted for their inability to reproduce the results of some *in vivo* experiments. However, a recent study by Ahlstedt et al. found that VQ-1 reduced GBM tumor size in rats, albeit no significant increase in survival rate was

observed, and further investigation was recommended.[26] Presumably, compounds with even higher potency than VQ-1 may demonstrate a better *in vivo* activity, and investigation of such compounds would allow access to a better candidate for the treatment of GBM.

4.1.3 History of vacquinol-1

Before its novel use as an antitumor agent against GBM, VQ-1 was earlier investigated for significantly different pharmaceutical applications. Originally, VQ-1 was synthesized in an investigation to discover more potent derivatives of quinine and chloroquine as antimalarials during the worldwide rise in resistance from 1950s to 1970s.[27-30] This investigation led to the discovery and marketing of the antimalarial drug mefloquine, a derivative of VQ-1 (Figure 4-1).[30,31]

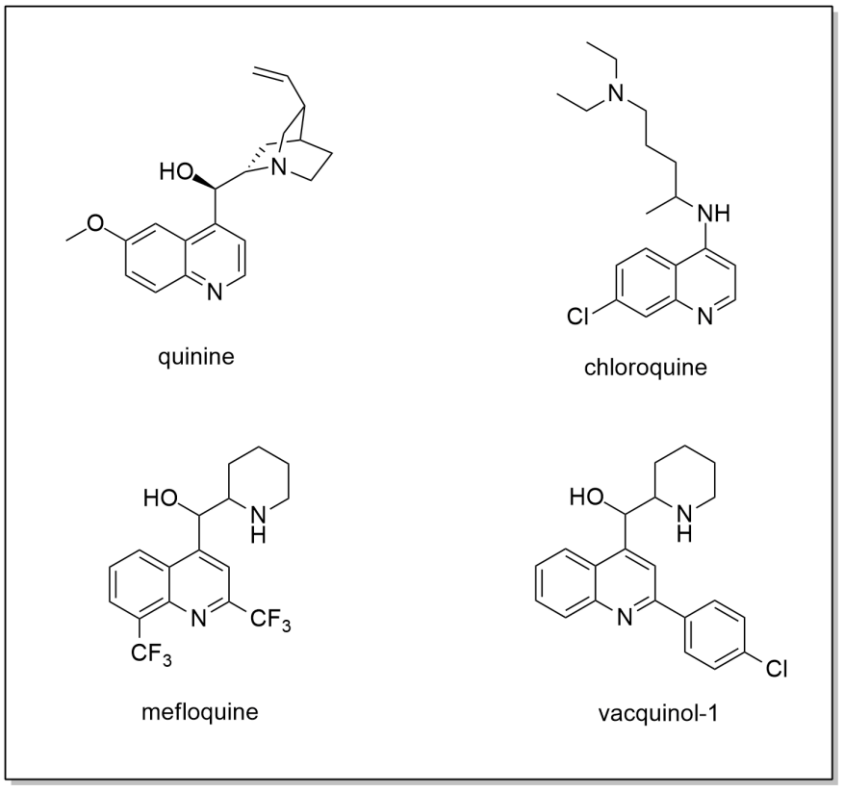

Figure 4-1. Structural comparison of antimalarial scaffolds.

In addition to their antimalarial activity, other VQ-1 analogs have been synthesized towards applications in inhibition of the biofilm infection caused by the gram-negative bacteria; *Vibrio*

chlorae.[32] Another application of VQ-1 scaffolds is the inhibition of proto-oncogene enzymes inositol-5'-phophatase 1 (SHIP1) and inositol-5'-phophatase 2 (SHIP2) (Figure 4-2).[33] This diversity in biological activity of the VQ-1 scaffold justifies the investigation of this α-hydroxyalkyl piperidine scaffold in the treatment of GBM.

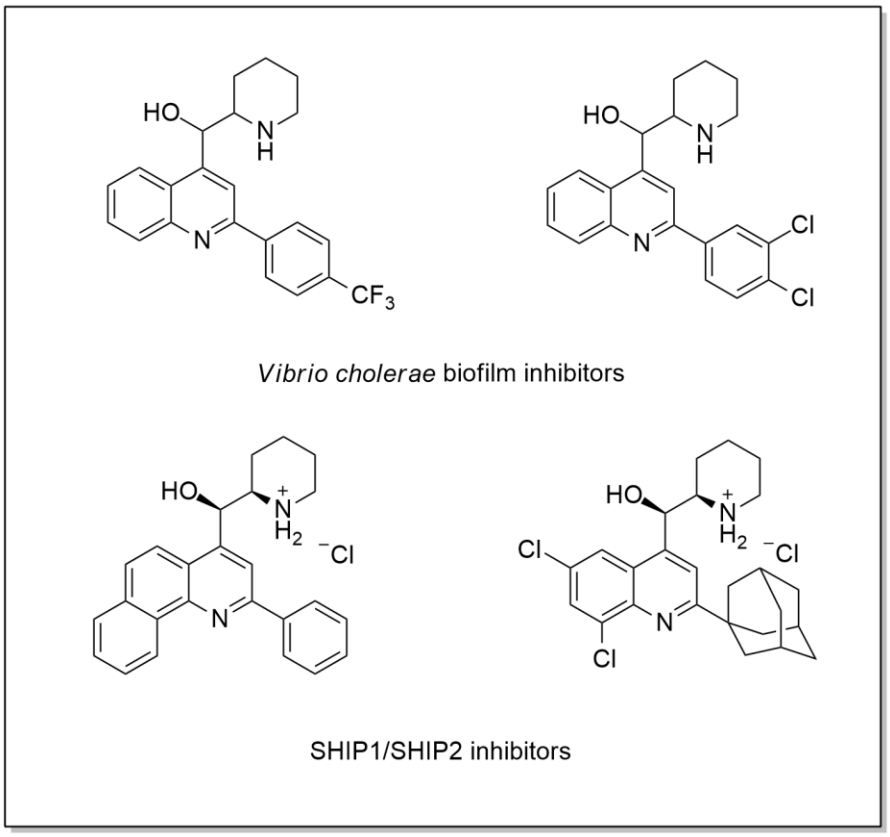

Figure 4-2. VQ-1 analogs and their pharmaceutical applications.

4.1.4 Structure and biological activity of VQ-1

As shown below in Figure 4-3, VQ-1 has four possible stereoisomers due to the presence of two contiguous stereogenic centers in its structure. These stereoisomers could be categorized into two enantiomeric pairs: 1) *erythro* pairs where the amine and hydroxy functional groups are *anti*, and 2): *threo* pairs where the amine and hydroxy functional groups are *syn*.[34] The original study by Ernfors and co-workers determined the IC_{50} against GBM cells for VQ-1 to be roughly at 3.14 μM.[22] This reported IC_{50} value represents the activity of VQ-1 as a mixture of all stereoisomers.[22]

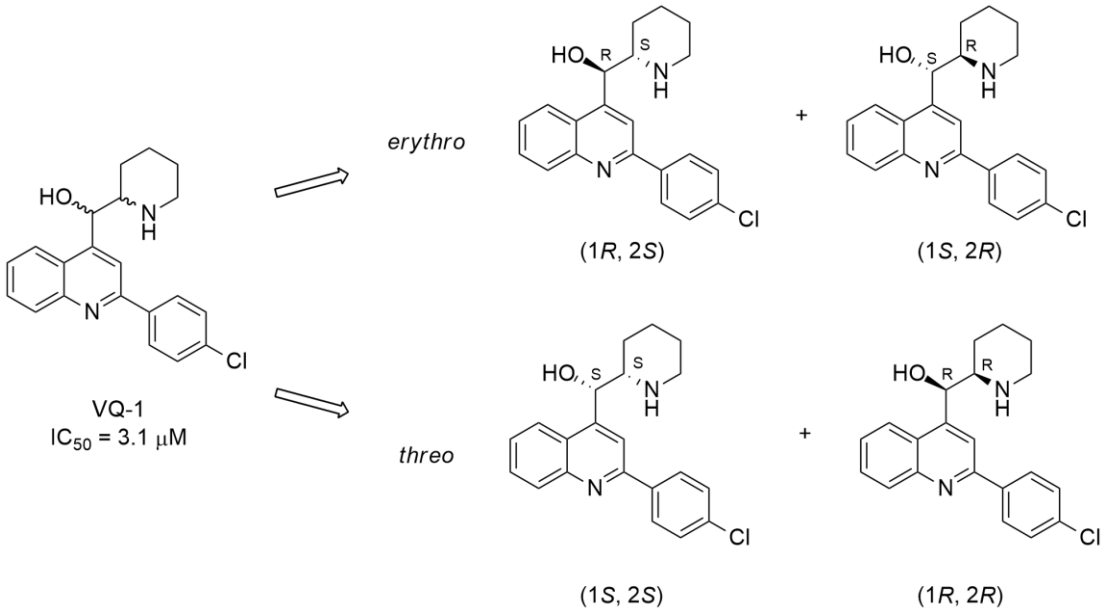

Figure 4-3. Biological activity of VQ-1 and its four possible stereoisomers.

4.1.5 Racemic synthesis of VQ-1 analogs and structure-activity relationship

In order to gain deeper understanding of the structure-activity relationship (SAR) of VQ-1, Ernfors and co-workers constructed a library of VQ-1 analogs using the synthetic route exemplified with VQ-1 shown in Scheme 4-2.[35] The synthesis begins with a Pfitzinger reaction between acetophenone **4-1** and isatin to obtain the 2,4-disubstituted quinoline **4-2**.[36] Subjecting intermediate **4-2** to a Fischer esterification protocol furnishes the methyl ester **4-3**.[37] Tricarbonyl intermediate **4-5** is obtained by a Claisen condensation reaction with ester **4-4**. Next, a tandem amide hydrolysis, saponification, and decarboxylation reaction, yields ketone intermediate **4-6**. Bromination at the α-position of ketone **4-6** followed by an intermolecular nucleophilic substitution reaction forms the piperidone derivative **4-7**. Lastly, sodium borohydride reduction on **4-7** furnishes VQ-1 and related analogs in seven steps with an overall yield of 0.8%.[35]

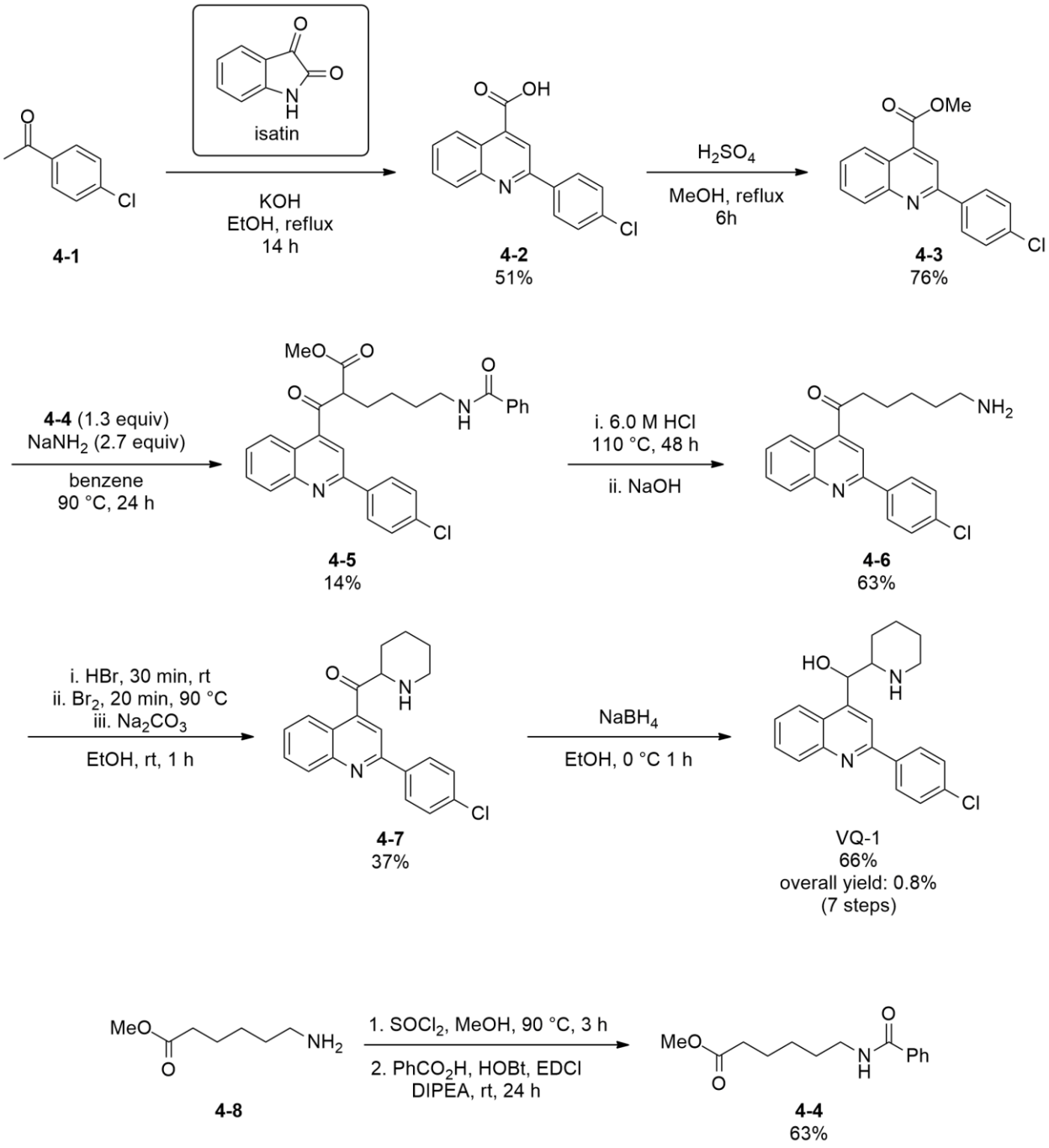

Scheme 4-2. Racemic synthesis of VQ-1 for SAR study.

The SAR study investigated four main structural features: the piperidine ring, the hydroxy group, quinoline substitutions, and modification to the 2-(4-chlorophenyl) moiety (Table 4-1).[22,35] The unfunctionalized piperidine unit was found to be essential for the biological activity as altering the piperidine to a pyridine or pyrrolidine, alkylating the amine, or a hydrogen atom resulted in

reduced activity against GBM (entries 2-5). Oxidation of the hydroxy unit to the ketone or the amide was poorly tolerated (entries 6-7), whereas installation of a methyl ether moiety instead of hydroxy showed similar activity (entry 8). Next, the 2-(4-chlorophenyl) was investigated and was found to be a comparatively sensitive pharmacophore as shown in entries 9-13. However, the biological activity improved when moving the chloride atom to the *meta* position (entry 14). In addition, switching the 2-(4-chlorophenyl) scaffold to a 4-chloroaniline group improved the IC_{50} (entry 15), although this improvement is hard to assess since two structural changes have occurred. It is ambiguous to attribute the increased potency to the methyl group on C6 of the quinoline moiety as an illustration of a *magic methyl effect*, or the introduction of an aniline moiety. Lastly, entries 16-18 show increased potency when substituents on C6-C8 of the quinoline ring are introduced. The most potent compound was found to be VQ-15 (entry 16), a phenyl ring fused to C7-C8 of the quinoline.

Though entries 14-18 of Table 4-1 illustrated better potency *in vitro* against GBM compared to VQ-1, the authors did not select them for further optimization due to either cytotoxicity effects, or they demonstrated poorer efficacy at shrinking GBM tumors in the *in vivo* zebrafish models. Based on these findings, VQ-1 was selected for further optimization, by altering the 2-(4-chlorophenyl) scaffold, and by developing a stereoselective synthesis to assess the biological activity of each stereoisomers.[22,35]

Table 4-1. Initial SAR study of VQ-1.

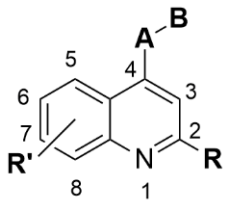

entry	A	B	R	R′	IC_{50} (μM)
1	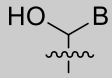	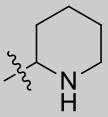	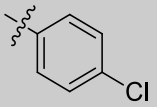	H (C5-C8)	3.14 ± 1.23
2		N/A	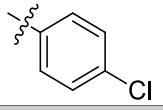	H (C5-C8)	> 50
3	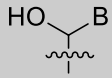	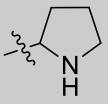	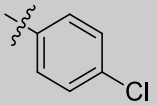	H (C5-C8)	8.32 ± 1.36
4	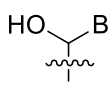	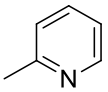	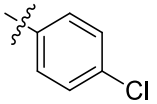	H (C5-C8)	> 50
5	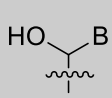	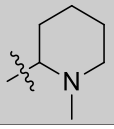	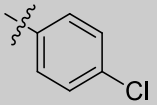	H (C5-C8)	> 25
6		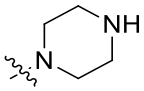	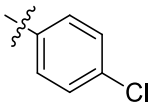	H (C5-C8)	> 50
7		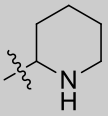	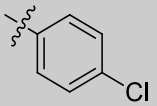	H (C5-C8)	> 50
8	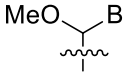	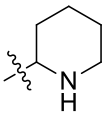	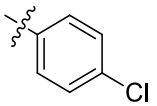	H (C5-C8)	3.62 ± 1.44
9	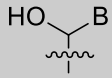	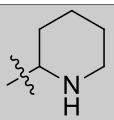		H (C5-C8)	> 50
10	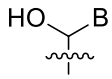	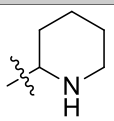	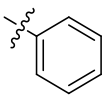	H (C5-C8)	> 25
11	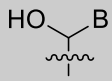	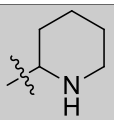	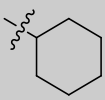	H (C5-C8)	12.7 ± 4.3

12	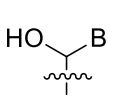	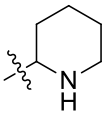	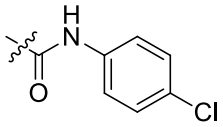	H (C5, C6-C7) CF_3 (C8)	> 50
13	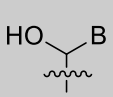	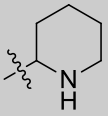	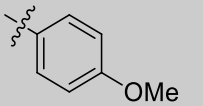	H (C5-C8)	7.59 ± 2.65
14	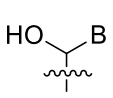	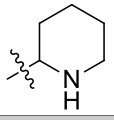	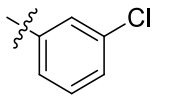	H (C5-C8)	2.13 ± 0.87
15	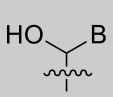	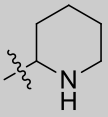	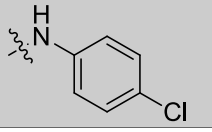	H (C5, C7-C8) CH_3 (C6)	0.71 ± 0.21
16	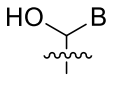	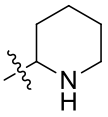	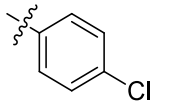	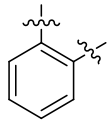 (C7-C8) H (C5-C6)	0.39 ± 0.12
17	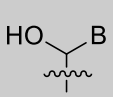	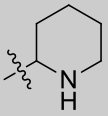	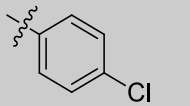	H (C6, C8) Cl (C5, C7)	1.10 ± 0.87
18	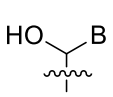	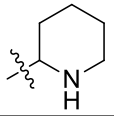	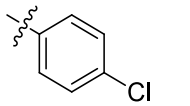	H (C5-C7) Cl (C8)	1.03 ± 0.73

4.1.6 Stereoselective synthesis of VQ-1

Due to the abundance of literature examples that show how enantioenriched drugs have better potency, less toxicity, and fewer side effects,[38] it was imperative at this stage of the biological activity study to synthesize the four stereoisomers of VQ-1 and assess their potency individually. For this reason, the authors developed a stereoselective synthesis in a similar fashion to the studies of Linington and co-workers to gain access to the four stereoisomers (Scheme 4-3).[32] Their synthetic approach began with using enantioenriched *tert*-butyl 2-formylpiperidine-1-carboxylate (*S*)-**4-9**, which undergoes an alkylation reaction from the turbo Grignard activated 2,4-dibromoquinoline intermediate **4-10** to furnish the amino alcohol **4-11** as a mixture of *(R,S) erythro* and *(S,S) threo* isomers.[39] Amino alcohol **4-11** was subjected to a Suzuki-Miyaura cross-coupling with boronic acid **4-12** followed by acidic deprotection of the *tert*-butyloxycarbonyl (Boc) group

to afford the HCl salt derivative of VQ-1 **4-13**. The stereoisomers could be obtained individually by basification of salt **4-13** then HPLC separation.[34] To obtain the two remaining stereoisomers, *(S,R) erythro* and *(R,R) threo*, the same synthesis described above is applied starting from the enantiomer of (*S*)-**4-9**.[34]

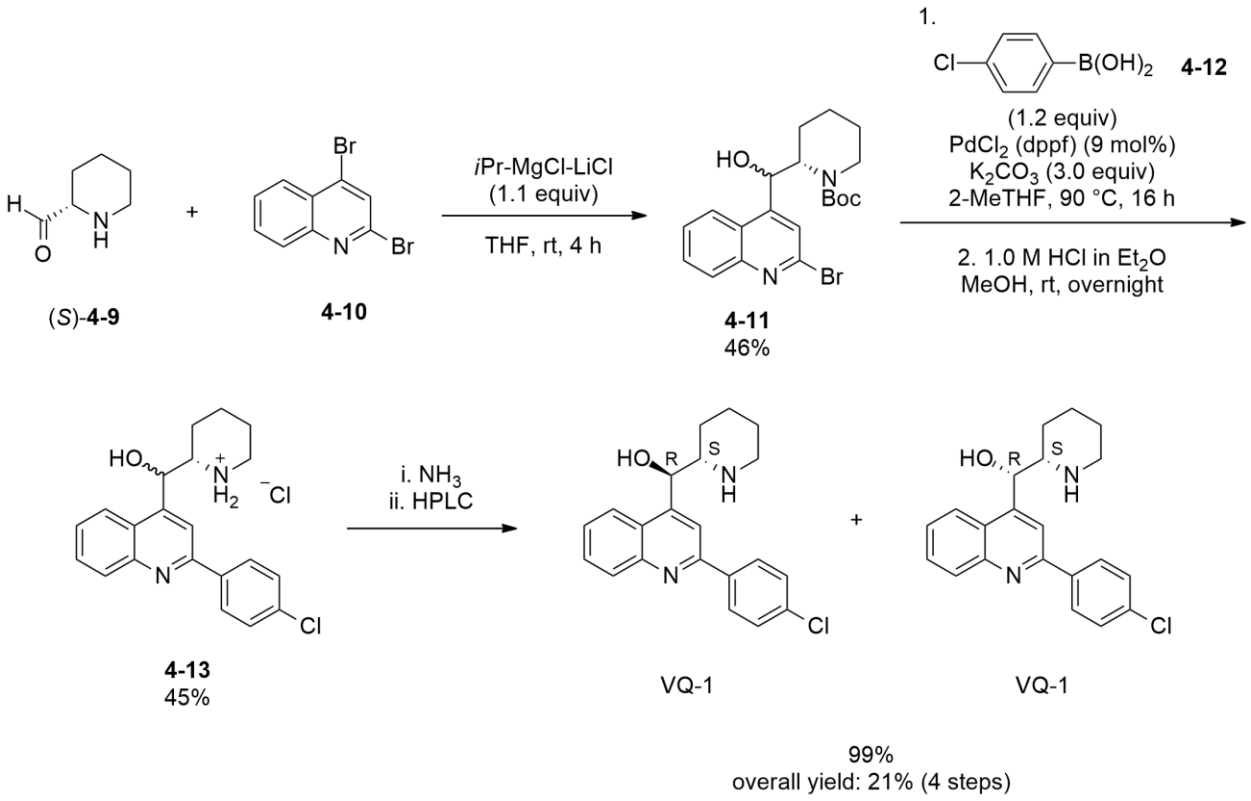

Scheme 4-3. Stereoselective synthesis of VQ-1.

After successfully obtaining the four stereoisomers of VQ-1, they were tested for their biological activity (Figure 4-4). The authors found that the *erythro* isomers were the most active isomers compared to their *threo* counterparts.[34] Furthermore, it was found the *erythro* isomer *(R,S)* more effectively penetrate the blood-brain barrier (BBB). This feature is exceedingly beneficial, as GBM candidate drugs not being able to penetrate BBB is a common problem.[40] Based on these findings, modifications to the stereoselective synthesis was applied to obtain a higher *erythro*:*threo* ratio. This objective was achieved by replacing the Boc protecting group on **9** with a trityl (Tr) group and completing the synthesis without further modification to obtain a 9:1 *erythro*:*threo* ratio

with an improved overall yield of ~60%.[34] Another library of compounds was made by changing the cross-coupling partner in the Suzuki-Miyaura step, however, all the analogs that were obtained showed poor biological activity.[34] The potency of VQ-1 stereoisomers establishes an opportunity for further optimization and a pathway towards the treatment of this type of cancer.

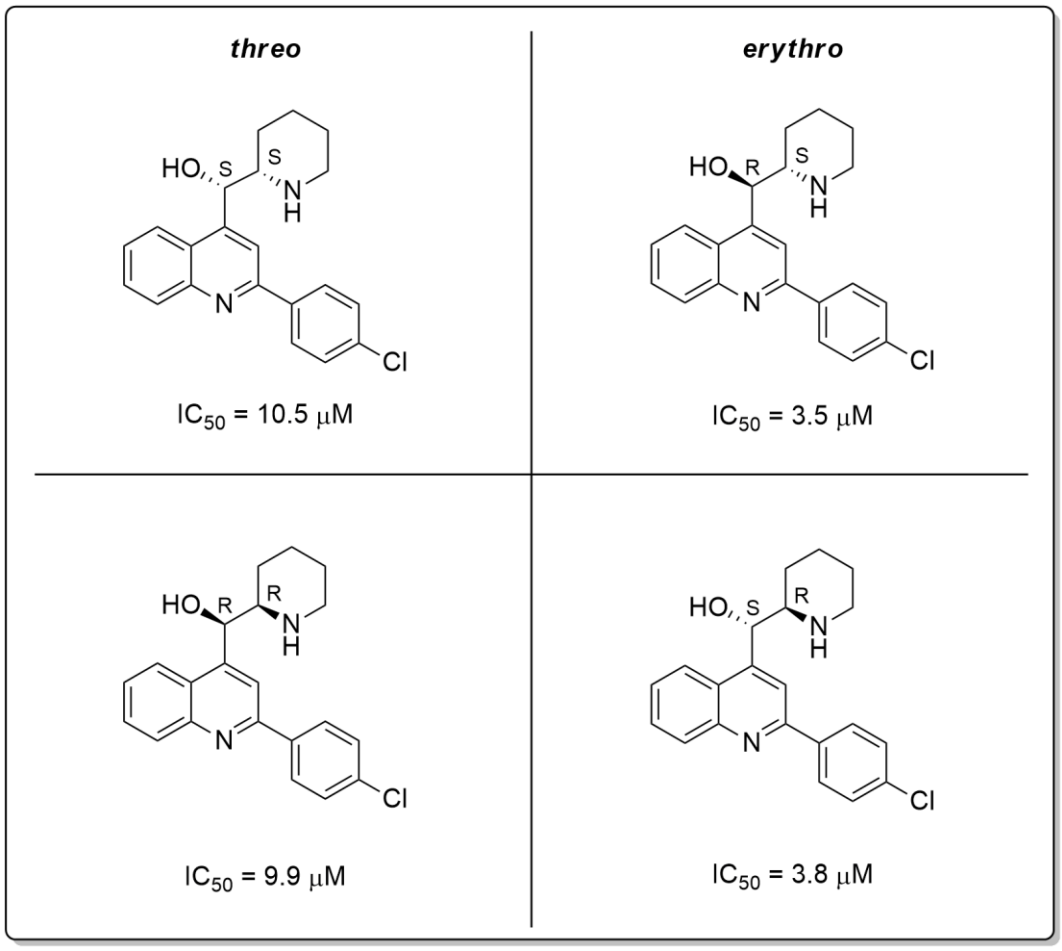

Figure 4-4. IC_{50} values of the four stereoisomers of VQ-1.

4.2 Recent Advancement in the SAR of VQ-1

In the recent years, the Hall Group has made efforts into expanding the library of VQ-1 analogs in search of better biological activity against GBM cells. Initially, Samantha Kwok synthesized a small library of VQ-1 analogs by varying the functional group at the *para* position of the 2-(4-chlorophenyl) moiety and tested their biological activity against U251 GBM cell lines *in vitro* at Dr. Godbout's laboratory in the Department of Oncology at the University of Alberta.[41] These

analogs were synthesized stereoselectively to obtain each stereoisomer independently. There was significant increase in potency when the chlorine atom was replaced by a bromine atom. Nevertheless, a decrease in potency was observed when the chlorine atom was replaced with hydrogen atom, methyl, or methoxy groups (Figure 4-5).[41]

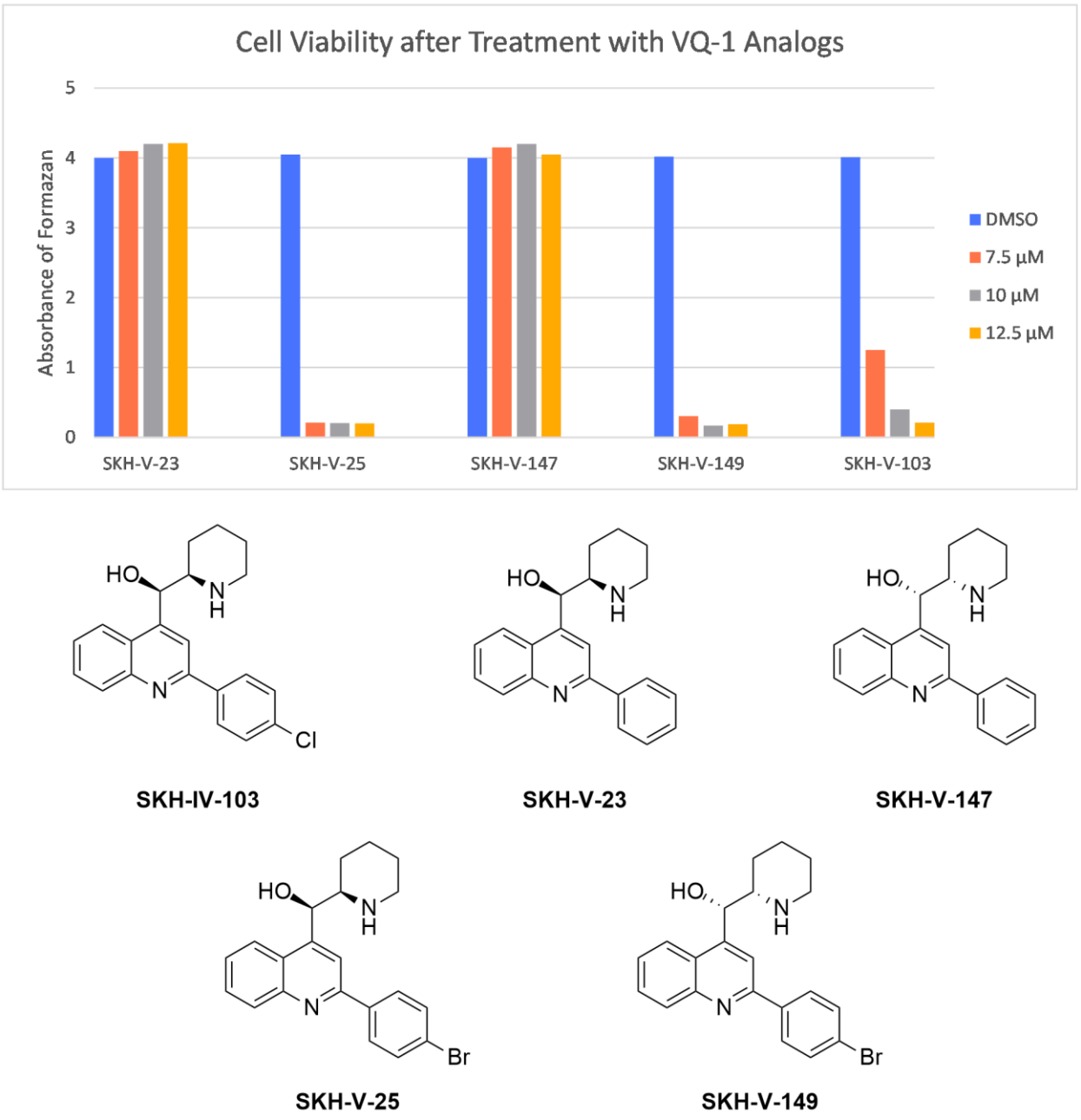

Figure 4-5. Biological activity of VQ-1 analogs synthesized by Kwok.

Encouraged by the preliminary findings of Kwok, the Hall Group made efforts into expanding the library of VQ-1 analogs seeking to further increase *in vitro* potency. Using the same methodology of replacing the chlorine atom at the *para* position with different functional groups, McDonald synthesized a larger library of *threo* racemates of VQ-1 analogs, where their performance against GBM cells was evaluated by Dr. Saket Jain from the Godbout laboratories.[42] Figure 4-6 illustrates the performance of selected compounds of McDonald's library of VQ-1 analogs. It was observed in McDonald's study that replacing the chlorine atom with bulky alkyl substituents is most beneficial for the biological activity as shown from the performance of analogs **RMH-VI-177** and **RMH-VIII-111** with *i*-Pr and *tert*-Bu groups respectively. On the other hand, smaller alkyl groups such as **RMH-VIII-103** and **RMH-VIII-105** showed no to insignificant activity compared to the bulkier alkyl substituents. Longer alkyl chain analog **RMH-VIII-119** demonstrated significant activity at 10 μM and 5 μM, albeit not as powerful as the bulkier **RMH-VIII-111**. A noteworthy observation was *N*-methylated dehydropiperidinyl quinoline VQ-1 analog **RMH-VIII-131,** which demonstrated excellent activity at 10 μM and 5μM. Furthermore, with a rigid cyclic alkyl substituent of **RMH-VIII-135** produced significantly reduced activity compared to **RMH-VIII-111**.[42] It is worth noting that **RMH-VIII-111** exhibited superior potency against GBM cells compared to **SKH-IV-103** (the original VQ-1). From these observations, analog **RMH-VIII-111** was selected as the lead compound for further SAR optimization.

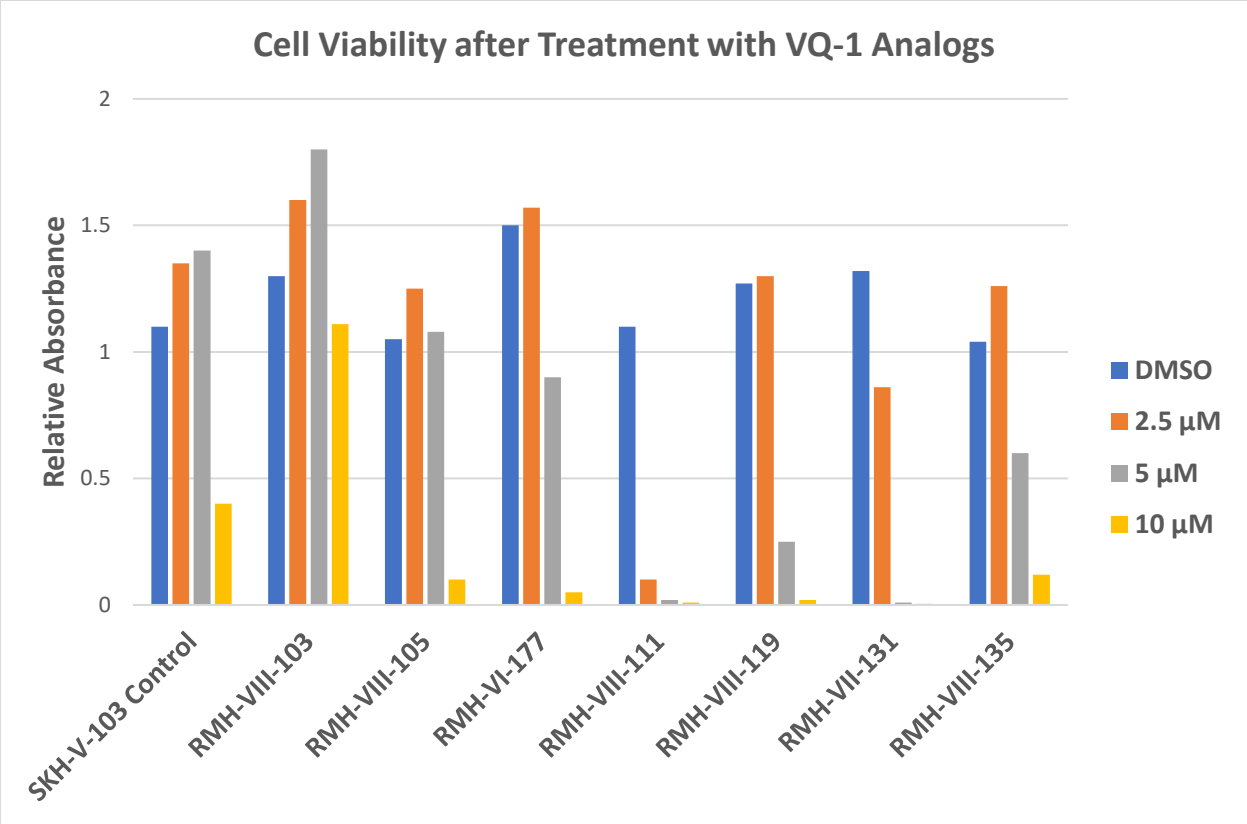

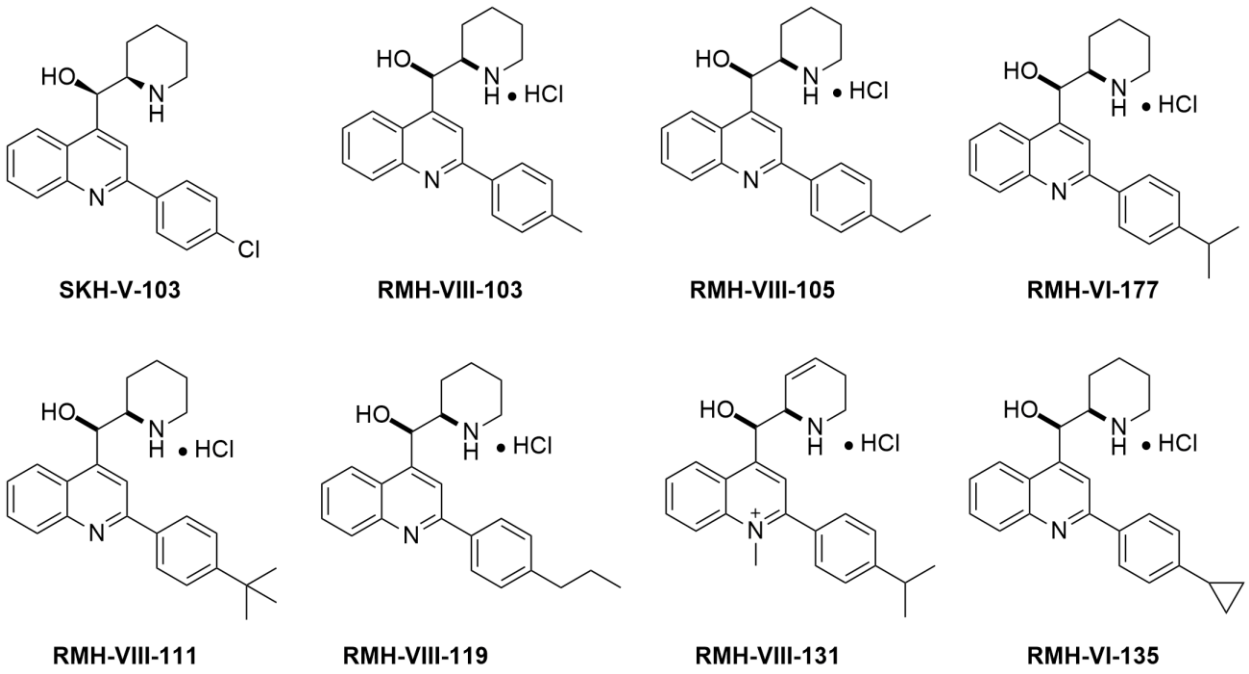

Figure 4-6. Biological activity of VQ-1 analogs synthesized by McDonald.

4.3 Objectives

The construction of a library of VQ-1 analogs led to the discovery of the lead candidate **RMH-VIII-111**. The lead candidate was chosen after observing that bulky alkyl groups at the *para* position of the 2-aryl quinolinyl substituent demonstrate better biological activity than VQ-1. However, opportunities to further optimize the lead candidate remain. The first consideration is to determine the extent to which large alkyl groups improve the efficacy against GBM cells by replacing the *tert*-butyl group of the drug candidate with larger alkyl groups such as adamantyl groups. Another modification to consider is the synthesis of quinolinium derivatives of the lead compound and compare their biological activity as quinolinium derivatives show promising activity as demonstrated by **RMH-VIII-131**. Lastly, after selecting the best drug candidate from the aforementioned SAR studies, the four stereoisomers of the drug will be synthesized, and their biological activity will be compared.

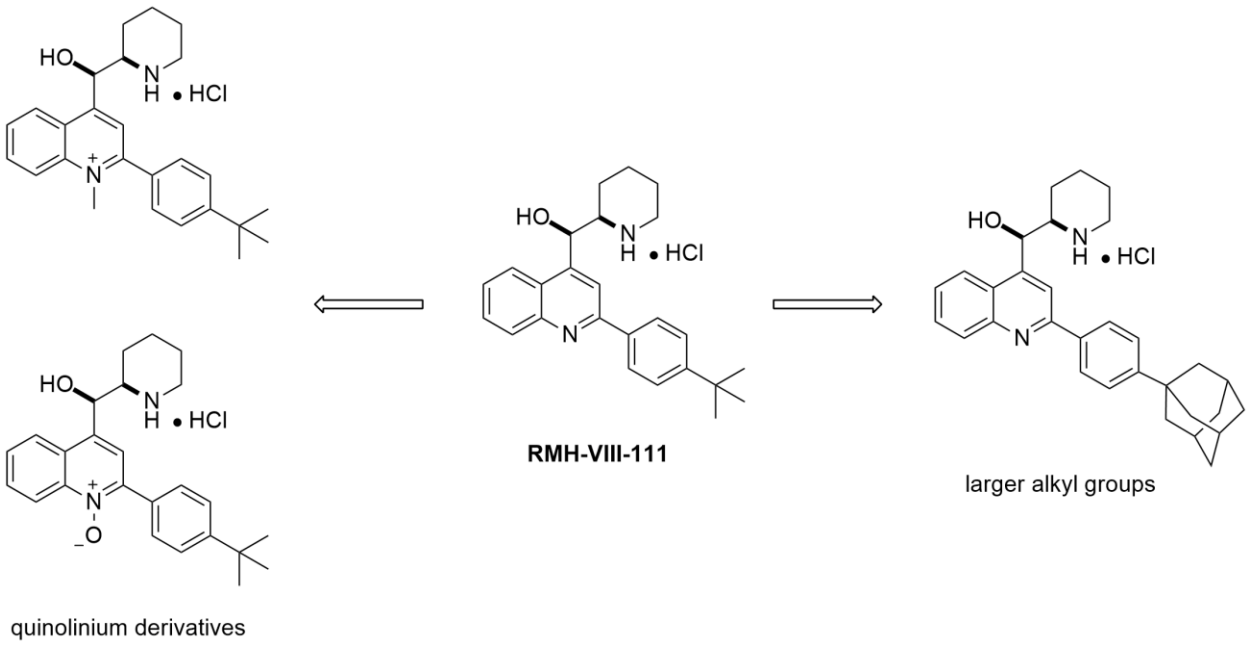

Figure 4-7. Potential modification on the drug candidate **RMH-VIII-111** to improve the biological activity

4.4 Synthesis of New VQ-1 Analogs

4.4.1 Synthesis of adamantyl substituted VQ-1 analog

I initiated the synthesis of the new adamantyl substituted VQ-1 analog by using an indium-catalyzed Friedel–Crafts alkylation of 1-bromoadamantane in benzene, followed by a Friedel–Crafts acylation that furnished the *para*-acetophenone **4-14**.[43] Next, a Pfitzinger reaction using compound **4-14** and isatin afforded quinoline carboxylic acid **4-15**.[36] A thionyl chloride mediated esterification in methanol of **4-15** yielded the corresponding methyl ester, which was subject to lithium borohydride reduction to furnish quinoline alcohol **4-16**. The desired quinoline aldehyde **4-17** was obtained via an oxidation reaction using Dess–Martin Periodinane (DMP) on alcohol **4-16**. The synthetic route of quinoline aldehyde **4-17** is shown in Scheme 4-4.

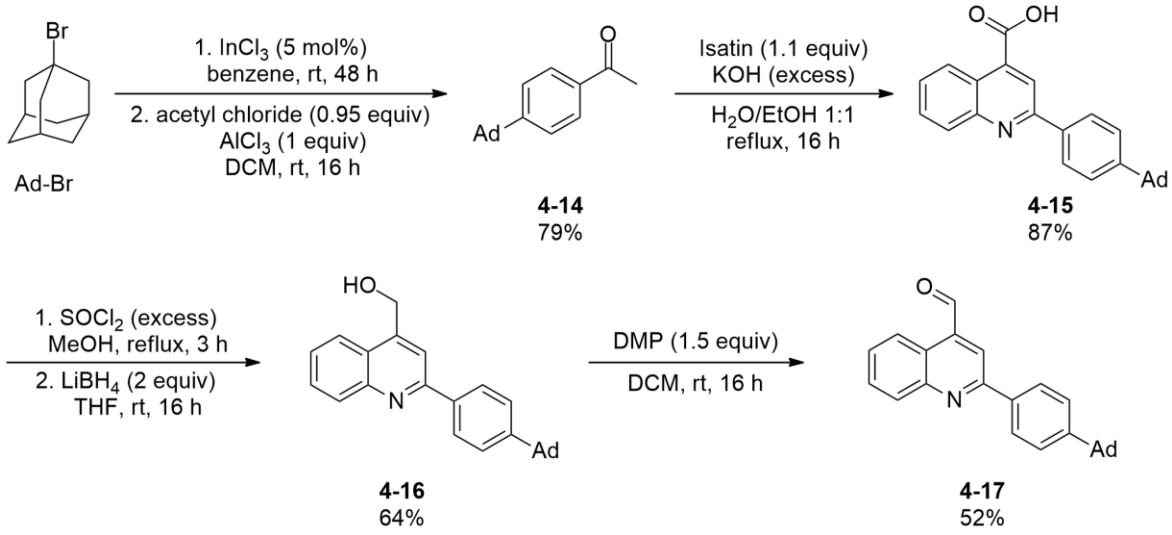

Scheme 4-4. Synthetic route towards quinoline aldehyde **4-17**.

The next step was to assemble the β-amino alcohol scaffold for the VQ-1 analog *via* an allylboration reaction (Scheme 4-5). To set up this key reaction, piperidinyl allylic boronate *(rac)*-**4-18** was prepared by the catalytic racemic borylative migration reaction conditions optimized by Kim and Hall.[44] Subjecting the key intermediates **4-17** and *(rac)*-**4-18** to a thermal allylboration reaction afforded the racemate of *threo* dehydro-VQ-1 scaffold **4-19** after silica gel purification. The synthesis was finalized by a hydrogenation of the endocyclic alkene using

Adams' catalyst (PtO_2) followed by BOC deprotection to furnish the corresponding VQ-1 analog **MEH-VI-117**.

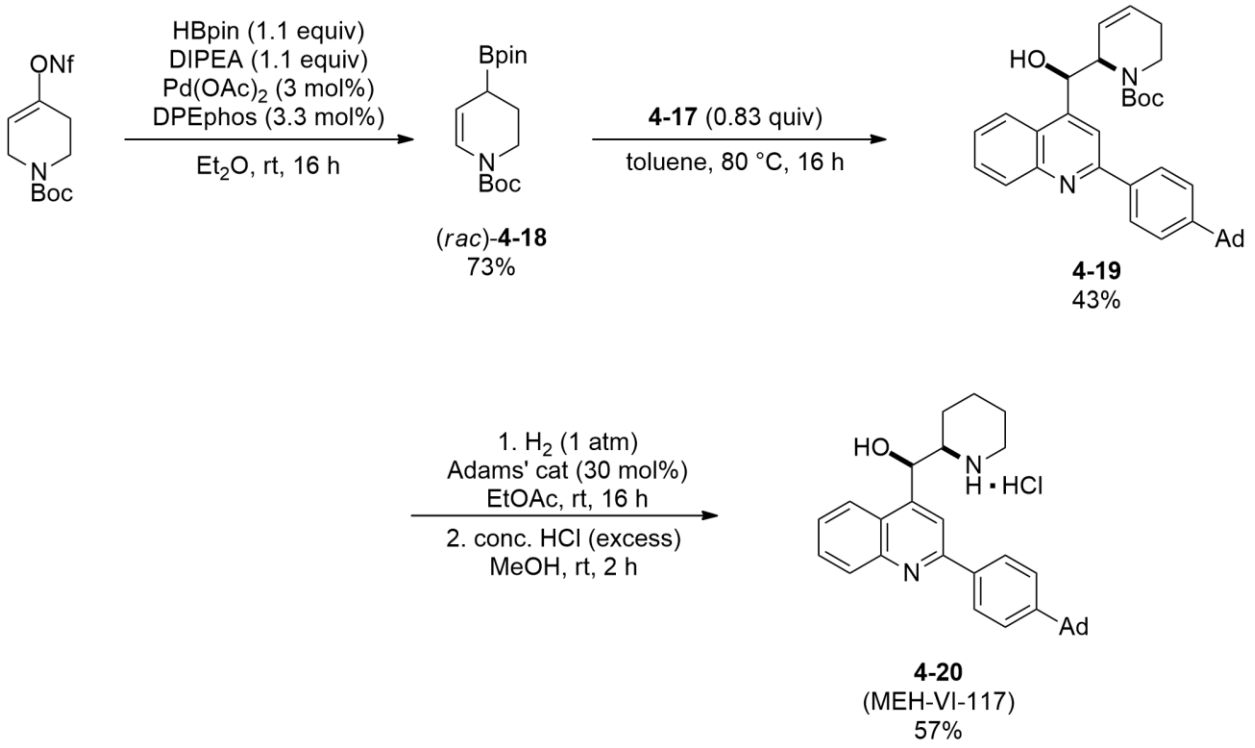

Scheme 4-5. Synthesis of VQ-1 analog **MEH-VI-117**.

4.4.2 Synthesis of quinolinium derivatives of RMH-VIII-111

The quinolinium derivatives of **RMH-VIII-111** were synthesized in a similar fashion to the synthetic route discussed in Section 4.4.1 from commercially available 4′-*tert*-butylacetophenone, albeit with slight modification. Formation of *N*-oxide or *N*-methyl quinolinium derivatives of the corresponding β-amino alcohol was planned after the endocyclic alkene reduction to avoid any potential reduction of the quinolinium derivatives. Thus, the *N*-oxide VQ-1 analog **MEH-VII-53** was obtained by an *N*-oxidation step using *m*CPBA, whereas the *N*-methyl VQ-1 analog **MEH-VII-95** was afforded *via N*-methylation using Simmons–Smith conditions.[42]

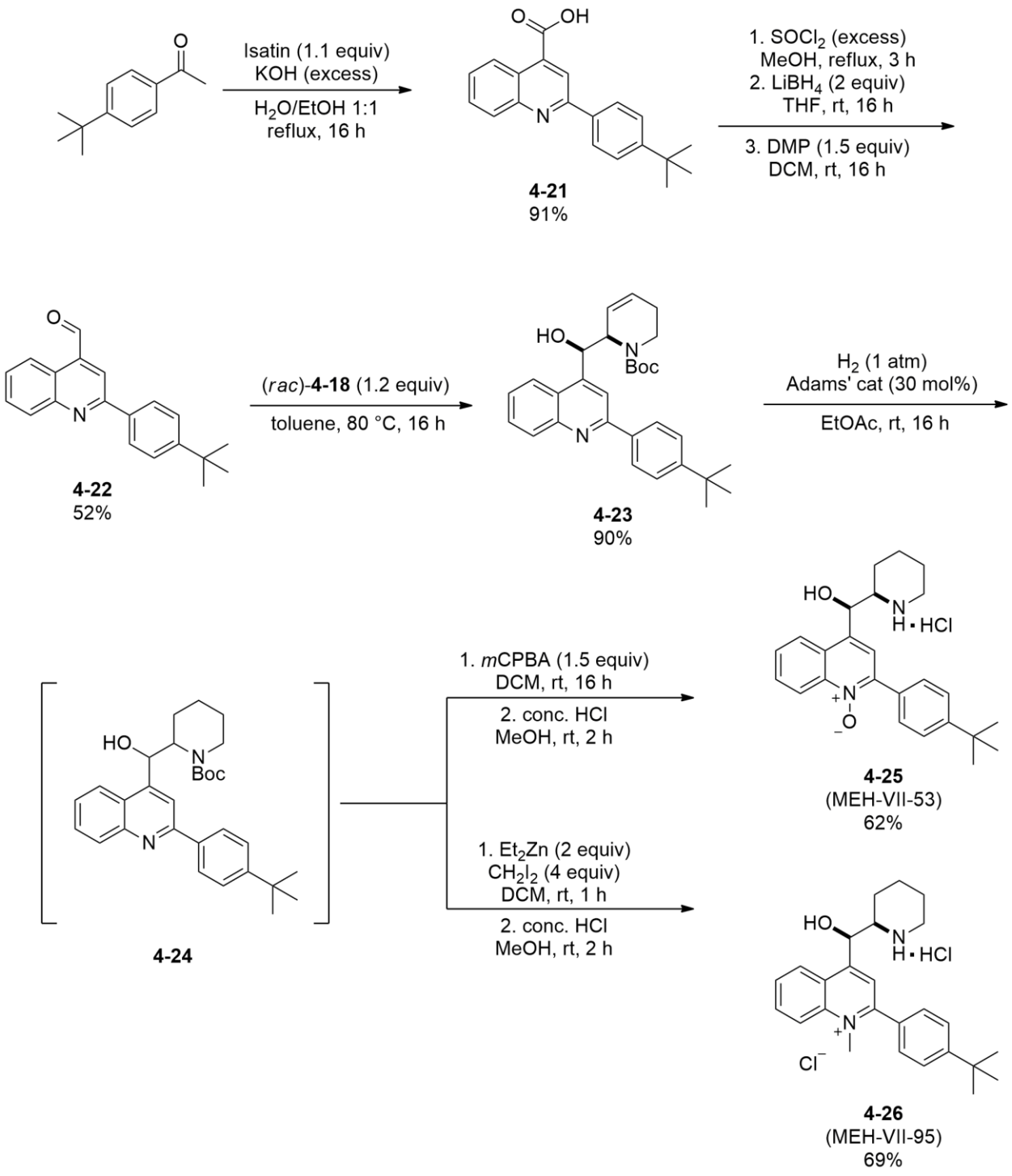

Scheme 4-6. Synthesis of VQ-1 analog **MEH-VII-53** and **MEH-VII-95**.

4.5 Biological Activity of the Newly Synthesized VQ-1 Analogs

After the new VQ-1 analogs were obtained, they were submitted to Dr. Mansi Garg from the Godbout laboratory for biological testing. The potency of the new analogs against U251 GBM cells and patient derived GBM cell line A4-004 was determined using the CellTiter 96® AQueous One Solution Cell Proliferation Assay (MTS).[45] The colourimetric *in vitro* assay set-up is as follows: GBM cells are incubated in a 96-well plate, then the cells are dosed with varying concentration of the VQ-1 analog of interest, in addition to Owen's reagent [3-(4,5-dimethylthiazol-2-yl)-5-(3-carboxymethoxyphenyl)-2-(4-sulfophenyl)-2H-tetrazolium (MTS), and phenazine ethosulfate (PES), an electron coupling reagent (Scheme 4-7).[45] When exposed to living cells, MTS and PES will undergo bioreduction to a colored formazan product *via* dehydrogenase enzymes, which use the cellular redox cofactors nicotinamide adenine dinucleotide phosphate (NADPH) or nicotinamide adenine dinucleotide (NADH). The colored solution is then analyzed using UV-Vis spectrophotometry at 490 nm, where the population of survived cells is inversely proportional to the measured absorbance.[45] To ensure the accuracy of the results, DMSO is commonly used as a negative control, along with **SKH-IV-103** as a positive control.[45]

The MTS assay compared the newly synthesized compounds **MEH-VI-117**, **MEH-VII-53**, and **MEH-VII-95** (Figure 4-8) at 10.0, 5.0, 2.5, and 1.25 μM respectively for U251 cells, and at 20.0, 10.0, 5.0, 2.5, and 1.25 μM respectively for the patient derived GBM cells A4-004. The potency of the new compounds were also compared relative to **RMH-VIII-111**, and compound **SKH-IV-103** serves as a positive control of the enantioenriched *threo* (*R*,*R*) VQ-1. The assay showed the *N*-oxide and *N*-methyl quinolinium derivatives have no benefits in the case of the saturated piperidine rings as most of the GBM cells survived even at higher drug concentrations. However, the adamantyl-containing analog **MEH-VI-117** showed comparable potency to **RMH-VIII-111** in both assays, which highlight the importance of bulky alkyl groups at the *para* position. Considering the results of biological activity and ease of preparation,

RMH-VIII-111 was selected as the lead drug candidate towards an independent synthesis and evaluation of all four stereoisomers.

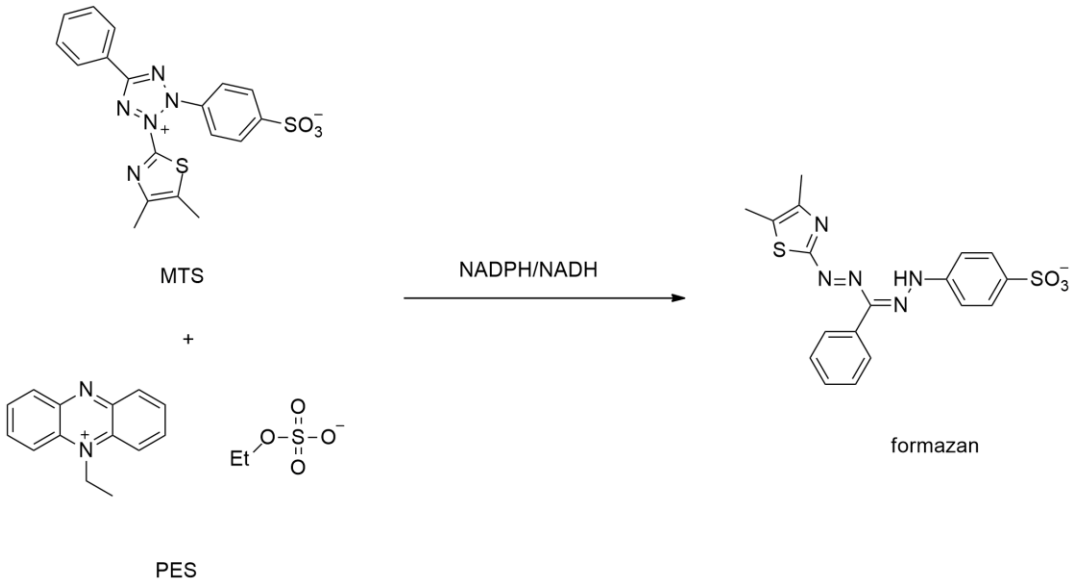

Scheme 4-7. Bioreduction of MTS to formazan.

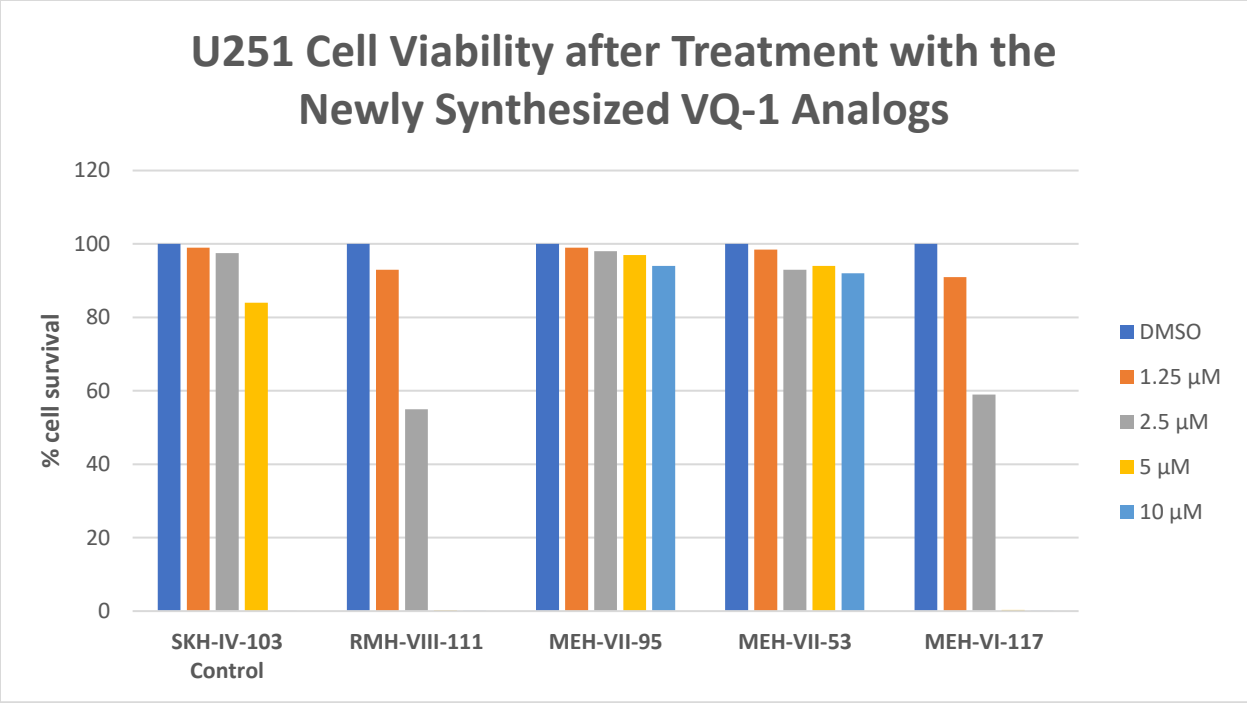

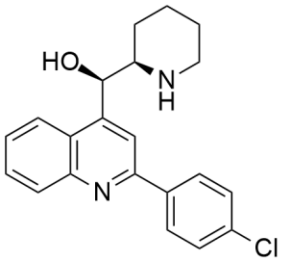

SKH-V-103

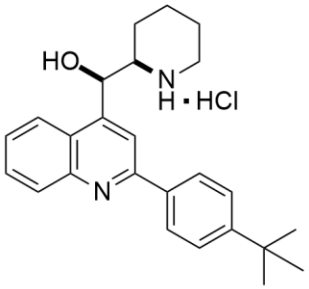

RMH-VIII-111

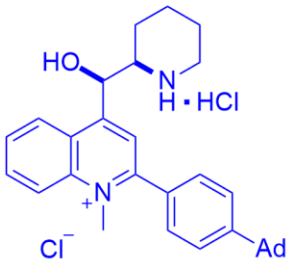

4-26
(MEH-VII-95)

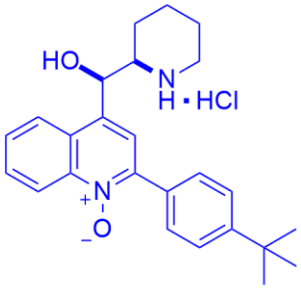

4-25
(MEH-VII-95)

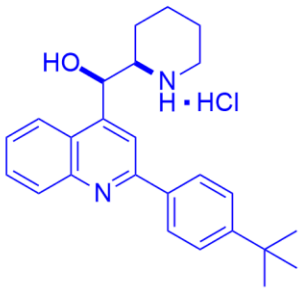

4-20
(MEH-VI-117)

Figure 4-8. Biological activity of the newly synthesized VQ-1 analogs against GBM cells U251. Analogs in black were synthesized by previous Hall Group members. Analogs in blue are newly synthesized by the author.

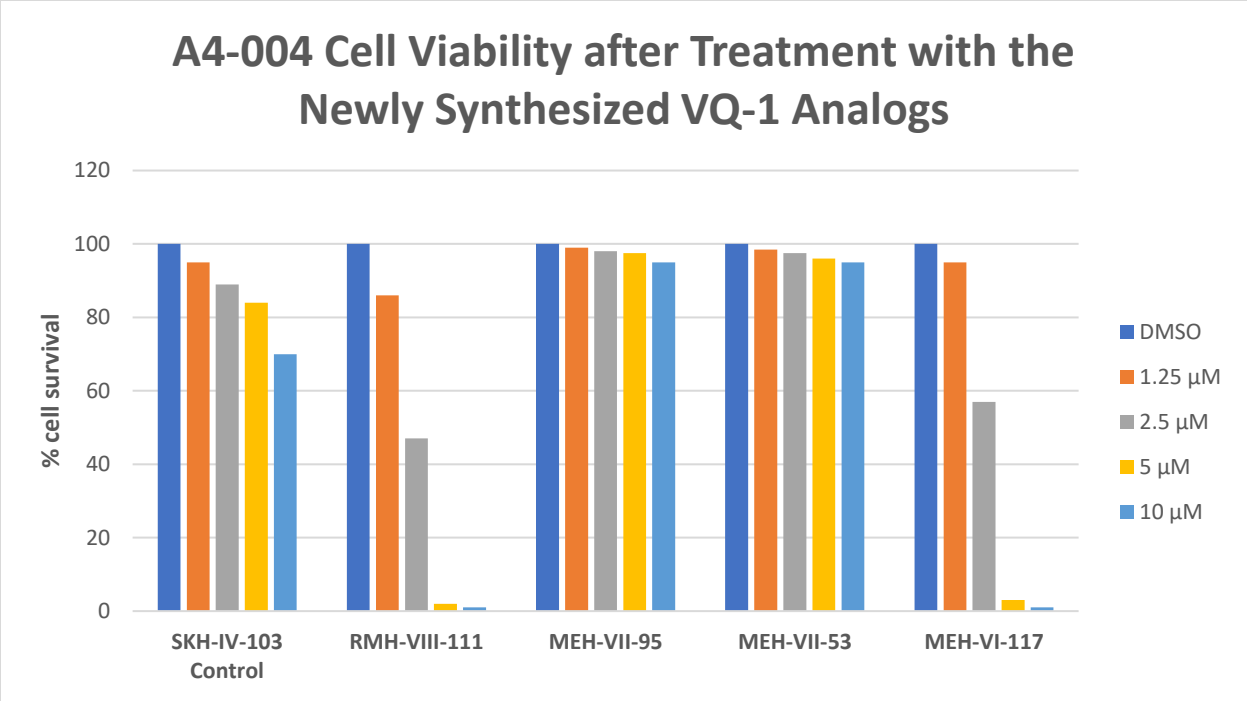

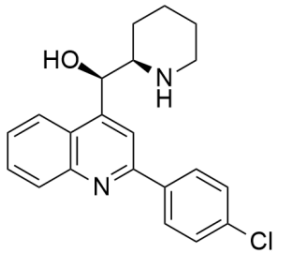

SKH-V-103

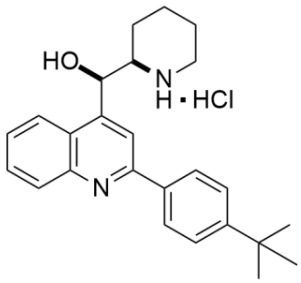

RMH-VIII-111

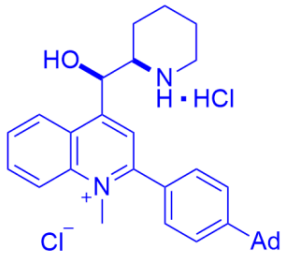

4-26
(MEH-VII-95)

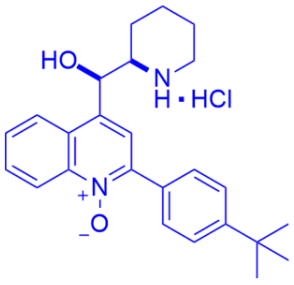

4-25
(MEH-VII-95)

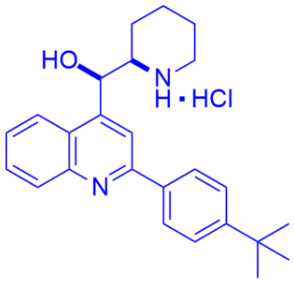

4-20
(MEH-VI-117)

Figure 4-9. Biological activity of the newly synthesized VQ-1 analogs against patient derived GBM cells. Analogs in black were synthesized by previous Hall Group members. Analogs in blue are newly synthesized by the author.

4.6 Synthetic Strategy Towards the Synthesis of all Stereoisomers of RMH-VIII-111

Inspired by the successful attempt from the Hall Group at synthesizing all four stereoisomers of mefloquine in 2013,[46] a retrosynthetic analysis towards the formation of all four stereoisomers of compound **RMH-VIII-111** is shown in Scheme 4-8. The key steps of this synthesis are the unique enantioselective borylative migration reaction using (+)-TANIAPHOS and the subsequent stereoselective aldehyde allylboration. VQ-1 analog **4-27** could be prepared by the catalytic hydrogenation of the key dehydro-intermediate **4-31** and the subsequent Boc deprotection, whereas its diastereomer **4-28** could be obtained from hydrogenation, alcohol inversion, and deprotection. Similarly, the other stereoisomers **4-29** and **4-30** could be accessed from the allylboration product **4-32** using (–)-TANIAPHOS.

Compared to the synthetic strategy employed by Ernfors and co-workers, the proposed synthetic route is convergent and amenable to selectively obtain each stereoisomer independently. This strategy utilizes two parallel synthetic routes: one to obtain the enantioenriched allylic boronate intermediate **4-18** and the other to access aldehyde **4-22**. The routes converge at this point to obtain VQ-1 analogs **4-27** and **4-29** in three steps, whereas analogs **4-28** and **4-30** can be accessed in five steps.

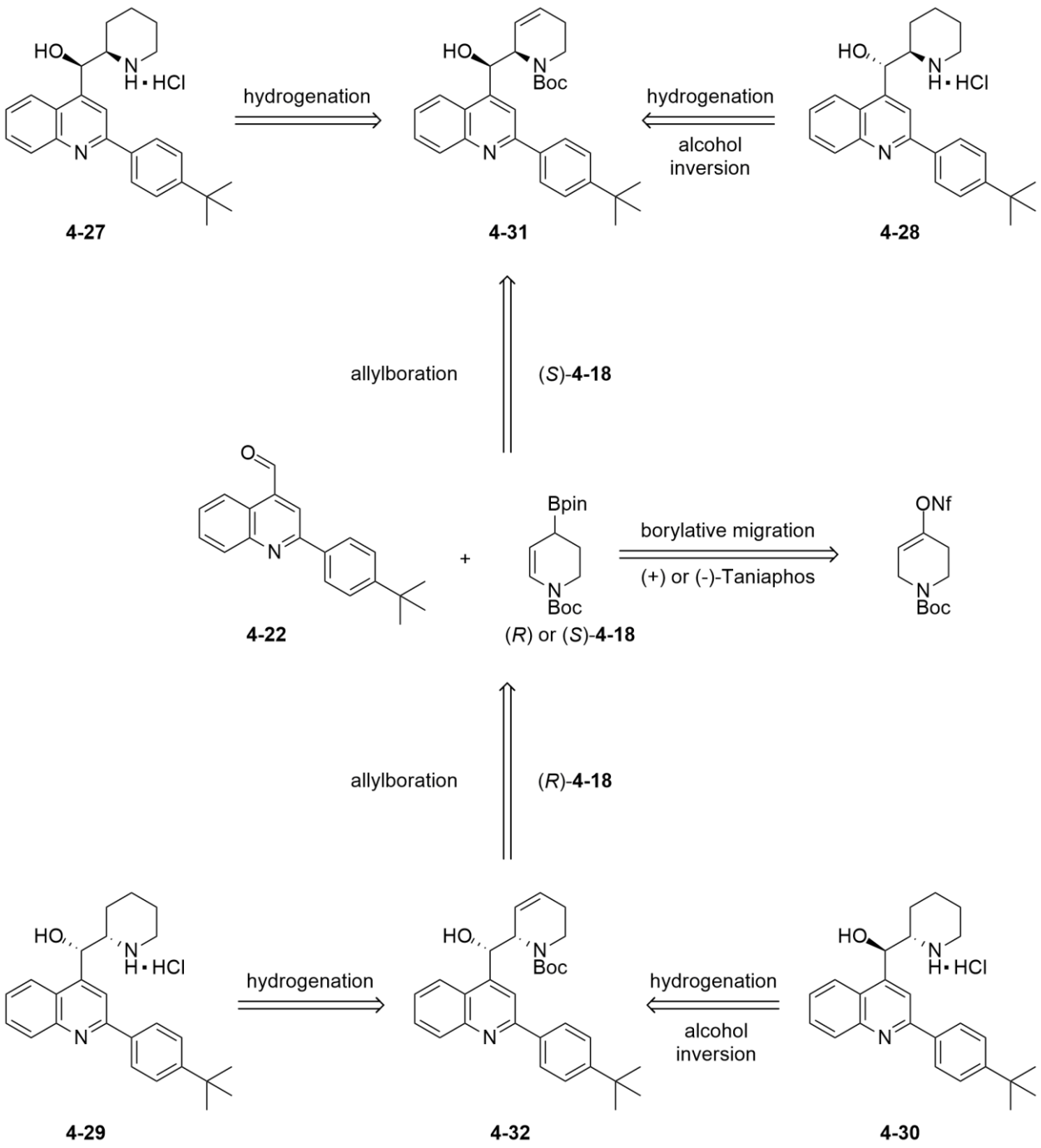

Scheme 4-8. Retrosynthetic analysis of the four stereoisomers of the VQ-1 analog **RMH-VIII-111**.

4.7 Synthesis of all Four Stereoisomers of VQ-1 analog RMH-VIII-111

Obtaining access to the two key intermediates in the synthesis of the stereoisomers is crucial to set up the key stereoselective aldehyde allylboration step. The aldehyde intermediate **4-22** was synthesized from a Pfitzinger reaction using commercially available 4′-*tert*-butylacetophenone followed by an esterification, a reduction, and a subsequent oxidation reaction (*vide supra,* Scheme 4-6). The piperidinyl allylic boronate intermediate (*S*)-**4-18** was obtained utilizing the unique enantioselective borylative migration reaction with Kim and Hall's optimized conditions with (+)-Taniaphos (Scheme 4-9)[44].

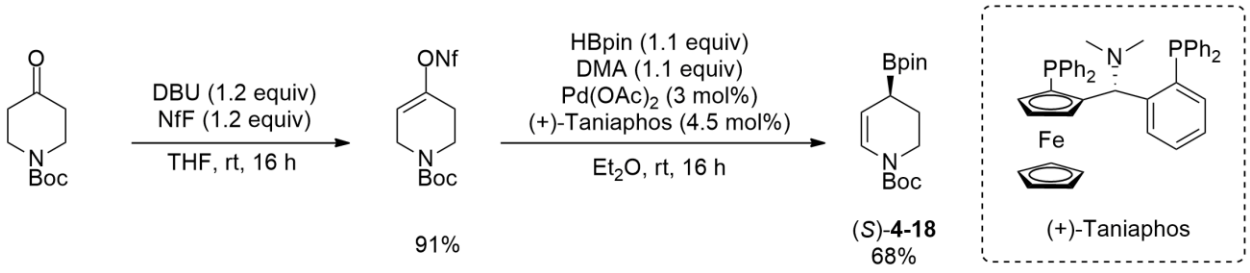

Scheme 4-9. Synthesis of enantioenriched piperidinyl allylic boronate (S)-**4-18**.

With the two main intermediates in hands, the stage was set for the stereoselective aldehyde allylboration reaction. Indeed, thermal allylboration between (*S*)-**4-18** and **4-22** afforded the *threo R,R* isomer of β-amino alcohol **4-31** in good yields and high enantiomeric excess (Scheme 4-10a). The stereoselectivity could be explained by Zimmerman-Traxler transition state as illustrated in Scheme-4-10b. Similarly, the *S,S* enantiomer **4-32** was obtained from allylic boronate (*R*)-**4-18** made by using (–)-Taniaphos in the borylative migration step.

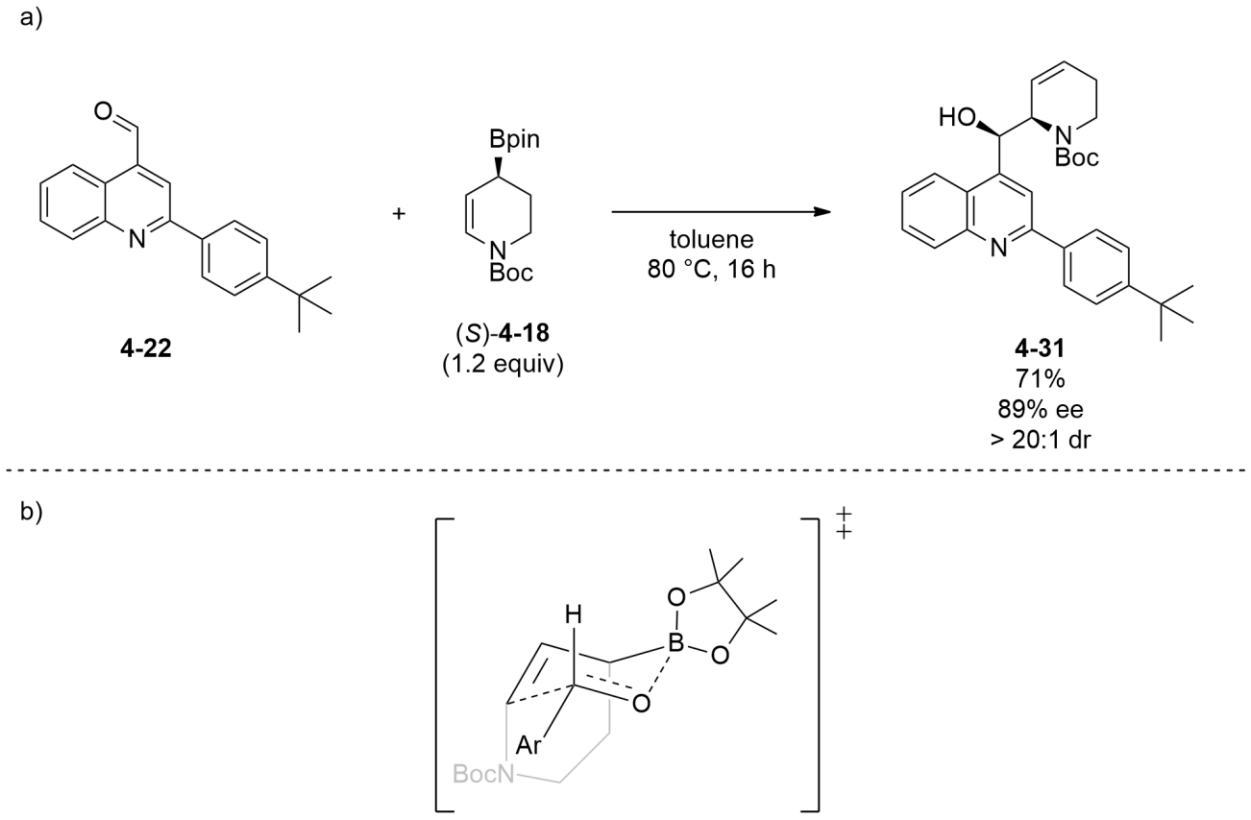

Scheme 4-10. a) Synthesis of **4-31** via a stereoselective thermal allylboration reaction. b) Rationale for the observed stereochemistry of the allylboration product.

The next stage was to finalize the synthesis of the *threo* enantiomers **4-27** and **4-29**. This was accomplished by heterogeneous catalyzed hydrogenation of the endocyclic alkene of the corresponding dehydro-derivatives using Adams' catalyst followed by Boc group removal under acidic conditions to obtain the corresponding salts **4-27** and **4-29** (Scheme 4-11). For the synthesis of the *erythro* enantiomers, inversion of the stereogenic secondary alcohol center is necessary. This was achieved as described by Ding and Hall using a direct oxidation of the secondary alcohol using Dess–Martin periodinane followed by a diastereoselective $CeCl_3$-$NaBH_4$ reduction to obtain the *erythro* dehydro-derivatives **4-33** and **4-34**.[46] The synthesis was finalized by applying the aforementioned hydrogenation and Boc deprotection to compounds **4-33** and **4-34** to obtain the *erythro* enantiomers **4-28** and **4-30** respectively (Scheme 4-12).

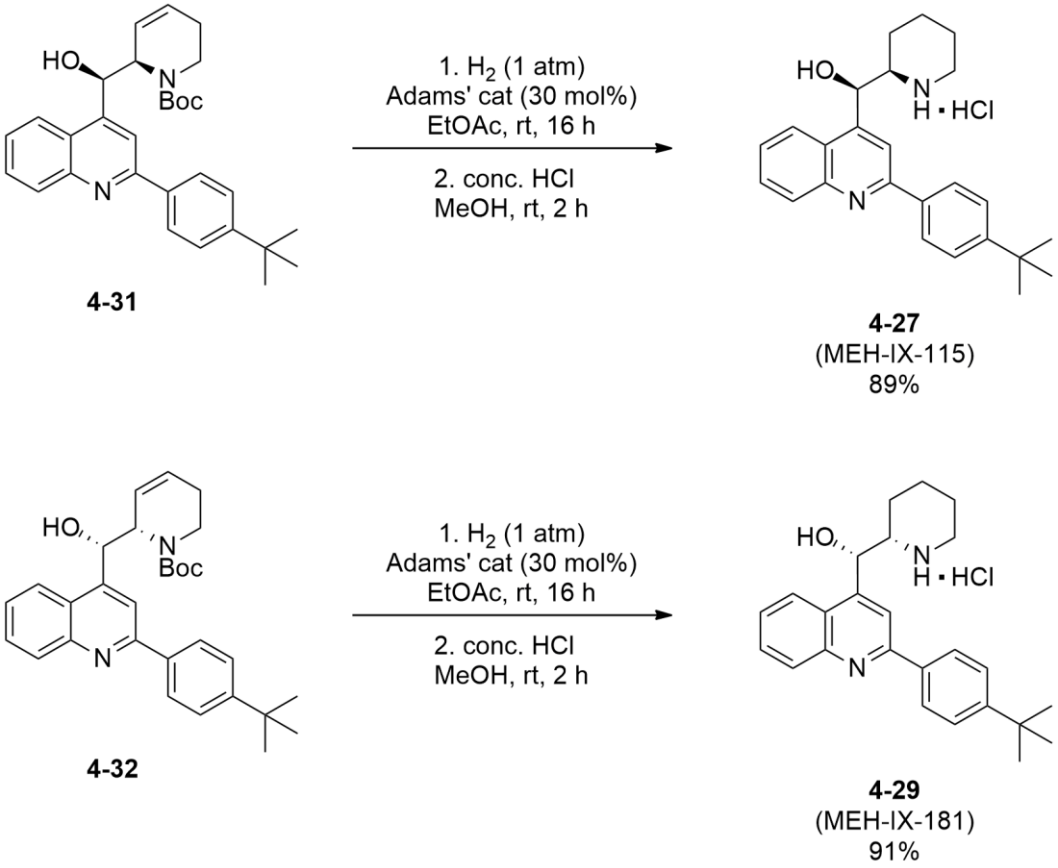

Scheme 4-11. Synthesis of the threo enantiomers **4-27** and **4-29**.

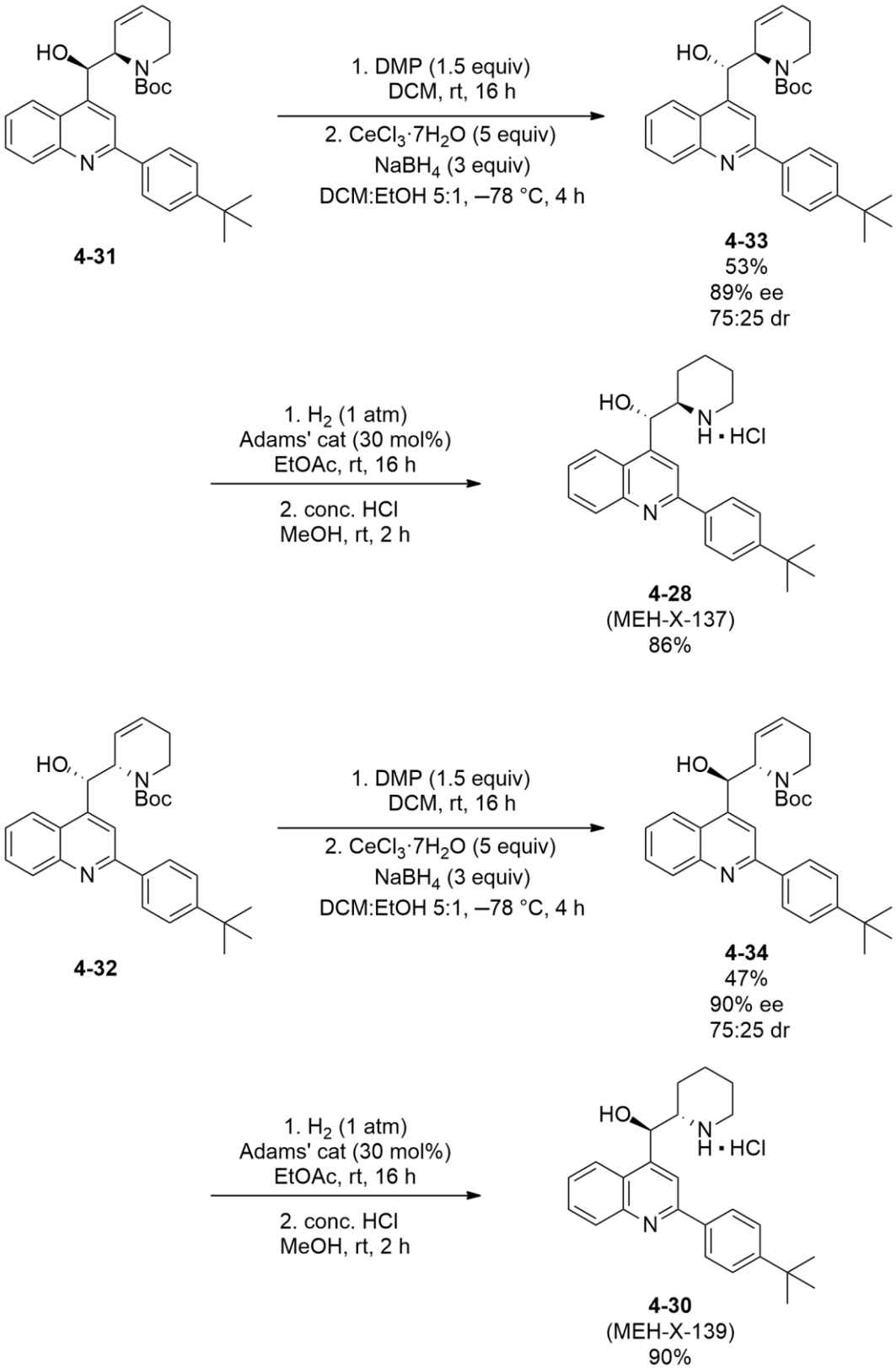

Scheme 4-12. Synthesis of the erythro enantiomers **4-28** and **4-30**.

Examination of the stereochemistry of the four stereoisomers was crucial before conducting any biological activity testing. Separation of the analogs in their free amine form is a challenging process. Therefore, the chiral separation of the Boc protected derivatives was performed instead *via* a co-injection experiment (Figure 4-9). This experiment confirmed the synthesis of all four stereoisomers individually. In addition, there was no undesired epimerization observed during the inversion of secondary alcohol as supported by the co-injection experiment. Credit for the determining the HPLC conditions of the experiments is attributed to Mr. Ed Fu. After confirming the synthesis and purity of the four stereoisomers of VQ-1 analog **RMH-VIII-111**, the samples were submitted to the Godbout laboratories for biological testing.

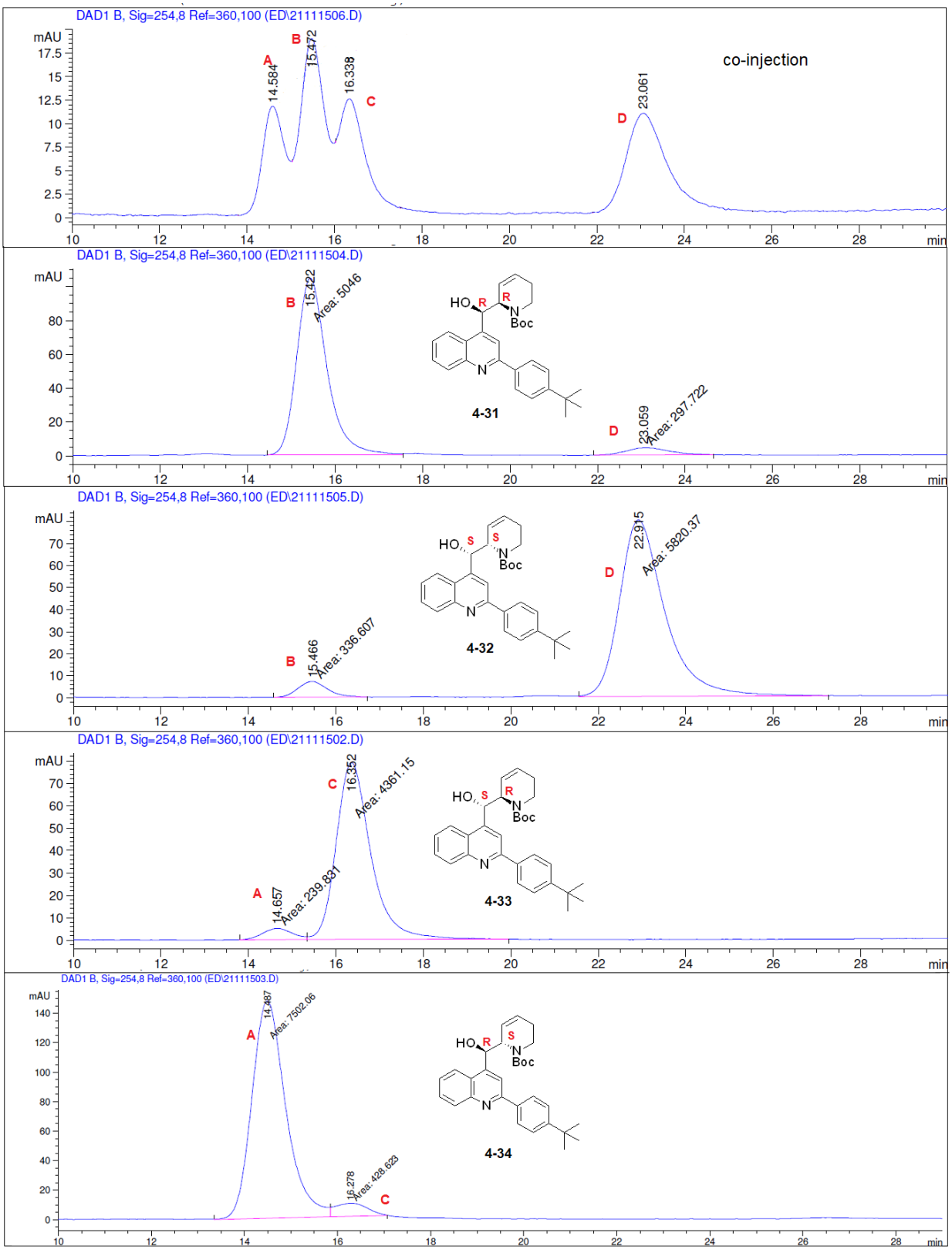

Figure 4-10. Chiral HPLC chromatograms of the four stereoisomers with their co-injection experiment at the top.

4.8 Biological Testing of Separate Stereoisomers

The newly synthesized stereoisomers were submitted to Dr. Mansi Garg in the laboratory of Dr. Godbout to test their biological activity against the growth of GBM cells. The potency of each stereoisomer against U251 GBM cells and patient derived GBM cell line A4-004 was determined using the MTS assay detailed in Section 4.5. Similar to the previous assay, DMSO was used as a negative control, along with **SKH-VI-103** as a positive control.

The MTS assay compared the IC_{50} values against GBM cells of the four separate stereoisomers. In addition, the potency of each stereoisomer was compared relative to **RMH-VIII-111** and **SKH-IV-103**. To our surprise, the newly synthesized stereoisomers had similar IC_{50} values and comparable performance to the racemic **RMH-VIII-111** analog (Table 4-2). These findings might be attributed to the binding strength of the *tert*-butyl substituent at the para-position of the 2-aryl ring overriding the effect of spatial orientation of the compounds that was observed in the case of the original VQ-1 analog. From these findings, **RMH-VIII-111** was selected as the best candidate for subsequent *in vivo* testing.

Table 4-2. IC_{50} values of the newly synthesized VQ-1 analogs in the treatment of GBM.

	IC_{50} (μM)	
Compound	**U251**	**A4-004**
4-27	2.5 ± 0.4	3.2 ± 0.7
4-29	2.7 ± 0.2	2.4 ± 0.4
4-28	2.6 ± 0.3	2.5 ± 0.4
4-30	2.4 ± 0.4	2.5 ± 0.4
RMH-VIII-111	2.5 ± 0.1	2.4 ± 0.2
SKH-IV-103	5.6 ± 0.5	24 ± 6

4.9 Summary and Future Work

In summary, new VQ-1 analogs were synthesized and tested for their biological activity against GBM cells. The result of the biological testing shows a correlation between the performance and bulky functional groups as shown in **RMH-VIII-111** and **MEH-VI-117**. On the other hand, quinolinium derivatives did not show promising results. Additionally, the four stereoisomers of the best analog of this study, **RMH-VIII-111**, were independently synthesized selectively using a convergent strategy and stereoselective methods. The biological activity of the newly synthesized stereoisomers to induce GBM cell death were determined and showed similar inhibition profiles to the racemic analog **RMH-VIII-111**. Based on these results, the simplest set of diastereomers **RMH-VIII-111** was selected for *in vivo* testing using mice implanted with GBM cells.

4.10 Experimental

4.10.1 General information

All reactions were performed under nitrogen atmosphere in flame dried glassware, unless stated otherwise. Tetrahydrofuran (THF), dichloromethane (DCM) and toluene were purified using a cartridge solvent purification system. Diethyl ether (Et_2O) was distilled over CaH_2. Cyclopentyl methyl ether (CPME) was purchased from Sigma-Aldrich and used as received. *N,N*-Diisopropylethylamine (DIPEA) was purchased from Sigma-Aldrich and distilled over CaH_2 under nitrogen prior to use. *N,N*-dimethylaniline (DMA) and 1,8-diazabicyclo[5.4.0.]undec-7-ene (DBU) were purchased from Sigma Aldrich and Combi-Blocks Inc., respectively, and distilled over CaH_2 under vacuum prior to use. Pinacolborane was purchased from Oakwood Chemicals and used without further purification. 1-*tert*-Butoxycarbonyl-4-piperidone, 1-carbobenzoxy-4-piperidone, perfluorobutanesulfonyl fluoride (NfF) and tris(dibenzylideneacetone)dipalladium(0) were purchased from Combi-Blocks Inc. and used as purchased without further purification. Palladium(II) acetate, Taniaphos, and DPEphos were purchased from STREM Chemicals. Thin layer chromatography (TLC) was performed on Merck Silica Gel 60 F254 plates and visualized using UV light, phosphomolybdic acid (PMA) stain, and $KMnO_4$ stain. Flash chromatography was

performed on ultra-pure silica gel 230-400 mesh. Nuclear magnetic resonance (NMR) spectra were recorded on Agilent/Varian INOVA-400, INOVA 500, INOVA-600 or INOVA-700 MHz instruments. The residual solvent proton (^{1}H) and carbon (^{13}C) signals were used as internal references. ^{1}H NMR data are represented as follows: Chemical Shift in ppm (δ) downfield from trimehtylsilane (multiplicity, coupling constant, integration). The following abbreviations are used in reporting NMR data: s, singlet; br s, broad singlet; t, triplet; app t, apparent triplet; dd, doublet of doublets; dt, doublet of triplets; m, multiplet. The error of coupling constants from ^{1}H NMR spectra is estimated to be ± 0.3 Hz. High-resolution mass spectra were recorded by the University of Alberta Mass Spectrometry Services Laboratory using electrospray ionization (ESI) method. Infrared spectra were obtained from a Nicolet Magna-IR machine with frequencies expressed in cm^{-1}. The enantiomeric excess ratios for optically enriched compounds were determined using a HPLC Agilent instrument with a Chiralcel-OD or Chiralpak IA or IB or IC column as specified in the following individual procedures.

4.10.2 Preparation of quinoline-4-carboxaldehyde derivatives

4.10.2.1 Preparation of quinoline-4-carboxylic acid derivatives

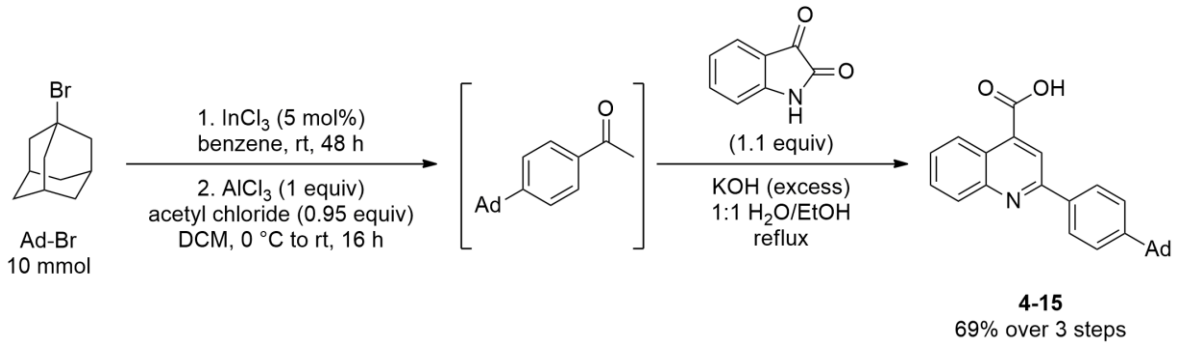

2-(4-(Adamantan-1-yl)phenyl)quinoline-4-carboxylic acid (4-15). $InCl_3$ (111 mg, 0.500 mmol) was introduced in a flame dried round-bottom flask charged with a stir bar. The flask was heated using a heat gun for 1–2 min under vacuum. 1-Bromoadamantane (2.15 g, 10.0 mmol) was added to the flask followed by benzene (22.0 g, 282 mmol). The reaction flask was covered with aluminum foil and stirred under nitrogen atmosphere for 48 h at room temperature. The reaction

mixture was then diluted with pentane (100 mL) and washed with water until neutral. The organic layer dried over Na_2SO_4, filtered, and concentrated *in vacuo*. The obtained crude product was directly used as is in the next step without further purification. The crude 1-phenyladamantane was mixed with $AlCl_3$ (1.33 g, 10 mmol) in a flame dried round-bottom flask charged with a stir bar. The flask was evacuated and backfilled with nitrogen 3 times before adding DCM (25.0 mL) and stirred at 0 °C for 10 min. Acetyl chloride (746 mg, 9.50 mmol) was added to the solution, then the reaction mixture was warmed up to room temperature and stirred for 16 h. The reaction mixture was quenched with water at 0 °C and extracted with EtOAc (50.0 mL × 3). The combined organic layers were washed with HCl (aq. 1.0 M), water and brine, dried over Na_2SO_4, filtered, and concentrated *in vacuo*. The obtained crude product was used directly in the following Pfitzinger reaction without further purification. In a round-bottom flask charged with a stir bar, potassium hydroxide (10.0 g, 178 mmol) was added and mixed with distilled water (15.0 mL) until a clear solution formed. Isatin (1.62 g, 11.0 mmol) was added to the basic solution, forming a dark red solution. Crude acetophenone derivative was added to the solution followed by EtOH (15.0 mL) and the reaction mixture was kept under reflux for 16 h. The mixture was cooled to rt and acidified with 6.0 M aq. HCl till the free carboxylic acid precipitated out of solution. The acid was collected by vacuum filtration and washed with water and pentane. The solid was dried under vacuum at 60 °C to afford 4-quinoline carboxylic acid **4-15** (2.65 g. 69%): **m.p.** = 241.2-243.7 °C; **^{1}H NMR** (500 MHz, DMSO-d_6) δ 8.62 (d, J = 8.5 Hz, 1H), 8.35 (s, 1H), 8.21 (d, J = 8.4 Hz, 2H), 8.11 (d, J = 8.4 Hz, 1H), 7.80 (t, J = 7.6 Hz, 1H), 7.64 (t, J = 7.6 Hz, 1H), 7.54 (d, J = 8.4 Hz, 1H), 2.12 –1.68 (m, 15H); **^{13}C NMR** (126 MHz, DMSO-d_6): δ 167.9, 155.7, 152.7, 148.4, 135.4, 129.9, 129.5, 127.1, 126.9, 125.7, 125.3, 123.5, 118.4, 42.7, 42.4, 36.1, 35.9, 28.4, 28.3; **IR** (microscope, cm^{-1}) 3056, 3031, 2901, 2847, 2658, 1699, 1588, 1544, 1447, 1260; **HRMS** (ESI-TOF): for $C_{26}H_{24}NO_2$ $(M–H)^-$: calcd. 382.1813; found 382.1808.

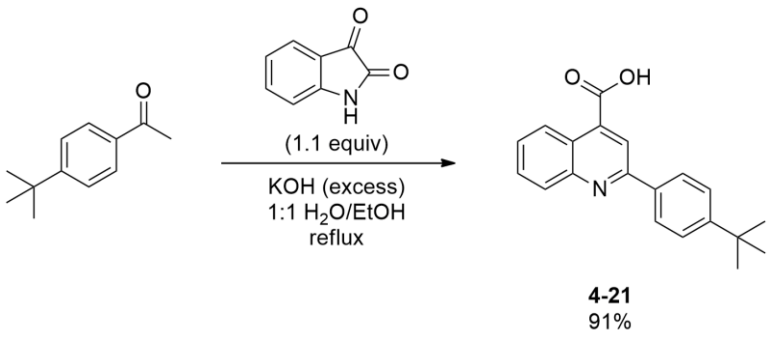

4-21
91%

2-(4-(*tert*-Butyl)phenyl)quinoline-4-carboxylic acid (4-21). Synthesized according to the Pfitzinger reaction procedure described above for **4-15** with isatin (3.37 g, 22.9 mmol) and 1-(4-(*tert*-butyl)phenyl)ethenone (3.84 g, 21.8 mmol) to afford yellow solid (6.05 g, 91%): **m.p.** =204.9-207.2 °C; **^{1}H NMR** (500 MHz, DMSO-d_6) δ 8.63 (d, *J* = 8.5 Hz, 1H), 8.42 (s, 1H), 8.20 (dt, *J* = 8.5 Hz, 2.0 Hz, 2H), 8.14 (d, *J* = 8.5 Hz, 1H), 7.83 (ddd, *J* = 8.5 Hz, 7.0 Hz, 1.5 Hz, 1H), 7.68 (ddd, *J* = 8.5 Hz, 7.0 Hz, 1.5 Hz, 1H), 7.56 (dt, *J* = 8.5 Hz, 2.0 Hz, 2H), 1.33 (s, 9H); **^{13}C NMR** (125 MHz, DMSO-d_6) δ 167.7, 155.7, 152.6, 148.4, 138.2, 135.2, 130.0, 129.6, 127.4, 126.9, 125.7, 125.5, 123.4, 118.7, 34.5, 31.0; **IR** (microscope, cm^{-1}) 3349, 3082, 2962, 2903, 2869, 1699, 1656, 1594, 1419, 1366, 1231, 1112; **HRMS** (ESI) for $(M+H)^+$: $C_{20}H_{20}NO_2$: calcd. 306.1489; found 306.1489.

*4.10.2.2 Synthesis of Aldehydes **4-17** and **4-22***

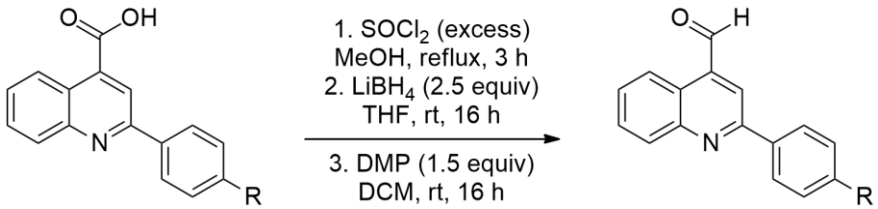

R = Ad, ^{t}Bu

General procedure A. To a solution of quinoline-4-carboxylic acid (3.50 mmol) in MeOH (30.0 mL) at 0 °C, $SOCl_2$ (2.08 g, 17.5 mmol) was added dropwise. After the addition of thionyl chloride was completed, the reaction mixture was stirred under reflux for 3 h. The volatiles were removed *in vacuo*. The residue was dissolved in ethyl acetate (50.0 mL), washed with a saturated aqueous

solution of $NaHCO_3$ (40 mL × 3). Then, the organic layer was washed with water, brine and dried over anhydrous Na_2SO_4, filtered and concentrated *in vacuo* to afford the corresponding ester, which was used in the next reduction step without further purification. In a flame dried round-bottom flask charged with a stir bar, the crude ester was mixed with THF (30.0 mL) under nitrogen atmosphere. Then, $LiBH_4$ (191 mg, 8.75 mmol) was added to the solution and stirred at room temperature for 16 h. The reaction mixture was quenched with water (40.0 mL) and extracted with EtOAc (50 mL × 3). The combined organic layers were washed with brine, dried over Na_2SO_4, filtered, and concentrated *in vacuo* to afford the corresponding alcohol, and used in the next oxidation step. In flame dried round-bottom flask charged with a stir bar, a solid mixture of the crude alcohol and Dess-Martin Periodinane (2.23 g, 5.25 mmol) was dissolved in DCM (25.0 mL). The reaction mixture was stirred under nitrogen atmosphere for 16 h. The reaction mixture was quenched with 1.0 M sodium hydroxide solution (40 mL) and extracted with EtOAc (50 mL × 3). The organic layers were combined and then washed with water until the pH was 7, brine, dried over Na_2SO_4, filtered, and concentrated *in vacuo* to obtain the crude aldehyde. Flash chromatography (1:11 EtOAc:hexanes) was used to isolate the desired aldehyde.

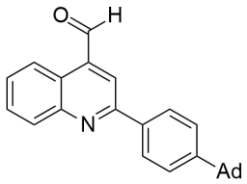

2-(4-(Adamantan-1-yl)phenyl)quinoline-4-carbaldehyde (4-17). Prepared by the general procedure A using carboxylic acid **4-15** (1.34 g, 3.50 mmol). Flash chromatography afforded a yellow viscous oil (428 mg, 33%): **m.p.** = 142.4-145.1 °C; **^{1}H NMR** (500 MHz, $CDCl_3$) δ 10.59 (s, 1H), 8.99 (d, *J* = 8.3, 1H), 8.30–8.23 (m, 2H), 8.19 (d, *J* = 8.5, 2H), 7.81 (ddd, *J* = 8.3, 6.9, 1.3 Hz, 1H), 7.69 (ddd, *J* = 8.2, 6.9, 1.2 Hz, 1H), 7.57 (d, *J* = 8.5 Hz, 2H), 2.19–1.74 (m, 15H); **^{13}C NMR** (125 MHz, $CDCl_3$) δ 193.2, 157.5, 153.6, 149.5, 141.9, 137.7, 135.8, 133.4, 131.9, 130.3, 130.2, 128.7, 127.2, 125.7, 124.2, 122.8, 43.1, 36.8, 36.5, 29.1; **IR** (microscope, cm^{-1}) 3056, 2903, 2847,

1704, 1594, 1544, 1448, 1240; **HRMS** (ESI) for $(M+H)^+$: $C_{26}H_{26}NO$: calcd. 368.2009; found 368.2010.

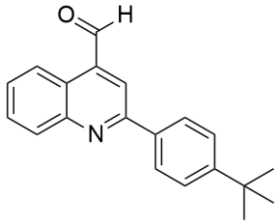

2-(4-(*tert*-Butyl)phenyl)quinoline-4-carbaldehyde (4-22). Prepared by the general procedure A using carboxylic acid **4-21** (1.07 g, 3.50 mmol). Flash chromatography afforded a yellow solid (709 mg, 52%): **m.p.** = 73.6-75.8 °C; **^{1}H NMR** (700 MHz, DMSO-d_6) δ 10.59 (s, 1H) 8.96 (d, *J* = 8.4 Hz, 1H), 8.69 (s, 1H), 8.27 (d, *J* = 8.4 Hz, 2H), 8.19 (d, *J* = 8.4 Hz, 1H), 7.88 (t, *J* = 7.0 Hz, 1H), 7.77 (t, *J* = 7.0 Hz, 1H), 7.62 (d, *J* = 8.4 Hz, 2H), 1.35 (s, 9H); **^{13}C NMR** (175 MHz, DMSO-d_6) δ 194.9, 156.5, 153.0, 148.5, 137.7, 135.0, 130.4, 129.6, 128.7, 127.0, 125.8, 124.3, 124.2, 122.2, 34.6, 31.0. **IR** (microscope, cm^{-1}) 3064, 2962, 2903, 2867, 2744, 1704, 1595, 1545, 1337, 1240; **HRMS** (ESI) for $(M+H)^+$: $C_{20}H_{20}NO$: calcd. 290.1539; found 290.1539.

4.10.3 Synthesis of allyl piperidinyl boronates

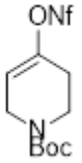

***tert*-Butyl 4-(((perfluorobutyl)sulfonyl)oxy)-5,6-dihydropyridine-1(2*H*)-carboxylate.** In a flame dried round bottom flask equipped with a stir bar, 1-Boc-4-piperidone (5.0 g, 25 mmol) was dissolved in THF (130 mL) under a nitrogen atmosphere. The solution was cooled down to 0 °C using an ice-bath and stirred for 5 min. DBU (4.5 mL, 30 mmol) and perfluorobutanesulfonyl fluoride (5.4 mL, 30 mmol) were added respectively. The ice-bath was removed, and the solution was allowed to stir at room temperature overnight. The reaction mixture was quenched by slow addition of water and extracted with Et_2O (100 mL × 3). The organic layers were washed with

brine, dried over Na_2SO_4, filtered and concentrated *in vacuo*. The brown crude oil was then purified by silica gel (15% Et_2O/pentane). Spectral data are in accordance with the literature:[44] **^{1}H NMR** (400 MHz, $CDCl_3$): δ 5.77 (s, 1H), 4.11–3.99 (m, 2H), 3.63 (t, J = 5.7 Hz, 2H), 2.48–2.39 (m, 2H), 1.47 (s, 9H).

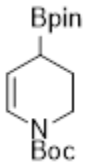

***tert*-Butyl 4-(4,4,5,5-tetramethyl-1,3,2-dioxaborolan-2-yl)-3,4-dihydropyridine-1(*2H*)-carboxylate ((*rac*)-4-18)**. In a flame dried round bottom flask equipped with a stir bar, palladium acetate (54 mg, 0.24 mmol) and DPEphos (140 mg, 0.26 mmol) were mixed with freshly distilled Et_2O (24 mL) and stirred at room temperature for 10 min. DIPEA (1.5 mL, 8.8 mmol), pinacolborane (1.3 mL, 8.8 mmol) and *tert*-butyl-4-(nonafluorobutylsulfonyloxy)-5,6-dihydropyridine-1(*2H*)-carboxylate **3-1** (3.9 g, 8.0 mmol) were added respectively, and the mixture was stirred at room temperature for 16 h. The mixture was filtered through a short silica plug (100% Et_2O) and the filtrate was concentrated *in vacuo*, the crude product was purified by silica gel (15% Et_2O/pentane) which provided the allylic boronate as a colorless oil (1.66 g, 67% yield). Spectral data are in accordance with the literature:[44] **^{1}H NMR** (700 MHz, $CDCl_3$, rotamers are present): δ 6.84–6.71 (m, 1H), 5.02–4.76 (m, 1H), 3.62–3.44 (m, 2H), 1.92–1.77 (m, 3H), 1.45 (s, 9H), 1.21 (s, 12H); **^{13}C NMR** (176 MHz, $CDCl_3$, rotamers are present): δ 152.7, 152.3, 124.5, 124.2, 106.3, 105.8, 83.4, 83.4, 80.3, 80.2, 42.4, 41.3, 28.4, 24.8, 24.7, 23.3, 18.3.

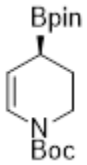

(*4S*)-*tert*-Butyl 4-(4,4,5,5-tetramethyl-1,3,2-dioxaborolan-2-yl)-3,4-dihydropyridine-1(*2H*)-carboxylate (*(S)*-4-18). In a flame dried round bottom flask equipped with a stir bar, palladium acetate (25 mg,

0.11 mmol) and (+)-Taniaphos (110 mg, 0.17 mmol) were mixed with CPME (12 mL) and stirred at room temperature for 10 min. *N*,*N*-dimethylaniline (510 µL, 4.1 mmol), pinacolborane (590 µL, 4.1 mmol) and *tert*-butyl-4-(nonafluorobutylsulfonyloxy)-5,6-dihydropyridine-1(*2H*)-carboxylate **3-1** (1.8 g, 3.7 mmol) were added respectively, and the mixture was stirred at room temperature for 16 h. The mixture was filtered through a short silica plug (100% Et_2O) and the filtrate was concentrated *in vacuo*, the crude product was purified by flash chromatography (15% Et_2O/pentane) which provided the allylic boronate as a colorless oil (910 mg, 79% yield). Spectral data are in accordance with the literature:[44] **^{1}H NMR** (700 MHz, $CDCl_3$, rotamers are present): δ 6.84–6.71 (m, 1H), 5.02–4.76 (m, 1H), 3.62–3.44 (m, 2H), 1.92–1.77 (m, 3H), 1.45 (s, 9H), 1.21 (s, 12H); **^{13}C NMR** (176 MHz, $CDCl_3$, rotamers are present): δ 152.7, 152.3, 124.5, 124.2, 106.3, 105.8, 83.4, 83.4, 80.3, 80.2, 42.4, 41.3, 28.4, 24.8, 24.7, 23.3, 18.3.

4.10.4 Synthesis of racemic VQ-1 analogs

4.10.4.1 Synthesis of racemic Boc protected dehydro-VQ-1 analogs

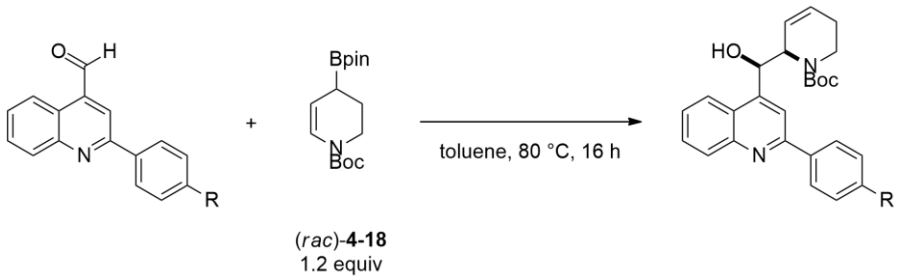

General procedure B. In a flame dried reaction tube with charged with stir bar, quinoline aldehyde (0.500 mmol) was added, followed by allylic piperidinyl boronate (*rac*)-**4-18** (185 mg, 0.600 mmol) and dissolved in toluene (1.00 mL). The reaction tube was sealed, heated to 80 °C, and stirred for 16 h. The reaction mixture was cooled down to rt then concentrated *in vacuo*. The crude oil purified by flash chromatography (20% EtOAc/Hexanes) to afford the allylboration product.

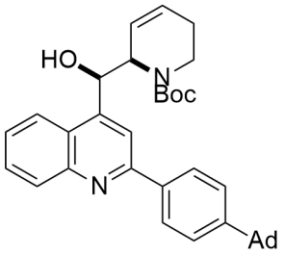

***tert*-Butyl 2-((2-(4-(adamantan-1-yl)phenyl)quinolin-4-yl)(hydroxy)methyl)-5,6-dihydropyridine-1(2H)-carboxylate (4-19)**. Prepared by general procedure B using aldehyde **4-17** (184 mg, 0.500 mmol). Flash chromatography afforded a pale-yellow solid (142 mg, 45%): **^{1}H NMR** (500 MHz, $CDCl_3$, rotamers are present): δ 8.20 (d, *J* = 8.1 Hz, 1H), 8.16–7.89 (m, 4H), 7.69 (t, *J* = 7.5 Hz, 1H), 7.56–7.45 (m, 3H), 6.08–5.73 (m, 1H), 5.63–5.40 (m, 1H), 5.16–4.82 (m, 1H), 4.36–4.03 (m, 1H), 3.19–2.91 (m, 1H), 2.37–0.98 (m, 28H); **^{13}C NMR** (126 MHz, $CDCl_3$, rotamers are present): δ 152.8, 148.6, 141.7, 130.5, 129.3, 128.0, 127.4, 126.0, 125.4, 123.4, 122.0, 117.6, 81.1, 73.0, 43.4, 43.2, 36.9, 36.4, 29.0, 28.5, 28.1; **HRMS** (ESI) for $(M+H)^+$ $C_{36}H_{43}N_2O_3$: calcd. 551.3268; found 551.3264.

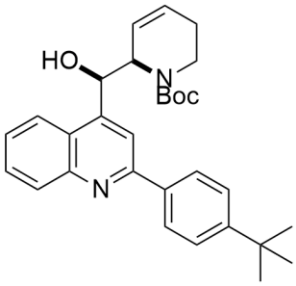

***tert*-Butyl 2-((2-(4-(*tert*-butyl)phenyl)quinolin-4-yl)(hydroxy)methyl)-5,6-dihydropyridine-1(2H)-carboxylate (4-23)**. Prepared by general procedure B using aldehyde **4-22** (144 mg, 0.500 mmol). Flash chromatography afforded a white solid (213 mg, 90%): **m.p.** = 103.7-105.3 °C; **^{1}H NMR** (500 MHz, $CDCl_3$, rotamers are present): δ 8.19–7.94 (m, 5H), 7.69 (t, *J* = 7.7 Hz, 1H), 7.53 (d, *J* = 8.4 Hz, 2H), 7.48 (t, *J* = 7.4 Hz, 1H), 6.01–5.46 (m, 3H), 5.09–4.85 (m, 1H), 4.38–4.10 (m, 1H), 2.95 (m, 1H), 2.21–1.96 (m, 2H), 1.51 (s, 9H), 1.37 (s, 9H); **^{13}C NMR** (126 MHz, $CDCl_3$, rotamers are present): δ 157.3, 157.1, 152.5, 148.6, 136.9, 130.5, 129.1, 127.7, 127.3, 125.9, 125.7, 125.3, 124.2, 123.4, 117.5, 81.0, 80.2, 72.8, 60.4, 58.2, 57.0, 38.4, 37.3, 34.7, 31.3, 28.4, 28.0,

27.9, 24.7, 24.3, 21.0, 14.2; **IR** (microscope, cm^{-1}) 3016, 2966, 1682, 1420, 1366, 1169; **HRMS** (ESI) for $(M+H)^+$ $C_{30}H_{37}N_2O_3$: calcd. 473.2799; found 473.2798.

*4.10.4.2 Synthesis of VQ-1 analog **MEH-VI-117***

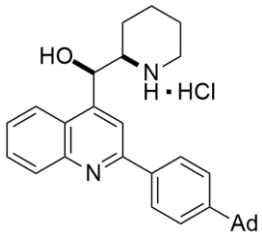

(2-(4-(Adamantan-1-yl)phenyl)quinolin-4-yl)(piperidin-2-yl)methanol hydrochloride (**4-20)**. In a flame dried 10 mL pear-shaped flask charged with a stir bar, Adams' catalyst (6.2 mg, 27 μmol) was mixed with the dehydro Boc protected VQ-1 analog **4-19** (50 mg, 91 μmol). The flask was evacuated and backfilled with nitrogen for three cycles. Ethyl acetate (5.0 mL) was added to the flask via syringe and mixture was stirred for 5 min. The solution was purged with a hydrogen balloon for 10 min. The balloon was then moved into the flask's headspace, and the reaction then stirred for 16 h. Hydrogen gas was released then the mixture was filtered through a silica plug with (100% EtOAc) and the filtrate was concentrated *in vacuo*. The saturated Boc VQ-1 analog intermediate was purified on an HPLC Agilent instrument using a XDB-C18 column, (9.4 × 250mm, 5μm) with the following instrument conditions and eluent: 3.0 mL/min, 40 °C M.P.A: 0.1% formic acid in H_2O M.P.B: 0.1% formic acid in acetonitrile. The purified analog was dissolved in methanol (1.0 mL) and the solution was added to a 1-dram vial with stir bar under air. Concentrated hydrochloric acid (200 μL) was added dropwise to the solution and the reaction was stirred at rt for 2 h. The solvent was evaporated *in vacuo* giving the HCl salt of VQ-1 analog **4-20** as a brown solid (25 mg, 57%): **^{1}H NMR** (500 MHz, CD_3OD) δ 8.59 (d, J = 8.5 Hz, 1H), 8.56 (s, 1H), 8.47 (d, J = 8.5 Hz, 1H), 8.23–8.15 (m, 3H), 8.02 (t, J = 7.6 Hz, 1H), 7.79 (d, J = 8.2 Hz, 2H), 5.79 (d, J = 5.8 Hz, 1H), 3.66 (dd, J = 7.7, 3.1 Hz, 1H), 3.41 (d, J = 12.5 Hz, 1H), 2.96 (t, J = 12.4 Hz, 1H), 2.20–1.43 (m, 21H); **^{13}C NMR** (126 MHz, CD_3OD) δ 159.3, 159.0, 156.4, 140.0, 136.1, 131.1, 130.5, 129.6, 127.8, 126.6, 126.2, 122.6, 121.6, 71.0, 62.3, 46.3, 44.0, 38.1, 37.7, 30.32,

27.22, 23.2, 22.8; **IR** (microscope, cm^{-1}) 3208, 3099, 3065, 2932, 2906, 2492, 2404, 1635, 1421, 1109; **HRMS** (ESI) for $(M)^+$ $C_{30}H_{37}N_2O$: calcd. 453.2906; found 453.2899.

*4.10.4.3 Synthesis of VQ-1 analog **MEH-VII-53***

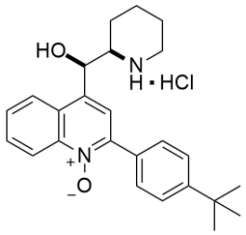

2-(4-(tert-butyl)phenyl)-4-((R)-hydroxy((R)-piperidin-2-yl)methyl)quinoline 1-oxide hydrochloride (4-25). The saturated Boc protected VQ-1 analog intermediate **4-24** was prepared and purified by HPLC according to the hydrogenation procedure mentioned in Section 4.9.4.2 using the dehydro Boc protected VQ-1 analog **4-23** (50 mg, 110 μmol) and Adams' catalyst (7.2 mg, 32 μmol). In a flame dried round bottom flask charged with a stir bar, compound **4-24** was dissolved in DCM (5.0 mL) and the solution was cooled down to 0 °C. *m*-Chloroperoxybenzoic acid (27 mg, 160 μmol) was added to the solution, then reaction was stirred at 0 °C for 1 h and warmed to rt for 16 h. The reaction mixture was quenched with saturated $NaHCO_3$ solution (10 mL) and extracted with DCM (30 mL × 3). The combined organic layers were washed with water, brine, dried over Na_2SO_4, filtered, and concentrated *in vacuo* to obtain the corresponding *N*-oxide derivative, which was used in the next deprotection step. Using the deprotection conditions mentioned in Section 4.9.4.2 afforded the VQ-1 **4-25** as a brown film (28 mg, 62%): **^{1}H NMR** (500 MHz, CD_3OD) δ 8.71 (d, *J* = 8.7 Hz, 1H), 8.64 (d, *J* = 7.7 Hz, 1H), 8.33 (s, 1H), 8.28 (t, *J* = 7.5 Hz, 1H), 8.15–8.01 (m, 3H), 7.76 (d, *J* = 7.7 Hz, 2H), 5.85–5.77 (m, 1H), 3.64 (d, *J* = 7.8 Hz, 1H), 3.38 (d, *J* = 11.4 Hz, 1H), 2.94 (t, *J* = 11.7 Hz, 1H), 2.03–1.69 (m, 5H), 1.55 (d, *J* = 14.9 Hz, 1H), 1.41 (s, 9H); **^{13}C NMR** (126 MHz, CD_3OD) δ 157.5, 155.1, 154.8, 140.1, 136.6, 131.9, 131.7, 128.4, 128.3, 127.2, 126.6, 124.3, 119.5, 70.5, 62.3, 46.4, 36.1, 31.5, 27.3, 23.2, 22.9; **IR** (microscope, cm^{-1}) 3211, 3078, 2960, 2867, 2709, 2494, 1604, 1446, 1364, 1270, 1109; **HRMS** (ESI) for $(M)^+$ $C_{25}H_{31}N_2O_2$: calcd. 391.2386; found 391.2376.

*4.10.4.4 Synthesis of VQ-1 analog **MEH-VII-95***

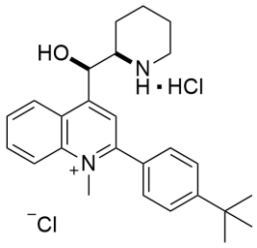

2-(4-(tert-Butyl)phenyl)-4-(hydroxy(piperidin-2-yl)methyl)-1-methylquinolin-1-ium chloride hydrochloride (4-26). The saturated Boc protected VQ-1 analog intermediate **4-24** was prepared and purified by HPLC according to the hydrogenation procedure mentioned in Section 4.9.4.2 using the dehydro Boc protected VQ-1 analog **4-23** (50 mg, 110 μmol) and Adams' catalyst (7.2 mg, 32 μmol). In a flame dried reaction tube charged with a stir bar under argon atmosphere, DCM (2.0 mL) was added and kept at –78 °C for 10 min. Diethylzinc solution in hexanes (200 μL, 1.0 M, 200 μmol) was added and followed by diiodomethane (110 mg, 400 μmol) and stirred at –78 °C for 15 min. Compound **4-24** was dissolved in DCM (1.0 mL) and the solution was added to the reaction tube dropwise. After the addition was complete, the reaction tube was warmed to room temperature and stirred for 1 h. The reaction was quenched with saturated aqueous solution of Na_2EDTA (100 μL) followed by $NaHCO_3$ (10 mL) and extracted with DCM (30 mL × 3). The combined organic layers were washed with water, brine, dried over Na_2SO_4, filtered, and concentrated *in vacuo* to obtain the corresponding *N*-methyl derivative, which was used in the next deprotection step. Using the deprotection conditions mentioned in Section 4.9.4.2 afforded the VQ-1 **4-26** as a yellow film (33 mg, 69%): **^{1}H NMR** (500 MHz, CD_3OD) δ 8.66 (d, *J* = 7.8 Hz, 1H), 8.62 (d, *J* = 8.9 Hz, 1H), 8.33 (ddd, *J* = 8.7, 7.1, 1.2 Hz, 1H), 8.25 (s, 1H), 8.11 (t, *J* = 7.7 Hz, 1H), 7.85–7.72 (m, 4H), 5.81 (d, *J* = 5.6 Hz, 1H), 4.51 (s, 3H), 3.64 (s, 1H), 3.37 (d, *J* = 12.9 Hz, 1H), 2.93 (td, *J* = 13.0, 3.0 Hz, 1H), 1.99–1.82 (m, 4H), 1.79–1.67 (m, 1H), 1.59–1.49 (m, 1H), 1.43 (s, 9H); **^{13}C NMR** (126 MHz, CD_3OD) δ 161.4, 158.2, 157.1, 141.52, 136.9, 132.0, 131.2, 130.8, 127.7, 127.6, 127.0, 125.2, 121.6, 70.6, 62.3, 46.4, 43.6, 36.1, 31.5, 27.3, 23.2, 22.8. **IR**

(microscope, cm^{-1}) 3214, 3060, 2958, 2868, 2711, 2492, 1607, 1432, 1363, 1256, 1113; **HRMS** (ESI) for $(M)^+$ $C_{26}H_{33}N_2O$: calcd. 389.2587; found 389.2586.

4.10.5 Synthesis of stereoisomers of RMH-VIII-111

4.10.5.1 Synthesis of threo stereoisomers

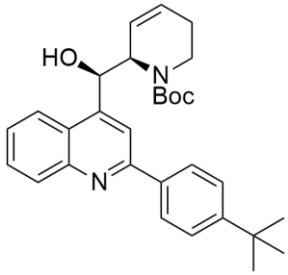

(*R*)-*tert*-Butyl 2-((*R*)-(2-(4-(*tert*-butyl)phenyl)quinolin-4-yl)(hydroxy)methyl)-5,6-dihydropyridine-1(2H)-carboxylate (4-31). Prepared by general procedure B using aldehyde **4-20** (144 mg, 0.500 mmol) and (*S*)-**4-18** (185 mg, 0.600 mmol). Flash chromatography afforded a white solid (167 mg, 71%): **^{1}H NMR** (500 MHz, $CDCl_3$, rotamers are present): δ 8.19–7.94 (m, 5H), 7.69 (t, *J* = 7.7 Hz, 1H), 7.53 (d, *J* = 8.4 Hz, 2H), 7.48 (t, *J* = 7.4 Hz, 1H), 6.01–5.46 (m, 3H), 5.09–4.85 (m, 1H), 4.38–4.10 (m, 1H), 2.95 (m, 1H), 2.21–1.96 (m, 2H), 1.51 (s, 9H), 1.37 (s, 9H); **^{13}C NMR** (126 MHz, $CDCl_3$, rotamers are present): δ 157.3, 157.1, 152.5, 148.6, 136.9, 130.5, 129.1, 127.7, 127.3, 125.9, 125.7, 125.3, 124.2, 123.4, 117.5, 81.0, 80.2, 72.8, 60.4, 58.2, 57.0, 38.4, 37.3, 34.7, 31.3, 28.4, 28.0, 27.9, 24.7, 24.3, 21.0, 14.2; **IR** (microscope, cm^{-1}) 3402, 3016, 2966, 1682, 1420, 1366, 1169; **HRMS** (ESI) for $(M+H)^+$ $C_{30}H_{37}N_2O_3$: calcd. 473.2799; found 473.2798; **$[\alpha]_D^{20}$**: 68.5 (*c* = 0.600, $CHCl_3$); **HPLC** (Chiralpak IB) 3:97 iso-propanol:hexanes, 0.5 mL/min, 20 °C, λ = 254 nm, T_{major} = 15.4 min, T_{minor} = 23.1 min, er = 94.5:5.5.

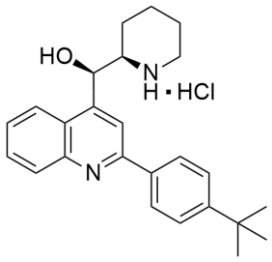

(*R*)-(2-(4-(*tert*-Butyl)phenyl)quinolin-4-yl)((R)-piperidin-2-yl)methanol hydrochloride (4-27). Prepared according to the hydrogenation, HPLC purification and deprotection protocols described in Section 4.9.4.2 using analog **4-31** (25 mg, 55 μmol) and Adams' catalyst (3.6 mg, 16 μmol). White solid (20 mg, 89%): **^{1}H NMR** (400 MHz, CD_3OD) δ 8.60 (d, *J* = 8.4 Hz, 1H), 8.54 (s, 1H), 8.46 (d, *J* = 8.4 Hz, 1H), 8.21 (t, *J* = 7.2 Hz, 1H), 8.16 (d, *J* = 8.4 Hz, 2H), 8.02 (t, *J* = 7.2 Hz, 1H), 7.83 (d, *J* = 8.4 Hz, 2H), 5.75 (d, *J* = 6.4 Hz, 1H) 3.65 (m, 1H), 3.42 (d, *J* = 12.8 Hz, 1H), 2.97 (td, *J* = 13.2 Hz, 3.2 Hz, 1H), 1.98–1.43 (m, 15H); **^{13}C NMR** (100 MHz, CD_3OD) δ 158.2, 155.9, 135.4, 130.4, 129.7, 127.5, 126.0, 125.4, 122.3, 120.8, 70.4, 61.7, 45.7, 35.6, 30.8, 26.6, 22.7, 22.2, 10.10; **IR** (solid, cm-1): 3200–2500, 3055, 2935, 1634, 1423, 1113; **HRMS** (ESI) for $(M)^+$ $C_{25}H_{31}N_2O$: calcd. 375.2431; found 375.2431; **[α]$_D^{20}$**: –21.2 (*c* = 2.60, CH_3OH).

4.10.5.2 Synthesis of erythro stereoisomers

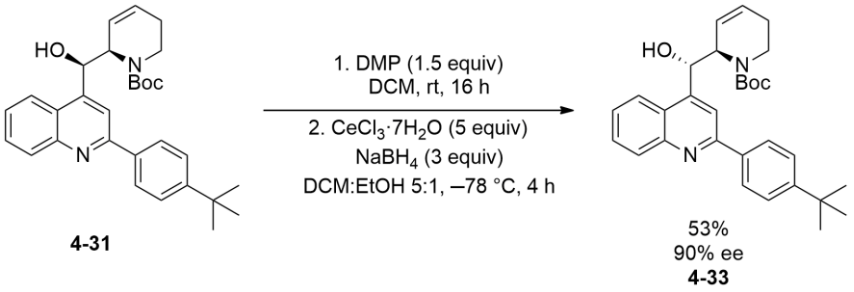

(*R*)-*tert*-Butyl 2-((*S*)-(2-(4-(*tert*-butyl)phenyl)quinolin-4-yl)(hydroxy)methyl)-5,6-dihydropyridine-1(2H)-carboxylate (4-33). In flame dried round-bottom flask charged with a stir bar, a solid mixture of compound **4-31** (100 mg, 212 μmol) and Dess-Martin Periodinane (134 mg, 318 μmol) was dissolved in DCM (5.00 mL). The reaction mixture was stirred under nitrogen atmosphere for 16 h. The reaction mixture was quenched with 1.0 M sodium hydroxide solution

(10.0 mL) and extracted with EtOAc (30 mL × 3). The organic layers were combined, washed water till neutral, brine, dried over Na_2SO_4, filtered, and concentrated *in vacuo* to obtain the crude ketone, which was used in the following reduction reaction without further purification. In a round bottom flask charged with a stir bar, $CeCl_3 \cdot 7H_2O$ (420 mg, 1.06 mmol) was mixed with EtOH (3.00 mL). The crude ketone was dissolved in DCM (15.0 mL) and added to the reaction flask. The reaction mixture was cooled to –78 °C. After stirring for 10 minutes, solution of $NaBH_4$ (25.0 mg, 636 μmol) in EtOH (1.5 mL) solution was added over one hour. After two hours, the reaction was quenched with water and the mixture was allowed to warm to room temperature. The aqueous layer was extracted with EtOAc (30 mL × 3). The organic layers were combined, washed with brine, dried over Na_2SO_4, filtered, concentrated *in vacuo* to obtain the crude erythro isomer, which was purified by HPLC using the conditions described in Section 4.9.4.2 to obtain the analog **4-33** as white solid (53.0 mg, 53%): **^{1}H NMR** (500 MHz, $CDCl_3$) rotamers are present: δ 8.40 (br s, 1H), 8.19 (d, J = 8.5 Hz, 1H), 8.11 (d, J = 8.4 Hz, 2H), 7.71 (ddd, J = 8.3, 6.8, 1.3 Hz, 1H), 7.62–7.48 (m, 3H), 5.99 (s, 1H), 5.84 (s, 1H), 5.39 (s, 1H), 4.90 (s, 1H), 4.13 (br s, 1H), 3.07 (br s, 1H), 2.13 (s, 1H), 1.99 (s, 1H), 1.80–1.13 (m, 20H); **^{13}C NMR** (126 MHz, $CDCl_3$) rotamers are present: δ 159.7, 152.7, 148.4, 147.5, 136.9, 130.4, 129.4, 127.4, 125.8, 122.4, 116.4, 73.5, 56.2, 34.8, 31.4, 28.6, 24.7, 17.6. **IR** (microscope, cm^{-1}) 3993, 3039, 3007, 2965, 1683, 1598, 1419, 1168; **HRMS** (ESI) for $(M+H)^+$ $C_{30}H_{37}N_2O_3$: calcd. 473.2799; found 473.2796; **$[\alpha]_D^{20}$**: 100 (c = 0.440, $CHCl_3$); **HPLC** (Chiralpak IB) 3:97 iso-propanol:hexanes, 0.5 mL/min, 20 °C, λ = 254 nm, T_{minor} = 14.7 min, T_{major} = 16.4 min, er = 94.6:5.4.

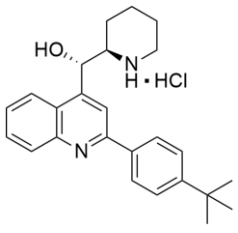

(*S*)-(2-(4-(*tert*-Butyl)phenyl)quinolin-4-yl)((*R*)-piperidin-2-yl)methanol hydrochloride (4-28). Prepared according to the hydrogenation, HPLC purification and deprotection protocols

described in Section 4.9.4.2 using analog **4-33** (25 mg, 55 µmol) and Adams' catalyst (3.6 mg, 16 µmol). White solid (21 mg, 90%): **m.p.** = 86.3-87.8 °C; **^{1}H NMR** (500 MHz, CD_3OD) δ 8.70 (d, *J* = 8.5 Hz, 1H), 8.51 (s, 1H), 8.47 (dd, *J* = 8.6, 1.0 Hz, 1H), 8.21 (ddd, *J* = 8.3, 7.0, 1.0 Hz, 1H), 8.12 (d, *J* = 8.5 Hz, 2H), 8.04 (ddd, *J* = 8.3, 7.0, 1.0 Hz, 1H), 7.82 (d, *J* = 8.5 Hz, 2H), 6.14 (d, *J* = 2.7 Hz, 1H), 3.73 (d, *J* = 12.3 Hz, 1H), 3.53–3.38 (m, 1H), 3.18 (td, *J* = 12.6, 2.9 Hz, 1H), 1.94–1.63 (m, 4H), 1.42 (m, 11H); **^{13}C NMR** (126 MHz, CD_3OD) δ 159.5, 159.0, 156.0, 139.7, 136.2, 131.4, 130.4, 129.5, 128.2, 126.0, 122.5, 120.8, 69.8, 60.8, 46.4, 36.2, 31.4, 23.0, 22.7; **IR** (microscope, cm^{-1}) 3217, 3067, 2980, 2866, 2707, 1633, 1604, 1419, 1115; **HRMS** (ESI) for $(M)^+$ $C_{25}H_{31}N_2O$: calcd. 375.2431; found 375.2428; **[α]$_D^{20}$**: 7.96 (*c* = 1.01, CH_3OH).

4.11 References

[1] Taylor, O. G.; Brzozowski, J. S.; Skelding, K. A. *Front. Oncol.* **2019**, *9*.

[2] Thakkar, J. P.; Dolecek, T. A.; Horbinski, C.; Ostrom, Q. T.; Lightner, D. D.; Barnholtz-Sloan, J. S.; Villano, J. L. *Cancer Epidemiol. Biomarkers Prev.* **2014**, *23*, 1985.

[3] Ohgaki, H.; Kleihues, P. *J. Neuropathol. Exp. Neurol.* **2005**, *64*, 479.

[4] Ohgaki, H.; Kleihues, P. *Am. J. Pathol.* **2007**, *170*, 1445.

[5] Ohgaki, H.; Kleihues, P. *Clin. Cancer Res.* **2013**, *19*, 764.

[6] Rossi, J.; Giaccherini, L.; Cavallieri, F.; Napoli, M.; Moratti, C.; Froio, E.; Serra, S.; Fraternali, A.; Ghadirpour, R.; Cozzi, S.; Ciammella, P.; Iaccarino, C.; Pascarella, R.; Valzania, F.; Pisanello, A. *BMC Neurol.* **2020**, *20*, 382.

[7] Urbańska, K.; Sokołowska, J.; Szmidt, M.; Sysa, P. *Contemp. Oncol. (Pozn)* **2014**, *18*, 307.

[8] American Society of Clinical Oncology. Brain Tumor: Grades and Prognostic Factors. **2021**. https://www.cancer.net/cancer-types/brain-tumor/grades-and-prognostic-factors. (accessed January 11, 2022).

[9] Kleihues, P.; Ohgaki, H. *Neuro-Oncol.* **1999**, *1*, 44.

[10] Perkins, A.; Liu, G. *Am Fam Physician* **2016**, *93*, 211.

[11] Shi, Y.; Lim, S. K.; Parada, L. F. *Cell Res.* **2014**, *24*, 910.

[12] Barbashina, V.; Salazar, P.; Ladanyi, M.; Rosenblum, M. K.; Edgar, M. A. *Am. J. Surg. Pathol.* **2007**, *31*, 1196.

[13] Appin, C. L.; Gao, J.; Chisolm, C.; Torian, M.; Alexis, D.; Vincentelli, C.; Schniederjan, M. J.; Hadjipanayis, C.; Olson, J. J.; Hunter, S.; Hao, C.; Brat, D. J. *Brain Pathol.* **2013**, *23*, 454.

[14] Takeuchi, H.; Kitai, R.; Hosoda, T.; Yamada, S.; Hashimoto, N.; Kikuta, K.-i.; Shimizu, Y.; Kimura, H. *J. Neurooncol.* **2016**, *127*, 337.

[15] Zhang, P.; Xia, Q.; Liu, L.; Li, S.; Dong, L. *Front. Mol. Biosci.* **2020**, *7*.

[16] Rodriguez, F. J.; Orr, B. A.; Ligon, K. L.; Eberhart, C. G. *Oncotarget* **2012**, *3*.

[17] Vasilev, A.; Sofi, R.; Rahman, R.; Smith, S. J.; Teschemacher, A. G.; Kasparov, S. *Brain Sci.* **2020**, *10*, 75.

[18] Lee, S. Y. *Genes & Diseases* **2016**, *3*, 198.

[19] Bastiancich, C.; Bastiat, G.; Lagarce, F. *Drug Discov Today* **2018**, *23*, 416.

[20] Lathia, J. D.; Mack, S. C.; Mulkearns-Hubert, E. E.; Valentim, C. L. L.; Rich, J. N. *Genes Dev.* **2015**, *29*, 1203.

[21] Cantrell, J. N.; Waddle, M. R.; Rotman, M.; Peterson, J. L.; Ruiz-Garcia, H.; Heckman, M. G.; Quiñones-Hinojosa, A.; Rosenfeld, S. S.; Brown, P. D.; Trifiletti, D. M. *Mayo Clin. Proc.* **2019**, *94*, 1278.

[22] Kitambi, S. S.; Toledo, E. M.; Usoskin, D.; Wee, S.; Harisankar, A.; Svensson, R.; Sigmundsson, K.; Kalderén, C.; Niklasson, M.; Kundu, S.; Aranda, S.; Westermark, B.; Uhrbom, L.; Andäng, M.; Damberg, P.; Nelander, S.; Arenas, E.; Artursson, P.; Walfridsson, J.; Nilsson, K. F.; Hammarström, L. G. J.; Ernfors, P. *Cell* **2017**, *170*, 407.

[23] Hann, M. M.; Oprea, T. I. *Curr. Opin. Chem. Biol.* **2004**, *8*, 255.

[24] Gilbertson, Richard J. *Cell* **2014**, *157*, 289.

[25] Lee, J.; Kotliarova, S.; Kotliarov, Y.; Li, A.; Su, Q.; Donin, N. M.; Pastorino, S.; Purow, B. W.; Christopher, N.; Zhang, W.; Park, J. K.; Fine, H. A. *Cancer Cell* **2006**, *9*, 391.

[26] Ahlstedt, J.; Förnvik, K.; Zolfaghari, S.; Kwak, D.; Hammarström, L. G.; Ernfors, P.; Salford, L. G.; Redebrandt, H. N. *Oncotarget* **2018**, *9*, 8391.

[27] Buchman, E.; Howton, D. *J. Am. Chem. Soc.* **1946**, *68*, 2718.

[28] Senear, A.; Sargent, H.; Mead, J.; Koepfli, J. *J. Am. Chem. Soc.* **1946**, *68*, 2695.

[29] Winstein, S.; Jacobs, T. L.; Levy, E. F.; Seymour, D.; Linden, G. B.; Henderson, R. B. *J. Am. Chem. Soc.* **1946**, *68*, 2714.

[30] Pinder, R. M.; Burger, A. *J. Med. Chem.* **1968**, *11*, 267.

[31] Fernandez-Alvaro, E.; Hong, W. D.; Nixon, G. L.; O'Neill, P. M.; Calderon, F. *J. Med. Chem.* **2016**, *59*, 5587.

[32] León, B.; Fong, J. C.; Peach, K. C.; Wong, W. R.; Yildiz, F. H.; Linington, R. G. *Org. Lett.* **2013**, *15*, 1234.

[33] Fuhler, G. M.; Brooks, R.; Toms, B.; Iyer, S.; Gengo, E. A.; Park, M.-Y.; Gumbleton, M.; Viernes, D. R.; Chisholm, J. D.; Kerr, W. G. *Mol. Med.* **2012**, *18*, 65.

[34] Hammarström, L. G. J.; Harmel, R. K.; Granath, M.; Ringom, R.; Gravenfors, Y.; Färnegårdh, K.; Svensson, P. H.; Wennman, D.; Lundin, G.; Roddis, Y.; Kitambi, S. S.; Bernlind, A.; Lehmann, F.; Ernfors, P. *J. Med. Chem.* **2016**, *59*, 8577.

[35] Färnegårdh, K.; Gravenfors, Y.; Ernfors, P.; Hammarström, L. G. J.; Kitambi, S. Compounds and Use for Treating Cancer. WO Patent 2015/033228 A2, March 12, 2015.

[36] Pfitzinger, W. *Journal für Praktische Chemie* **1886**, *33*, 100.

[37] Fischer, E.; Speier, A. *Ber. Dtsch. Chem. Ges.* **1895**, *28*, 3252.

[38] McConathy, J.; Owens, M. J. *Prim. Care Companion. J. Clin. Psychiatry.* **2003**, *5*, 70.

[39] Li-Yuan Bao, R.; Zhao, R.; Shi, L. *ChemComm* **2015**, *51*, 6884.

[40] Tan, S. K.; Jermakowicz, A.; Mookhtiar, A. K.; Nemeroff, C. B.; Schürer, S. C.; Ayad, N. G. *Front. Pharmacol.* **2018**, *9*.

[41] Kwok, S. Application and Substrate Scope Expansion of a Unique Borylative Migration Transformation. M.Sc. Thesis, The University of Alberta, 2016.

[42] McDonald, R. Preparation and Application of Cyclic Chiral Organoboron Compounds for the Stereoselective Synthesis of Vacquinol-1 Analogs, and Trisubstituted Cyclobutylboronates. M.Sc. Thesis, The University of Alberta, 2019.

[43] Mosset, P.; Grée, R. *Synlett* **2013**, *24*, 1142.

[44] Kim, Y.-R.; Hall, D. G. *Org. Biomol. Chem.* **2016**, *14*, 4739.

[45] *CellTiter 96® AQueous One Solution Cell Proliferation Assay*; Technical Bulletin #TB112; Promega Corporation: Madison, W., 2012, 1-12.

[46] Ding, J.; Hall, D. G. *Angew. Chem. Int. Ed.* **2013**, *52*, 8069.

Chapter 5: Conclusions and Future Perspectives

5.1 Conclusions and Future Perspectives

The discovery and development of natural and synthetic bioactive piperidine-containing compounds has been of importance for many decades. The potential medicinal properties of these compounds make the establishment of new and convenient methods of synthesizing and using the piperidine scaffold desirable. In addition, optimizing these methods to be stereoselective to afford chiral piperidines enables access to enantiopure building blocks for the synthesis of pharmaceutically relevant chemicals. To this end, this thesis described efforts towards new methods of synthesis and application of enantioenriched piperidines in drug discovery.

In Chapter 1, a brief discussion about general methods of synthesizing functionalized piperidine derivatives was presented. The strengths and weaknesses of each method were discussed. Furthermore, a variety of synthetic applications of chiral allylic boronic esters were described and their potential in the synthesis of enantioenriched piperidines was illustrated. This discussion highlighted the need for the continuous development of powerful synthetic methods to access chiral piperidines, setting the stage for this thesis and its objectives.

In Chapter 2, my efforts to study the effect of the alkenyl boronate side product in the borylative migration reaction were discussed. These efforts, in addition to the experimental and computational mechanistic studies performed by Dr. Helen Clement and Dr. Claude Legault respectively, provided insights regarding the borylative migration reaction to complete the picture of the catalytic cycle of the reaction. The mechanistic details can contribute towards the design of a borylative migration reaction of pre-functionalized piperidines to expand the scope of this transformation. In addition, this mechanistic study illustrates the potential to obtain functionalized piperidines with contiguous stereocenters in only a few steps (Scheme 5-1). Furthermore, there is still room for improving the chemo- and enantioselectivity based on the outcomes of the current optimized conditions. Different additives and/or bases could be explored to produce the desired heterocyclic allylic boronic ester exclusively in a higher enantioselective fashion.

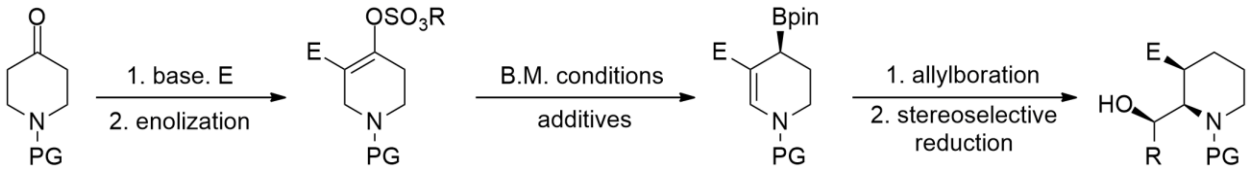

Scheme 5-1. Suggestions for expanding the substrate scope of the borylative migration.

In Chapter 3, an optimization of a synthetic method to obtain novel enantionenriched 2-substituted piperidines using stereospecific C_{sp}^3–C_{sp}^3 allyl-allyl cross-coupling is presented. The method was inspired by Morken's allyl-allyl cross-coupling protocol between cinnamyl electrophiles and allyl boronic esters nucleophiles. The current method is only optimized for electrophiles bearing a cinnamic moiety. Thus, there is still room for improvement to incorporate alkyl-allylic substituted electrophiles. Furthermore, the method was optimized to exclusively obtain the *γ*-linear products, which leaves an opportunity to reoptimize this protocol or use different approaches to obtain the other 3 regioisomers. Other transition metals or ligands can be considered to favor the branched and/or the *α*-substituted piperidine products. For example, Feringa and co-workers reported an allyl-allyl cross-coupling reaction favoring the branched product using copper catalysis with incorporation of phosphoramidite ligands.[1] In addition, *α*-substituted piperidines might be synthesized by finding a suitable ligand that favors the [3-3′] elimination from the *γ*-palladium species (Scheme 3-8, compound 3-10).[2] This opens the door to synthesize different enantioenriched piperidinyl regioisomers from the same piperidinyl allylic boronic ester intermediate depending on suitable conditions (Figure 5-2).

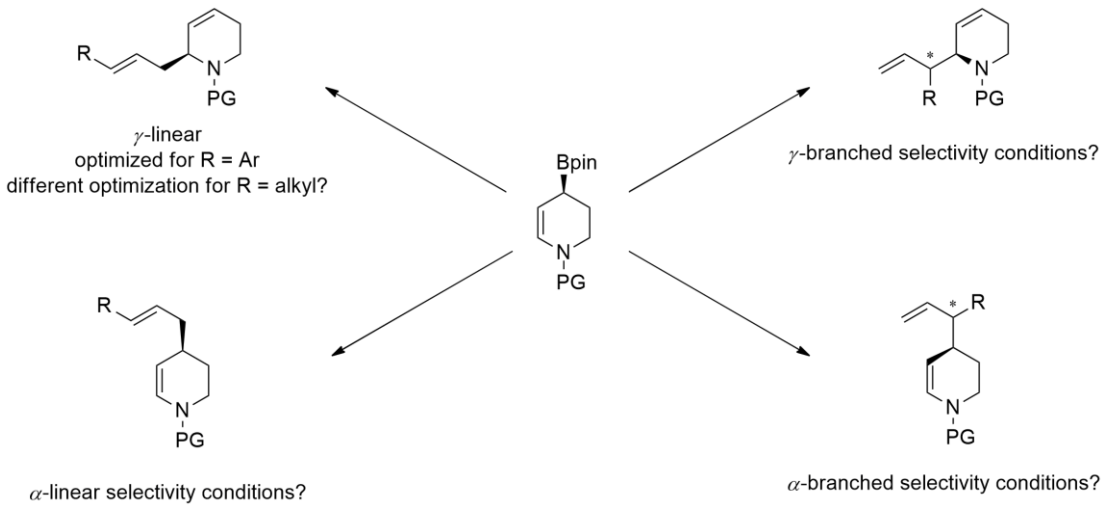

Figure 5-1. Potential diversification of the allyl-allyl cross-coupling reaction.

Finally, in Chapter 4, the synthesis and biological testing of new vaquinol-1 (VQ-1) analogs for the treatment of GBM were discussed. The borylative migration method enabled access to various VQ-1 analogs. To date, *in vitro* studies suggest that the VQ-1 analog bearing a *tert*-butyl substituent at the *para*-position of the 2-aryl ring is the best candidate for the treatment of GBM. Therefore, the four stereoisomers of this candidate were synthesized to determine which optically active isomer is the most potent against GBM cell lines. Based on the ongoing *in vitro* studies, the next step is to test the biological activity of the best stereoisomer *in vivo*. However, if this candidate is deemed not suitable for further biological testing by exhibiting low potency or high toxicity *in vivo*, further SAR studies are required. For example, the benzo[h]quinoline analog VQ-15 (Table 4-1, entry 16) showed better *in vitro* potency against GBM than the original VQ-1. Optimizing this derivative to mitigate its toxicity might be beneficial in seeking a better analog. A general synthetic plan for VQ-15 analogs is shown in Scheme 5-2.[3] The 7,8-benzoquinoline core structure of VQ-15 can be synthesized *via* Doebner–Miller reaction, which can be derivatized to the corresponding aldehyde to perform a stereoselective aldehyde allylboration.

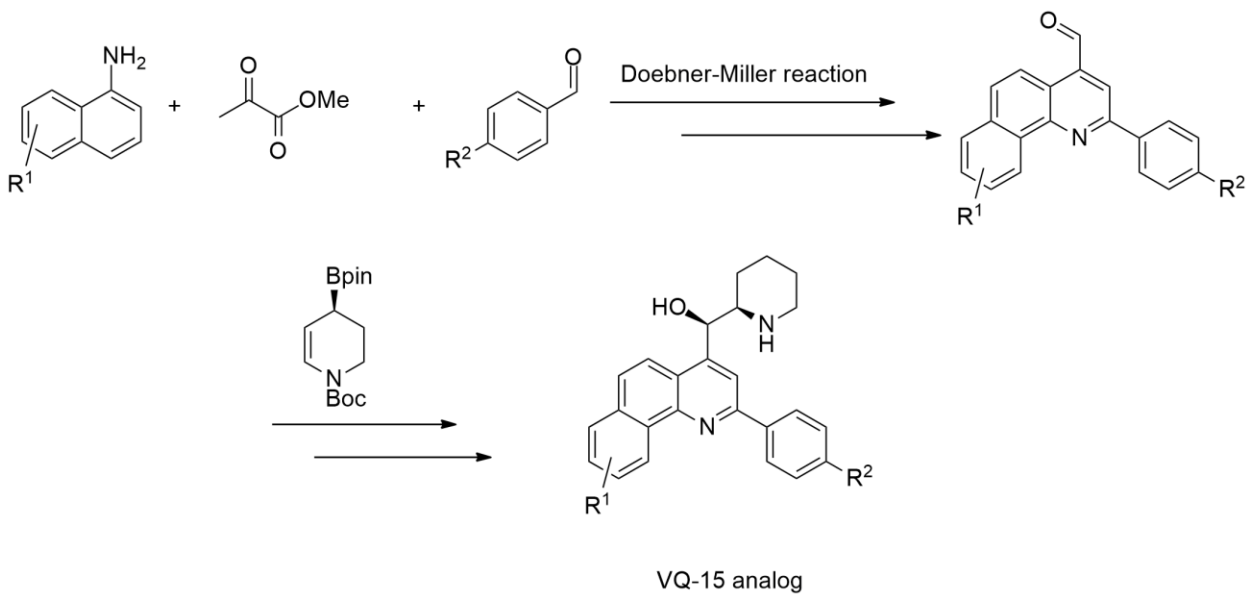

Scheme 5-2. Synthetic plan for VQ-15 analogs.

Overall, this thesis describes my contribution towards expanding the scope of of methods to synthesize enantioselective piperidine in organic chemistry and medicinal chemistry. This field of research is continuously growing attesting the importance of optically pure piperidines in the pharmaceutical industry. Advancements in this field will promote ease of access to a large library of pharmaceutically relevant piperidines, with the goal of providing a new variety of cures and treatments for various diseases.

5.2 References

[1] Hornillos, V.; Pérez, M.; Fañanás-Mastral, M.; Feringa, B. L. *J. Am. Chem. Soc.* **2013**, *135*, 2140.

[2] Ding, J.; Rybak, T.; Hall, D. G. *Nat. Commun.* **2014**, *5*, 5474.

[3] Lei, S.; Jingjing, X.; Jingjing, B.; Zhiguo, Z.; Tongxin, L.; Xiaolan, Y.; Guisheng, Z. *Chin. J. Org. Chem.* **2018**, *38*, 3016.

Bibliography

[1] Gao, B.; Yang, B.; Feng, X.; Li, C. *Nat. Prod. Rep.* **2022**, *39*, 139.

[2] Parmar, V. S.; Jain, S. C.; Bisht, K. S.; Jain, R.; Taneja, P.; Jha, A.; Tyagi, O. D.; Prasad, A. K.; Wengel, J.; Olsen, C. E.; Boll, P. M. *Phytochemistry* **1997**, *46*, 597.

[3] Butler, M. S. *Nat. Prod. Rep.* **2008**, *25*, 475.

[4] Cordell, G. A.; Quinn-Beattie, M. L.; Farnsworth, N. R. *Phytother. Res.* **2001**, *15*, 183.

[5] Warnhoff, E. W. *Bull. Hist. Chem.* **1998**, *22*, 29.

[6] Shoba, G.; Joy, D.; Joseph, T.; Majeed, M.; Rajendran, R.; Srinivas, P. *Planta Med.* **1998**, *64*, 353.

[7] Bano, G.; Raina, R.; Zutshi, U.; Bedi, K.; Johri, R.; Sharma, S. *Eur. J. Clin. Pharmacol.* **1991**, *41*, 615.

[8] Atal, C.; Dubey, R. K.; Singh, J. *J. Pharmacol. Exp. Ther.* **1985**, *232*, 258.

[9] Platel, K.; Srinivasan, K. *Nahrung* **2000**, *44*, 42.

[10] Platel, K.; Srinivasan, K. *Int. J. Food Sci. Nutr.* **1996**, *47*, 55.

[11] Felpin, F. X.; Lebreton, J. *ChemInform* **2005**, *36*.

[12] Stansbury, J.; Saunders, P. R.; Zampieron, E. *J. Restor. Med.* **2013**, *2*, 94.

[13] Achan, J.; Talisuna, A. O.; Erhart, A.; Yeka, A.; Tibenderana, J. K.; Baliraine, F. N.; Rosenthal, P. J.; D'Alessandro, U. *Malar. J.* **2011**, *10*, 144.

[14] WHO: Guidelines for Malaria. 2022. https://app.magicapp.org/#/guideline/6236, accessed April 5th, 2022

[15] Baumann, M.; Baxendale, I. R. *Beilstein J. Org. Chem.* **2013**, *9*, 2265.

[16] Welsch, M. E.; Snyder, S. A.; Stockwell, B. R. *Curr. Opin. Chem. Biol.* **2010**, *14*, 347.

[17] Vitaku, E.; Smith, D. T.; Njardarson, J. T. *J. Med. Chem.* **2014**, *57*, 10257.

[18] WHO Model Lists of Essential Medicines. 2021.

https://apps.who.int/iris/rest/bitstreams/1374779/retrieve, accessed April 6th, 2022

[19] Gründer, G.; Hippius, H.; Carlsson, A. *Nat. Rev. Drug Discov.* **2009**, *8*, 197.

[20] Wagstaff, A. J.; Cheer, S. M.; Matheson, A. J.; Ormrod, D.; Goa, K. L. *Drugs* **2002**, *62*, 655.

[21] Wong, W.; Bai, X.-C.; Sleebs, B. E.; Triglia, T.; Brown, A.; Thompson, J. K.; Jackson, K. E.; Hanssen, E.; Marapana, D. S.; Fernandez, I. S.; Ralph, S. A.; Cowman, A. F.; Scheres, S. H. W.; Baum, J. *Nat. Microbiol.* **2017**, *2*, 17031.

[22] Peter, H.; Joris, D.; Nollaig, H.; Wafae, I.; Johan, A.; Mark, W. *Haematologica* **2018**, *103*, e204.

[23] Rueping, M.; Antonchick, A. P. *Angew. Chem. Int. Ed.* **2007**, *46*, 4562.

[24] Wang, S.-G.; You, S.-L. *Angew. Chem. Int. Ed.* **2014**, *53*, 2194.

[25] Studer, M.; Wedemeyer-Exl, C.; Spindler, F.; Blaser, H.-U. *Monatsh. Chem.* **2000**, *131*, 1335.

[26] Legault, C. Y.; Charette, A. B. *J. Am. Chem. Soc.* **2005**, *127*, 8966.

[27] Ye, Z.-S.; Chen, M.-W.; Chen, Q.-A.; Shi, L.; Duan, Y.; Zhou, Y.-G. *Angew. Chem. Int. Ed.* **2012**, *51*, 10181.

[28] Renom-Carrasco, M.; Gajewski, P.; Pignataro, L.; de Vries, J. G.; Piarulli, U.; Gennari, C.; Lefort, L. *Chem. Eur. J.* **2016**, *22*, 9528.

[29] Huang, W.-X.; Yu, C.-B.; Ji, Y.; Liu, L.-J.; Zhou, Y.-G. *ACS Catal.* **2016**, *6*, 2368.

[30] Kita, Y.; Iimuro, A.; Hida, S.; Mashima, K. *Chem. Lett.* **2014**, *43*, 284.

[31] Chen, M.-W.; Ye, Z.-S.; Chen, Z.-P.; Wu, B.; Zhou, Y.-G. *Org. Chem. Front.* **2015**, *2*, 586.

[32] Li, W.; Zhang, S.; Yu, X.; Feng, X.; Yamamoto, Y.; Bao, M. *J. Org. Chem.* **2021**, *86*, 10773.

[33] Chen, M.-W.; Ji, Y.; Wang, J.; Chen, Q.-A.; Shi, L.; Zhou, Y.-G. *Org. Lett.* **2017**, *19*, 4988.

[34] Vinogradov, M. G.; Turova, O. V.; Zlotin, S. G. *Adv. Synth. Catal.* **2021**, *363*, 1466.

[35] Moyano, A.; Rios, R. *Chem. Rev.* **2011**, *111*, 4703.

[36] Cao, M.-H.; Green, N. J.; Xu, S.-Z. *Org. Biomol. Chem.* **2017**, *15*, 3105.

[37] Rowland, B. G.; Rowland, B. E.; Zhang, Q.; Antilla, C. J. *Curr. Org. Chem.* **2006**, *10*, 981.

[38] Fochi, M.; Caruana, L.; Bernardi, L. *Synthesis* **2014**, *46*, 135.

[39] Xie, M.; Lin, L.; Feng, X. *Chem. Rec.* **2017**, *17*, 1184.

[40] Liu, X.; Zheng, H.; Xia, Y.; Lin, L.; Feng, X. *Acc. Chem. Res.* **2017**, *50*, 2621.

[41] Rahman, A.; Lin, X. *Org. Biomol. Chem.* **2018**, *16*, 4753.

[42] Klier, L.; Tur, F.; Poulsen, P. H.; Jørgensen, K. A. *Chem. Soc. Rev.* **2017**, *46*, 1080.

[43] Kobayashi, S.; Komiyama, S.; Ishitani, H. *Angew. Chem. Int. Ed.* **1998**, *37*, 979.

[44] Yao, S.; Saaby, S.; Hazell, R. G.; Jørgensen, K. A. *Chem. Eur. J.* **2000**, *6*, 2435.

[45] Mancheño, O. G.; Gómez Arrayás, R.; Adrio, J.; Carretero, J. C. *J. Org. Chem.* **2007**, *72*, 10294.

[46] Mandai, H.; Mandai, K.; Snapper, M. L.; Hoveyda, A. H. *J. Am. Chem. Soc.* **2008**, *130*, 17961.

[47] Chu, J. C. K.; Dalton, D. M.; Rovis, T. *J. Am. Chem. Soc.* **2015**, *137*, 4445.

[48] Han, B.; Li, J.-L.; Ma, C.; Zhang, S.-J.; Chen, Y.-C. *Angew. Chem. Int. Ed.* **2008**, *47*, 9971.

[49] Li, Q.-Z.; Ma, L.; Dong, L.; Chen, Y.-C. *ChemCatChem* **2012**, *4*, 1139.

[50] Jian, T.-Y.; Sun, L.-H.; Ye, S. *Chem. Commun.* **2012**, *48*, 10907.

[51] Rong, Z.-Q.; Wang, M.; Chow, C. H. E.; Zhao, Y. *Chem. Eur. J.* **2016**, *22*, 9483.

[52] Felpin, F.-X.; Lebreton, J. *Eur. J. Org. Chem.* **2003**, 3693.

[53] Fu, G. C.; Grubbs, R. H. *J. Am. Chem. Soc.* **1992**, *114*, 7324.

[54] Pachamuthu, K.; Vankar, Y. D. *J. Organomet. Chem.* **2001**, *624*, 359.

[55] Cossy, J.; Willis, C.; Bellosta, V.; Bouzbouz, S. *Synlett* **2000**, *2000*, 1461.

[56] Alexander, J. B.; La, D. S.; Cefalo, D. R.; Hoveyda, A. H.; Schrock, R. R. *J. Am. Chem. Soc.* **1998**, *120*, 4041.

[57] La, D. S.; Alexander, J. B.; Cefalo, D. R.; Graf, D. D.; Hoveyda, A. H.; Schrock, R. R. *J. Am. Chem. Soc.* **1998**, *120*, 9720.

[58] Cefalo, D. R.; Kiely, A. F.; Wuchrer, M.; Jamieson, J. Y.; Schrock, R. R.; Hoveyda, A. H. *J. Am. Chem. Soc.* **2001**, *123*, 3139.

[59] Sattely, E. S.; Cortez, G. A.; Moebius, D. C.; Schrock, R. R.; Hoveyda, A. H. *J. Am. Chem. Soc.* **2005**, *127*, 8526.

[60] Dolman, S. J.; Sattely, E. S.; Hoveyda, A. H.; Schrock, R. R. *J. Am. Chem. Soc.* **2002**, *124*, 6991.

[61] Cossy, J.; Dumas, C.; Pardo, D. G. *Eur. J. Org. Chem.* **1999**, 1693.

[62] Cossy, J.; Mirguet, O.; Pardo, D. G. *Synlett* **2001**, *2001*, 1575.

[63] Jarvis, S. B. D.; Charette, A. B. *Org. Lett.* **2011**, *13*, 3830.

[64] Van Brabandt, W.; Van Landeghem, R.; De Kimpe, N. *Org. Lett.* **2006**, *8*, 1105.

[65] Mollet, K.; Catak, S.; Waroquier, M.; Van Speybroeck, V.; D'hooghe, M.; De Kimpe, N. *J. Org. Chem.* **2011**, *76*, 8364.

[66] Roughley, S. D.; Jordan, A. M. *J. Med. Chem.* **2011**, *54*, 3451.

[67] Davis, F. A.; Reddy, R. E.; Szewczyk, J. M.; Reddy, G. V.; Portonovo, P. S.; Zhang, H.; Fanelli, D.; Zhou, P.; Carroll, P. J. *J. Org. Chem.* **1997**, *62*, 2555.

[68] Liu, G.; Cogan, D. A.; Ellman, J. A. *J. Am. Chem. Soc.* **1997**, *119*, 9913.

[69] Semina, E.; Colpaert, F.; Van Hecke, K.; De Kimpe, N.; Mangelinckx, S. *Eur. J. Org. Chem.* **2015**, 4847.

[70] Kavala, M.; Mathia, F.; Kožíšek, J.; Szolcsányi, P. *J. Nat. Prod.* **2011**, *74*, 803.

[71] Fustero, S.; Jiménez, D.; Moscardó, J.; Catalán, S.; del Pozo, C. *Org. Lett.* **2007**, *9*, 5283.

[72] Liu, J.-D.; Chen, Y.-C.; Zhang, G.-B.; Li, Z.-Q.; Chen, P.; Du, J.-Y.; Tu, Y.-Q.; Fan, C.-A. *Adv. Synth. Catal.* **2011**, *353*, 2721.

[73] Sun, Z.; Winschel, G. A.; Zimmerman, P. M.; Nagorny, P. *Angew. Chem. Int. Ed.* **2014**, *53*, 11194.

[74] Mulet, C.; Escolano, M.; Llopis, S.; Sanz, S.; Ramírez de Arellano, C.; Sánchez-Roselló, M.; Fustero, S.; del Pozo, C. *Adv. Synth. Catal.* **2018**, *360*, 2885.

[75] Fustero , S.; del Pozo, C.; Mulet, C.; Lazaro, R.; Sánchez-Roselló, M. *Chem. Eur. J.* **2011**, *17*, 14267.

[76] Hall, D. G. *Boronic Acids*; 2nd Edition, Wiley: Weinheim, 2011.

[77] Sandford, C.; Aggarwal, V. K. *Chem. Commun.* **2017**, *53*, 5481.

[78] McKillop, A.; Sanderson, W. R. *Tetrahedron* **1995**, *51*, 6145.

[79] Mlynarski, S. N.; Karns, A. S.; Morken, J. P. *J. Am. Chem. Soc.* **2012**, *134*, 16449.

[80] Edelstein, E. K.; Grote, A. C.; Palkowitz, M. D.; Morken, J. P. *Synlett* **2018**, *29*, 1749.

[81] Nave, S.; Sonawane, R. P.; Elford, T. G.; Aggarwal, V. K. *J. Am. Chem. Soc.* **2010**, *132*, 17096.

[82] Kennedy, J. W. J.; Hall, D. G. *J. Am. Chem. Soc.* **2002**, *124*, 11586.

[83] Rauniyar, V.; Zhai, H.; Hall, D. G. *J. Am. Chem. Soc.* **2008**, *130*, 8481.

[84] Lou, S.; Moquist, P. N.; Schaus, S. E. *J. Am. Chem. Soc.* **2006**, *128*, 12660.

[85] Chen, J. L.-Y.; Aggarwal, V. K. *Angew. Chem. Int. Ed.* **2014**, *53*, 10992.

[86] Lachance, H.; Hall, D. G. *Allylboration of Carbonyl Compounds*. In *Organic Reactions*; Denmark, S. E., Ed. 2009, p 1–574.

[87] Clement, H. A.; Hall, D. G. *Recent Advances in the Stereoselective Additions of Allylic Boronates to Carbonyl Compounds*. In *PATAI'S Chemistry of Functional Groups*; Rappoport, Z., Ed. 2020, p 1–86.

[88] Buskes, M. J.; Blanco, M.-J. *Molecules* **2020**, *25*, 3493.

[89] Zhao, S.; Gensch, T.; Murray, B.; Niemeyer, Z. L.; Sigman, M. S.; Biscoe, M. R. *Science* **2018**, *362*, 670.

[90] Lehmann, J. W.; Crouch, I. T.; Blair, D. J.; Trobe, M.; Wang, P.; Li, J.; Burke, M. D. *Nat. Commun.* **2019**, *10*, 1263.

[91] Luo, Y.; Wales, S. M.; Korkis, S. E.; Roy, I. D.; Lewis, W.; Lam, H. W. *Chem. Eur. J.* **2018**, *24*, 8315.

[92] Lee, H.; Yun, J. *Org. Lett.* **2018**, *20*, 7961.

[93] Hu, J.; Ferger, M.; Shi, Z.; Marder, T. B. *Chem. Soc. Rev.* **2021**, *50*, 13129.

[94] Ito, H.; Ito, S.; Sasaki, Y.; Matsuura, K.; Sawamura, M. *J. Am. Chem. Soc.* **2007**, *129*, 14856.

[95] Guzman-Martinez, A.; Hoveyda, A. H. *J. Am. Chem. Soc.* **2010**, *132*, 10634.

[96] Park, J. K.; Lackey, H. H.; Ondrusek, B. A.; McQuade, D. T. *J. Am. Chem. Soc.* **2011**, *133*, 2410.

[97] Rivera-Chao, E.; Mitxelena, M.; Varela, J. A.; Fañanás-Mastral, M. *Angew. Chem. Int. Ed.* **2019**, *58*, 18230.

[98] Kojima, R.; Akiyama, S.; Ito, H. *Angew. Chem. Int. Ed.* **2018**, *57*, 7196.

[99] Chen, C.; Shen, X.; Chen, J.; Hong, X.; Lu, Z. *Org. Lett.* **2017**, *19*, 5422.

[100] Lee, H.; Han, J. T.; Yun, J. *ACS Catal.* **2016**, *6*, 6487.

[101] Ito, H.; Kunii, S.; Sawamura, M. *Nat. Chem.* **2010**, *2*, 972.

[102] Ge, Y.; Cui, X.-Y.; Tan, S. M.; Jiang, H.; Ren, J.; Lee, N.; Lee, R.; Tan, C.-H. *Angew. Chem. Int. Ed.* **2019**, *58*, 2382.

[103] Gao, X.; Hall, D. G. *J. Am. Chem. Soc.* **2003**, *125*, 9308.

[104] Hall, D. G.; Rybak, T.; Verdelet, T. *Acc. Chem. Res.* **2016**, *49*, 2489.

[105] Gao, X.; Hall, D. G. *J. Am. Chem. Soc.* **2005**, *127*, 1628.

[106] Penner, M.; Rauniyar, V.; Kaspar, L. T.; Hall, D. G. *J. Am. Chem. Soc.* **2009**, *131*, 14216.

[107] Touré, B. B.; Hall, D. G. *J. Org. Chem.* **2004**, *69*, 8429.

[108] Touré, B. B.; Hall, D. G. *Angew. Chem. Int. Ed.* **2004**, *43*, 2001.

[109] Lessard, S.; Peng, F.; Hall, D. G. *J. Am. Chem. Soc.* **2009**, *131*, 9612.

[110] Murata, M.; Oyama, T.; Watanabe, S.; Masuda, Y. *Synthesis* **2000**, *2000*, 778.

[111] Kim, Y.-R.; Hall, D. G. *Org. Biomol. Chem.* **2016**, *14*, 4739.

[112] Ding, J.; Rybak, T.; Hall, D. G. *Nat. Commun.* **2014**, *5*, 5474.

[113] Ding, J.; Hall, D. G. *Angew. Chem. Int. Ed.* **2013**, *125*, 8227.

[114] Ding, J.; Rybak, T.; Hall, D. G. *Nat. Commun.* **2014**, *5*, 1.

[115] Clement, H. A.; Hall, D. G. *Tetrahedron Lett.* **2018**, *59*, 4334.

[116] Lessard, S.; Peng, F.; Hall, D. G. *J. Am. Chem. Soc.* **2009**, *131*, 9612.

[117] Murata, M.; Oyama, T.; Watanabe, S.; Masuda, Y. *Synthesis* **2000**, *2000*, 778.

[118] Chow, W. K.; Yuen, O. Y.; Choy, P. Y.; So, C. M.; Lau, C. P.; Wong, W. T.; Kwong, F. Y. *RSC Adv.* **2013**, *3*, 12518.

[119] Ishiyama, T.; Murata, M.; Miyaura, N. *J. Org. Chem.* **1995**, *60*, 7508.

[120] Murata, M.; Watanabe, S.; Masuda, Y. *J. Org. Chem.* **1997**, *62*, 6458.

[121] Murata, M.; Oyama, T.; Watanabe, S.; Masuda, Y. *J. Org. Chem.* **2000**, *65*, 164.

[122] Lam, K. C.; Marder, T. B.; Lin, Z. *Organometallics* **2010**, *29*, 1849.

[123] Yamashita, M.; Nozaki, K. *Topics in Organometallic Chemistry, Springer, Cham* **2015**, 2.

[124] Yamamoto, Y.; Nogi, K.; Yorimitsu, H.; Osuka, A. *ChemistrySelect* **2017**, *2*, 1723.

[125] Murata, M.; Oda, T.; Sogabe, Y.; Tone, H.; Namikoshi, T.; Watanabe, S. *Chem. Lett.* **2011**, *40*, 962.

[126] Beletskaya, I. P.; Cheprakov, A. V. *Chem. Rev.* **2000**, *100*, 3009.

[127] Sommer, H.; Juliá-Hernández, F.; Martin, R.; Marek, I. *ACS Cent. Sci.* **2018**, *4*, 153.

[128] Mathew, J. S.; Klussmann, M.; Iwamura, H.; Valera, F.; Futran, A.; Emanuelsson, E. A. C.; Blackmond, D. G. *J. Org. Chem.* **2006**, *71*, 4711.

[129] Blackmond, D. G. *J. Am. Chem. Soc.* **2015**, *137*, 10852.

[130] Burés, J. *Angew. Chem. Int. Ed.* **2016**, *55*, 16084.

[131] Thomas, B. N.; Moon, P. J.; Yin, S.; Brown, A.; Lundgren, R. J. *Chem. Sci.* **2018**, *9*, 238.

[132] Nielsen, C. D. T.; Burés, J. *Chem. Sci.* **2019**, *10*, 348.

[133] Burés, J. *Angew. Chem. Int. Ed.* **2016**, *55*, 2028.

[134] Larsen, M. A.; Hennessy, E. T.; Deem, M. C.; Lam, Y.-h.; Saurí, J.; Sather, A. C. *J. Am. Chem. Soc.* **2020**, *142*, 726.

[135] Deardorff, D. R.; Niman, S. W.; Paulsen, M. I.; Sookezian, A.; Whalen, M. E.; Finlayson, C. J.; Frivold, C.; Brown, H. C.; Cannon, J. S. *ACS Omega* **2020**, *5*, 2005.

[136] Glasspoole, B. W.; Ghozati, K.; Moir, J. W.; Crudden, C. M. *Chem. Commun.* **2012**, *48*, 1230.

[137] Ding, J.; Hall, D. G. *Angew. Chem. Int. Ed.* **2013**, *52*, 8069.

[138] Jana, R.; Pathak, T. P.; Sigman, M. S. *Chem. Rev.* **2011**, *111*, 1417.

[139] Zhang, P.; Brozek, L. A.; Morken, J. P. *J. Am. Chem. Soc.* **2010**, *132*, 10686.

[140] Quasdorf, K. W.; Riener, M.; Petrova, K. V.; Garg, N. K. *J. Am. Chem. Soc.* **2009**, *131*, 17748.

[141] Brozek, L. A.; Ardolino, M. J.; Morken, J. P. *J. Am. Chem. Soc.* **2011**, *133*, 16778.

[142] Thomas, A. A.; Zahrt, A. F.; Delaney, C. P.; Denmark, S. E. *J. Am. Chem. Soc.* **2018**, *140*, 4401.

[143] Wright, S. W.; Hageman, D. L.; McClure, L. D. *J. Org. Chem.* **1994**, *59*, 6095.

[144] Granberg, K. L.; Bäckvall, J. E. *J. Am. Chem. Soc.* **1992**, *114*, 6858.

[145] Hartwig, J. F. *Inorg. Chem.* **2007**, *46*, 1936.

[146] Zhang, S.-L.; Huang, L.; Sun, L.-J. *Dalton Trans.* **2015**, *44*, 4613.

[147] Amatore, C.; Jutand, A.; M'Barki, M. A. *Organometallics* **1992**, *11*, 3009.

[148] Doebner, O. *Ber. Dtsch. Chem. Ges.* **1902**, *35*, 1136.

[149] Ardolino, M. J.; Morken, J. P. *Tetrahedron* **2015**, *71*, 6409.

[150] Kohlmann, J.; Braun, T.; Laubenstein, R.; Herrmann, R. *Chem. Eur. J.* **2017**, *23*, 12218.

[151] Yamamoto, Y.; Takada, S.; Miyaura, N.; Iyama, T.; Tachikawa, H. *Organometallics* **2009**, *28*, 152.

[152] Yamamoto, Y.; Takada, S.; Miyaura, N. *Chem. Lett.* **2006**, *35*, 1368.

[153] Yamamoto, Y.; Takada, S.; Miyaura, N. *Chem. Lett.* **2006**, *35*, 704.

[154] Sebelius, S.; Olsson, V. J.; Wallner, O. A.; Szabó, K. J. *J. Am. Chem. Soc.* **2006**, *128*, 8150.

[155] Meyers, A. I.; Dickman, D. A.; Bailey, T. R. *J. Am. Chem. Soc.* **1985**, *107*, 7974.

[156] Podyacheva, E.; Afanasyev, O. I.; Tsygankov, A. A.; Makarova, M.; Chusov, D. *Synthesis* **2019**, *51*, 2667.

[157] Liu, X.; Liu, S.; Wang, Q.; Zhou, G.; Yao, L.; Ouyang, Q.; Jiang, R.; Lan, Y.; Chen, W. *Org. Lett.* **2020**, *22*, 3149.

[158] Yang, B.; Wang, Z.-X. *Org. Lett.* **2019**, *21*, 7965.

[159] Guo, Y.; Shen, Z. *Organic & Biomolecular Chemistry* **2019**, *17*, 3103.

[160] Li, F.; Wang, Z.-H.; Zhao, L.; Xiong, F.-J.; He, Q.-Q.; Chen, F.-E. *Tetrahedron: Asymmetry* **2011**, *22*, 1337.

[161] Weix, D. J.; Markovic, D.; Ueda, M.; Hartwig, J. F. *Org. Lett.* **2009**, *11*, 2944.

[162] Yuan, Q.; Yao, K.; Liu, D.; Zhang, W. *Chem. Commun.* **2015**, *51*, 11834.

[163] Lin, L.-Z.; Che, Y.-Y.; Bai, P.-B.; Feng, C. *Org. Lett.* **2019**, *21*, 7424.

[164] Bai, X.-D.; Zhang, Q.-F.; He, Y. *Chem. Commun.* **2019**, *55*, 5547.

[165] Davis, C. R.; Luvaga, I. K.; Ready, J. M. *J. Am. Chem. Soc.* **2021**, *143*, 4921.

[166] Daley, R. A.; Topczewski, J. J. *Org. Biomol. Chem.* **2019**, *17*, 1709.

[167] Stambasky, J.; Malkov, A. V.; Kocovsky, P. *J. Org. Chem.* **2008**, *73*, 9148.

[168] Taylor, O. G.; Brzozowski, J. S.; Skelding, K. A. *Front. Oncol.* **2019**, *9*.

[169] Thakkar, J. P.; Dolecek, T. A.; Horbinski, C.; Ostrom, Q. T.; Lightner, D. D.; Barnholtz-Sloan, J. S.; Villano, J. L. *Cancer Epidemiol. Biomarkers Prev.* **2014**, *23*, 1985.

[170] Ohgaki, H.; Kleihues, P. *J. Neuropathol. Exp. Neurol.* **2005**, *64*, 479.

[171] Ohgaki, H.; Kleihues, P. *Am. J. Pathol.* **2007**, *170*, 1445.

[172] Ohgaki, H.; Kleihues, P. *Clin. Cancer Res.* **2013**, *19*, 764.

[173] Rossi, J.; Giaccherini, L.; Cavallieri, F.; Napoli, M.; Moratti, C.; Froio, E.; Serra, S.; Fraternali, A.; Ghadirpour, R.; Cozzi, S.; Ciammella, P.; Iaccarino, C.; Pascarella, R.; Valzania, F.; Pisanello, A. *BMC Neurol.* **2020**, *20*, 382.

[174] Urbańska, K.; Sokołowska, J.; Szmidt, M.; Sysa, P. *Contemp. Oncol. (Pozn)* **2014**, *18*, 307.

[175] American Society of Clinical Oncology. Brain Tumor: Grades and Prognostic Factors. **2021**. https://www.cancer.net/cancer-types/brain-tumor/grades-and-prognostic-factors. (accessed January 11, 2022).

[176] Kleihues, P.; Ohgaki, H. *Neuro-Oncol.* **1999**, *1*, 44.

[177] Perkins, A.; Liu, G. *Am Fam Physician* **2016**, *93*, 211.

[178] Shi, Y.; Lim, S. K.; Parada, L. F. *Cell Res.* **2014**, *24*, 910.

[179] Barbashina, V.; Salazar, P.; Ladanyi, M.; Rosenblum, M. K.; Edgar, M. A. *Am. J. Surg. Pathol.* **2007**, *31*, 1196.

[180] Appin, C. L.; Gao, J.; Chisolm, C.; Torian, M.; Alexis, D.; Vincentelli, C.; Schniederjan, M. J.; Hadjipanayis, C.; Olson, J. J.; Hunter, S.; Hao, C.; Brat, D. J. *Brain Pathol.* **2013**, *23*, 454.

[181] Takeuchi, H.; Kitai, R.; Hosoda, T.; Yamada, S.; Hashimoto, N.; Kikuta, K.-i.; Shimizu, Y.; Kimura, H. *J. Neurooncol.* **2016**, *127*, 337.

[182] Zhang, P.; Xia, Q.; Liu, L.; Li, S.; Dong, L. *Front. Mol. Biosci.* **2020**, *7*.

[183] Rodriguez, F. J.; Orr, B. A.; Ligon, K. L.; Eberhart, C. G. *Oncotarget* **2012**, *3*.

[184] Vasilev, A.; Sofi, R.; Rahman, R.; Smith, S. J.; Teschemacher, A. G.; Kasparov, S. *Brain Sci.* **2020**, *10*, 75.

[185] Lee, S. Y. *Genes & Diseases* **2016**, *3*, 198.

[186] Bastiancich, C.; Bastiat, G.; Lagarce, F. *Drug Discov Today* **2018**, *23*, 416.

[187] Lathia, J. D.; Mack, S. C.; Mulkearns-Hubert, E. E.; Valentim, C. L. L.; Rich, J. N. *Genes Dev.* **2015**, *29*, 1203.

[188] Cantrell, J. N.; Waddle, M. R.; Rotman, M.; Peterson, J. L.; Ruiz-Garcia, H.; Heckman, M. G.; Quiñones-Hinojosa, A.; Rosenfeld, S. S.; Brown, P. D.; Trifiletti, D. M. *Mayo Clin. Proc.* **2019**, *94*, 1278.

[189] Kitambi, S. S.; Toledo, E. M.; Usoskin, D.; Wee, S.; Harisankar, A.; Svensson, R.; Sigmundsson, K.; Kalderén, C.; Niklasson, M.; Kundu, S.; Aranda, S.; Westermark, B.; Uhrbom, L.; Andäng, M.; Damberg, P.; Nelander, S.; Arenas, E.; Artursson, P.; Walfridsson, J.; Nilsson, K. F.; Hammarström, L. G. J.; Ernfors, P. *Cell* **2017**, *170*, 407.

[190] Hann, M. M.; Oprea, T. I. *Curr. Opin. Chem. Biol.* **2004**, *8*, 255.

[191] Gilbertson, Richard J. *Cell* **2014**, *157*, 289.

[192] Lee, J.; Kotliarova, S.; Kotliarov, Y.; Li, A.; Su, Q.; Donin, N. M.; Pastorino, S.; Purow, B. W.; Christopher, N.; Zhang, W.; Park, J. K.; Fine, H. A. *Cancer Cell* **2006**, *9*, 391.

[193] Ahlstedt, J.; Förnvik, K.; Zolfaghari, S.; Kwak, D.; Hammarström, L. G.; Ernfors, P.; Salford, L. G.; Redebrandt, H. N. *Oncotarget* **2018**, *9*, 8391.

[194] Buchman, E.; Howton, D. *J. Am. Chem. Soc.* **1946**, *68*, 2718.

[195] Senear, A.; Sargent, H.; Mead, J.; Koepfli, J. *J. Am. Chem. Soc.* **1946**, *68*, 2695.

[196] Winstein, S.; Jacobs, T. L.; Levy, E. F.; Seymour, D.; Linden, G. B.; Henderson, R. B. *J. Am. Chem. Soc.* **1946**, *68*, 2714.

[197] Pinder, R. M.; Burger, A. *J. Med. Chem.* **1968**, *11*, 267.

[198] Fernandez-Alvaro, E.; Hong, W. D.; Nixon, G. L.; O'Neill, P. M.; Calderon, F. *J. Med. Chem.* **2016**, *59*, 5587.

[199] León, B.; Fong, J. C.; Peach, K. C.; Wong, W. R.; Yildiz, F. H.; Linington, R. G. *Org. Lett.* **2013**, *15*, 1234.

[200] Fuhler, G. M.; Brooks, R.; Toms, B.; Iyer, S.; Gengo, E. A.; Park, M.-Y.; Gumbleton, M.; Viernes, D. R.; Chisholm, J. D.; Kerr, W. G. *Mol. Med.* **2012**, *18*, 65.

[201] Hammarström, L. G. J.; Harmel, R. K.; Granath, M.; Ringom, R.; Gravenfors, Y.; Färnegårdh, K.; Svensson, P. H.; Wennman, D.; Lundin, G.; Roddis, Y.; Kitambi, S. S.; Bernlind, A.; Lehmann, F.; Ernfors, P. *J. Med. Chem.* **2016**, *59*, 8577.

[202] Färnegårdh, K.; Gravenfors, Y.; Ernfors, P.; Hammarström, L. G. J.; Kitambi, S. Compounds and Use for Treating Cancer. WO Patent 2015/033228 A2, March 12, 2015.

[203] Pfitzinger, W. *Journal für Praktische Chemie* **1886**, *33*, 100.

[204] Fischer, E.; Speier, A. *Ber. Dtsch. Chem. Ges.* **1895**, *28*, 3252.

[205] McConathy, J.; Owens, M. J. *Prim. Care Companion. J. Clin. Psychiatry.* **2003**, *5*, 70.

[206] Li-Yuan Bao, R.; Zhao, R.; Shi, L. *ChemComm* **2015**, *51*, 6884.

[207] Tan, S. K.; Jermakowicz, A.; Mookhtiar, A. K.; Nemeroff, C. B.; Schürer, S. C.; Ayad, N. G. *Front. Pharmacol.* **2018**, *9*.

[208] Kwok, S. Application and Substrate Scope Expansion of a Unique Borylative Migration Transformation. M.Sc. Thesis, The University of Alberta, 2016.

[209] McDonald, R. Preparation and Application of Cyclic Chiral Organoboron Compounds for the Stereoselective Synthesis of Vacquinol-1 Analogs, and Trisubstituted Cyclobutylboronates. M.Sc. Thesis, The University of Alberta, 2019.

[210] Mosset, P.; Grée, R. *Synlett* **2013**, *24*, 1142.

[211] *CellTiter 96® AQueous One Solution Cell Proliferation Assay*; Technical Bulletin #TB112; Promega Corporation: Madison, W., 2012, 1-12.

[212] Hornillos, V.; Pérez, M.; Fañanás-Mastral, M.; Feringa, B. L. *J. Am. Chem. Soc.* **2013**, *135*, 2140.

[213] Lei, S.; Jingjing, X.; Jingjing, B.; Zhiguo, Z.; Tongxin, L.; Xiaolan, Y.; Guisheng, Z. *Chin. J. Org. Chem.* **2018**, *38*, 3016.

Appendix 1: Selected Copies of NMR Spectra

^{1}H NMR for compound **3-5j** (400 MHz, $CDCl_3$)

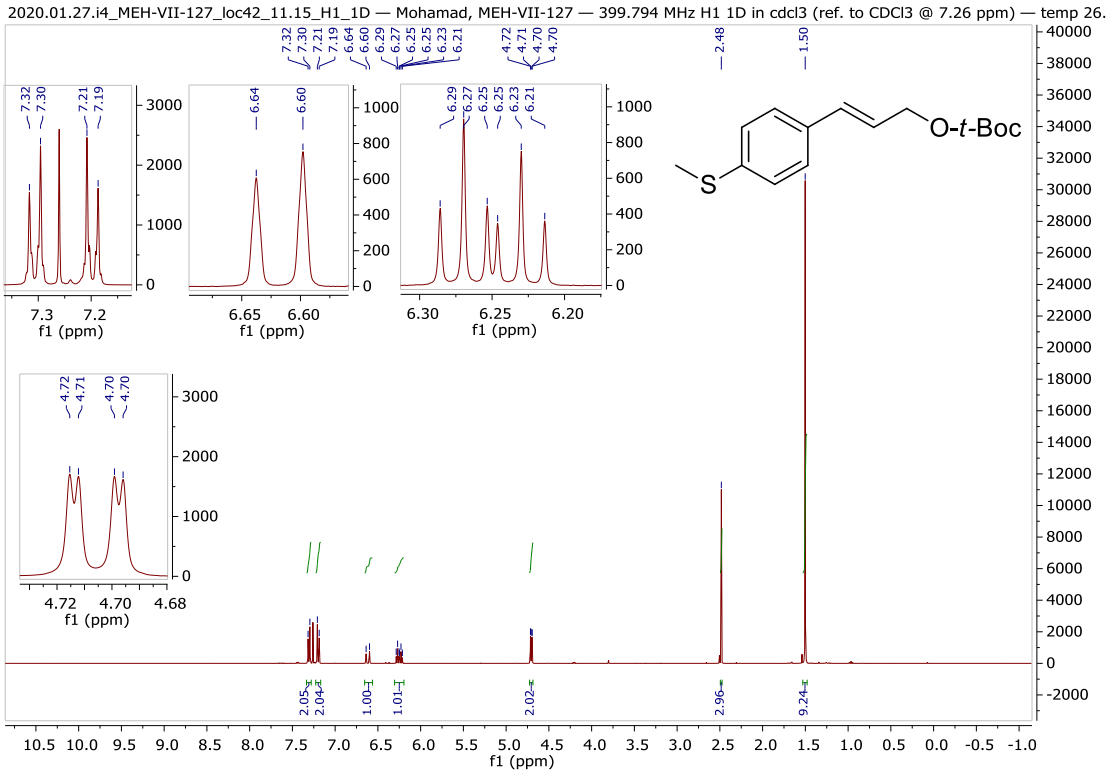

^{13}C NMR for compound **3-5j** (101 MHz, $CDCl_3$)

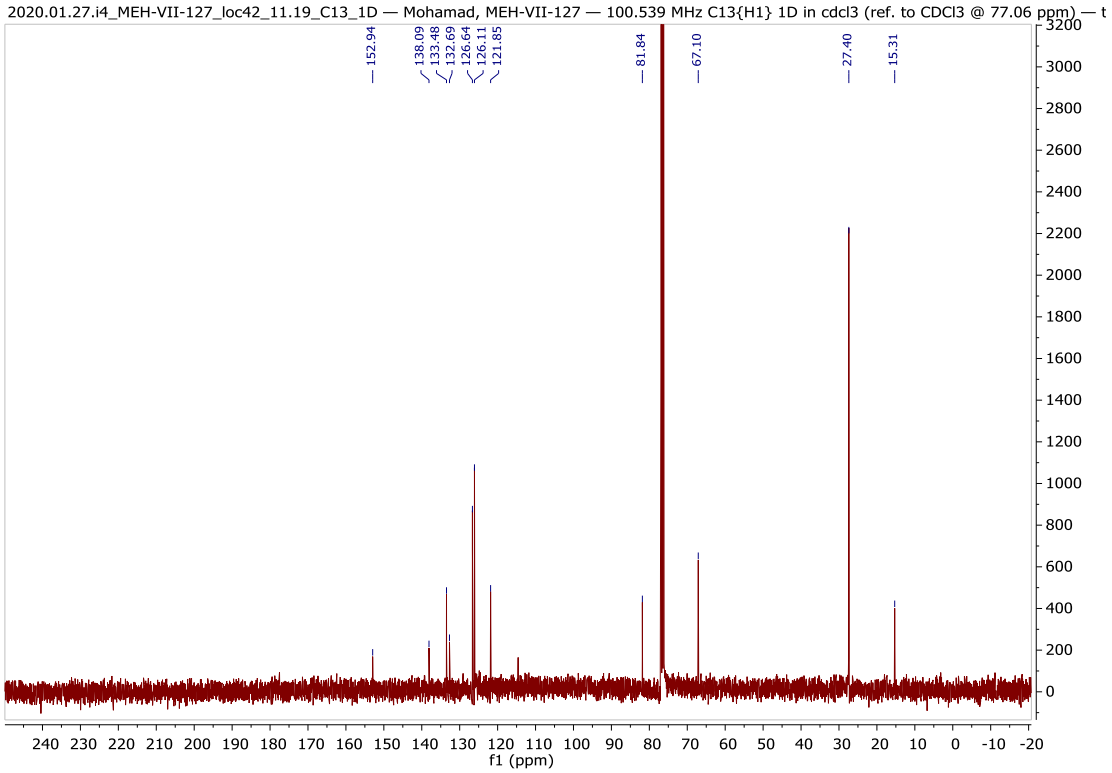

^{1}H NMR for compound **3-5g** (500 MHz, $CDCl_3$)

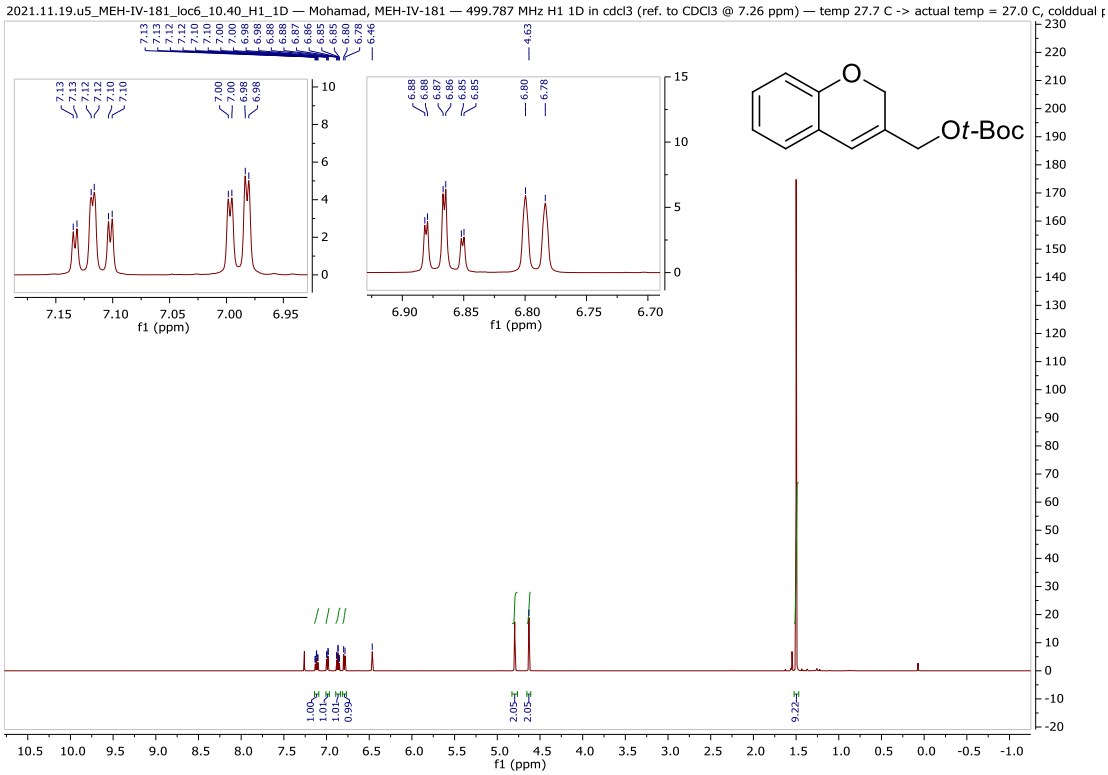

^{13}C NMR for compound **3-5g** (126 MHz, $CDCl_3$)

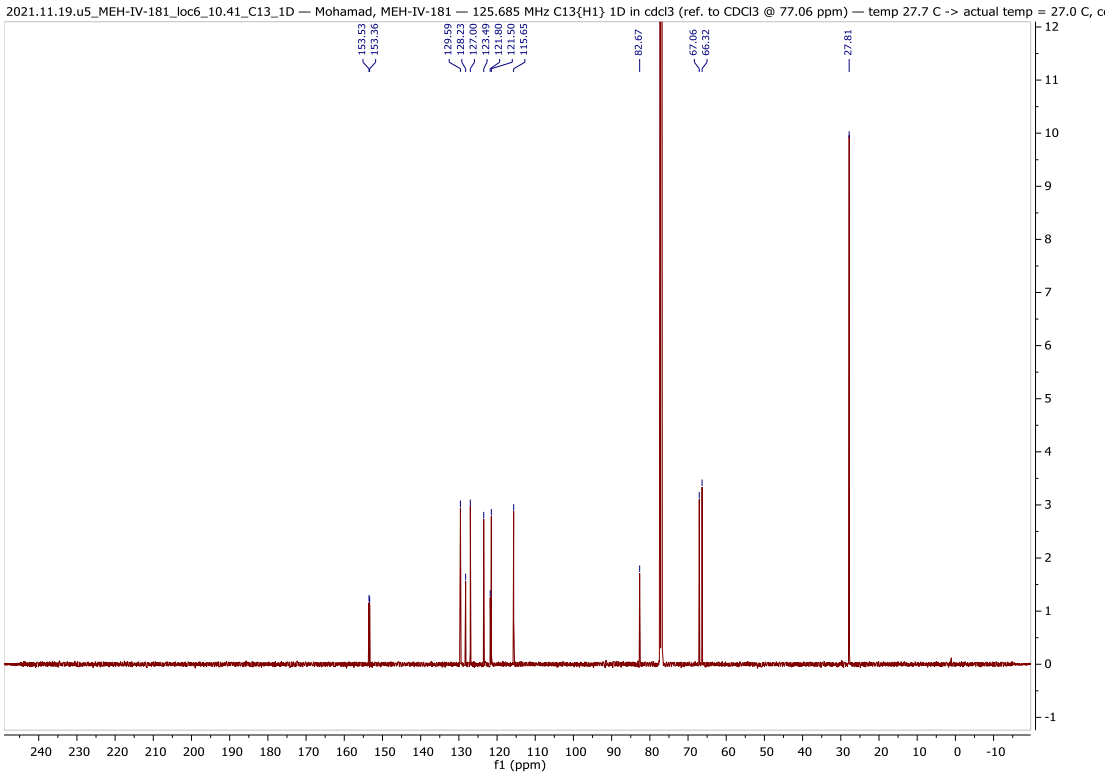

^{1}H NMR for compound ***(S)*-3-6a** (500 MHz, $CDCl_3$)

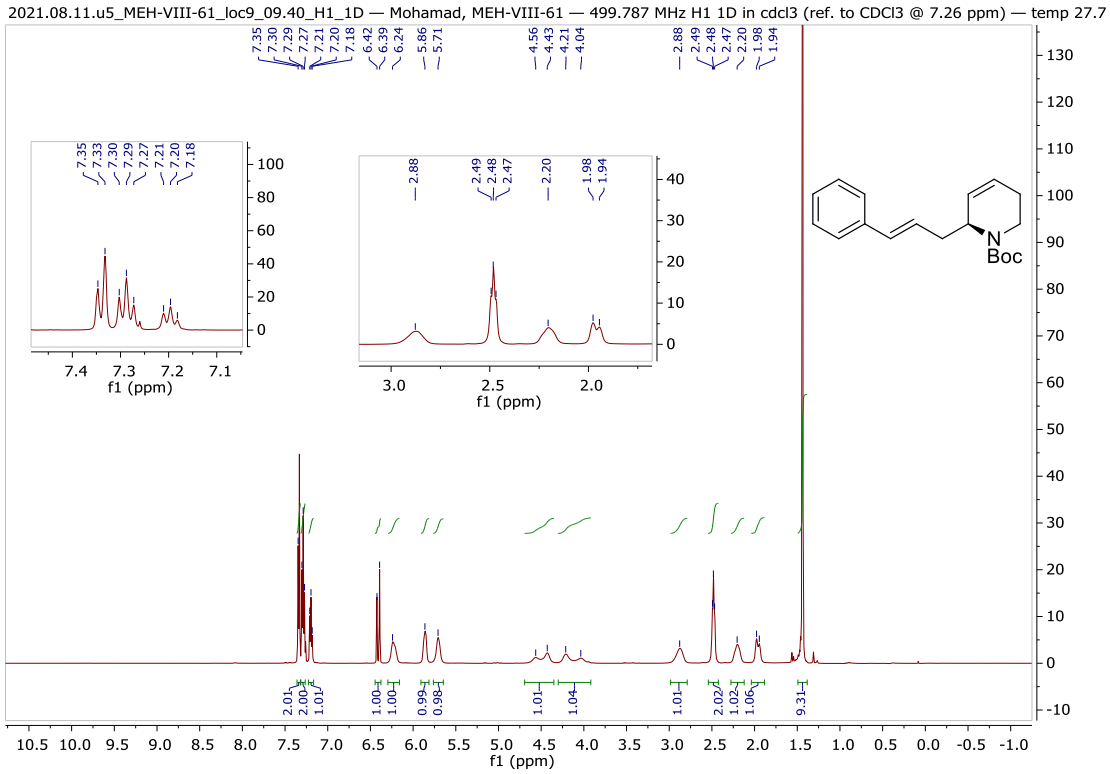

^{13}C NMR for compound ***(S)*-3-6a** (126 MHz, $CDCl_3$)

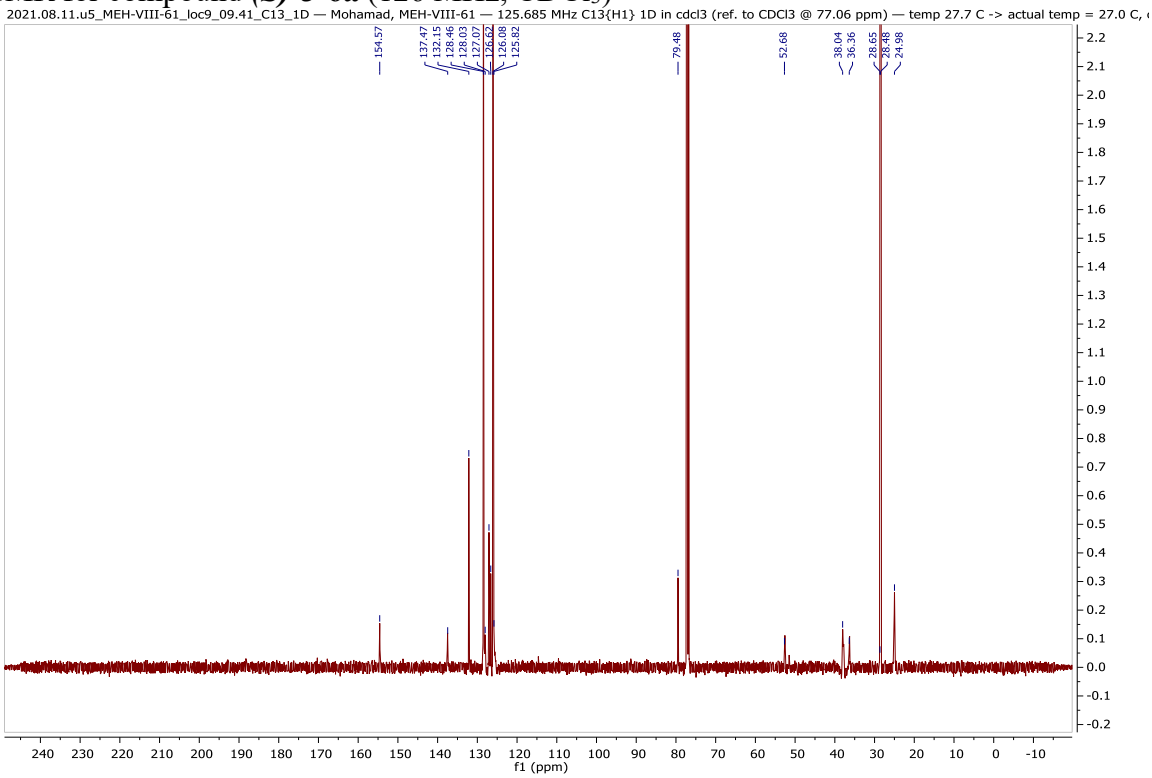

^{1}H NMR for compound **3-6b** (500 MHz, $CDCl_3$)

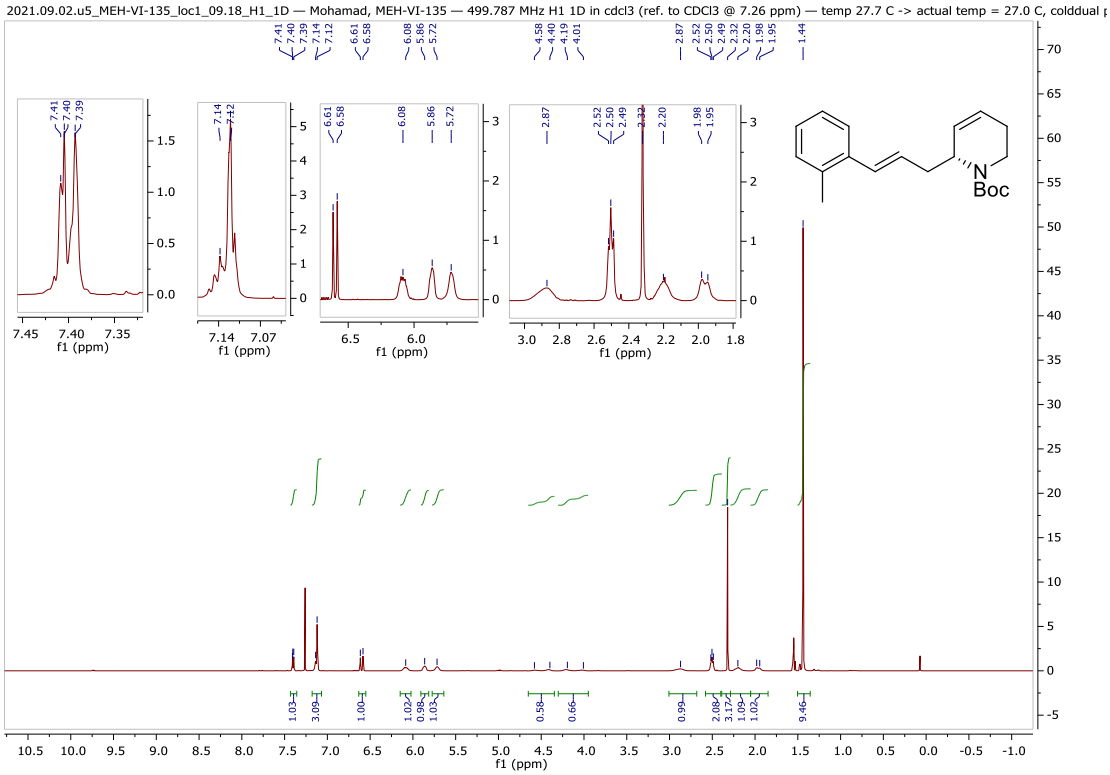

^{13}C NMR for compound **3-6b** (126 MHz, $CDCl_3$)

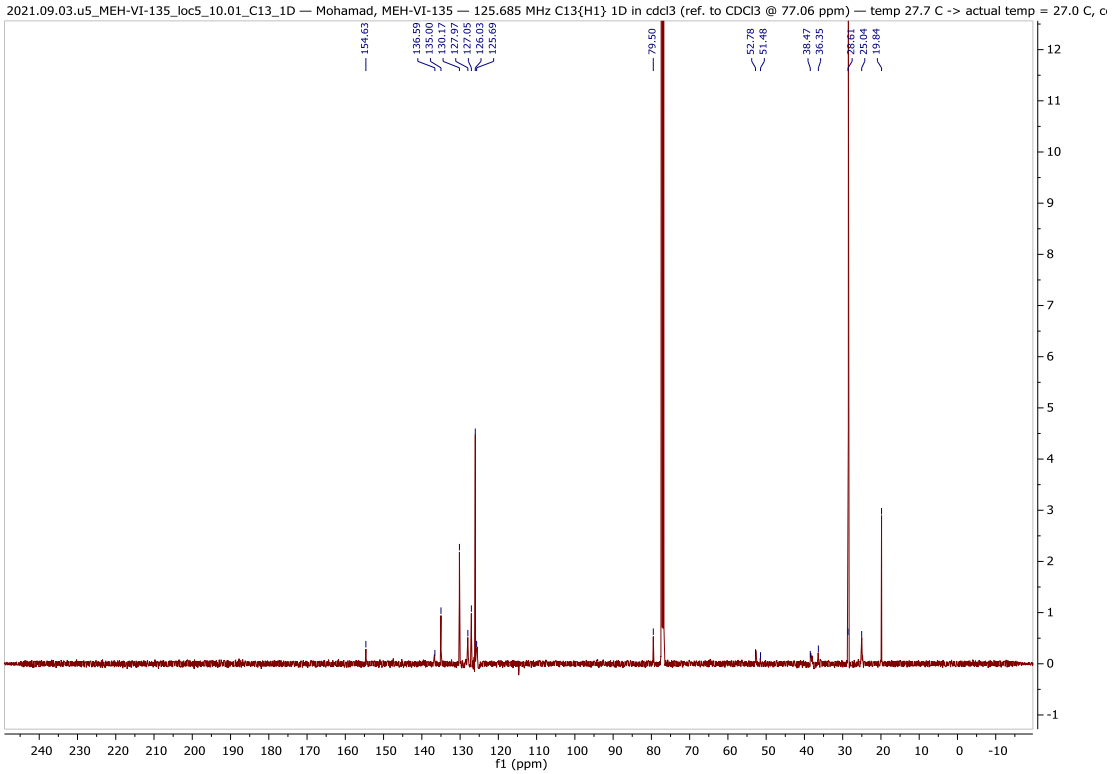

^{1}H NMR for compound **3-6c** (500 MHz, $CDCl_3$

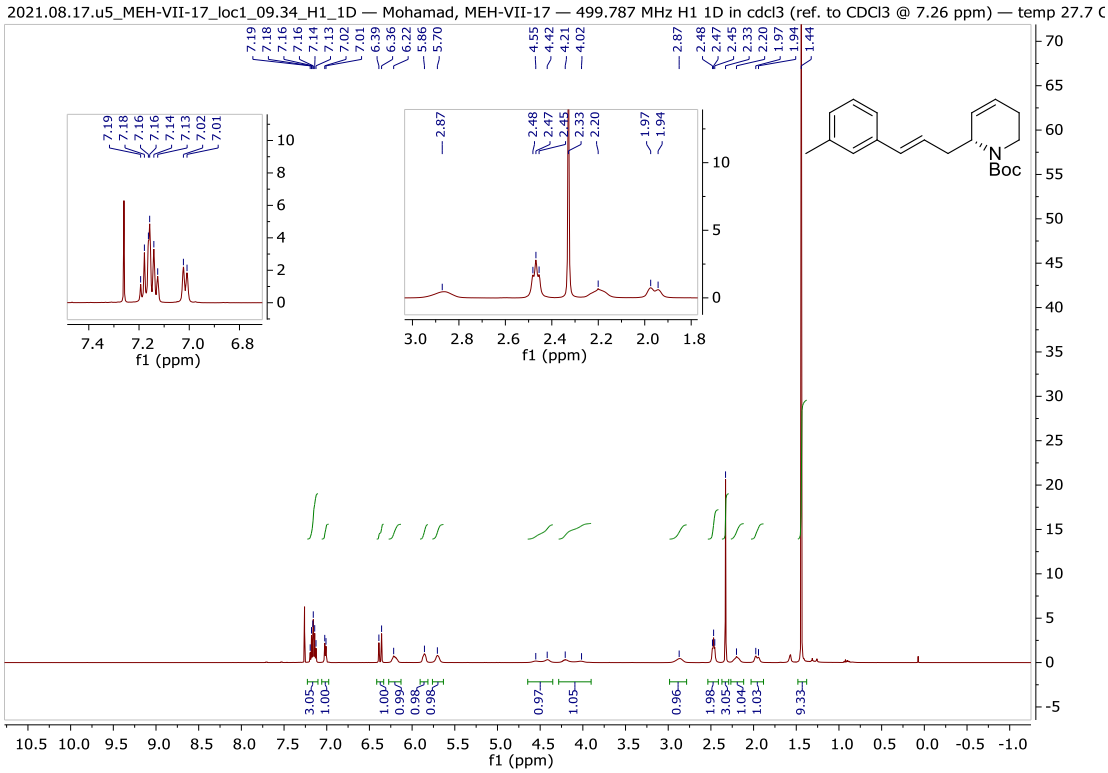

^{13}C NMR for compound **3-6c** (126 MHz, $CDCl_3$)

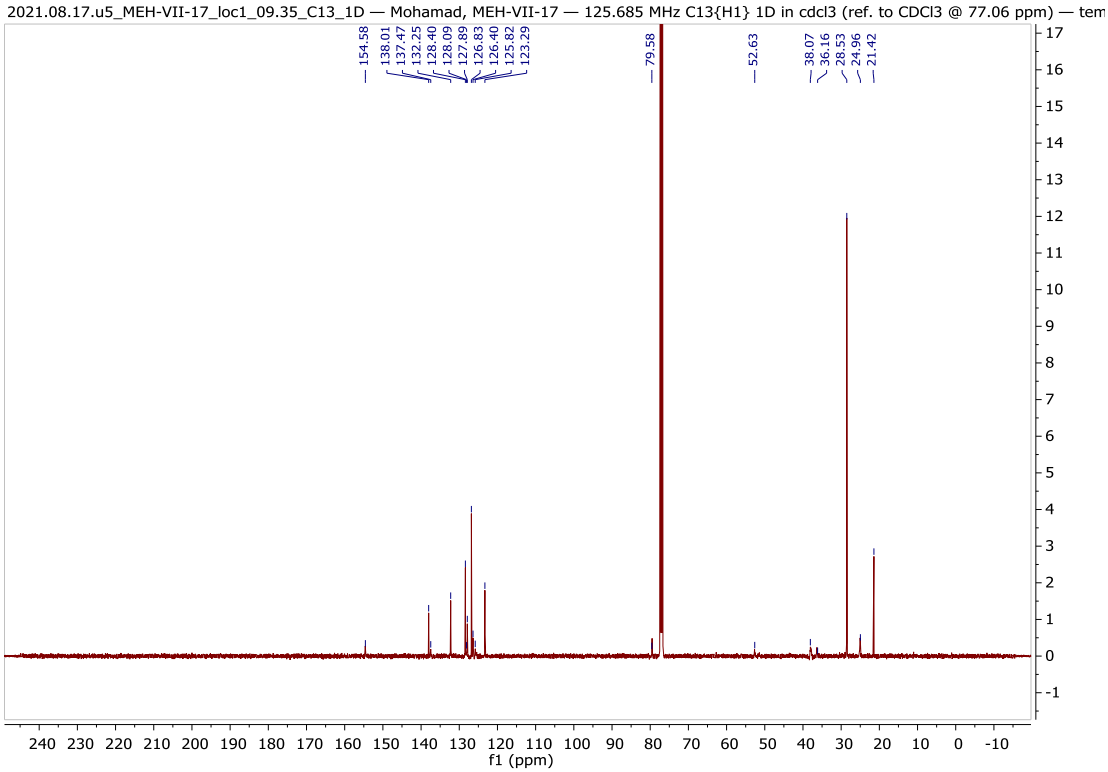

^{1}H NMR for compound **3-6d** (500 MHz, $CDCl_3$)

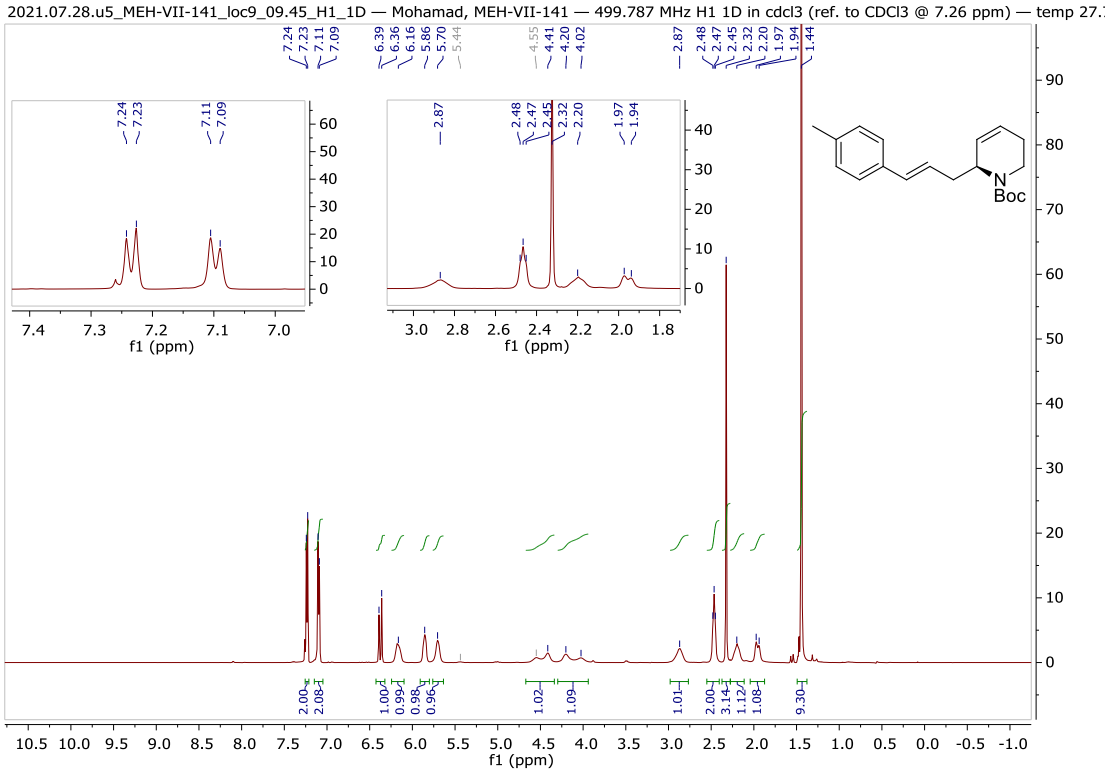

^{13}C NMR for compound **3-6d** (126 MHz, $CDCl_3$)

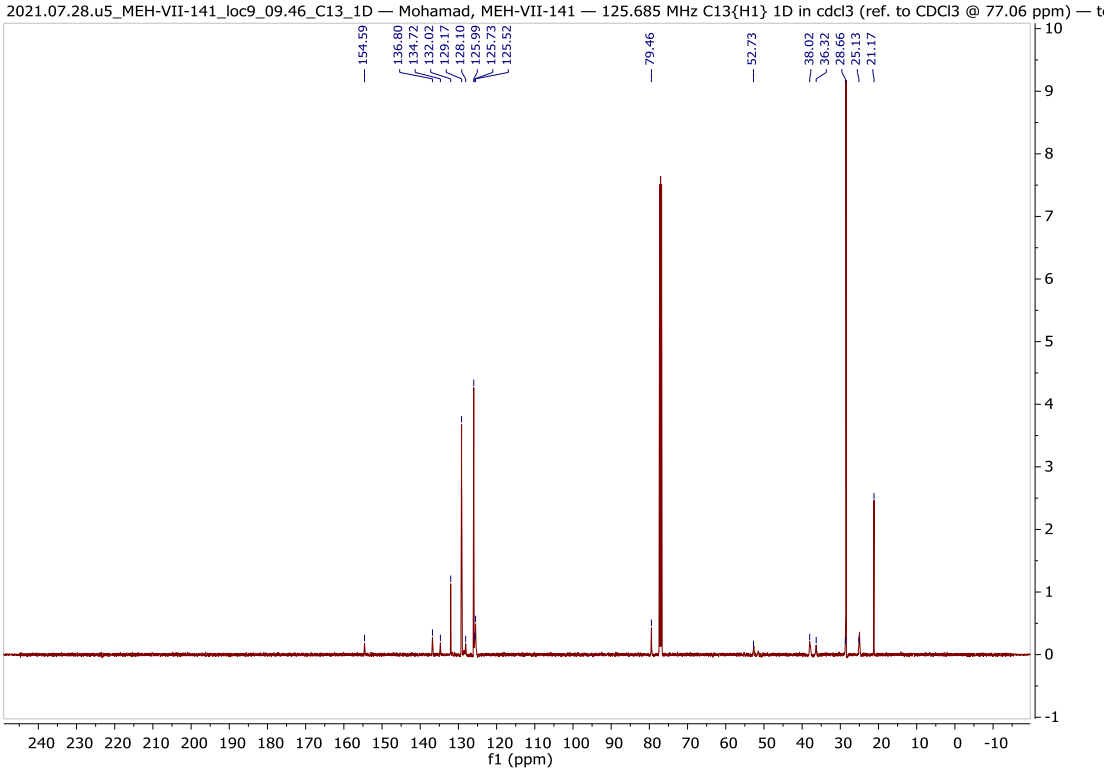

^{1}H NMR for compound **3-6e** (500 MHz, $CDCl_3$)

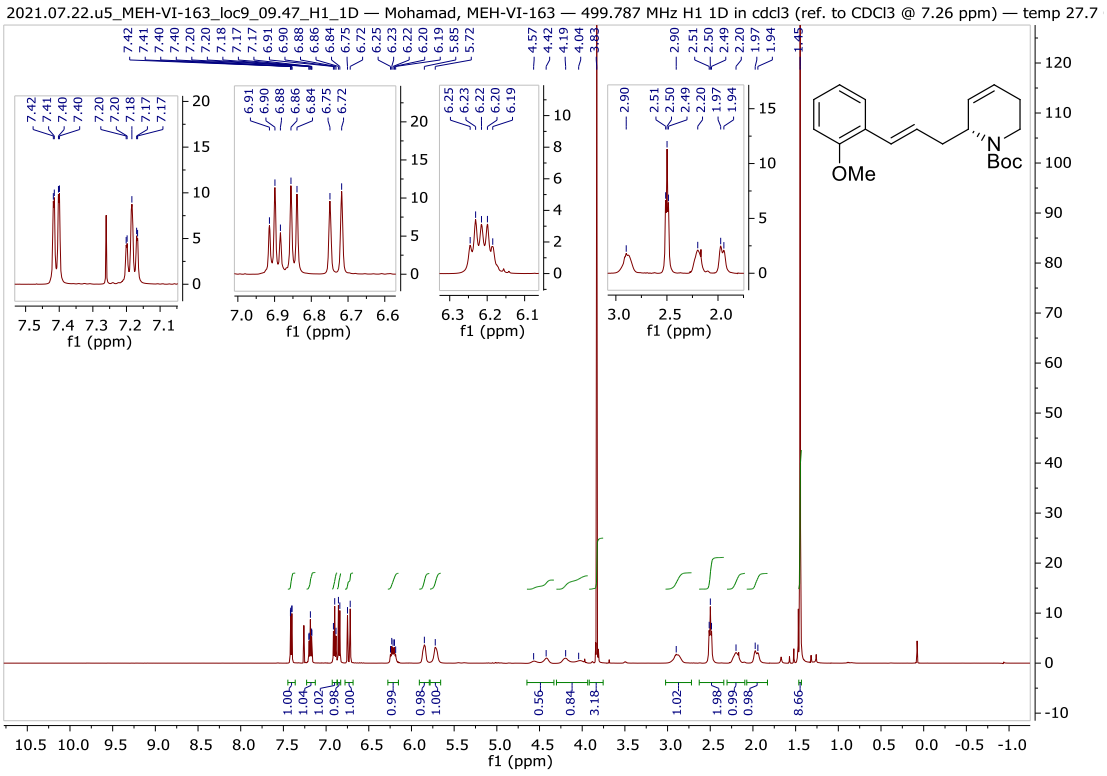

^{13}C NMR for compound **3-6e** (126 MHz, $CDCl_3$)

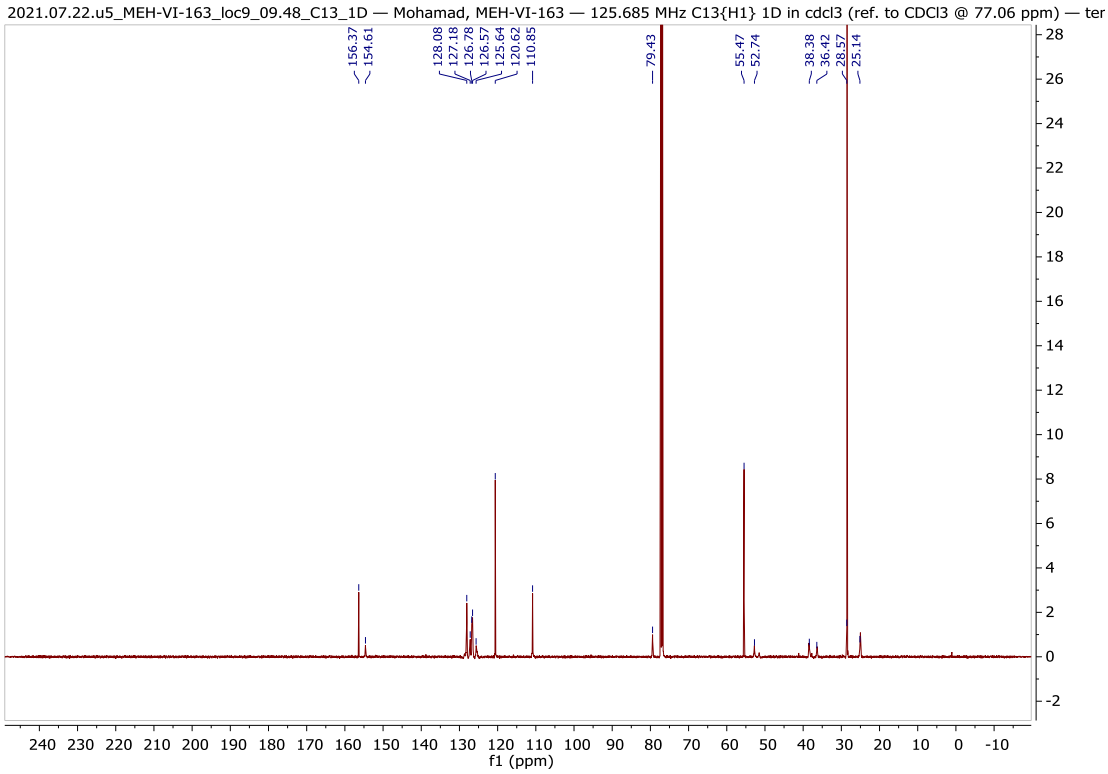

^{1}H NMR for compound **3-6f** (500 MHz, $CDCl_3$)

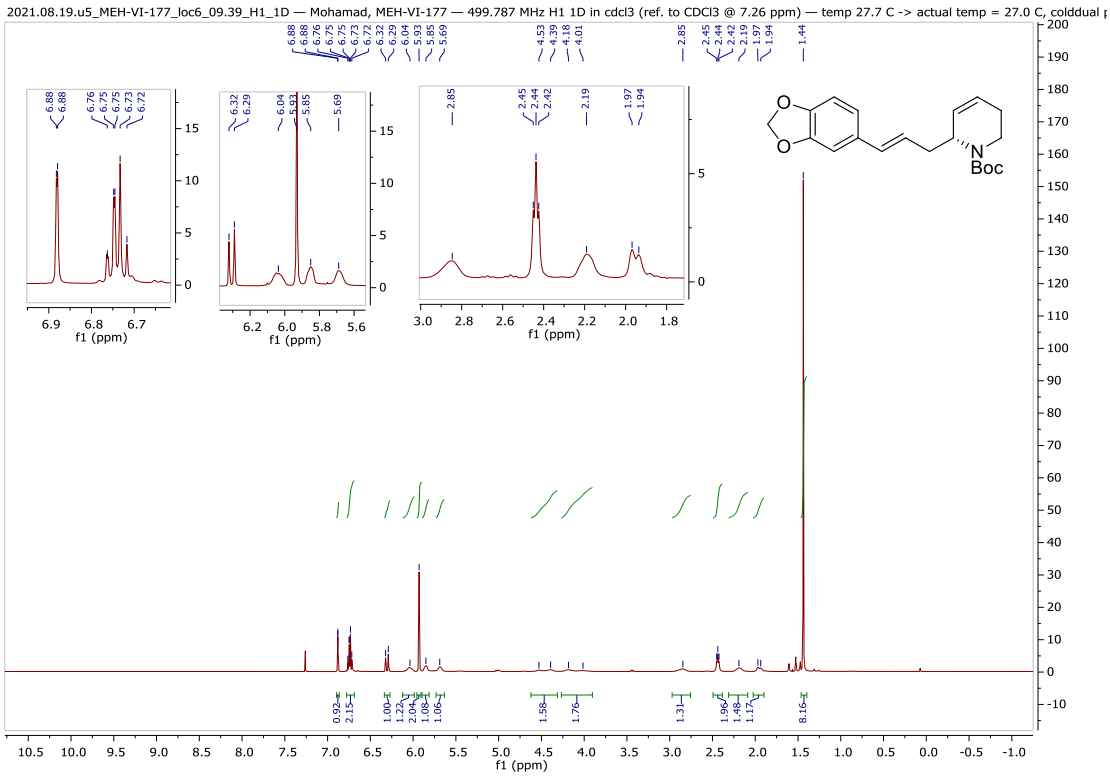

^{13}C NMR for compound **3-6f** (126 MHz, $CDCl_3$)

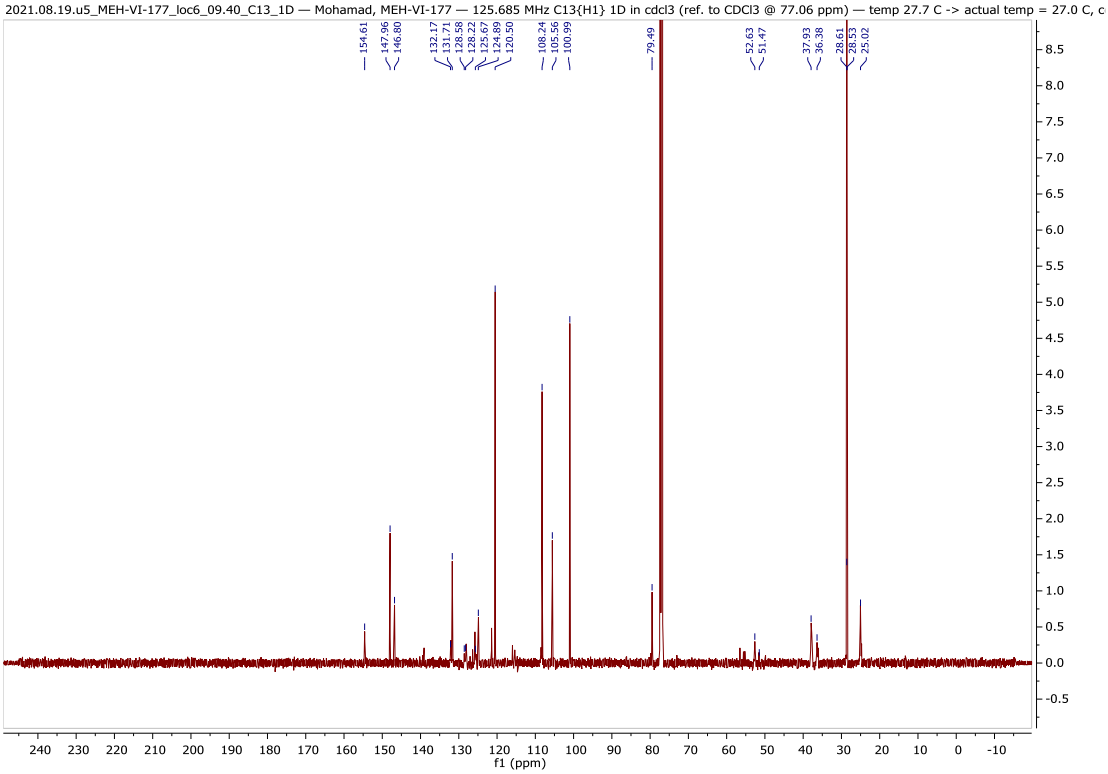

^{1}H NMR for compound **3-6g** (500 MHz, $CDCl_3$)

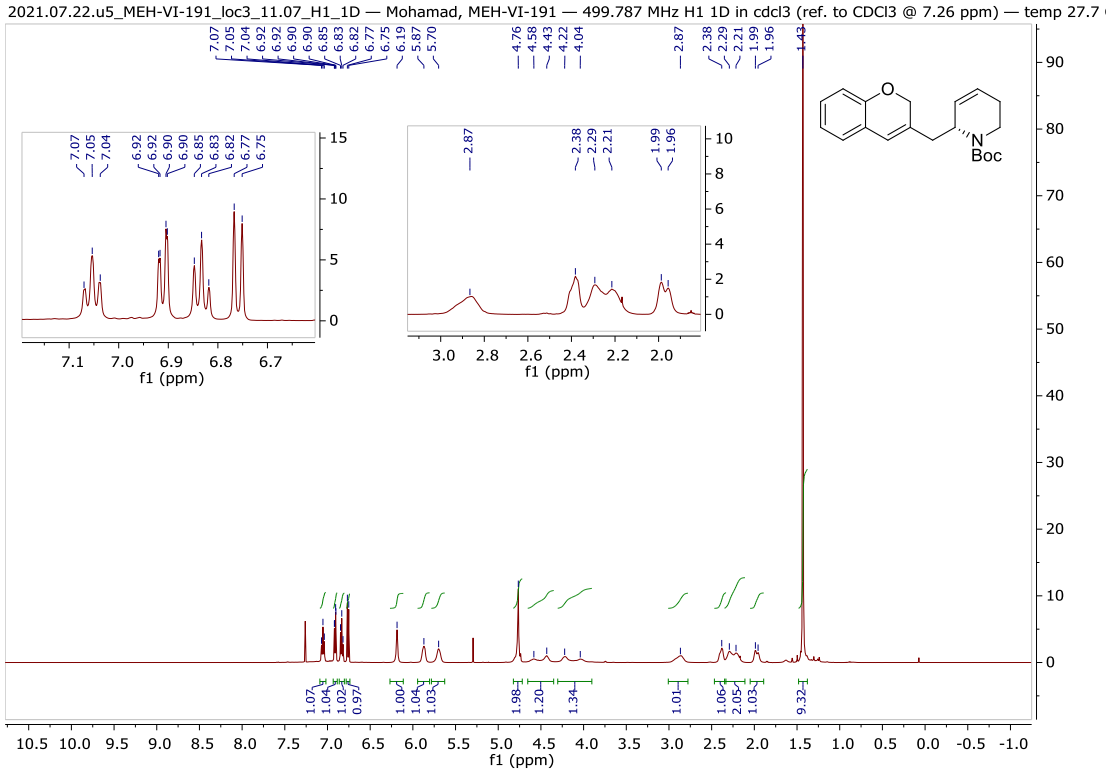

^{13}C NMR for compound **3-6g** (126 MHz, $CDCl_3$)

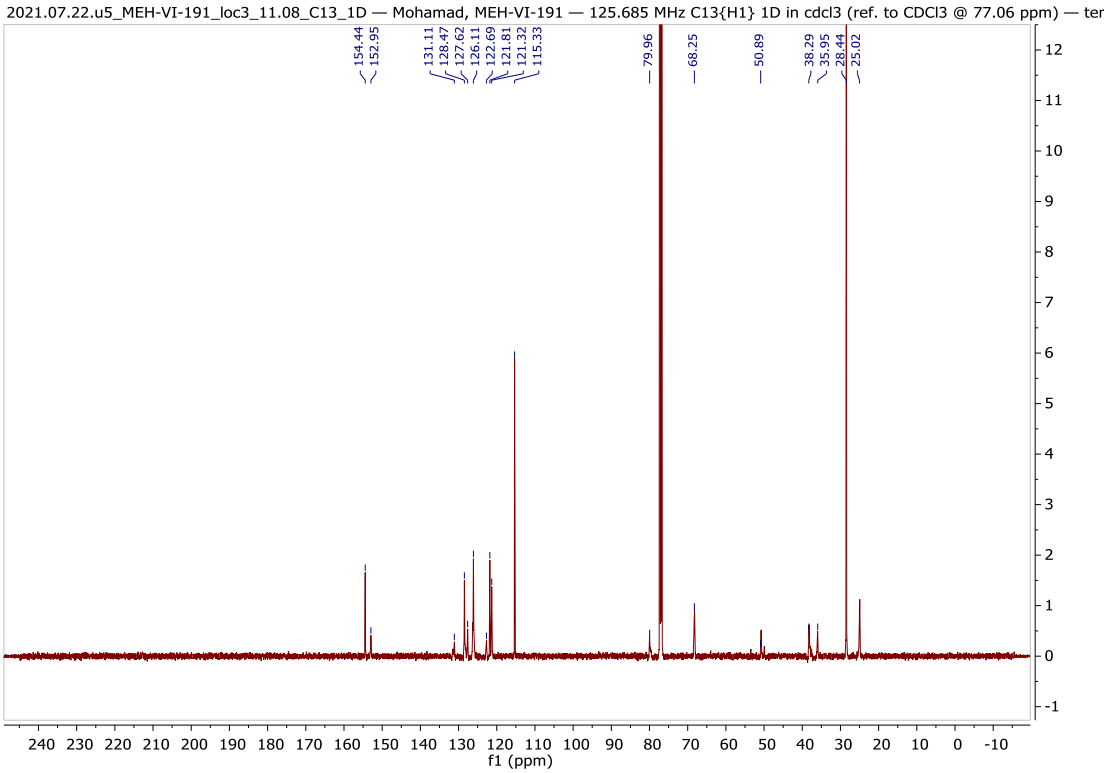

^{1}H NMR for compound **3-6h** (500 MHz, $CDCl_3$)

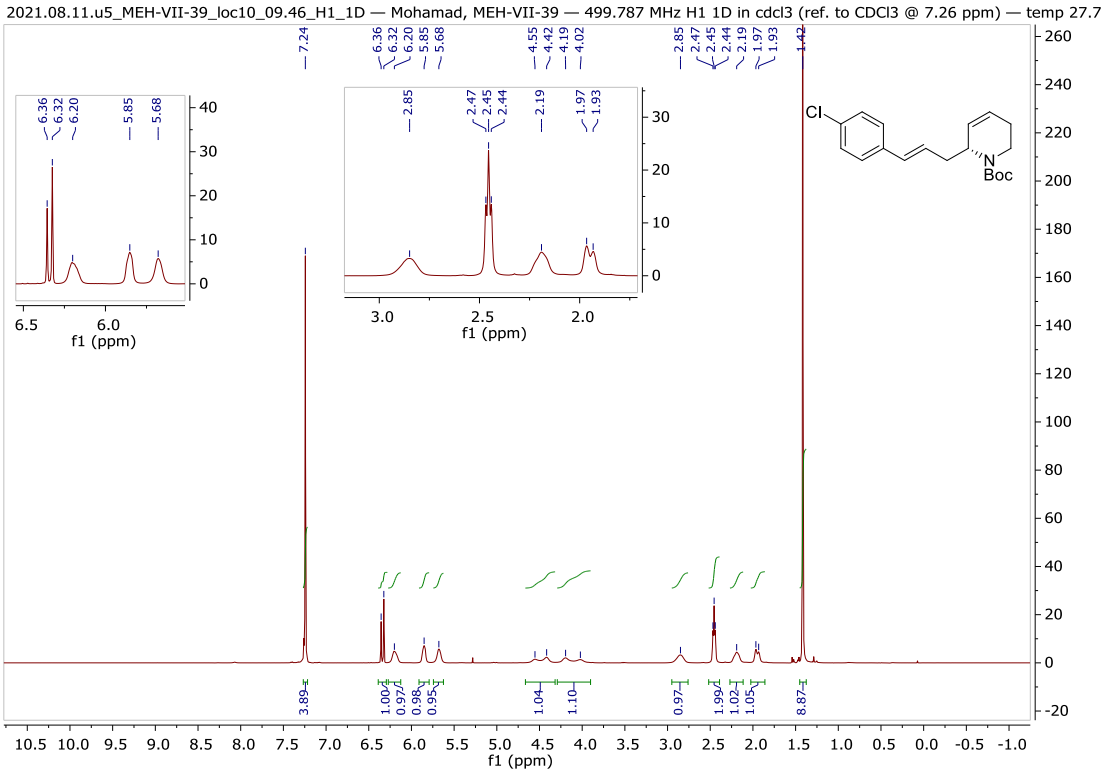

^{13}C NMR for compound **3-6h** (126 MHz, $CDCl_3$)

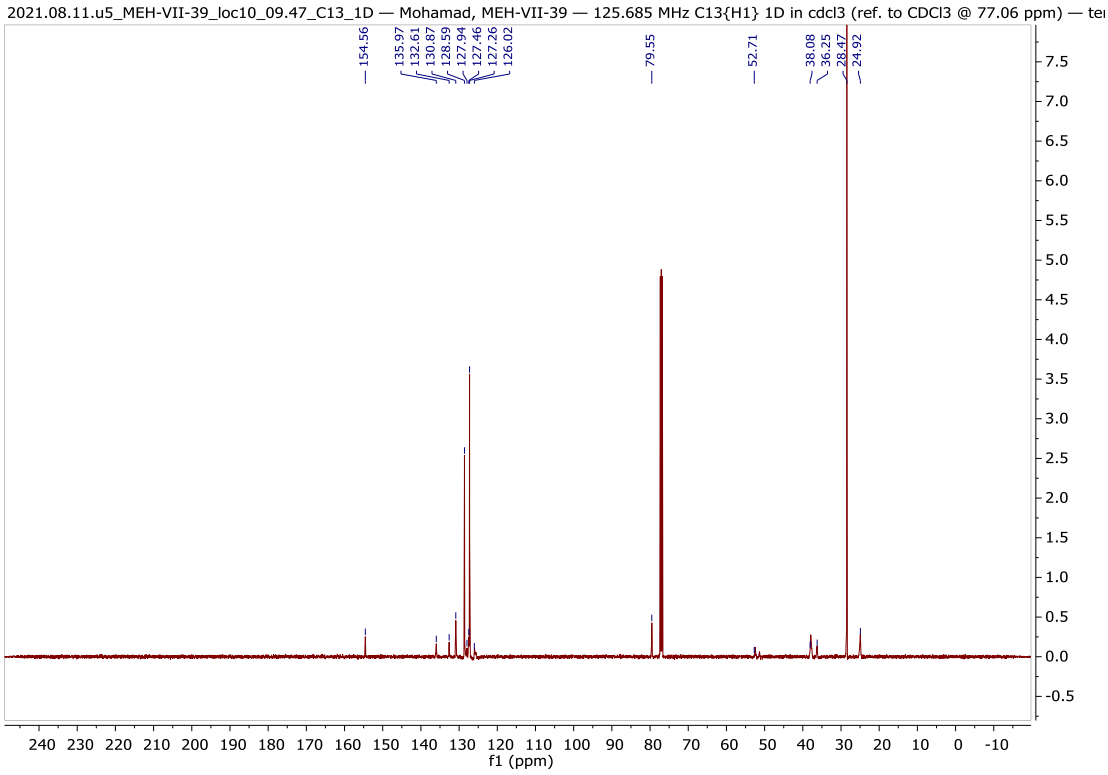

^{1}H NMR for compound **3-6i** (500 MHz, $CDCl_3$)

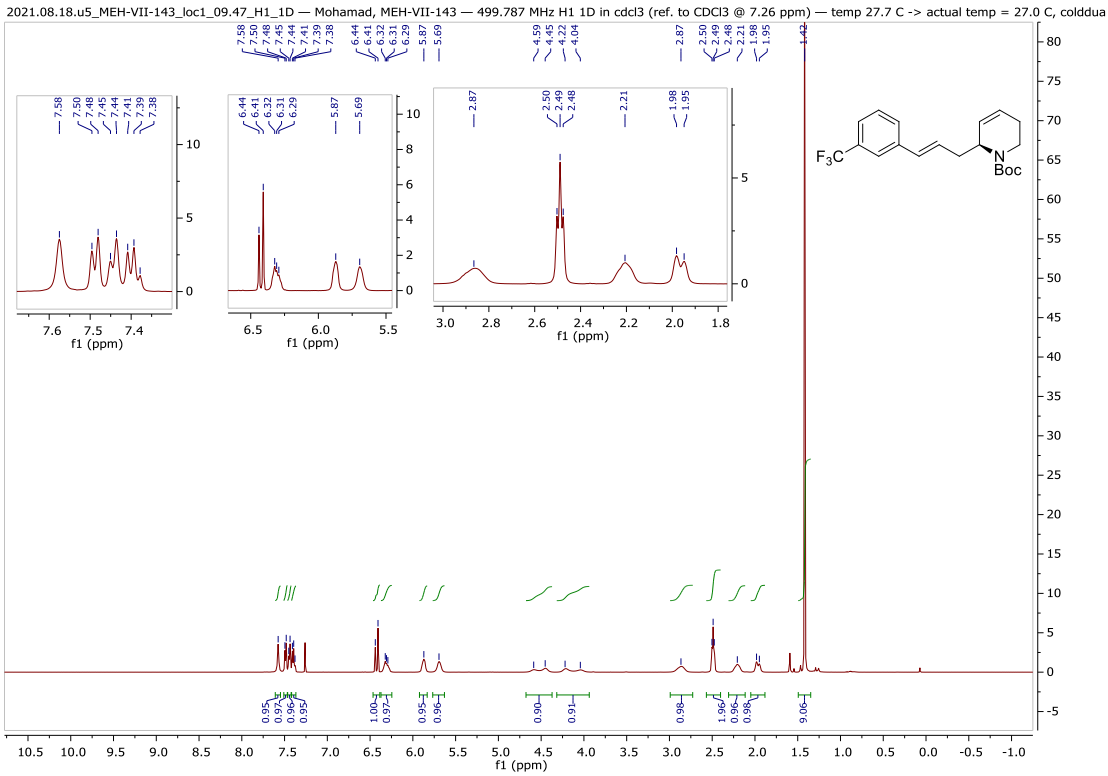

^{13}C NMR for compound **3-6i** (126 MHz, $CDCl_3$)

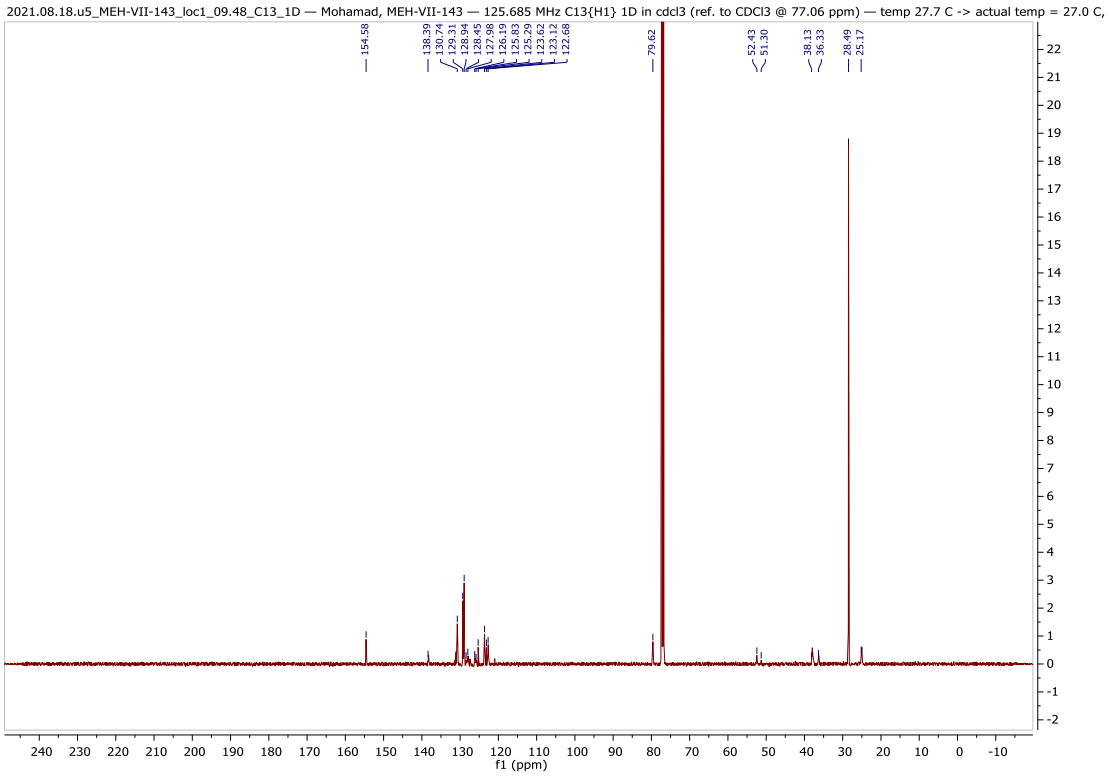

^{19}F NMR for compound **3-6i** (469 MHz, $CDCl_3$)

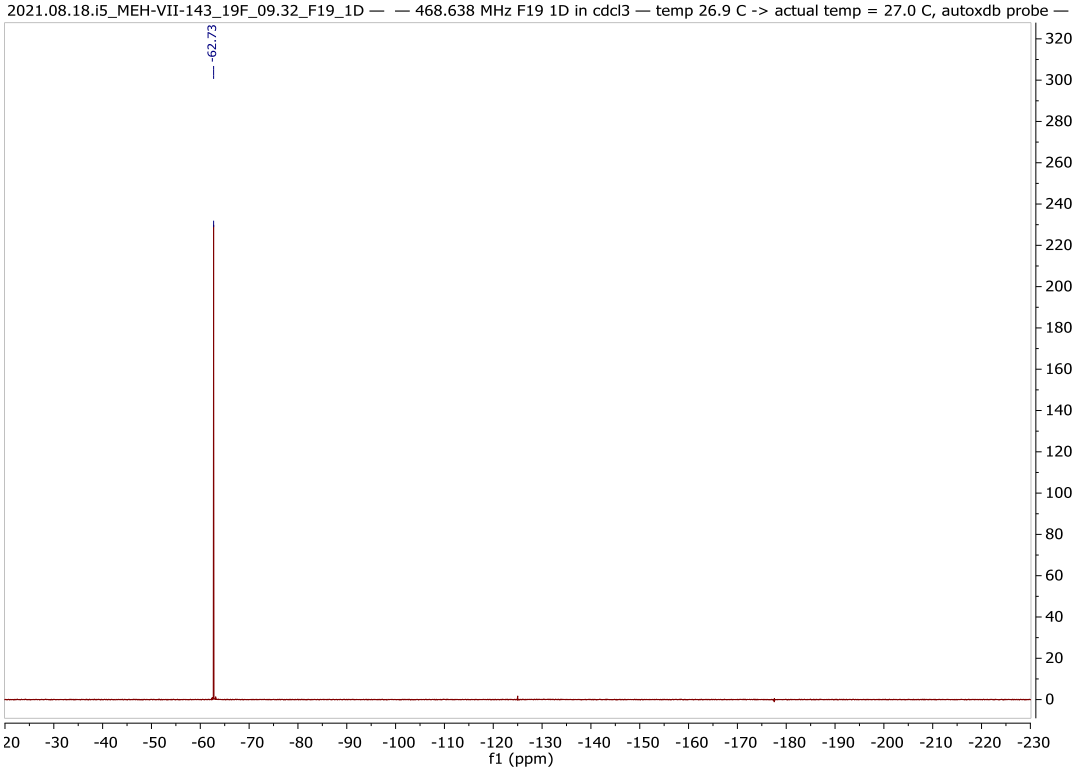

^{1}H NMR for compound **3-6j** (500 MHz, $CDCl_3$)

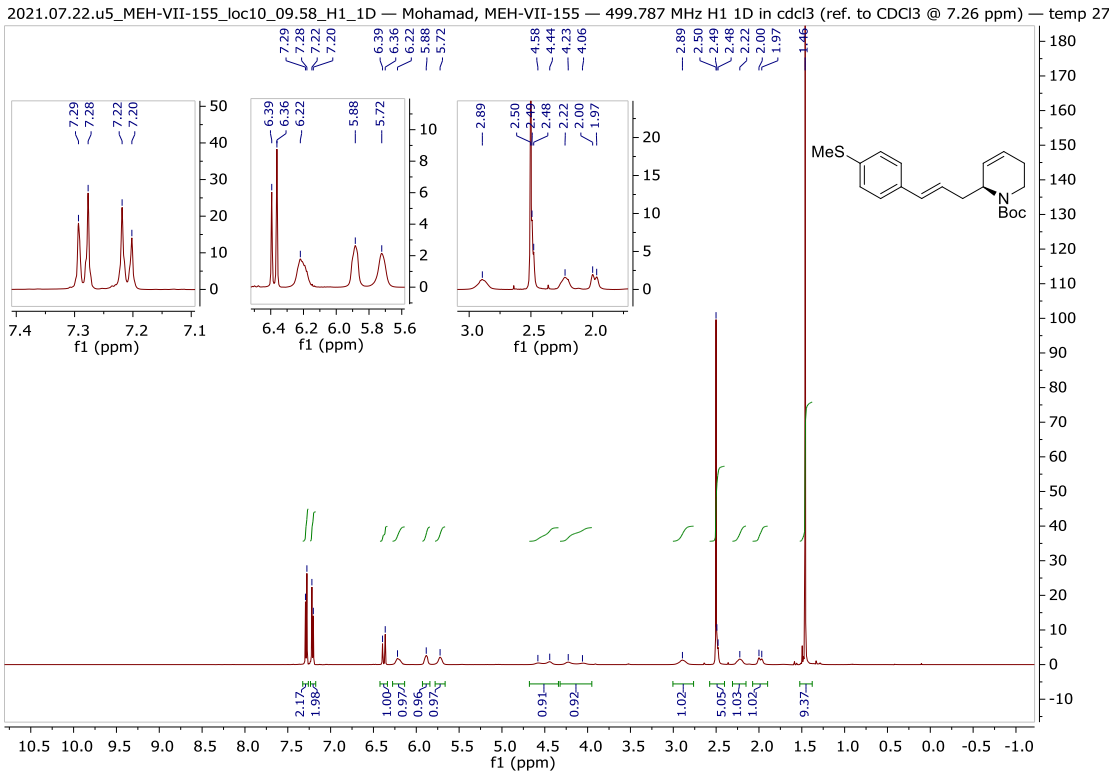

^{13}C NMR for compound **3-6j** (126 MHz, $CDCl_3$)

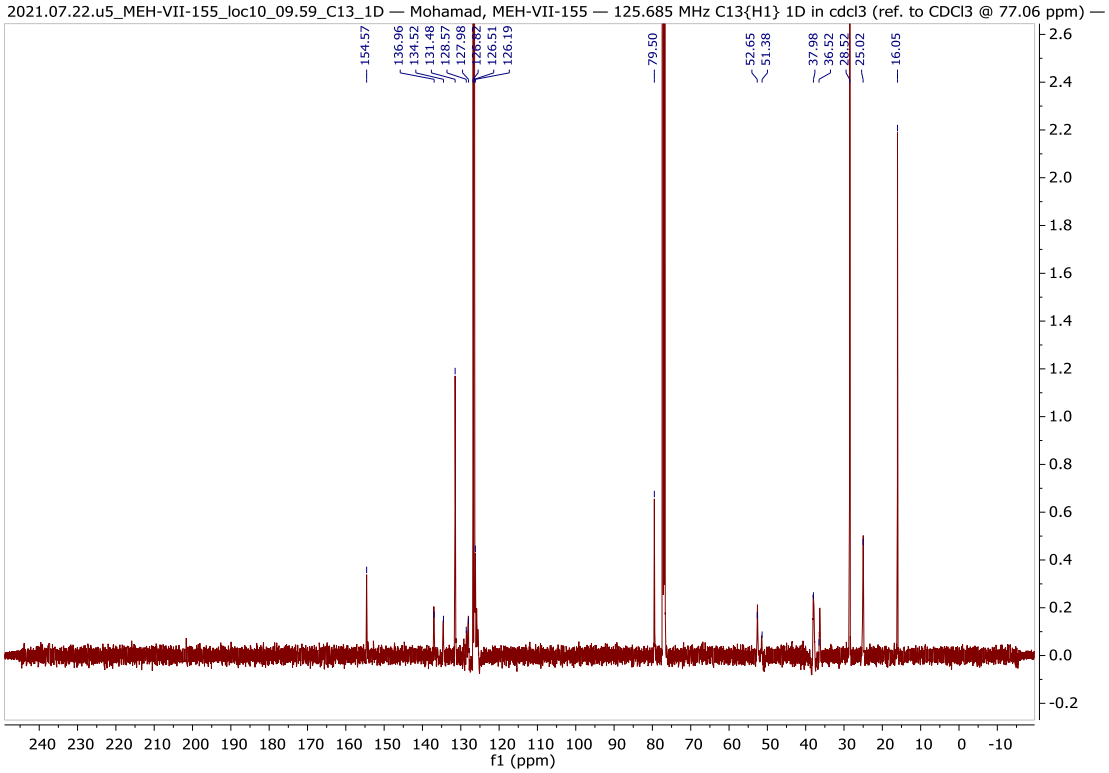

^{1}H NMR for compound **3-6k** (500 MHz, $CDCl_3$)

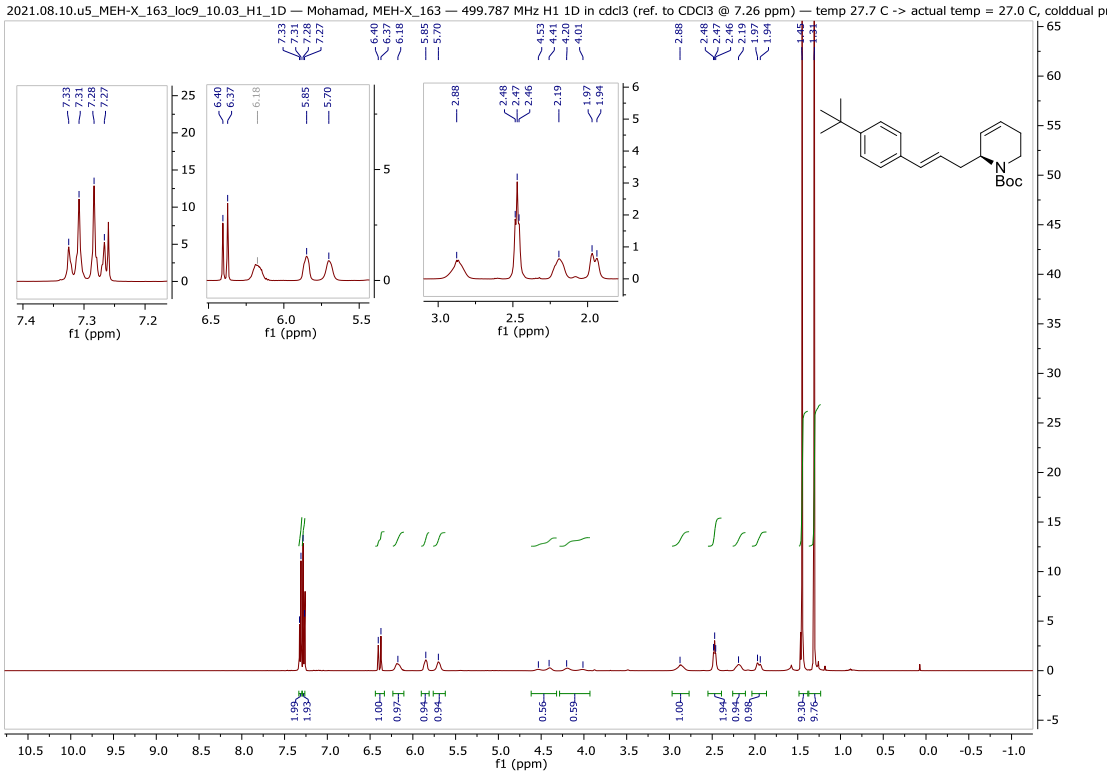

^{13}C NMR for compound **3-6k** (126 MHz, $CDCl_3$)

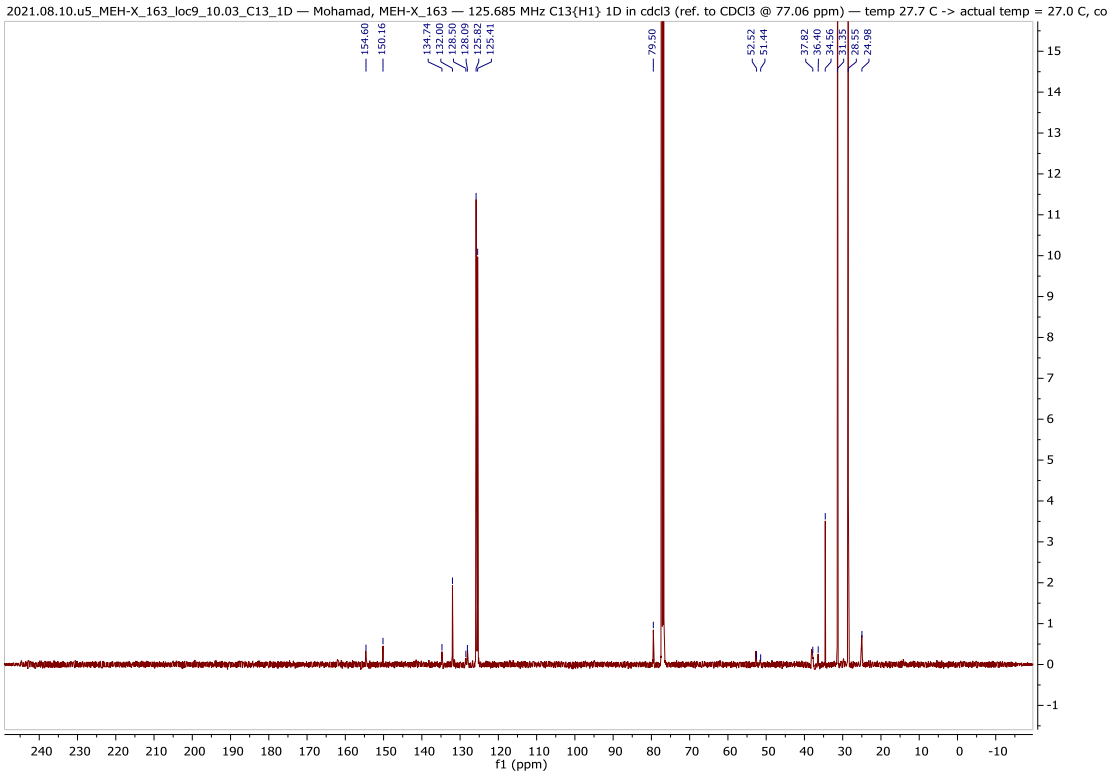

^{1}H NMR for compound **3-6l** (500 MHz, $CDCl_3$)

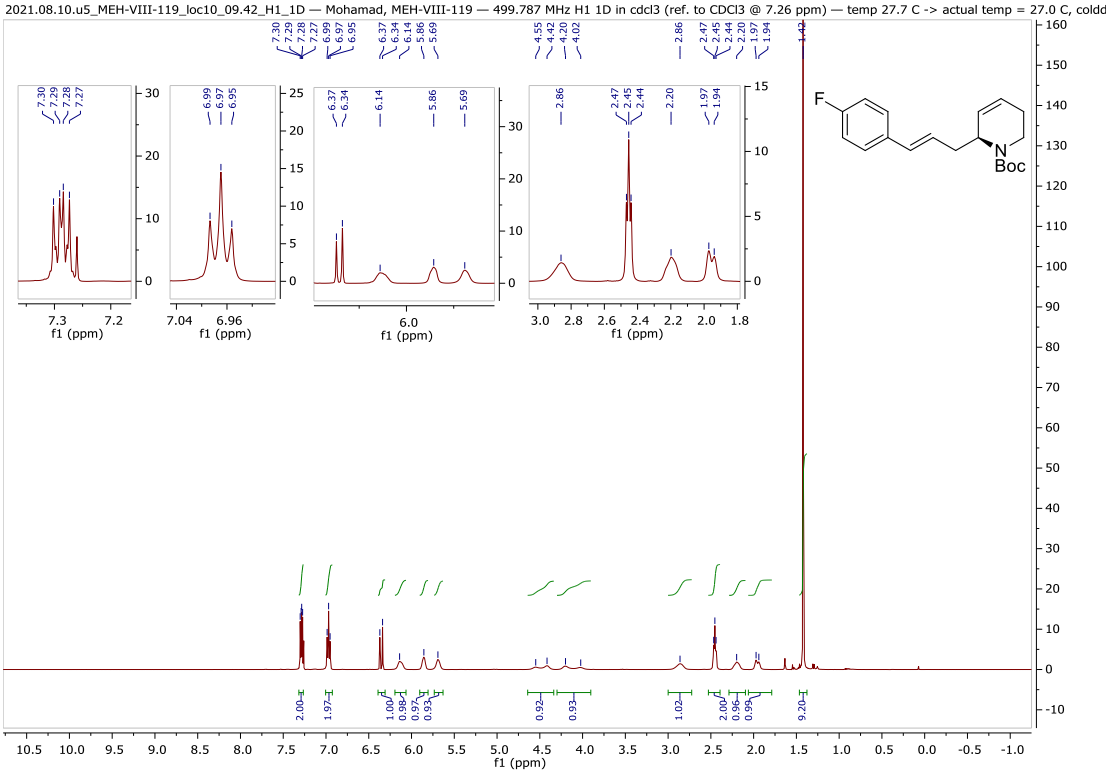

^{13}C NMR for compound **3-6l** (126 MHz, $CDCl_3$)

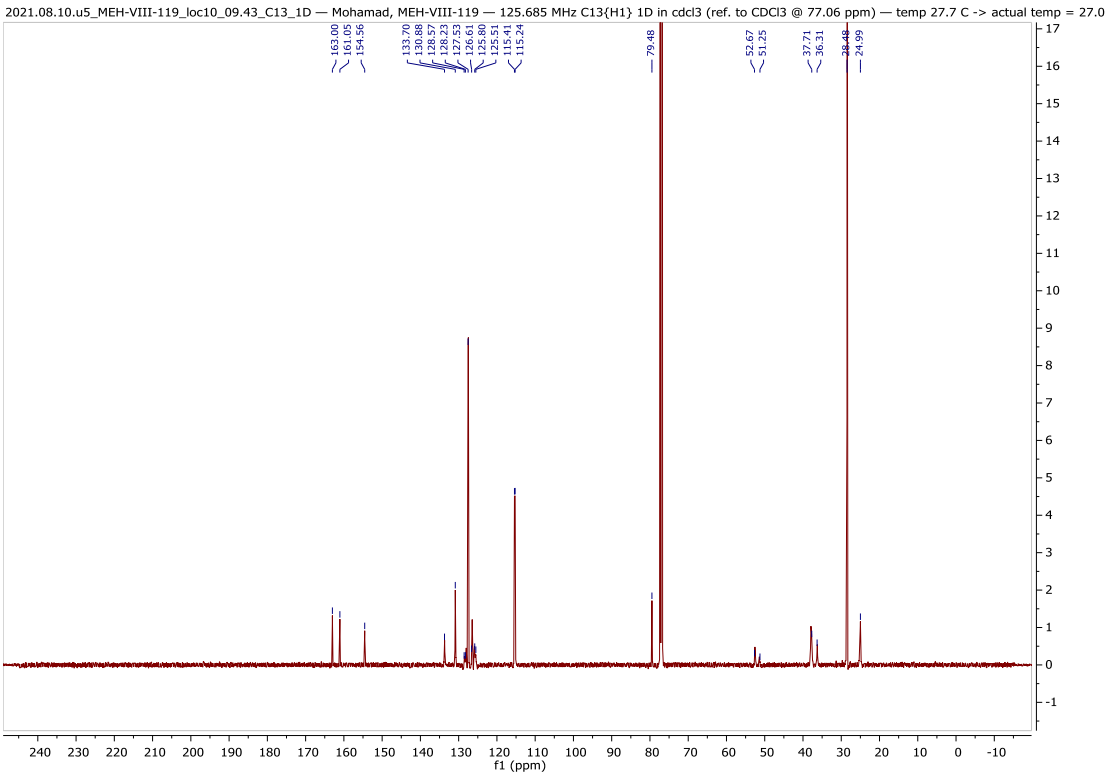

^{19}F NMR for compound **3-6l** (469 MHz, $CDCl_3$)

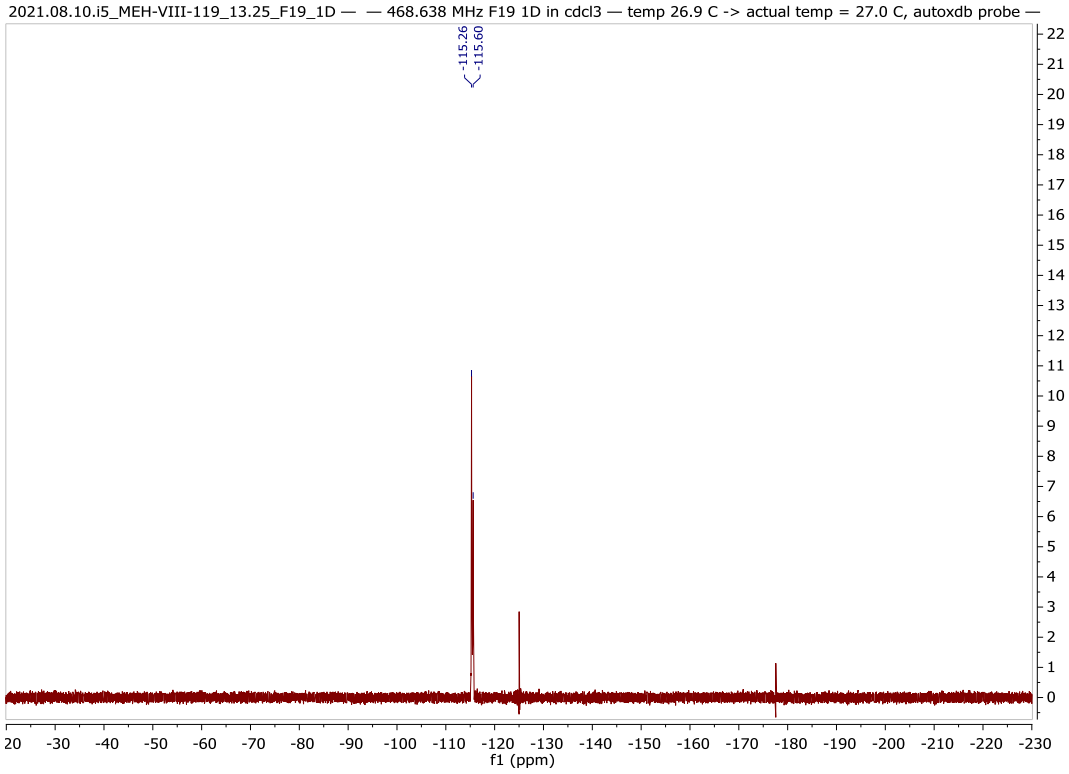

^{1}H NMR for compound **3-15** (500 MHz, $CDCl_3$)

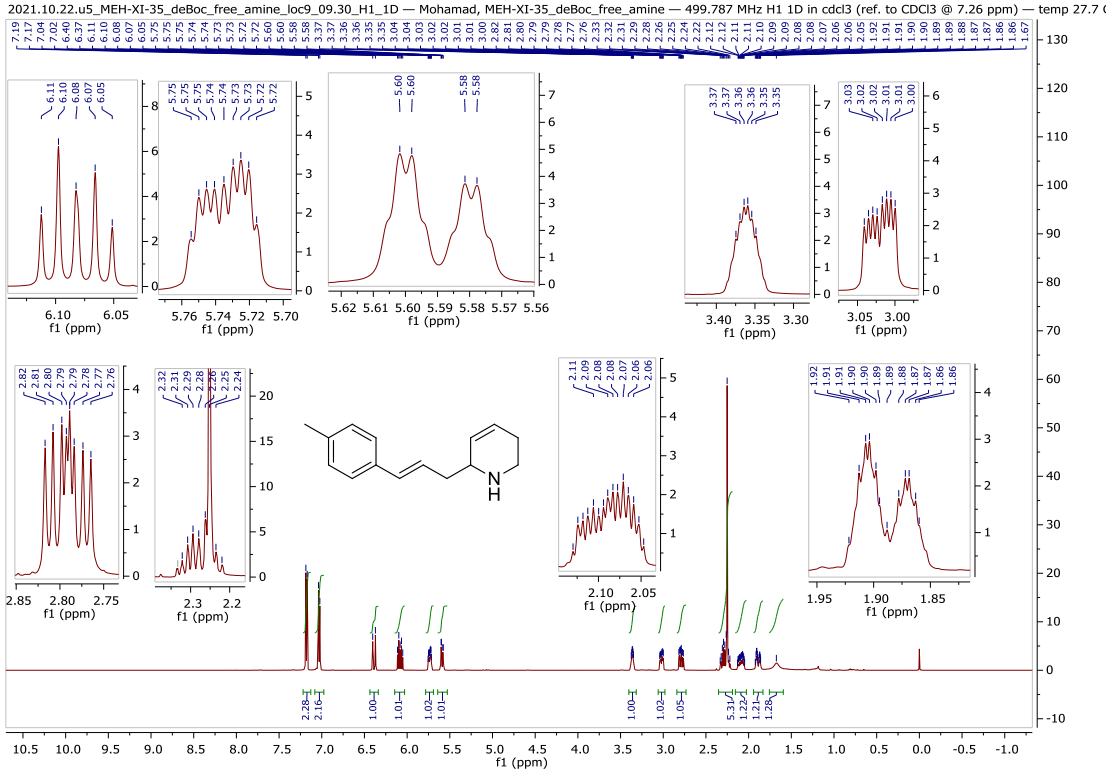

^{13}C NMR for compound **3-15** (126 MHz, $CDCl_3$)

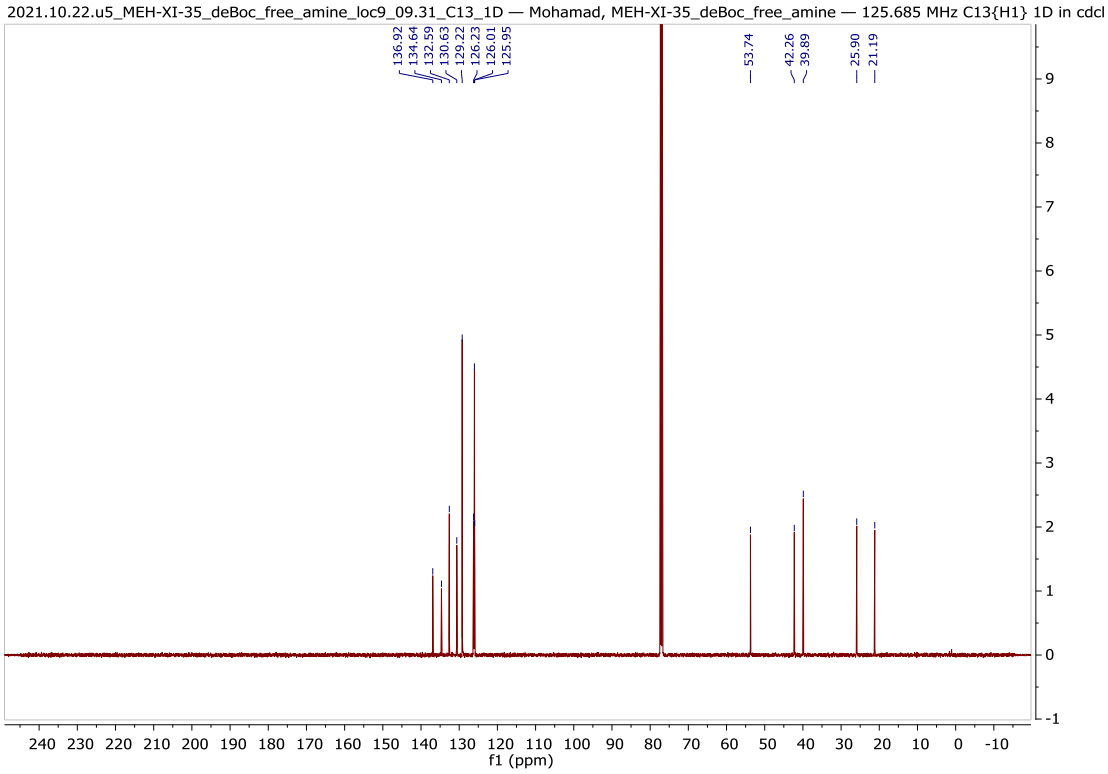

^{1}H NMR for compound **3-15** (500 MHz, $CDCl_3$ + 1 drop D_2O)

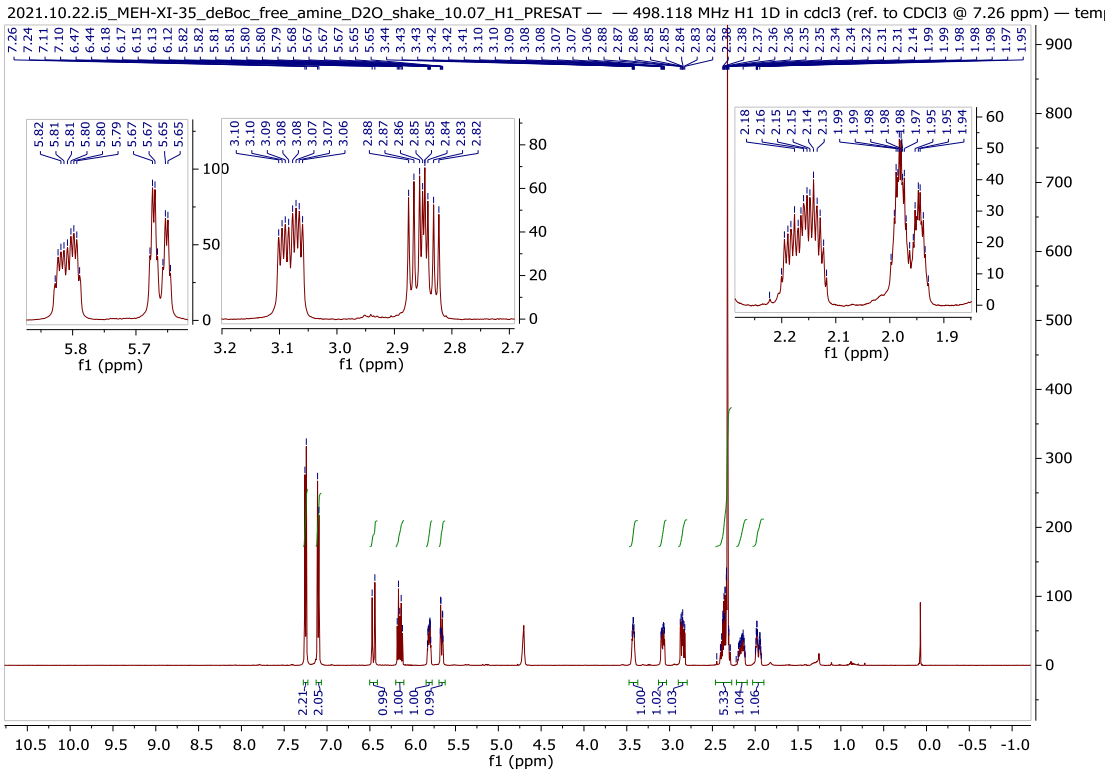

^{1}H NMR for compound (*rac*)-**3-6d′** (500 MHz, $CDCl_3$)

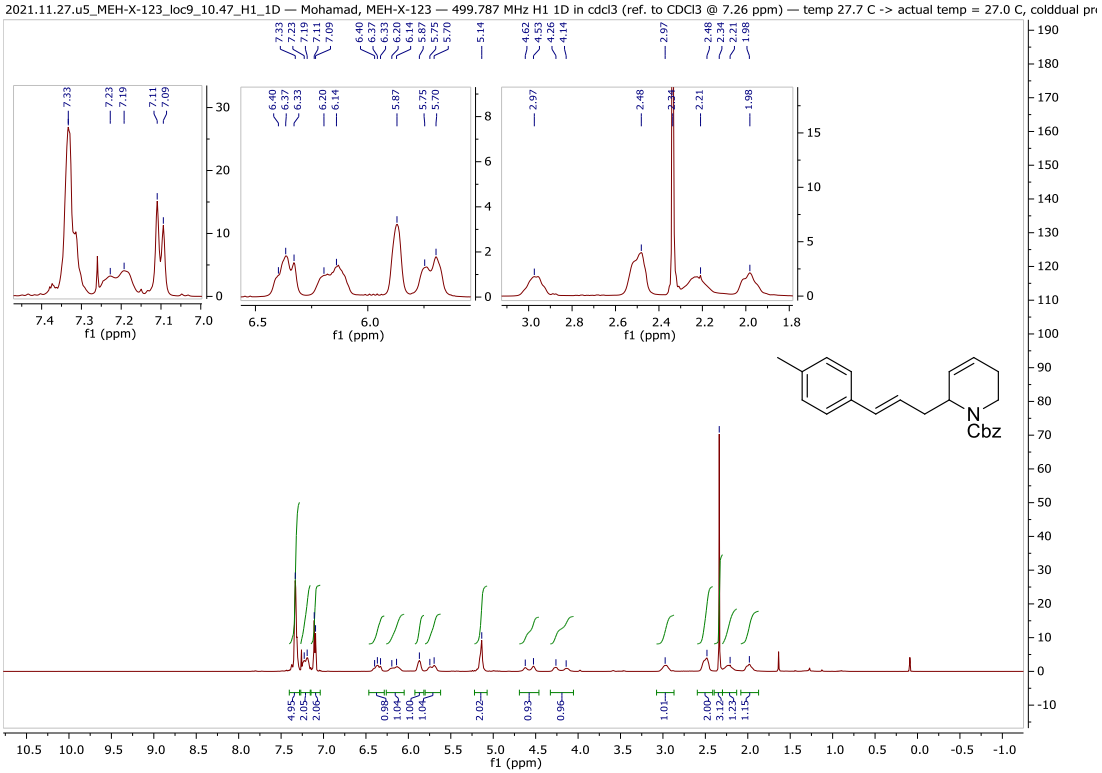

^{13}C NMR for compound (*rac*)-**3-6d′** (126 MHz, $CDCl_3$)

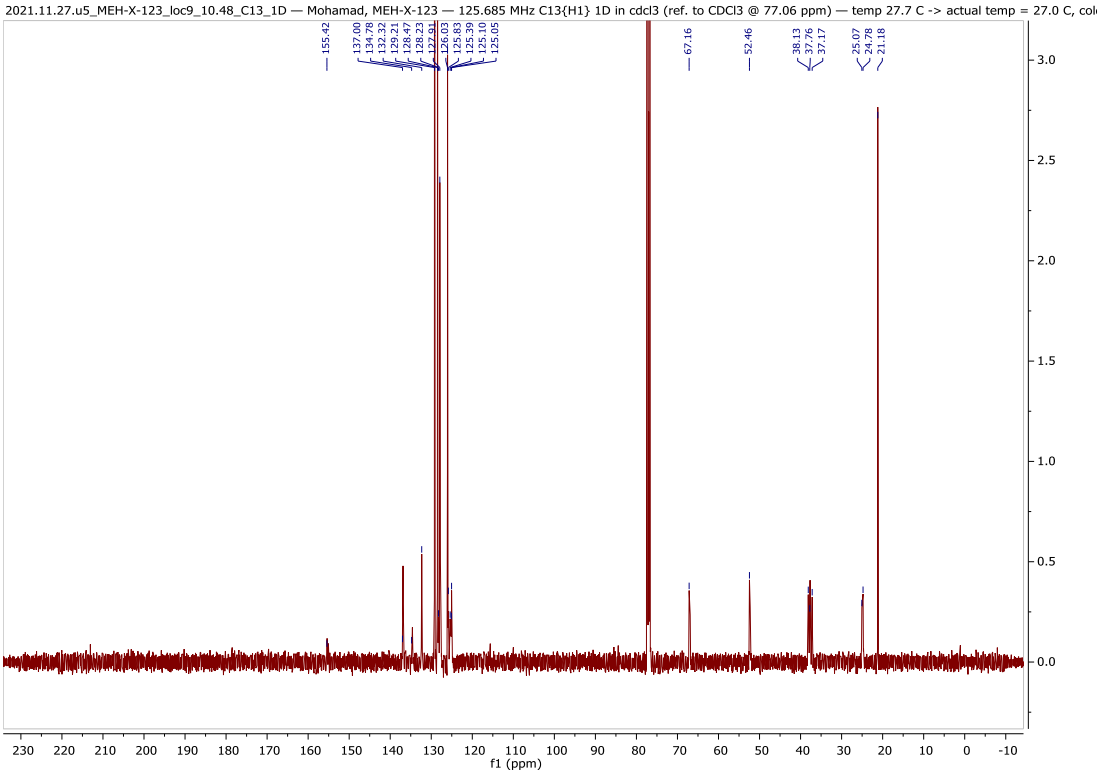

^{1}H NMR for compound **4-15** (500 MHz, DMSO-d_6)

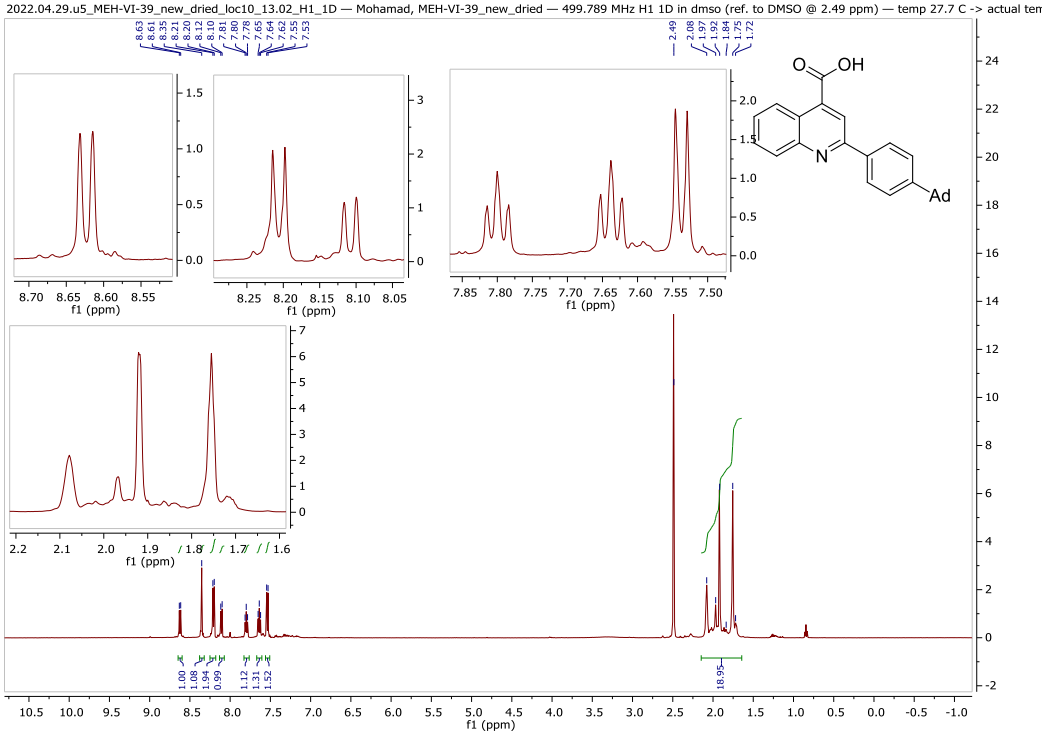

^{13}C NMR for compound **4-15** (500 MHz, DMSO-d_6)

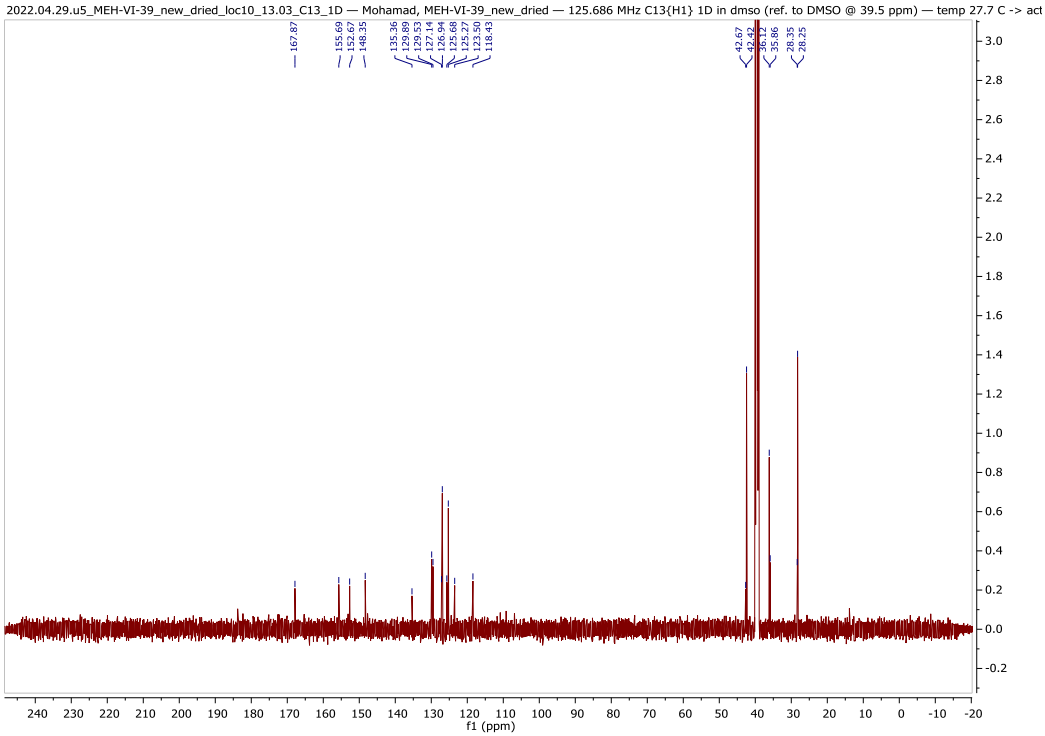

^{1}H NMR for compound **4-19** (500 MHz, $CDCl_3$)

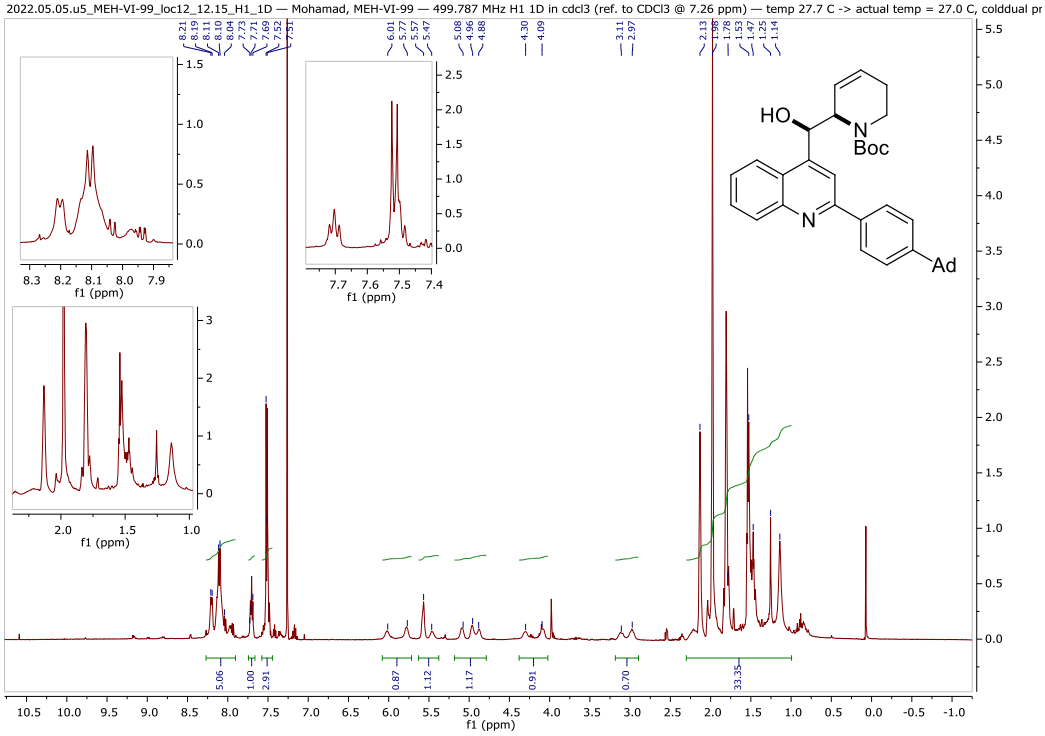

^{13}C NMR for compound **4-19** (500 MHz, $CDCl_3$)

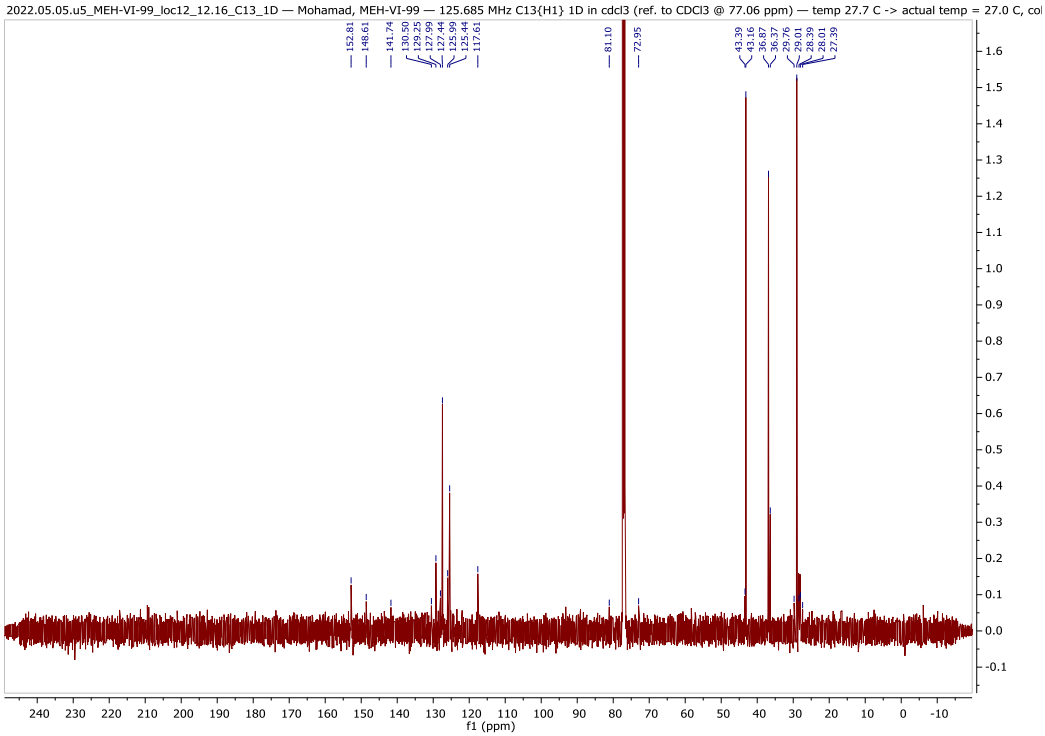

^{1}H NMR for compound **4-20** (500 MHz, CD_3OD)

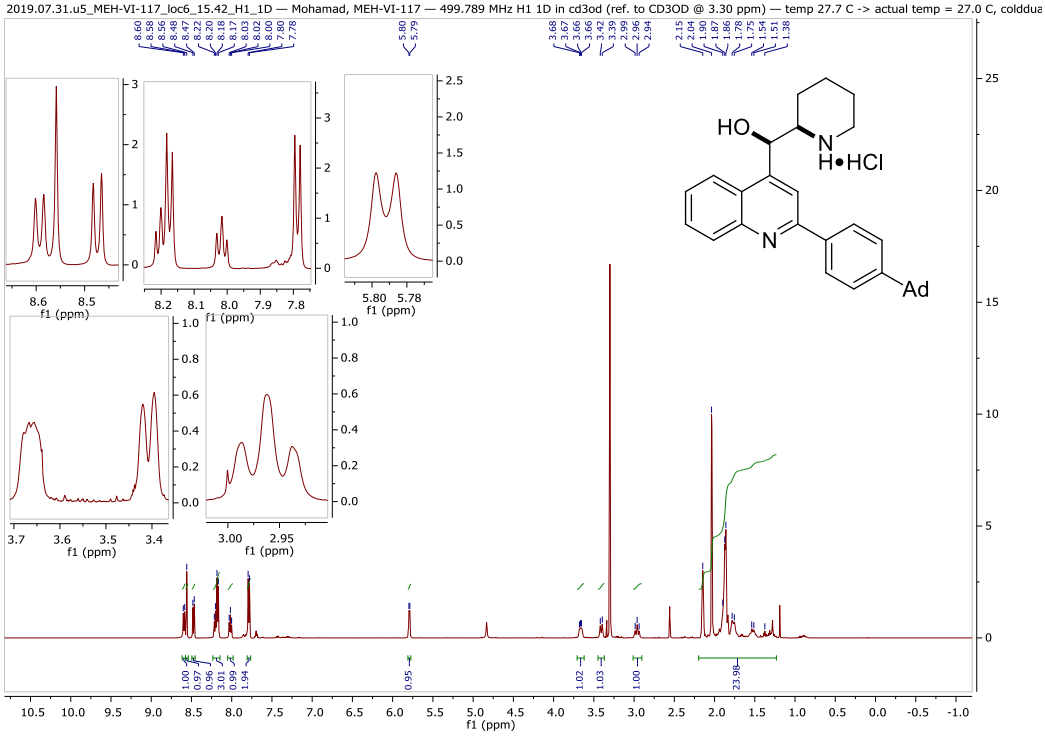

^{13}C NMR for compound **4-20** (500 MHz, CD_3OD)

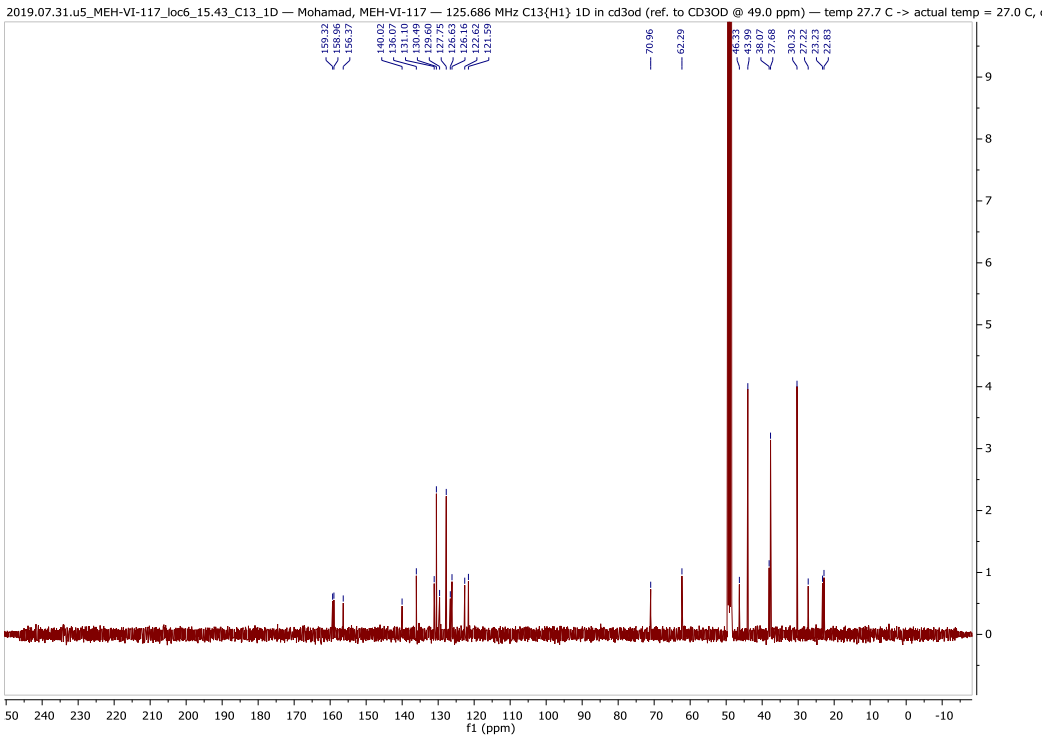

^{1}H NMR for compound **4-26** (500 MHz, CD_3OD)

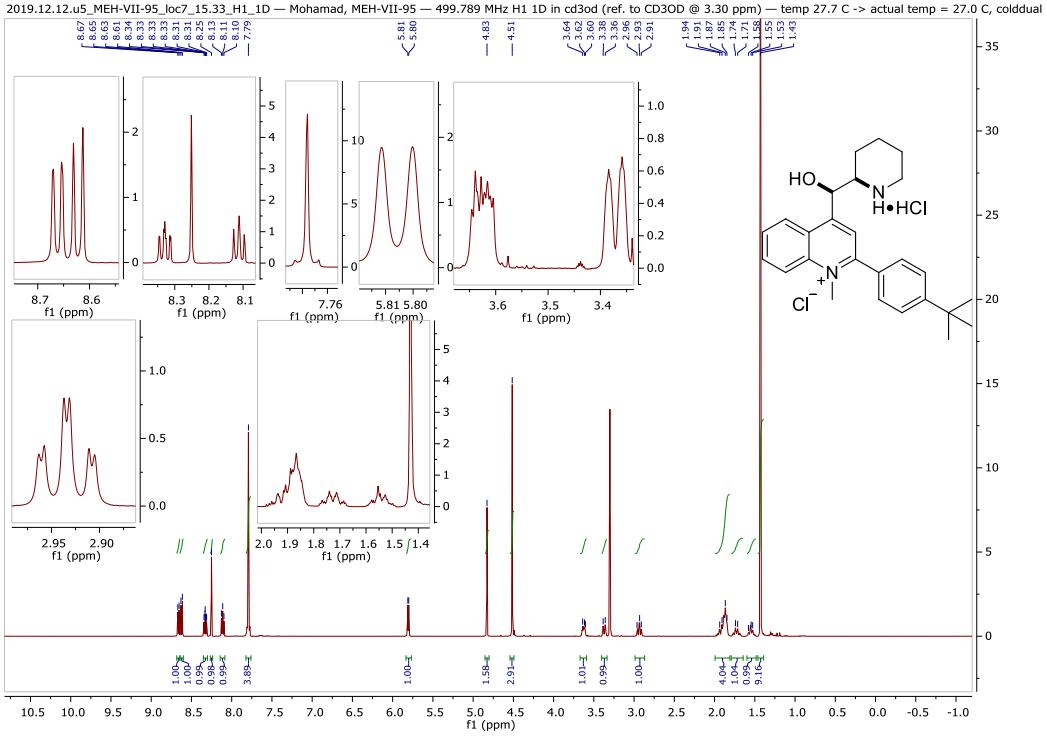

^{13}C NMR for compound **4-26** (500 MHz, CD_3OD)

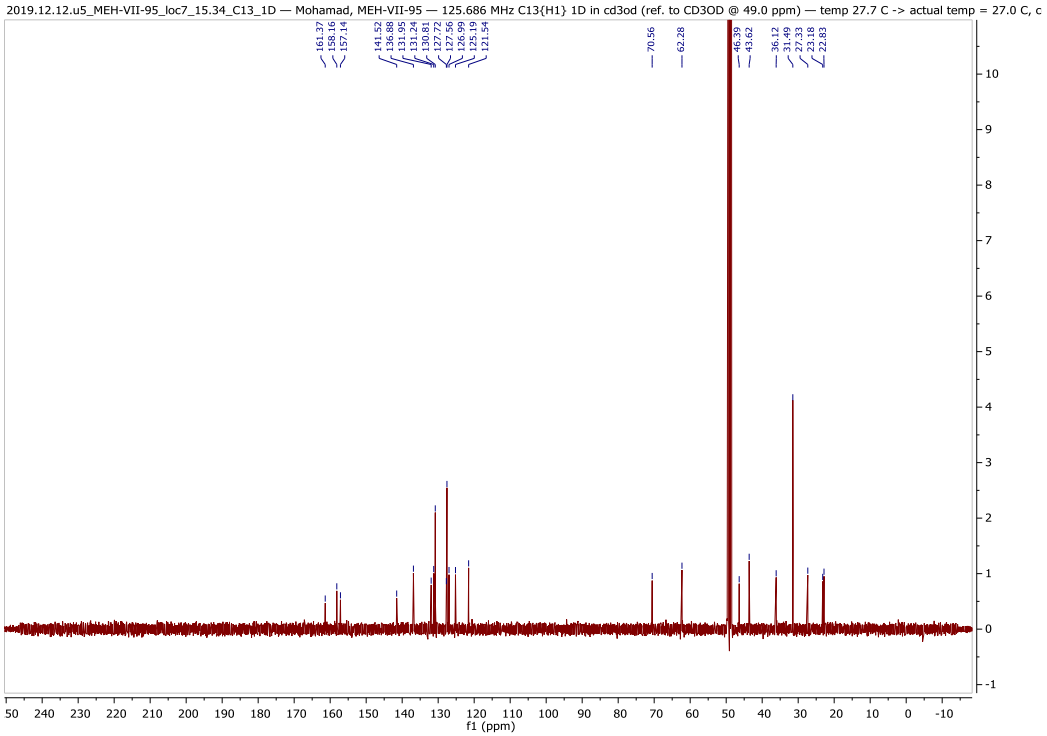

^{1}H NMR for compound **4-28** (500 MHz, CD_3OD)

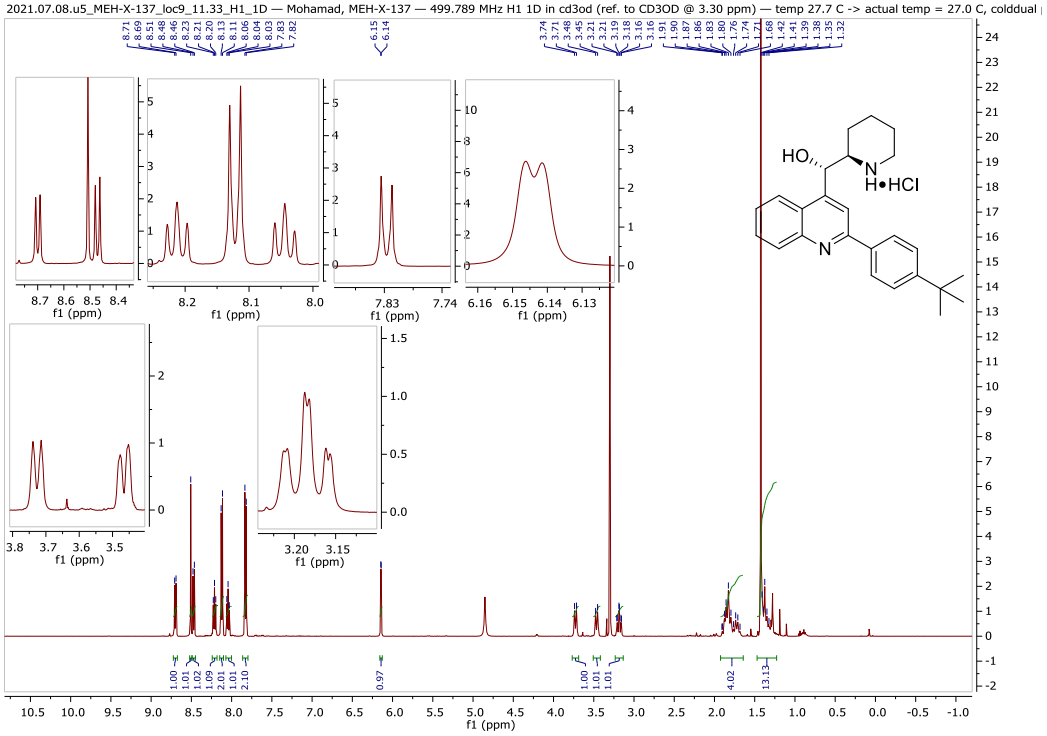

^{13}C NMR for compound **4-28** (500 MHz, CD_3OD)

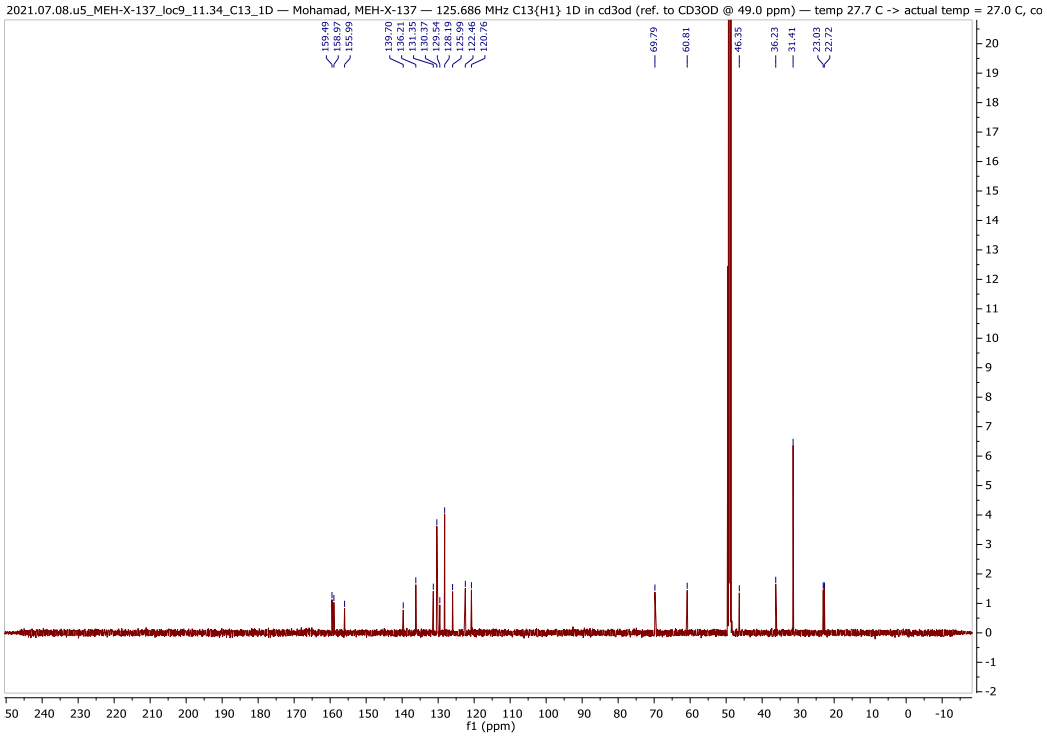

Appendix 2: Selected Chiral HPLC Chromatograms

HPLC trace for (±)-**3-6a** (top) and enantioenriched **3-6a** (bottom)

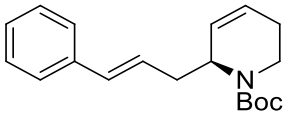

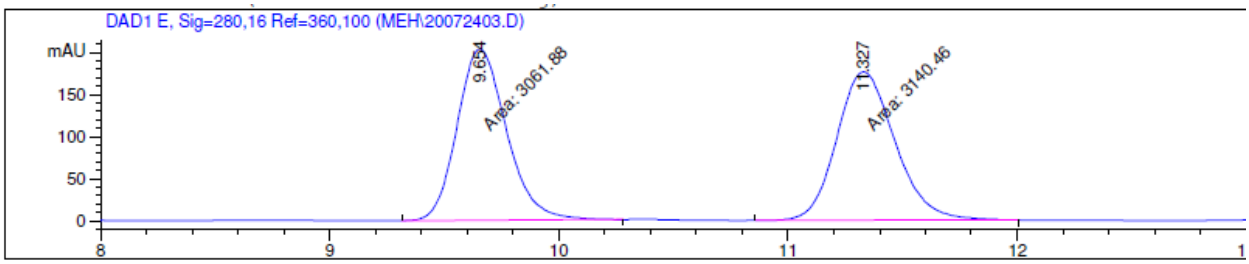

Signal 1: DAD1 E, Sig=280,16 Ref=360,100

Peak #	RetTime [min]	Type	Width [min]	Area [mAU*s]	Height [mAU]	Area %
1	9.654	MM	0.2499	3061.88403	204.22751	49.3666
2	11.327	MM	0.2959	3140.45874	176.89635	50.6334
Totals :				6202.34277	381.12386	

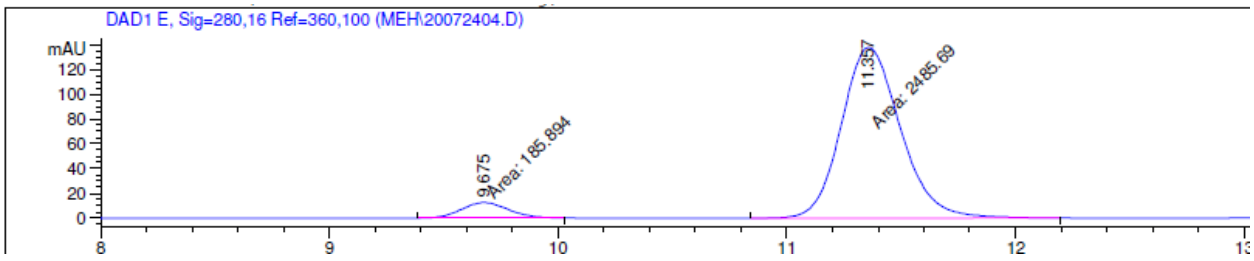

Peak #	RetTime [min]	Type	Width [min]	Area [mAU*s]	Height [mAU]	Area %
1	9.675	MM	0.2447	185.89436	12.66230	6.9582
2	11.357	MM	0.3004	2485.68579	137.90472	93.0418
Totals :				2671.58015	150.56702	

HPLC trace for (±)-**3-6b** (top) and enantioenriched **3-6b** (bottom)

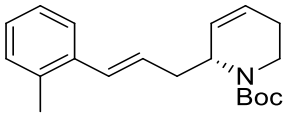

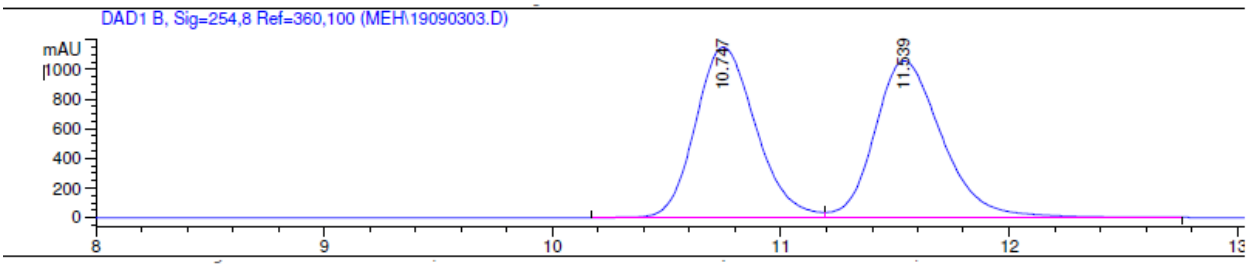

Peak #	RetTime [min]	Type	Width [min]	Area [mAU*s]	Height [mAU]	Area %
1	10.747	BV	0.2841	2.11436e4	1152.28040	49.3382
2	11.539	VB	0.3150	2.17108e4	1059.69092	50.6618
Totals :				4.28544e4	2211.97131	

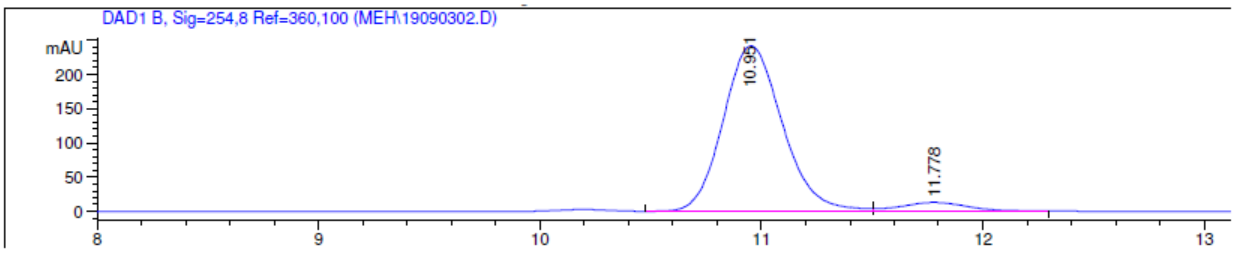

Peak #	RetTime [min]	Type	Width [min]	Area [mAU*s]	Height [mAU]	Area %
1	10.951	VV	0.2871	4503.35840	242.01489	94.2949
2	11.778	VB	0.3201	272.46707	12.91806	5.7051
Totals :				4775.82547	254.93295	

HPLC trace for (±)-**3-6c** (top) and enantioenriched **3-6c** (bottom)

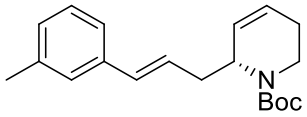

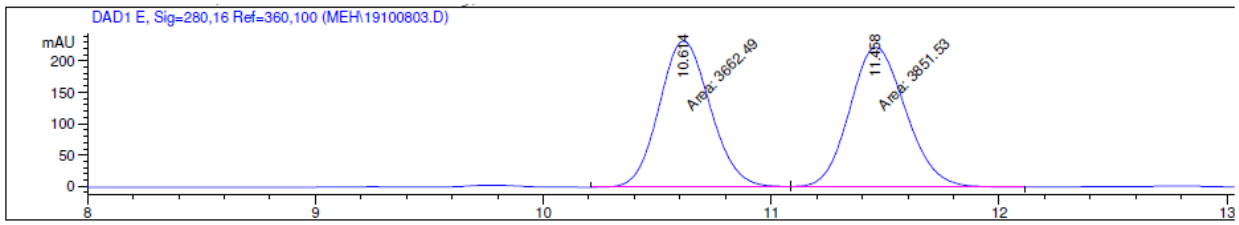

Peak #	RetTime [min]	Type	Width [min]	Area [mAU*s]	Height [mAU]	Area %
1	10.614	MF	0.2610	3662.48975	233.86827	48.7421
2	11.458	FM	0.2866	3851.53369	223.95952	51.2579
Totals :				7514.02344	457.82779	

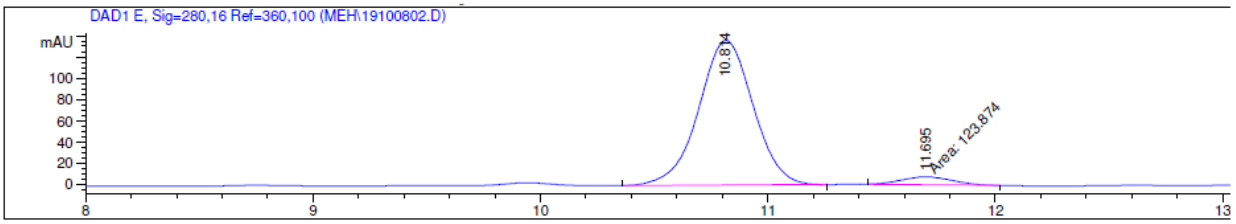

Peak #	RetTime [min]	Type	Width [min]	Area [mAU*s]	Height [mAU]	Area %
1	10.814	BP	0.2561	2267.71826	136.28812	94.8205
2	11.695	MM	0.2706	123.87367	7.62920	5.1795
Totals :				2391.59193	143.91731	

HPLC trace for (±)-**3-6d** (top) and enantioenriched **3-6d** from **3-5** (middle) and **3-5′** (bottom)

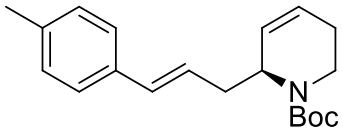

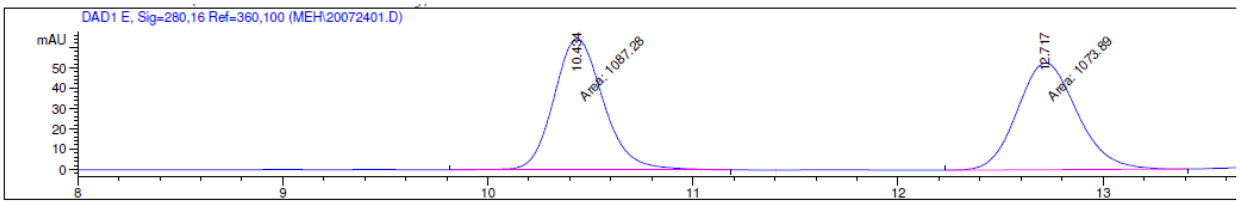

Peak #	RetTime [min]	Type	Width [min]	Area [mAU*s]	Height [mAU]	Area %
1	10.434	MM	0.2801	1087.28333	64.70607	50.3098
2	12.717	MM	0.3399	1073.89258	52.66484	49.6902
Totals :				2161.17590	117.37091	

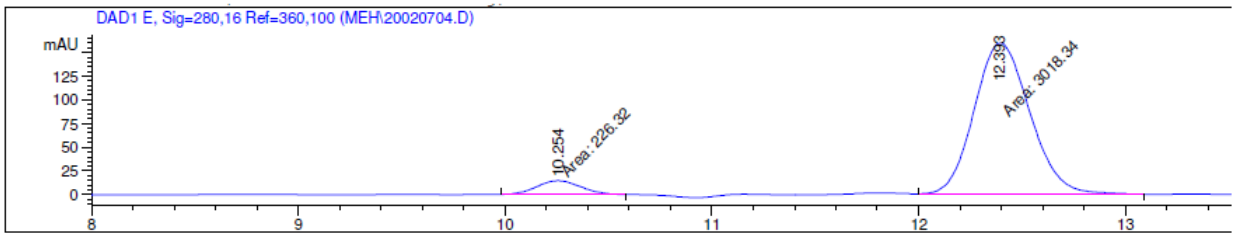

Peak #	RetTime [min]	Type	Width [min]	Area [mAU*s]	Height [mAU]	Area %
1	10.254	MM	0.2531	226.31989	14.90441	6.9752
2	12.393	MM	0.3145	3018.33789	159.94223	93.0248
Totals :				3244.65778	174.84664	

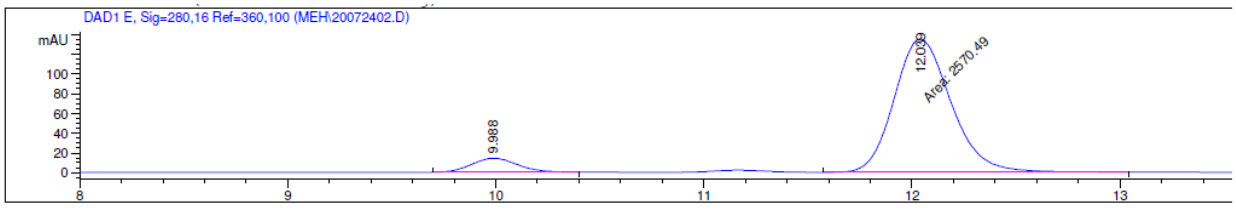

Peak #	RetTime [min]	Type	Width [min]	Area [mAU*s]	Height [mAU]	Area %
1	9.988	BB	0.2416	223.07236	14.33113	7.9852
2	12.039	MM	0.3166	2570.49121	135.30162	92.0148
Totals :				2793.56357	149.63275	

HPLC trace for (±)-**3-6e** (top) and enantioenriched **3-6e** (bottom)

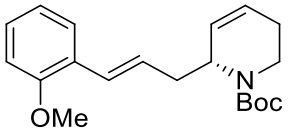

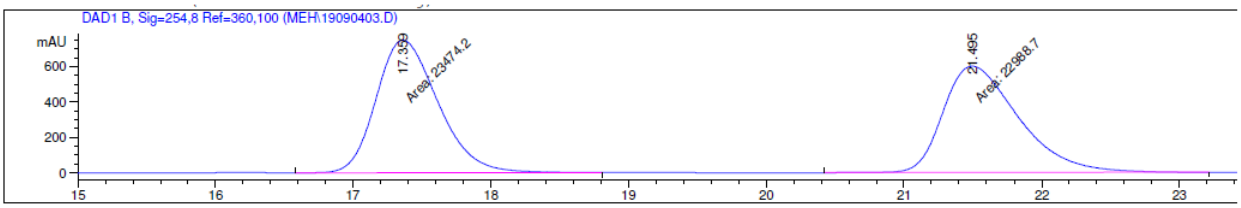

Peak #	RetTime [min]	Type	Width [min]	Area [mAU*s]	Height [mAU]	Area %
1	17.359	MM	0.5217	2.34742e4	749.90808	50.5225
2	21.495	MM	0.6371	2.29887e4	601.42139	49.4775
Totals :				4.64629e4	1351.32947	

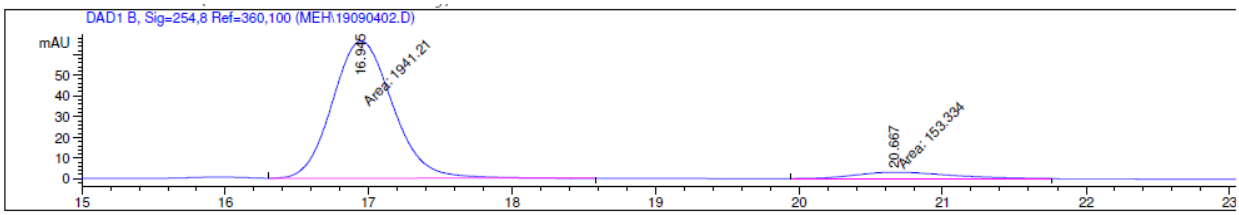

Peak #	RetTime [min]	Type	Width [min]	Area [mAU*s]	Height [mAU]	Area %
1	16.945	MM	0.4882	1941.21240	66.26708	92.6794
2	20.667	MM	0.7942	153.33423	3.21763	7.3206
Totals :				2094.54663	69.48471	

HPLC trace for (±)-**3-6f** (top) and enantioenriched **3-6f** (bottom)

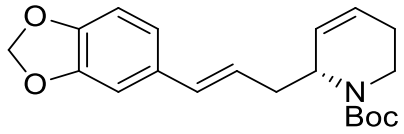

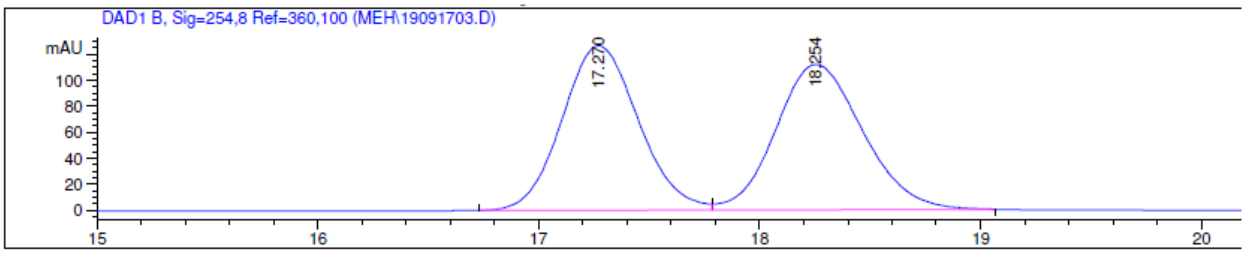

Peak #	RetTime [min]	Type	Width [min]	Area [mAU*s]	Height [mAU]	Area %
1	17.270	BV	0.3733	3056.04419	126.72529	49.8166
2	18.254	VB	0.4245	3078.54004	112.07335	50.1834
Totals :				6134.58423	238.79864	

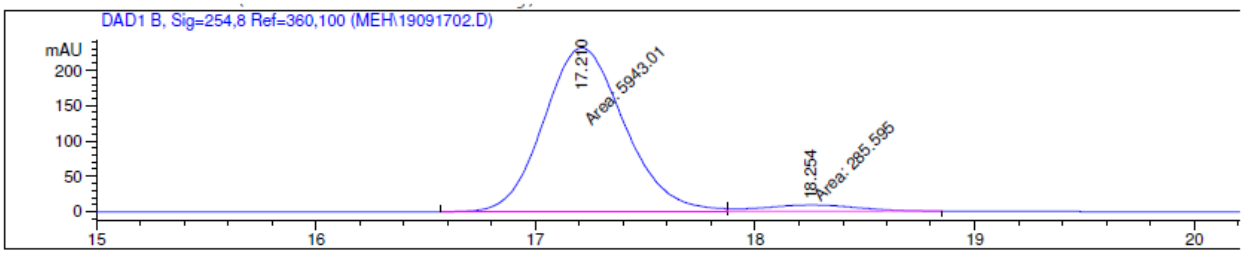

Peak #	RetTime [min]	Type	Width [min]	Area [mAU*s]	Height [mAU]	Area %
1	17.210	MF	0.4271	5943.01074	231.91661	95.4148
2	18.254	FM	0.5141	285.59528	9.25942	4.5852
Totals :				6228.60602	241.17603	

HPLC trace for (±)-**3-6g** (top) and enantioenriched **3-6g** (bottom)

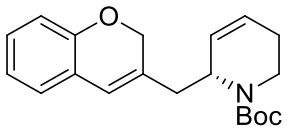

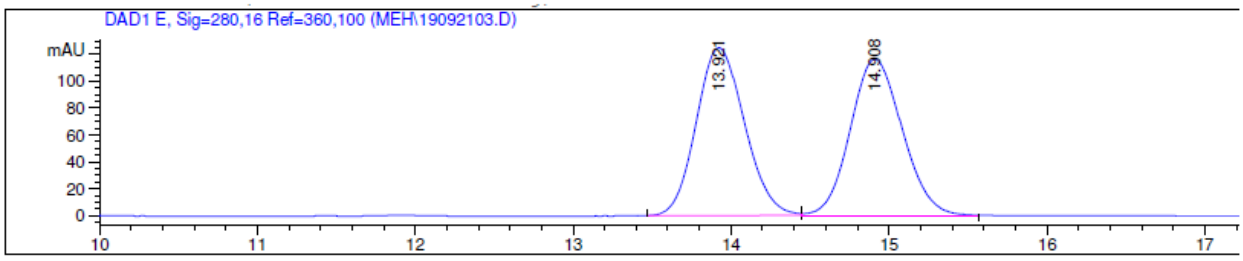

Peak #	RetTime [min]	Type	Width [min]	Area [mAU*s]	Height [mAU]	Area %
1	13.921	BV	0.3306	2676.27441	125.59457	49.9374
2	14.908	VB	0.3579	2682.98486	116.85542	50.0626
Totals :				5359.25928	242.45000	

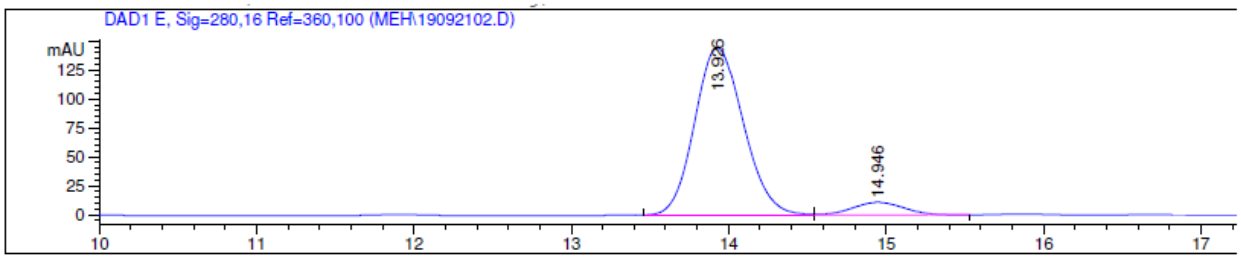

Peak #	RetTime [min]	Type	Width [min]	Area [mAU*s]	Height [mAU]	Area %
1	13.926	BB	0.3357	3128.53467	145.01659	92.4596
2	14.946	BP	0.3553	255.14180	11.13578	7.5404
Totals :				3383.67647	156.15237	

HPLC trace for (±)-**3-6h** (top) and enantioenriched **3-6h** (bottom)

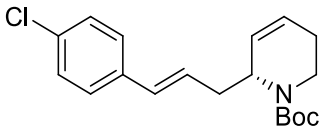

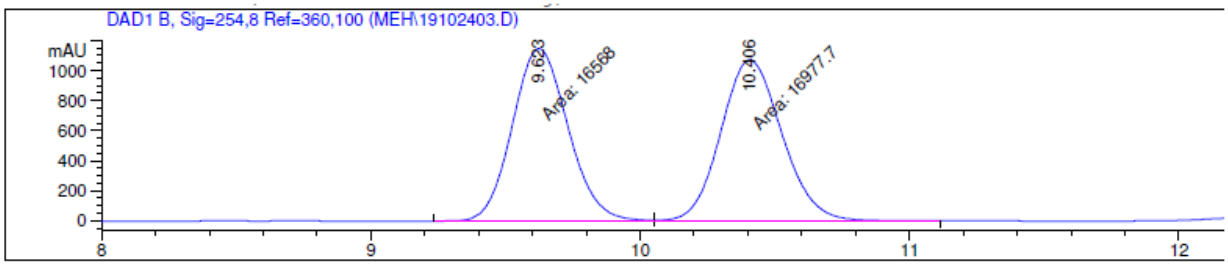

Peak #	RetTime [min]	Type	Width [min]	Area [mAU*s]	Height [mAU]	Area %
1	9.623	MF	0.2403	1.65680e4	1149.24426	49.3893
2	10.406	FM	0.2638	1.69777e4	1072.75830	50.6107
Totals :				3.35456e4	2222.00256	

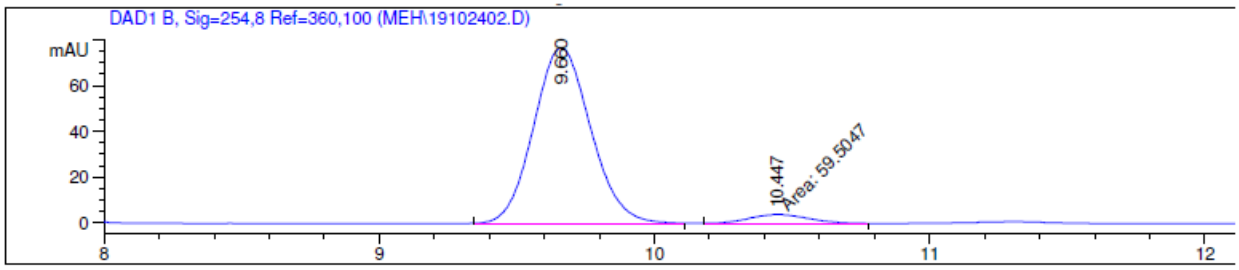

Peak #	RetTime [min]	Type	Width [min]	Area [mAU*s]	Height [mAU]	Area %
1	9.660	BB	0.2245	1111.93347	76.97248	94.9204
2	10.447	MM	0.2530	59.50470	3.91940	5.0796
Totals :				1171.43817	80.89188	

HPLC trace for (±)-**3-6i** (top) and enantioenriched **3-6i** (bottom)

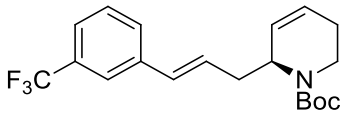

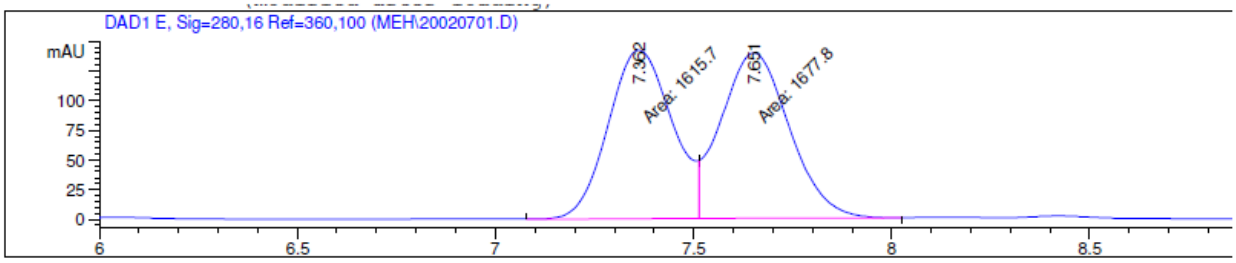

Peak #	RetTime [min]	Type	Width [min]	Area [mAU*s]	Height [mAU]	Area %
1	7.362	MF	0.1888	1615.70166	142.61624	49.0573
2	7.651	FM	0.1998	1677.79590	139.95151	50.9427
Totals :				3293.49756	282.56775	

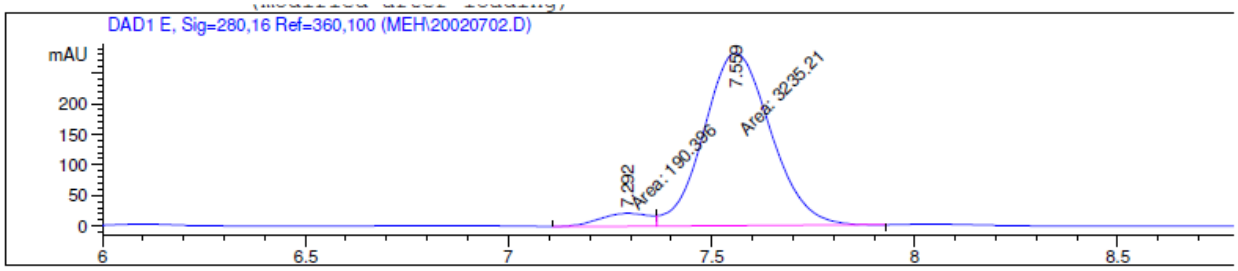

Peak #	RetTime [min]	Type	Width [min]	Area [mAU*s]	Height [mAU]	Area %
1	7.292	MF	0.1484	190.39609	21.38748	5.5580
2	7.559	FM	0.1909	3235.20874	282.40302	94.4420
Totals :				3425.60483	303.79049	

HPLC trace for (±)-**3-6j** (top) and enantioenriched **3-6j** (bottom)

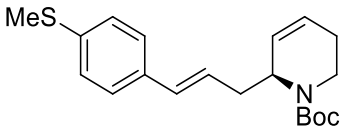

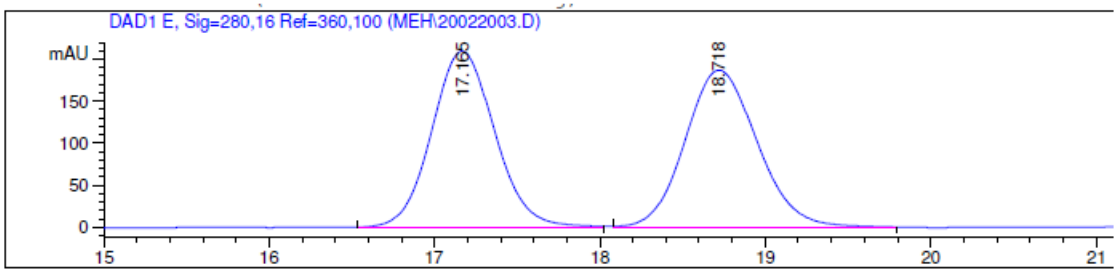

Peak #	RetTime [min]	Type	Width [min]	Area [mAU*s]	Height [mAU]	Area %
1	17.165	BB	0.4128	5576.94580	209.37207	49.4702
2	18.718	BB	0.4757	5696.39941	186.82304	50.5298
Totals :				1.12733e4	396.19511	

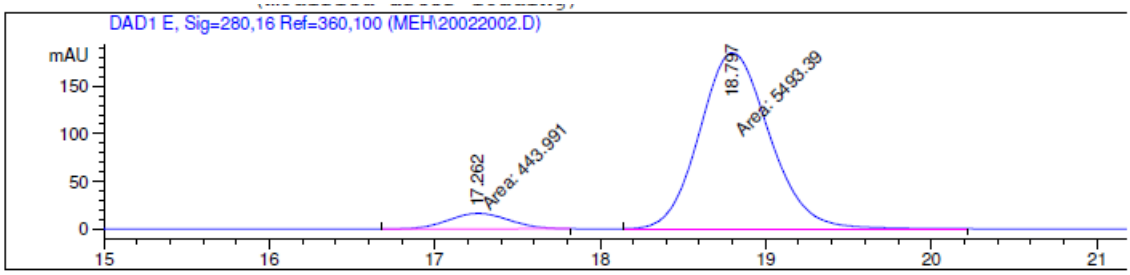

Peak #	RetTime [min]	Type	Width [min]	Area [mAU*s]	Height [mAU]	Area %
1	17.262	MM	0.4441	443.99146	16.66128	7.4779
2	18.797	MM	0.4943	5493.39355	185.22372	92.5221
Totals :				5937.38501	201.88501	

HPLC trace for (±)-**3-6k** (top) and enantioenriched **3-6k** (bottom)

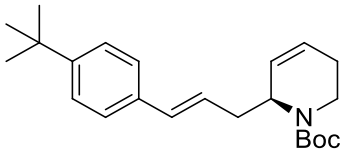

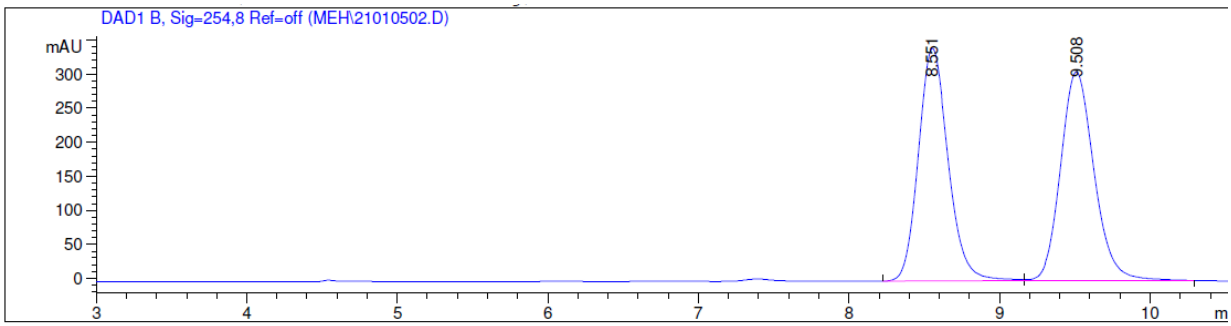

Peak #	RetTime [min]	Type	Width [min]	Area [mAU*s]	Height [mAU]	Area %
1	8.551	BV	0.2135	4733.62500	342.04077	49.9077
2	9.508	VB	0.2386	4751.13867	306.95721	50.0923
Totals :				9484.76367	648.99799	

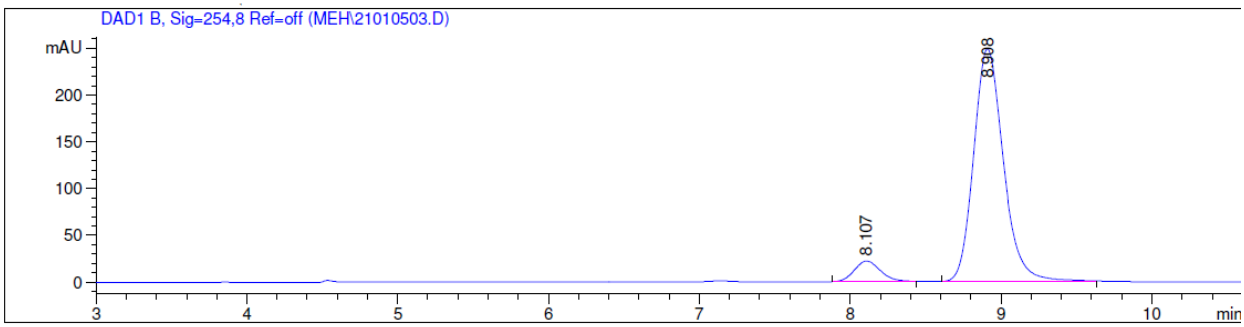

Peak #	RetTime [min]	Type	Width [min]	Area [mAU*s]	Height [mAU]	Area %
1	8.107	BB	0.1874	267.60303	22.08076	7.2773
2	8.908	BB	0.2100	3409.60352	248.60757	92.7227
Totals :				3677.20654	270.68833	

HPLC trace for (±)-**3-6l** (top) and enantioenriched **3-6l** (bottom)

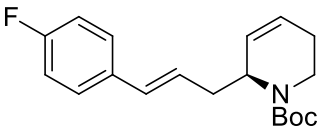

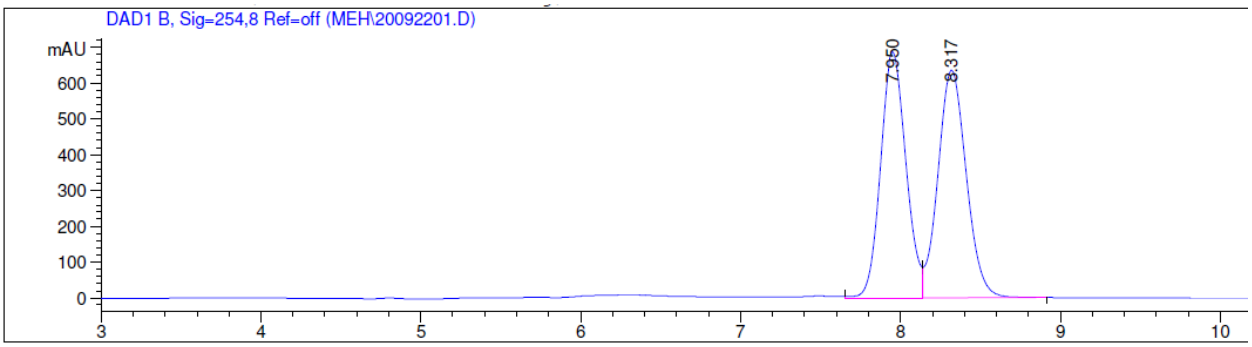

Signal 1: DAD1 B, Sig=254,8 Ref=off

Peak #	RetTime [min]	Type	Width [min]	Area [mAU*s]	Height [mAU]	Area %
1	7.950	VV	0.1718	7658.71240	688.23566	49.5030
2	8.317	VB	0.1892	7812.48877	636.35492	50.4970
Totals :				1.54712e4	1324.59058	

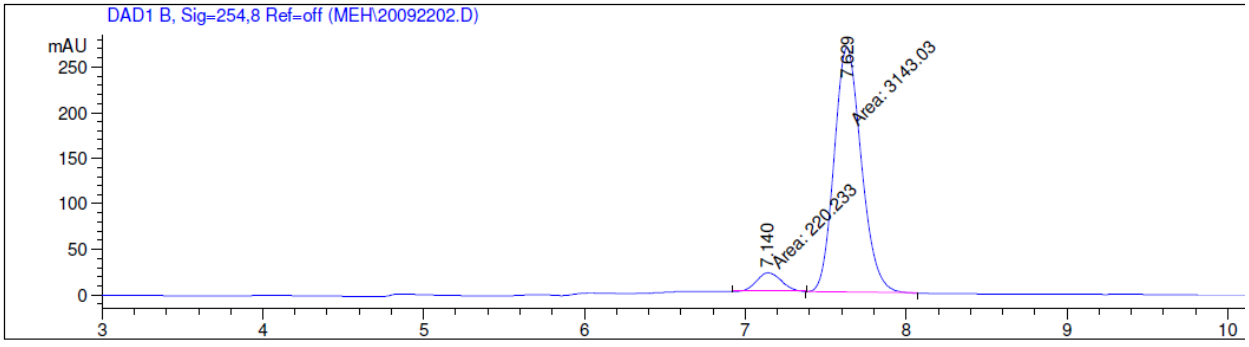

Peak #	RetTime [min]	Type	Width [min]	Area [mAU*s]	Height [mAU]	Area %
1	7.140	MM	0.1793	220.23280	20.47015	6.5482
2	7.629	MM	0.1952	3143.03320	268.30289	93.4518
Totals :				3363.26601	288.77304	